NONLINEAR MAGNETO-OPTIC EFFECTS IN OPTICALLY DENSE Rb VAPOR

A Dissertation

by

IRINA BORISOVNA NOVIKOVA

Submitted to the Office of Graduate Studies of
Texas A&M University
in partial fulfillment of the requirements for the degree of

DOCTOR OF PHILOSOPHY

May 2003

Major Subject: Physics

NONLINEAR MAGNETO-OPTIC EFFECTS
IN OPTICALLY DENSE Rb VAPOR

A Dissertation

by

IRINA BORISOVNA NOVIKOVA

Submitted to Texas A&M University
in partial fulfillment of the requirements
for the degree of

DOCTOR OF PHILOSOPHY

Approved as to style and content by:

George R. Welch
(Chair of Committee)

Marlan O. Scully
(Member)

Alexei V. Sokolov
(Member)

Phillip R. Hemmer
(Member)

Edward S. Fry
(Head of Department)

May 2003

Major Subject: Physics

ABSTRACT

Nonlinear Magneto-Optic Effects
in Optically Dense Rb Vapor. (May 2003)

Irina Borisovna Novikova, Diploma, Moscow State Engineering Physics Institute
Chair of Advisory Committee: Dr. George R. Welch

Nonlinear magneto-optical effects, originated from atomic coherence, are studied both theoretically and experimentally in thermal Rb vapor. The analytical description of the fundamental properties of coherent media are based on the simplified three- and four-level systems, and then verified using numerical simulations and experimental measurements. In particular, we analyze the modification of the long-lived atomic coherence due to various physical effects, such as reabsorption of spontaneous radiation, collisions with a buffer gas atoms, etc.

We also discuss the importance of the high-order nonlinearities in the description of the polarization rotation for the elliptically polarized light. The effect of self-rotation of the elliptical polarization is also analyzed.

Practical applications of nonlinear magneto-optical effects are considered in precision metrology and magnetometery, and for the generation of non-classical states of electromagnetic field.

To my father, Boris.

ACKNOWLEDGMENTS

There are many people who influenced and contributed to the work presented here, and I am grateful to each and every one of them.

I would like to wholeheartedly thank my advisor, Prof. George R. Welch for the constant support, guidance and advice, which provided the best environment for my research and academic development. I also want to thank Dr. Andrey B. Matsko, whose enthusiasm, talent and energy inspired most of the ideas described in this dissertation, and who taught me what it takes to be a scientist. My special appreciation is for Dr. Vladimir A. Sautenkov and Vladimir L. Velichansky, the people who taught me everything I know about the experimental work. I am very grateful to Prof. D. Budker and his group: V. V. Yashchuk, D. Kimball, S. Rochester and the others, for inviting me to visit their laboratory at U. C. Berkeley university, for sharing their ideas and for always inspiring discussions. I also would like to acknowledge the important contributions of M. O. Scully, Yu. V. Rostovtsev, A. S. Zibrov, M. D. Lukin, M. Fleischhauer, M. S. Zubairy, and C. J. Bednar.

It is my pleasure to thank M. Akulshin, E. S. Fry, L. Hollberg, J. Kitching, O. Kocharovskaya, R. Kolesov, R. P. Lucht, Yu. Malakyan, A. F. Narducci, H. Robinson, D. Sarkisyan, A. V. Sokolov, A. Taichenachev, V. V. Vassiliev, Th. Walter, A. Weis, R. Wynands, and V. Yudin for useful discussions. I also want to acknowledge the support of the Office of Naval Research and the Welch Foundation.

Finally, I would like to thank all my friends and family, especially my husband, Eugeniy Mikhailov, for the constant moral, physical and computer support and inspiration.

TABLE OF CONTENTS

CHAPTER Page

I INTRODUCTION 1

- A. Goals and motivation 1
- B. Review of coherence effects on the Zeeman sublevels 3
- C. Review of nonlinear magneto-optic effects 5

II NONLINEAR MAGNETO-OPTIC ROTATION IN THREE-LEVEL Λ SYSTEM 9

- A. Optical Bloch equations for general Λ scheme 9
  - 1. Maxwell's equations for the electromagnetic field propagating in atomic vapor 9
  - 2. Interaction of light with a three-level Λ system 13
  - 3. The effect of relaxation processes 16
- B. The nonlinear Faraday effect in a three-level Λ system . . . 20
  - 1. Alkali atoms in the external magnetic field 20
  - 2. Coherent population trapping in a Λ system 21
  - 3. The solution for the case of a homogeneously broadened transition 24
- C. Nonlinear Faraday effect in hot atomic vapor: the influence of Doppler broadening 27
- D. Normalization conditions for the $F = 1 \rightarrow F = 0$ transitions 33

III NONLINEAR FARADAY EFFECT IN DENSE Rb VAPOR . . 35

- A. Experimental setup 35
  - 1. Diode lasers 35
  - 2. Polarization rotation measurements 39
- B. Absorption and polarization rotation on various Rb transitions 40
- C. Enhancement of the nonlinear Faraday rotation with atomic density 46
- D. Experimental study of the NMOR resonance line-shape . . 48

IV THE EFFECT OF RADIATION TRAPPING ON ZEEMAN COHERENCE 54

- A. Radiation trapping in two-level and three-level systems . . 56

CHAPTER Page

- B. Radiation trapping and nonlinear magneto-optic rotation: theory . . . 60
- C. Radiation trapping and nonlinear magneto-optic rotation: experiment . . . 63

V MODIFICATION OF THE NONLINEAR FARADAY ROTATION IN THE PRESENCE OF BUFFER GAS . . . 72

- A. The effect of velocity-changing collisions on Zeeman coherence 75
  - 1. Low buffer gas pressure . . . 78
  - 2. High buffer gas pressure . . . 84
- B. The shape of NMOR resonances in the presence of buffer gas . . . 87
- C. Detection on non-resonant impurities using the nonlinear Faraday effect . . . 89

VI ELLIPTICITY-DEPENDENT MAGNETO-OPTICAL ROTATION VIA MULTI-PHOTON COHERENCE . . . 94

- A. Analysis of NMOR in M interaction scheme . . . 98
  - 1. Coherent population trapping in an M level scheme . 99
  - 2. Equations of motion . . . 101
  - 3. Solution based on the modified Schrödinger equations 102
- B. Polarization rotation for the $F = 2 \to F' = 1$ transition . . 108
- C. NMOR in atoms with large values of angular momentum . 110
- D. Experimental study of ellipticity-dependent MNOR in Rb vapor . . . 112
  - 1. The experiments with ^{87} Rb vapor . . . 114
  - 2. Polarization rotation of elliptically polarized light for large magnetic fields . . . 118
  - 3. NMOR for atoms with higher angular momentum . . 121

VII SELF-ROTATION OF THE ELLIPTICAL POLARIZATION AND ITS APPLICATION FOR THE GENERATION OF SQUEEZED VACUUM . . . 126

- A. Theory of self-rotation of the elliptical polarization 127
  - 1. Double-Λ level configuration . . . 127
  - 2. X level configuration . . . 132
- B. The influence of ac-Stark shifts on EIT resonance 135
- C. Experimental results . . . 140

CHAPTER Page

1. Large self-rotation 140
2. Self-rotation on the Rb D_1 line 141
3. Self-rotation on the Rb D_2 line 146
4. Self-rotation in cells with buffer gas 152

D. Application of self-rotation to generation of squeezed vacuum 154
1. Squeezing of vacuum fluctuations in general self-rotating medium 156
2. The perspectives of squeezed vacuum generation in Rb vapor 159

VIII APPLICATION OF THE NONLINEAR FARADAY EFFECT FOR HIGH-PRECISION MAGNETOMETRY 163

A. Optical methods of magnetic field measurements 163
B. Magnetometer based on the nonlinear Faraday effect in optically dense Rb vapor 166
1. Factors limiting the sensitivity of the magnetic field detection 166
2. Estimation of the sensitivity for Rb vapor 167
3. Experiments with buffered cells 173

C. Compensation of ac-Stark shifts 174

IX SUMMARY AND CONCLUSIONS 182

REFERENCES 184

APPENDIX A 210

VITA 217

LIST OF TABLES

TABLE Page

I Parameters of the atomic cells used in the experiments. Neon is used as a buffer gas for all cells except the one with 0.12Torr of Kr. 39

II Comparison between theoretical prediction and experimental estimation for minimum detectable magnetic fields for different cells and laser beam diameters. 174

III Transition probability coefficients for the ^{87}Rb D_1 line. 215

IV Transition probability coefficients for the ^{87}Rb D_2 line. 216

LIST OF FIGURES

FIGURE Page

1 Allowed transitions for the $F = 1 \rightarrow F' = 0$ in a) Faraday configuration (magnetic field is along the light propagation direction); b) Voigt configuration (the magnetic field is parallel to the light polarization). 12

2 Idealized three-level Λ system. 14

3 a) Open Λ scheme ; b) closed Λ scheme. 19

4 a) Three-level open Λ system, based on the Zeeman sublevels. . . . 24

5 (a) Scheme of interaction of an electromagnetic wave with atomic transition $|b\rangle,\ F = 1 \rightarrow |a\rangle,\ F' = 0$. (b) Simplification of the scheme (a) to the three-level Λ system 34

6 The schematic and the photo of the external cavity diode laser used in the experiments. 37

7 The schematic and photo of the experimental setup used in the experiments. 38

8 (a) The polarization rotation angle ϕ at magnetic field $B = 0.2$ G as a function of the laser frequency;(b) transmitted intensity under maximum CPT condition ($B = 0$) (solid line) and for large magnetic field $B = 2.8$ G (dashed line). Zero detuning corresponds to the $F = 2 \rightarrow F' = 1$ transition. Laser power $P = 2$ mW, laser beam diameter $d = 2$ mm, atomic density $N = 5.6 \cdot 10^{11}\mathrm{cm}^{-3}$. The additional peaks are due to contamination of the cell by ^{85}Rb. . 42

FIGURE Page

9 The polarization rotation angle ϕ (left column) and the transmitted laser intensity (middle column) as a function of the applied magnetic field. The interaction of the linearly polarized laser light with the magnetic sublevels on different transitions are shown in right column. The transitions, drawn in solid lines, contribute to CPT; those drawn in dashed lines do not contribute to a dark state. To avoid the modification of the resonance shapes due to propagation effects, we considered optically thin Rb vapor ($N = 8 \cdot 10^{10}\text{cm}^{-3}$). Laser power $P = 2$ mW, laser beam diameter $d = 2$ mm. 44

10 (a) The polarization rotation angle ϕ at magnetic field $B = 0.2$ G as a function of the laser frequency;(b) transmitted intensity under maximum CPT condition ($B = 0$) (solid line) and for large magnetic field $B = 2.8$ G (dashed line). Zero detuning corresponds to the center of the absorption line of the $F = 2 \rightarrow F'$ transition. Laser power $P = 2$ mW, laser beam diameter $d = 4$ mm, atomic density $N = 5.6 \cdot 10^{10}\text{cm}^{-3}$. The additional peak at 1 GHz is due to contamination of the cell by ^{85}Rb. Sub-Doppler structures observed on both transmission and rotation resonances are due to the redistribution of atomic population by retroreflected light. . . . 45

11 The experimental dependence of the maximum rotation angle of polarization on atomic density; the dashed line is to guide the eyes. 46

12 The experimental dependence of the rotation slope $d\phi/dB$ for $B = 0$ on atomic density (dots); dashed line is to guide the eyes. . . 47

13 The experimental dependence of the transmission through the cell on atomic density (dots) for $B = 0$; the dashed line is to guide the eyes. 48

14 Polarization rotation and transmission resonances in the ^{87}Rb cell without buffer gas. The laser is tuned at the $F = 2 \rightarrow F' = 1$ resonance of the D_1 line. 50

FIGURE Page

15 Experimentally observed dark resonances (solid line) and their best fit (dotted line) using Eq.(3.10). The laser intensity is (a) 2.0 mW; (b) 1.5 mW; (c) 1.0 mW; (d) 0.5 mW; (e) 0.25 mW; laser beam diameter $d = 2$ mm. The laser is tuned to the $F = 2 \rightarrow F' = 1$ resonance of the D_1 line. Atomic density is $5.6 \cdot 10^{11}\text{cm}^{-3}$. . 52

16 Experimentally observed dark resonance and its best fit using theoretical lineshape, calculated in high and low laser power limits (Eq.(3.10)and Eq.(3.8) correspondingly). The laser power is 2.0 mW, laser beam diameter $d = 2$ mm. The laser is tuned to the $F = 2 \rightarrow F' = 1$ resonance of the D_1 line. Atomic density is $5.6 \cdot 10^{11}\text{cm}^{-3}$. Inset: the relative deviation of the experimental data from the best fitting functions. 53

17 (a) Two-level atom interacting with a coherent field E and incoherent pump R; (b) Three-level atom interacting with coherent fields E_+ and E_- and incoherent pump $R = 2\gamma_r \bar{n}_{th}$; (c) is the same atom as in (b) shown in the basis of "dark" $|y\rangle = (E_-|+\rangle - E_+|-\rangle)/\sqrt{|E_+|^2 + |E_-|^2}$ and "bright" states $|x\rangle = (E_+|+\rangle + E_-|-\rangle) /\sqrt{|E_+|^2 + |E_-|^2}$, and $E = \sqrt{|E_+|^2 + |E_-|^2}$. Incoherent pump leads to transferring of the population from the "dark" state to the "bright" state and, therefore, to absorption of the fields. 57

18 Idealized three-level system used for analytical theoretical calculations. 60

19 The dependence of rotation rate $d\phi/dB$ on transmission through the system $I_{\text{out}}/I_{\text{in}}$ for the beam with diameter $d = 2$ mm: experimental (dots), prior theory with $\gamma_0 = 0.004\gamma_r$ (dashed line), and obtained by numerical simulation including radiation trapping (solid line). 64

FIGURE Page

20 The dependence of rotation rate $d\phi/dB$ on the absorption $1 - I_{out}/I_{in}$: for the laser beam diameter $d = 2$ mm and the cell without buffer gas (empty circles) and with buffer gas (filled circles); for the laser beam diameter $d = 5$ mm and the cell without buffer gas (empty triangles). Solid lines are to guide the eyes. The laser is tuned on the $F = 2 \rightarrow F' = 1$ transition of the ^{87}Rb D$_1$ line. As it follows from Eq. (4.20) the rotation rate plotted as a function of the absorption characterizes the EIT dephasing rate γ_0. The bigger $d\phi/dB$ for a fixed absorption, the less γ_0. The absorption serves as a measure of the vapor pressure via optical density (see Eq. (4.19)). 66

21 The incoherent pumping rate R/γ_0 due to radiation trapping as a function of absorption $1 - I_{out}/I_{in}$: calculated by applying Eq. (4.20) to the experimental data: for the cell without buffer gas (empty circles) and with buffer gas (filled circles), and obtained by numerical simulation for the laser beam diameter $d = 2$ mm and the cell without buffer gas (solid line). 67

22 The incoherent pumping rate R/γ_0 due to radiation trapping as a function of atomic density N: calculated by applying Eq. (4.20) to the data (dots) and obtained by numerical simulation (solid and dashed lines) for the laser beams with diameters $d = 2$ mm (dashed line) and $d = 5$ mm (solid line). 68

23 Polarization rotation rate $d\phi/dB$ and transmission I_{out}/I_{in} of linearly polarized coherent laser radiation through an atomic cell as a function of laser detuning from the ^{87}Rb $F = 2 \rightarrow F' = 1$ transition. Data are presented for cells with (from top to bottom) 0 Torr, 0.12 Torr, 1 Torr, 10 Torr, and 30 Torr of buffer gas. For each nonzero buffer gas pressure, some frequency may be found such that zero polarization rotation is observed. 77

24 (a) The EIT contrast, (b) the rotation rate $\left.\frac{d\phi}{dB}\right|_{B=0}$, and (c) the polarization rotation angle ϕ for $B = 100$mG as functions of the laser frequency in the ^{87}Rb cell with 0.12 Torr Kr buffer gas. Zero detuning corresponds to the $F = 2 \rightarrow F' = 1$ transition. The atomic density is $N = 5.2 \cdot 10^{11}$cm^{-3}. 79

FIGURE Page

25 The polarization rotation (left column) and transmitted intensity (right column) as functions of the applied magnetic field for different laser detunings in ^{87}Rb cell with 0.1 Torr Kr buffer gas. The transmitted intensity is normalized to the transmission without EIT (for large magnetic field). Zero detuning corresponds to the $F = 2 \to F' = 1$ transition. Note the scale difference for each graph. The atomic density $N = 5.2 \cdot 10^{11}\mathrm{cm}^{-3}$. 81

26 Dipole moments for the transitions the $F = 1 \to F' = 0, 1$; solid arrows show the transition which take part in the dark states formation; dotted arrows are used for the other transitions. 82

27 Polarization rotation rate $d\phi/dB$ $(B = 0)$ for the D_2 line of ^{87}Rb in an atomic cell with (a) no buffer gas (the additional rotation peak at a detuning about 1 GHz is due to residual ^{85}Rb); (b) 0.12 Torr of Kr; and (c) 1 Torr of Ne. Laser power is 2.5 mW, the temperature is adjusted for each cell so that the total transmission on the $F = 2 \to F'$ transition is about 80%. Zero laser detuning is chosen to coincide with the center of the absorption peak of the $F = 2 \to F'$ transition. 85

28 Same as for Fig. 24 in ^{87}Rb cell with 10 Torr Ne buffer gas. The atomic density $N = 2.1 \cdot 10^{12}\mathrm{cm}^{-3}$. 86

29 Same as for Fig. 25 in ^{87}Rb cell with 10 Torr Ne buffer gas. The atomic density $N = 2.1 \cdot 10^{12}\mathrm{cm}^{-3}$. 88

30 (a) The polarization rotation angle as a function of magnetic field. Inset: central narrow resonance; dotted line - lorentzian fit. (b) The transmission of the laser field through the cell. Inset: central narrow absorption resonance, corresponding to the narrow rotation. 90

31 (a) The maximum polarization rotation angle and (b) the width of the rotation resonance for both narrow and wide structures. On (a) the dashed line represents the square-root fit, the dotted line is to guide the eyes. On (b) the best linear fits are shown for both curves. 91

FIGURE Page

32 Energy level schemes for (a) Λ-system; (b) N-system; (c) M-system. 98

33 a) Energy level scheme for ^{87}Rb atoms. This scheme may be decomposed into a superposition of b) Λ-system and c) M-system. Transition probabilities are shown for each individual transition. . . 99

34 Generalized M interaction scheme. Here $\Omega_{i-} = E_-\wp_{a_ib_i}/\hbar$, $\Omega_{i+} = E_+\wp_{a_ib_{i-1}}/\hbar$. 111

35 Energy level scheme for ^{85}Rb atoms. This scheme may be decomposed into a superposition of a) M-system and b) triple-Λ system. Transition probabilities are shown for each individual transition. . . 113

36 The normalized slope of the nonlinear magneto-optic rotation as a function of the ellipticity of the incident light. Experimental data are shown for opposite values of ellipticity and two different values of laser power: P=2 mW (hollow up triangles for positive ellipticity and hollow down triangles for negative ellipticity) and P=1 mW (solid up triangles for positive ellipticity and solid down triangles for negative ellipticity). The results of the numerical simulations for the case of 2 mW laser power are shown by a solid line. Absolute values of the nonlinear Faraday rotation for the linear polarization were $d\phi/dB(B=0) = 4.5$ rad/G and 6 rad/G for P=2 mW and P=1 mW respectively. 115

37 The normalized slope of nonlinear magneto-optic rotation as a function of the ellipticity of the incident light for the Λ scheme (transition $F = 1 \rightarrow F' = 1$) and $M + \Lambda$ scheme (transition $F = 2 \rightarrow F' = 1$). Dotted lines are to guide the eyes. Input laser power is P=2 mW, the atomic densities are chosen to provide 85% absorption on each transition. The absolute value of the nonlinear Faraday rotation of linear polarization were $d\phi/dB(B = 0) =$ 1.8 rad/G and 4.5 rad/G for the $F = 1, 2 \rightarrow F' = 1$ transitions respectively. 116

FIGURE Page

38 The normalized slope of nonlinear magneto-optic rotation as a function of the ellipticity of the incident light for two different beam diameters: $d = 2$ mm (squares) and $d = 10$ mm (diamonds). In both cases the laser power is kept at 2 mW. Absolute values of the nonlinear Faraday rotation for the linear polarization were $d\phi/dB(B = 0) = 4.5$ rad/G and 30 rad/G respectively. 117

39 (a) The normalized slope of nonlinear magneto-optic rotation as a function of the ellipticity of the incident light for various atomic densities. Laser power is 2 mW, beam diameter $d = 2$ mm. Inset: Absolute value of the nonlinear Faraday rotation of linear polarization as a function of atomic density. (b) The output ellipticity ϵ as a function of the ellipticity of the incident light for various atomic densities. Dotted line is for unchanged ellipticity. Inset: Transmission $I_{\text{out}}/I_{\text{in}}$ of linear polarization as a function of atomic density. 119

40 The polarization rotation angle as a function of laser detuning for ellipticity $\epsilon = 25^o$ and magnetic field $B = 0.35$ G. The components of the rotation due to various processes are also shown. Zero detuning corresponds to the $F = 2 \to F' = 1$ transition. The small peak on the right is due to contamination of the cell with ^{85}Rb isotope. 120

41 (a) The polarization rotation angle as a function of magnetic field for opposite values of ellipticity. (b) The ellipticity of the transmitted light as a function of magnetic field. Input ellipticity is shown as a dashed line. 122

42 The normalized slope of nonlinear magneto-optic rotation as a function of the ellipticity of the incident light for the $F = 3 \to F' = 2$ transition of ^{85}Rb (diamonds), and for the $F = 2 \to F' = 1$ transition of ^{87}Rb (circles). Input laser power is P=2 mW, the atomic densities are chosen to provide 85% absorption on each transition. Absolute values of the nonlinear Faraday rotation for linear polarization were $d\phi/dB(B = 0) = 2.9$ rad/G and 4.5 rad/G respectively. Inset: the theoretical dependences for naturally broadened Rb isotopes, from Eqs. (6.51) and (6.58). . . . 123

FIGURE Page

43 The polarization rotation angle in ^{85}Rb as a function of laser detuning for ellipticity $\epsilon = 25^o$ and magnetic field $B = 0.35G$. The components of the rotation due to various processes are also shown. Zero detuning corresponds to the cross-resonance $F = 3 \to F' = 2.3$ transition. The distortions of the resonances are due to reflected light beam. 124

44 Atoms in a double-Λ configuration interacting with two circularly polarized fields E_+ and E_-. Field $E_\pm$ is resonant with transitions $a_1 \to b_\mp$ and off-resonant with transitions $a_2 \to b_\mp$. The splitting between a_1 and a_2 is Δ. We assume that the angular matrix elements, and consequently the Rabi frequencies, of the $a_2 \to b_+$ and $a_2 \to b_-$ transitions have opposite sign, as for the ^{87}Rb D_1 line. . 128

45 Atoms in an X configuration interacting with two circularly polarized fields E_+ and E_-. 133

46 Position of the EIT resonance (in terms of longitudinal magnetic field B) as a function of the degree of the incoming light ellipticity. Experimental data are shown as dots and theoretical results are shown as lines. Curves (1) and (4) correspond to the transitions $F = 2 \to F' = 1'$ and $F = 2 \to F' = 2'$, with intensity $1.1\,\mathrm{mW/cm^2}$; curves (2) and (3) correspond to the same transitions and intensity $0.54\,\mathrm{mW/cm^2}$. The measured values of the intensities are 1.2 and $0.6\,\mathrm{mW/cm^2}$. 137

47 Position of the EIT resonance (in terms of longitudinal magnetic field B) for the transition $F = 2 \to F' = 1'$ for various densities N of Rb vapor. Laser intensity is $1.1\,\mathrm{mW/cm^2}$. 138

48 Position of the EIT resonance (in terms of longitudinal magnetic field B) for the transition $F = 2 \to F' = 1'$ for the Rb cell with 30 Torr of Ne buffer gas and the one without buffer gas. Laser intensity is $1.1\,\mathrm{mW/cm^2}$. 139

49 Large self-rotation of elliptical polarization of the light propagating through vapor of ^{87}Rb vs laser detuning. Zero detuning corresponds to the $F = 2 \to F' = 1$ transition. Two small peaks on the right are due to the contamination of the cell with small amount of ^{85}Rb. 140

FIGURE Page

50 The self-rotation angle for the $F = 2 \rightarrow F'$ transition of the ^{87}Rb D_1 line of as a function of laser frequency for different atomic densities. Zero detuning corresponds to the $F = 2 \rightarrow F' = 1$ transition. Laser power is $P = 5$ mW. Ellipticity of the beam is $\epsilon = 0.035$ rad. 142

51 Self-rotation parameter gL and transmission I_{out}/I_{in} measured as functions of atomic density for the ^{87}Rb D_1 line. Laser power is 5 mW. Ellipticity of the beam is $\epsilon = 0.035$ rad. 143

52 Self-rotation parameter gL and absorption coefficient $\alpha L = 1 - I_{out}/I_{in}$ measured as functions of laser intensity for the ^{87}Rb D_1 line. Atomic density is $N = 8.2{\times}10^{11}$cm^{-3}. Ellipticity of the beam is $\epsilon = 0.035$ rad. 144

53 Self-rotation parameter gL and transmission I_{out}/I_{in} for the ^{85}Rb D_1 line as functions of atomic density. The laser power is 5 mW. . . 145

54 The angle of self-rotation measured on the $F = 1 \rightarrow F'$ transition of the ^{87}Rb D_2 line as a function of laser detuning. Zero detuning is chosen to coincide with the center of absorption line. Laser power is $P = 5$ mW, ellipticity of the beam is $\epsilon = 0.035$ rad. 147

55 The nonlinearity parameter gL measured as a function of ^{87}Rb density. Laser power is $P = 5.0$ mW. 149

56 The self-rotation parameter gL measured as a function of light transmission through the cell. Solid circles are for laser power $P = 5.0$ mW and open circles correspond to power $P = 1.3$ mW. Each point of the graph represents a different value of atomic density. 150

57 The angle of self-rotation measured for the $F = 2 \rightarrow F'$ transition of the ^{85}Rb D_2 line as a function of laser detuning. Data are shown for different values of the laser power. Zero detuning is chosen to coincide with the center of absorption line. The atomic density is $N = 2 \times 10^{11}$ cm^{-3}. Ellipticity of the beam is $\epsilon = 0.035$ rad. 151

FIGURE Page

58 The angle of self-rotation measured for the $F = 2 \rightarrow F'$ transition of the ^{85}Rb D_2 line a function of laser detuning. Data are shown for different atomic densities. Zero detuning is chosen to coincide with the center of absorption line. The laser power is $P = 5$ mW. Ellipticity of the beam is $\epsilon = 0.035$ rad. 152

59 The self-rotation parameter measured as a function of light transmission through the cell. Solid circles correspond to the cell without buffer gas and open circles correspond to the cell with 1 Torr of Ne. Laser power is $P = 5.0$ mW. Each point of the graph represents a different value of atomic density. 153

60 The squeezing of vacuum fluctuations, as defined in Eq.(7.62), as a function of laser intensity. For each value of laser intensity, the squeezing is calculated for the optimum value of laser detuning and atomic density. 161

61 Estimated sensitivity of magnetic field measurements $\Delta B_{\min}$ as a function of laser beam diameter. Laser intensity $I_{\text{in}} \approx 2$ mW/cm^2, atomic density $N \approx 10^{12}$ cm^{-3}. 168

62 (a) Rotation rate $d\phi/dB$ as a function of atomic density in the cell without buffer gas; (b) Transmission through the cell; (c) estimated minimum detectable magnetic field $\Delta B_{\min}$. Solid dots are for laser beam diameter $d = 2$ mm, open dots are for $d = 12$ mm. 170

63 (a) Rotation rate $d\phi/dB$ as a function of laser frequency in the cell without buffer gas (dashed line) and with 0.12 torr Kr (solid line); (b) Transmission through the cell; (c) estimated minimum detectable magnetic field $\Delta B_{\min}$. Laser power $P_{\text{in}} = 2.5$ mW, beam diameter $d = 12$ mm. Atomic density is $N = 2 \times 10^{12}$ cm^{-3} for vacuum cell and $N = 10^{12}$ for the cell with buffer gas. The frequency of the transition $F = 2 \rightarrow F' = 1$ is chosen as zero detuning. The vertical dotted lines show the positions of the transitions $F = 2 \rightarrow F' = 1, 2$. 172

FIGURE Page

64 (a) Estimated sensitivity of magnetic field measurements ΔB_{min} as a function of atomic density for different cells: without buffer gas (open circles), with 0.12 torr Kr (squares) and with 0.3 torr Ne (diamonds). Laser power $P_{\text{in}} \approx 2.5$ mW, laser beam diameter $d = 2$ mm. The dimensions of all cells are the same (length ≈ 5 cm, diameter ≈ 2.5 cm). 175

65 (a) Measured rotation angle ϕ_{AC} for elliptical polarizations of 2°, 4° and 6° degrees. (b) Measured Faraday rotation slope, $\frac{d\phi}{dB}$ with linearly polarized light. Both (a) and (b) are for the ^{87}Rb D_1 line, with no buffer gas and atomic density $N = 1.5 \times 10^{12}\text{cm}^{-3}$. (c) Calculated rotation angle ϕ_{AC} for D_1 line. (d) Calculated Faraday rotation slope, $\frac{d\phi}{dB}$. 177

66 Same as Fig. 65a and b for the D_2 line and atomic density $N = 8 \times 10^{10}\text{cm}^{-3}$. Zero detuning corresponds to the resonance with transition $5s_{1/2}F = 2 \rightarrow 5p_{1/2}F' = 1$ for the D_1 line and to the center of the absorption on the transition $5s_{1/2}F = 2 \rightarrow 5p_{3/2}$ for the D_2 line. 178

67 (a) Calculated rotation angle ϕ_{AC} and (b) calculated Faraday rotation slope $d\phi/dB$ for motionless atoms. 179

68 (a) and (c) Measured rotation angle ϕ_{AC} for elliptical polarizations of 2°, 4° and 6° degrees. (b) and (d) Measured Faraday rotation slope, $\frac{d\phi}{dB}$ with linearly polarized light. Both (a) and (b) are for the ^{87}Rb D_1 line, (c) and (d) are for the ^{87}Rb D_2 line, in the cell with 0.12 torr of Kr buffer gas and atomic density $N = 1.5 \times 10^{12}\text{cm}^{-3}$. . . 181

69 Glass atomic cell with drops of liquid Rb. 211

70 Level scheme for the D_1 line of ^{87}Rb and ^{85}Rb. The splitting between the levels is given in MHz. 212

71 Same as Fig. 70 for the Rb D_2 line. 213

CHAPTER I

INTRODUCTION

A. Goals and motivation

The interaction of light with matter remains one of the major areas of research from the dawn of modern physics to the present. Recent advances in optical technology made it possible to control the properties of an individual atom via laser light, and therefore to create new media with unique optical properties. A glass cell with dilute atomic vapor (with pressure much below that of the atmosphere) may surpass the best solid-state devices, traditionally used in optics. Under the action of several light fields, resonant with various atomic transitions, most atoms can be prepared in a coherent superposition of energy states, so the properties of the atomic vapor are altered dramatically [1]. For examples, it becomes possible to reduce the speed of a light pulse, propagating in such a medium, down to a few meters per second, or even bring the light to a complete stop and store it for some time with no absorption of the pulse energy by the atoms. Further, the efficiency of many nonlinear processes, which results in the generation of additional light with a different frequency, may be increased dramatically up to the single-photon level, which is impossible in standard nonlinear crystals. This high nonlinearity also allows generating ultra-short light pulses, in which the duration of the pulse is smaller than the period of one oscillation of the electromagnetic field. Coherent phenomena also play an important role in astrophysics and solar physics, creation of a new type of matter (Bose-Einstein condensate), precision metrology (such as a frequency standard with the stability of one second per hundred billion years), quantum computing and information processing,

---

This dissertation follows the style and fomat of Physical Review A.

and many others.

The subject of my research is Nonlinear Magneto-Optical polarization Rotation (NMOR) [2,3]. For this phenomenon the coherent properties of the atomic vapor are determined by the polarization of a single resonant laser field. The modification of the associated atomic coherence in an external magnetic field results in the rotation of the light polarization direction, similar to the well-known Faraday effect in solids. However, because of the coherent nature of the interaction, the polarization rotation per atom is up to 10^{10} times stronger for the same value of the magnetic field than for the best magneto-optical crystals. The analysis of NMOR data allows deeper and clearer understanding of basic properties of coherent media, hardly achievable by other methods.

At the same time this effect may be applied for high-precision measurements of the magnetic field. It has been predicted, that a magnetometer based on highly coherent media should surpass in sensitivity all presently available devices [4,5]. The magnetometer based on the nonlinear Faraday effect is one of the promising realizations of such an apparatus.

The major objective of this research is to conduct a comprehensive analysis of the nonlinear magneto-optic effects in optically dense Rubidium vapor, and to evaluate the influence of various physical effects, such as collisions with buffer gas, trapping of spontaneous radiation, atomic motion, laser intensity spatial distribution, etc., on the light absorption and the polarization rotation. This information allows better understanding of the fundamental properties of the coherent phenomena in general and Zeeman coherence in particular. At the same time these factors have to be taken into account in order to find the optimum conditions for the operation of a nonlinear Faraday-based magnetometer.

B. Review of coherence effects on the Zeeman sublevels

The idea of interference of different atomic states was first proposed by W. Hanle [6] and later developed by many other physicists of that time [7–11] to explain the experimental results of Wood and Ellett [12]. They observed a complete depolarization of the spontaneous emission of mercury vapor excited by linearly polarized light in the presence of a magnetic field, while the linear polarization was preserved for zero magnetic field. Hanle proposed that atoms were excited into a coherent superposition of excited state magnetic sublevels; if the degeneracy of these levels is lifted (by a magnetic field), the time evolution of relative phase leads to the different polarization of spontaneous photons. The Hanle effect and the related quantum beat effect [13–15] became powerful tools in atomic and molecular spectroscopy as well as in solar physics [16]. The interference of the non-degenerate states in the presence of non-zero external field (level crossing) was also demonstrated and applied for precision spectroscopy [11, 17, 18].

A similar coherence among ground-state sublevels can be created via optical pumping [19–21]. One of the most interesting phenomena, based on ground-state coherence, is coherent population trapping (CPT) [1, 22, 23]: under the combined action of several laser fields atoms are optically pumped into a coherent superposition of hyperfine or Zeeman sublevels which is decoupled from the light. Such a state is often called a "dark state", since it is associated with the suppression of the resonant fluorescence. The cancellation of linear absorption under CPT conditions is a manifestation of Electromagnetically Induced Transparency (EIT) [1, 24, 25].

Since the coherence between the magnetic sublevels is easily created and controlled by a properly polarized electro-magnetic field and an external magnetic field, coherent population trapping was initially demonstrated for Zeeman coherence excited by a multimode dye laser [26–28], and later extensively studied in a variety of experimental arrangements: in atomic beams [29, 30], thermal vapor cells [31–35], and cold clouds [36]. Similarly, the interference between Zeeman sublevels has to be taken into account in the experiments where hyperfine coherence is created by two laser fields [36–41]. The amplification without inversion due to Zeeman coherence [42, 43] and effective four-wave mixing in a degenerate two-level scheme [44] have been also demonstrated.

Steep dispersion associated with Zeeman coherence results in ultra-slow group velocity for the polarization pulse propagating in atomic vapor [45,46]. It also lead to various magneto-optical polarization effects, which are reviewed in the next section.

Coherent interaction allows efficient control over the properties of individual atoms by means of light field(s). In atomic optics coherent population transfer between magnetic sublevels [47–49] is widely used to create atomic mirrors and beam splitters [50–53], as well as an effective atomic interferometer for cold atoms [54].

furthermore, the properties of an electromagnetic field can be controlled by a coherently prepared medium. For example, an arbitrary state of the light in a cavity may be generated via strong coupling of atoms in a coherent superposition of the Zeeman states [55]. The possibility to transfer complete information about a light pulse to an atomic spin state and back [56, 57] allows storage, manipulation and releasing of laser pulses in well-controlled manner [58, 59], as well as transportation of the state of light between different spatial and temporal points, and multiplexing and time reversal of the restored pulse [60].

Although the majority of coherent phenomena are associated with coherent population trapping and cancellation of light absorption, under certain conditions the resonant coherent interaction may increase the absorption of the resonant light, giving rise to Electromagnetically Induced Absorption [61–64]. This effect occurs in the case of two resonant laser fields interacting with a degenerate two-level atomic system under the condition that the angular momentum of the excited state is higher than that of the lower state ($F' > F$). A quite similar effect has been observed in case of single laser excitation in the presence on magnetic field, and is called the enhanced absorption Hanle effect [34, 35, 65, 66]. The initial explanation of both effects was based on the redistribution of the atomic population among ground-state Zeeman sublevels due to the difference in the transition probabilities [61, 65]. These calculations, however, are valid only for closed (cycling) transitions, although experimentally EIA has been observed on open transitions as well [64, 66]. It is also possible that the enhancement of absorption occurs due to the spontaneous coherence transfer from excited to ground states [67]. This assumption provides good agreement with experimental results regardless of the "openness" of the transition [68]. Steep anomalous dispersion associated with EIA and the corresponding negative pulse delays have been demonstrated in [69, 70]. The effect of EIA has been proposed for highly selective four-wave mixing [71], noninvasive mapping of cold atomic samples [72], etc.

C. Review of nonlinear magneto-optic effects

The rotation of the polarization direction of light resonant with an atomic transition (linear resonant Faraday effect, Macaluso-Corbino effect) was discovered in 1898 by Macaluso and Corbino [73,74], and studied extensively [75–79] afterwards. This rotation, however, may be enhanced due to the interference of the ground-state magnetic sublevels and evolution of the Zeeman coherence in an external magnetic field, giving rise to a variety of nonlinear magneto-optical effects. Most of the experimental and theoretical work considers two specific cases of the magnetic field orientation with respect to the light propagation direction: longitudinal (Faraday configuration) and transverse (Voigt configuration) with analogy to the well-known Faraday [80] and Voigt (Cotton-Mutton) [81, 82] effects in magnetic crystals.

Many early experiments utilized the resonant forward scattering of the linearly polarized light to study magneto-optical interference effects. In these experiments the narrow resonances in the scattered light of the orthogonal polarization provide information about the populations and coherences among excited state [83, 84] and ground state [85–93] degenerate sublevels. Forward scattering spectroscopy is successfully used for measurement of the oscillator strength of various atomic transitions [78, 94–96] and for trace element detection [97–100].

Experiments in selective reflection spectroscopy [101, 102] in Cs vapor demonstrated that the Zeeman coherence induced by linearly polarized light leads to the appearance of resonances of subnatural width in polarization rotation of reflected light [103]. Anomalous deflection of a laser beam traversing the Cs cell due to Zeeman coherence has also been demonstrated [104].

Interest in nonlinear magneto-optical effects was revived in late 1980th with the almost simultaneous observation of strong nonlinear polarization rotation in Sm [105–107] and Cs [108–110]. Existing theoretical approaches provided an accurate description of the nonlinear Faraday [107, 111–115] and Voight [116–119] effects only for the simplest level configurations, and failed to adequately describe the atoms with high angular momentum [120]. For example, the importance of the hexadecapole moment ($\Delta m = 4$ coherence) in interpretation of resonant forward scattering features raised a heated discussion [85, 86, 92, 93].

Weis *et al.* developed a theoretical description of the nonlinear Faraday rotation for atoms with arbitrary angular momentum in the approximation of weak magnetic field and laser intensity [121, 122]. This theory includes a three-stage interaction process: initial excitation of ground-state coherence by a laser field, its evolution in the external magnetic field, and finally the scattering of the probe field on the modified Zeeman coherence, which results in the polarization rotation. This theory was later extended by Budker *et al.*, who took into account the alignment-to-orientation conversion process, which becomes dominant for a more powerful laser field [123]. An alternative approach to the description of the nonlinear Faraday rotation of strong laser field is based on the strong dependence of the refractive indices for two circularly polarized components of the electromagnetic field on the magnetic field in a coherent medium [124, 125]. Both theoretical approaches provide good agreement with experimental results in thermal Rb vapor [125–128]. The experimental and theoretical results for the Faraday effect in Ca, nonlinear with respect to both very high laser intensity and magnetic field, have been presented by Agarwal *et al.* [129].

Recent advance in laser trapping and cooling technology made possible the study of the optical properties of cold atoms. The absence of interatomic collisions and Doppler broadening of optical resonances lead to dramatic enhancement of linear Faraday effect in laser cooled Li [130] and Rb [131] atoms. Comparable enhancement of nonlinear magneto-optical effects is anticipated.

The observation of narrow Ramsey fringes in the nonlinear Faraday rotation spectrum in Rb atomic beam has been reported in experiments with separated optical fields [132]. Similar resonances were observed by Kanorsky *et al.* in Cs vapor cells with anti-relaxation wall coating, and explained in terms of multiple wall-collision-induced Ramsey resonances [133]. Nonlinear Faraday rotation with ultra-narrow width (~ 1 Hz) in a paraffin-coated Rb cell are reported by Budker *et al.* [134,135]. The narrow resonances, analogous to Ramsey fringes are also observed in atomic cells filled with inert buffer gas [136,137]. Modification of the magneto-optical polarization rotation due to collisions with buffer gas at high pressure is investigated in [138–141].

Rotation of the polarization direction of linearly polarized light is also an effective tool to study the population redistribution and ground-state coherence induced by a second laser field. The rotation of linear polarization of a weak probe field caused by the combined action of a longitudinal magnetic field and strong circularly polarized laser beam is analyzed in [142–145]; Patnaik and Agarwal [146, 147] have demonstrated that the presence of strong counter-propagating field may coherently control the polarization rotation of the probe field. It is also demonstrated both in forward scattering [148] and polarization rotation experiments [149] that spontaneous coherence transfer also results in the modification of the Faraday rotation by the ground-state coherence created by a second laser on different set of magnetic sublevels. Transfer of coherence between two transitions which are not connected by spontaneous emission is studied experimentally in [150].

CHAPTER II

NONLINEAR MAGNETO-OPTIC ROTATION IN THREE-LEVEL Λ SYSTEM

In this chapter we theoretically consider the interaction of linearly polarized light with atoms for the case of a simple Λ level scheme. We use semiclassical theory, assuming classical light fields and quantized atomic states.

The chapter is organized as follows. First, we derive the time evolution equations for the density matrix elements in a general Λ interaction scheme. Then, using these equations for the case of the magnetic sublevels we analyze the open and closed Λ system and prove their equivalence. Then we derive analytical expressions for the absorption and the polarization rotation angle of the electromagnetic field for homogeneously and non-homogeneously broadened optical transitions. Finally, we demonstrate, that the $F = 1 \rightarrow F = 0$ transition can be treated as a three-level Λ scheme with simple renormalization of the decay rates and atomic density.

A. Optical Bloch equations for general Λ scheme

1. Maxwell's equations for the electromagnetic field propagating in atomic vapor

The propagation of the electromagnetic field through a medium is described by Maxwell's equations [151, 152]:

$$\nabla \times \vec{E} = -\frac{1}{c}\frac{\partial \vec{B}}{\partial t}; \tag{2.1}$$

$$\nabla \times \vec{H} = \frac{4\pi}{c}\vec{j} + \frac{1}{c}\frac{\partial \vec{D}}{\partial t}; \tag{2.2}$$

$$\nabla \vec{D} = \rho \tag{2.3}$$

$$\nabla \vec{B} = 0. \tag{2.4}$$

Here $\vec{E}$ is the electric field, and $\vec{H}$ is the magnetic field, $\vec{D}$ is the displacement, $\vec{D} = \vec{E}+4\pi\vec{P}$, where $\vec{P}$ is the polarization of the medium, $\vec{B}$ is the magnetic induction, and $\vec{B} = \vec{H} + 4\pi\vec{M}$ where $\vec{M}$ is the magnetization of the medium; ρ and $\vec{j}$ are the electric charge and current densities in the medium.

We assume that no charges exist in an atomic vapor, $\rho = 0$ and $\vec{j} = 0$. We also consider only electric-dipole transitions, in which the propagating electromagnetic field induces the electric dipole moments of the atoms. In this case $\vec{B} \equiv \vec{H}$, and the equation for the electric component of the light field is:

$$-\nabla^2\vec{E} + \frac{1}{c^2}\frac{\partial^2\vec{E}}{\partial t^2} = -\frac{4\pi}{c^2}\frac{\partial^2\vec{P}}{\partial t^2} \tag{2.5}$$

Here $\vec{P}$ is the induced macroscopic polarization of the atomic vapor, which can be rewritten as a sum of induced dipole moments of individual atoms: $\vec{P} = N\langle\vec{d}\rangle$, where N is the number of atoms in the interaction region, and $\langle\vec{d}\rangle = -e\langle\vec{r}\rangle$ is the dipole moment of an individual atom averaged over the ensemble.

The average dipole moment can be easily found by using the density operator of the atomic system [1,153,154]:

$$\hat{\rho} = |\psi\rangle\langle\psi| = \sum_{\{\alpha\},\{\beta\}} \rho_{\alpha,\beta}|\alpha\rangle\langle\beta|, \tag{2.6}$$

where $\{|\alpha\rangle\}$ is a complete set of atomic states. In this case the average dipole moment can be written in terms of the dipole moments of the individual transitions and the density matrix elements of the atomic system:

$$\langle\vec{d}\rangle = Tr(\vec{d}\hat{\rho}) = -\sum_{\{\alpha\},\{\beta\}} e\langle\beta|\vec{r}|\alpha\rangle\rho_{\alpha,\beta} \tag{2.7}$$

The transition probability is determined by the dipole moment $e\langle\beta|\vec{r}|\alpha\rangle \neq 0$. The selection rules then follow from the basic properties of the wave-functions of the initial and final states of the electron. For uncoupled electrons in alkali atoms the state of the electron can be characterized by three quantum numbers [155–157]:

$$|\alpha\rangle = |n\ \ell\ m\rangle; \tag{2.8}$$
$$\psi_{n\ell m}(\vec{r}) = R_{n\ell}(r)Y_{\ell m}(\theta, \varphi).$$

Here n is the principle quantum number, ℓ and m are the angular momentum and the z-component of the angular momentum. [1] The selection rules for the electric-dipole transitions in atoms $\Delta n = 1$, $\Delta\ell = \pm 1$ and $\Delta m = 0, \pm 1$ follow from the orthogonality of the radial distribution functions $\{R_{n\ell}\}$ and spherical functions $\{Y_{\ell m}\}$. However, there are further restrictions due to the parity conservation, which results in additional selection rules for the electromagnetic field with different polarizations (Fig. 1). If the light propagates along the z axis, only circularly polarized light quanta can be absorbed and emitted, with the following selection rules: $\Delta m = 1$ for σ_+ polarization and $\Delta m = -1$ for σ_- polarization. If the quantization axis is perpendicular to the direction of the light propagation selection rules also depend on the angle between the z axis and direction of the electric field component of the electromagnetic wave: if they are parallel only $\Delta m = 0$ transitions are allowed (π-polarization). For any other geometry of the problem all types of transitions are allowed. The rotary transformation suggested by H. Lee and coworkers [158] allows a simple treatment of the general case.

In the following calculations we always consider a plane wave, circularly polarized in the $x - y$ plane propagating along the z direction. Then we can rewrite Eq.(2.5)

---

[1] Because of the spin-orbit interaction, the electron angular momentum in alkali atoms is not an independent operator. If the fine structure of the atomic energy levels is considered the total angular momentum j and its z-component m_j should be used instead. For the hyperfine structure due to the coupling with the nuclei spin the total atomic angular momentum F and its projection m_F define the spin state of an electron.

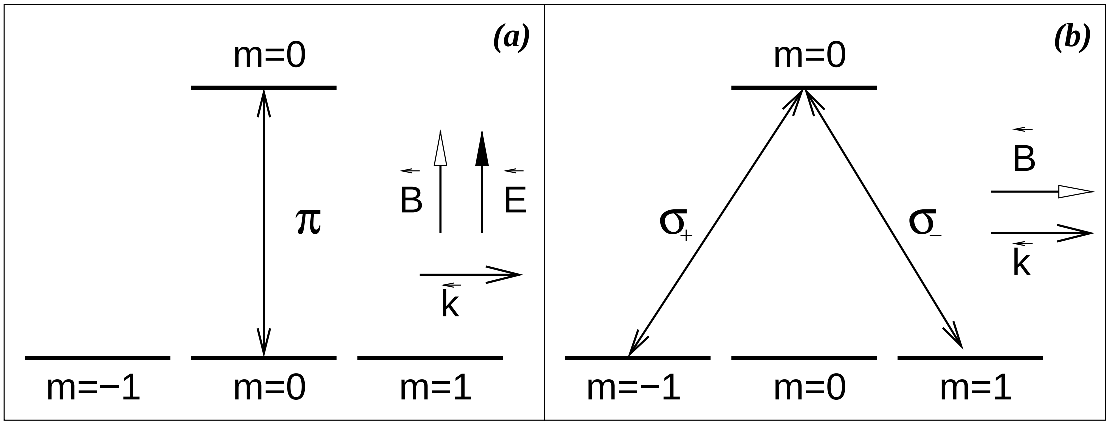

Fig. 1. Allowed transitions for the $F = 1 \to F' = 0$ in a) Faraday configuration (magnetic field is along the light propagation direction); b) Voigt configuration (the magnetic field is parallel to the light polarization).

in scalar form, using $\vec{E}(\vec{r}) = E_\pm(z)(\vec{e_x} \pm i\vec{e_y})/\sqrt{2}$:

$$-\frac{\partial^2 E_\pm}{\partial z^2} + \frac{1}{c^2}\frac{\partial^2 E_\pm}{\partial t^2} = \frac{4\pi}{c^2} N \sum_{\{\alpha,\beta\}} \wp_{\alpha,\beta} \frac{\partial^2}{\partial t^2} \rho^{(\pm)}_{\alpha,\beta}, \tag{2.9}$$

where $\wp^{(\pm)}_{\alpha,\beta} = -e\langle\beta|\frac{1}{2}(x \pm iy)|\alpha\rangle$ is the matrix element of the electric dipole moment of the transition. It is clear from the form of Eq.(2.9) that the amplitude of the electromagnetic field, propagating through the atomic vapor, is governed by the density matrix elements of the atoms. At the same time the properties of the density matrix elements are determined by the electromagnetic field in nonlinear processes, such as coherent population trapping.

It is convenient to extract the fast-oscillating time dependence of the electromagnetic field amplitude and write it down in the following form:

$$E(z,t) = \mathcal{E}(z,t)e^{ikz-i\nu t} + \mathcal{E}^*(z,t)e^{-ikz+i\nu t} \tag{2.10}$$

For all processes considered below, the characteristic changes of the amplitude and phase of the electromagnetic wave take place at the scale much larger than one cycle of the oscillations. In this case we can apply the slowly-varying amplitude approximation:

$$\frac{\partial\mathcal{E}}{\partial z} \ll k\mathcal{E}; \;\; \frac{\partial\mathcal{E}}{\partial t} \ll \omega\mathcal{E} \tag{2.11}$$

Then we can rewrite Eq.(2.9) for the amplitude $\mathcal{E}$, keeping only the first time and spatial derivatives of the slowly-varying amplitude:

$$\frac{\partial\mathcal{E}}{\partial z} + \frac{1}{c}\frac{\partial\mathcal{E}}{\partial t} = 2\pi i k N \sum_{\{\alpha,\beta\}} \wp_{\alpha,\beta}\tilde{\rho}_{\alpha,\beta}, \tag{2.12}$$

where $\rho_{\alpha,\beta} = \tilde{\rho}_{\alpha,\beta}e^{ikz-i\nu t}$.

2. Interaction of light with a three-level Λ system

In this section we derive the time-evolution equations for the density matrix elements for a general Λ scheme. The Hamiltonian describing the interaction of the electromagnetic field with the atom in the dipole approximation is [1,151,159,160]:

$$\hat{H}_I = -e\vec{r}\cdot\vec{E} = -er_E\cdot E, \tag{2.13}$$

where $r_E = \vec{r}\cdot\vec{E}/|E|$ is the projection of the electron displacement $\vec{r}$ on the direction of the electric field.

Let us consider three-level atoms interacting with two co-propagating electromagnetic waves, as shown in Fig. 2. We assume that levels $|b_{1,2}\rangle$ are coupled with $|a\rangle$ via the electromagnetic fields $E_{1,2}$, forming a Λ system. We assume that only one transition is allowed for each field, and the electric dipole transition between levels

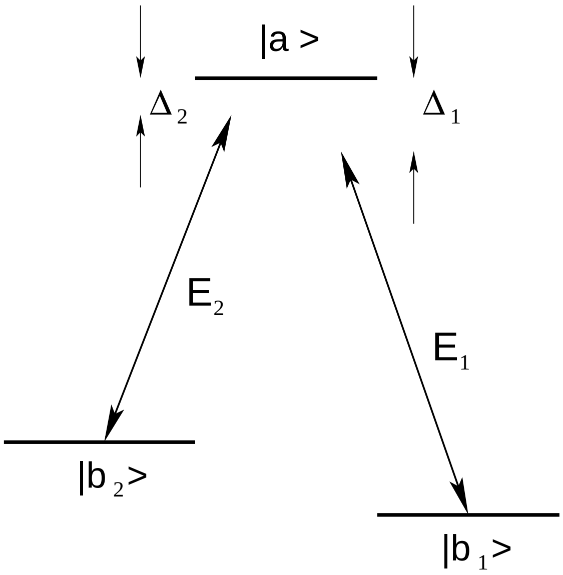

Fig. 2. Idealized three-level Λ system.

$|b_1\rangle$ and $|b_2\rangle$ is forbidden. The Hamiltonian for such a system can be written as:

$$\hat{H} = \hbar\omega_{b_1}|b_1\rangle\langle b_1| + \hbar\omega_{b_2}|b_2\rangle\langle b_2| + \hbar\omega_a|a\rangle\langle a| \tag{2.14}$$
$$+(\wp_{ab_1}E_1|a\rangle\langle b_1| + \wp_{b_1a}E_1|b_1\rangle\langle a|) + (\wp_{ab_2}E_2|a\rangle\langle b_2| + \wp_{b_2a}E_2|b_2\rangle\langle a|),$$

where $\wp_{ab_i} = \wp_{b_ia}$ is the dipole moment of the corresponding transition.

It is easy to show that there exists an atomic state $|\Psi\rangle$, such that $\hat{H}_I|\Psi\rangle = 0$:

$$|\Psi\rangle = \frac{\wp_{ab_1}\mathcal{E}_1|b_2\rangle - \wp_{ab_2}\mathcal{E}_2|b_1\rangle}{\sqrt{|\wp_{ab_1}\mathcal{E}_1|^2 + |\wp_{ab_2}\mathcal{E}_2|^2}}, \tag{2.15}$$

if the difference between the two laser frequencies matches the splitting between ground-state levels ($\omega_{b_1} - \omega_{b_2} = \nu_1 - \nu_2$). Note, that a match between the frequency of the lasers and the one-photon atomic transition is not required. A remarkable property of atoms in such state is that they do not interact with either electromagnetic field, and all atomic population is trapped in the dark state. This is the simplest realization of coherent population trapping (CPT).

The time evolution of the density operator for the atomic system is described by the Liouville - Von Neumann equation [1,153,154]:

$$\frac{d}{dt}\hat{\rho} = -\frac{i}{\hbar}\left[H, \hat{\rho}\right]. \tag{2.16}$$

Using the interaction Hamiltonian for our system (Eq.(2.14)) we derive the following system of equations, which describe the evolution of the density matrix elements:

$$\dot{\rho}_{b_{1,2}b_{1,2}} = \frac{i}{\hbar}\{\wp_{ab_{1,2}}E_{1,2}\rho_{ab_{1,2}} - \wp_{ab_{1,2}}E_{1,2}\rho_{b_{1,2}a}\}; \tag{2.17}$$

$$\begin{aligned} \dot{\rho}_{ab_{1,2}} &= -i(\omega_a - \omega_{b_{1,2}})\rho_{ab_{1,2}} + \frac{i}{\hbar}\ \wp_{ab_{1,2}}E_{1,2}(\rho_{b_{1,2}b_{1,2}} - \rho_{aa}) \\ &+\frac{i}{\hbar}\wp_{ab_{2,1}}E_{2,1}\rho_{b_{2,1}b_{1,2}}; \end{aligned} \tag{2.18}$$

$$\dot{\rho}_{b_1b_2} = -i(\omega_{b_1} - \omega_{b_2})\rho_{b_1b_2} + \frac{i}{\hbar}\wp_{ab_1}E_1\rho_{ab_2} - \frac{i}{\hbar}\wp_{ab_2}E_2\rho_{b_1a}. \tag{2.19}$$

Let us now separate the fast-oscillating time dependence in the atomic polarizations by making the substitutions:

$$\rho_{ab_{1,2}} = \tilde{\rho}_{ab_{1,2}}e^{-i\nu_i t}; \tag{2.20}$$

$$\rho_{b_1b_2} = \tilde{\rho}_{b_1b_2}e^{-i(\nu_1-\nu_2)t}. \tag{2.21}$$

Note that this is the same substitution that is necessary to derive the equation for the electromagnetic wave in the slowly-varying amplitude approximation Eq.(2.12). In the following we omit the use of the tilde and use the natation $\rho_{\alpha,\beta}$ for slowly varying matrix elements. We also use the definition Eq.(2.10) for the electromagnetic field and then make the rotating wave approximation by neglecting all the terms proportional to $e^{i(\omega_i+\nu_j)t}$. Indeed, under the conditions (2.11) the effect of these fast-oscillating terms is effectively time-averaged.

The time evolution of the slowly-varying density matrix elements for the three-level system can be written as:

$$\dot{\rho}_{b_{1,2}b_{1,2}} = i\Omega^*_{1,2}\rho_{ab_{1,2}} - i\Omega_{1,2}\rho_{b_{1,2}a}; \tag{2.22}$$

$$\dot{\rho}_{ab_{1,2}} = -i\Delta_{1,2}\rho_{ab_{1,2}} + i\Omega_{1,2}(\rho_{b_{1,2}b_{1,2}} - \rho_{aa}) + i\Omega_{2,1}\rho_{b_{2,1}b_{1,2}}; \tag{2.23}$$

$$\dot{\rho}_{b_1b_2} = -i(\Delta_1 - \Delta_2)\rho_{b_1b_2} + i\Omega^*_1\rho_{ab_2} - i\Omega_2\rho_{b_2a}. \tag{2.24}$$

Here $\Omega_i = \wp_{ab_i}\mathcal{E}_i/\hbar$ is the Rabi frequency, and $\Delta_i = (\omega_a - \omega_{b_i}) - \nu_i$ is the one-photon detuning of the electromagnetic field from the transition frequency.

These equations define the atomic populations and the polarization and polarizations for the three-level Λ scheme. The propagation equation for the electromagnetic fields Eq.(2.12) (in terms of Rabi frequencies) can be then written as:

$$\frac{\partial\Omega_i}{\partial z} + \frac{1}{c}\frac{\partial\Omega_i}{\partial t} = i\kappa_i\rho_{ab_i}. \tag{2.25}$$

The coefficient κ here is defined as:

$$\kappa_i = \frac{2\pi\nu_i}{\hbar c}N\wp^2_{ab_i} = \frac{3}{8\pi}N\lambda_i^2\gamma_{ab_i}, \tag{2.26}$$

where, λ_i is the wavelength of the corresponding transition, and $\gamma_{ab_i} = \frac{4\nu^3}{3\hbar c^3}\wp^2_{ab_i}$ is the radiative decay rate of level a [156].

3. The effect of relaxation processes

To provide an accurate description of the interaction of the light fields with real atoms, we need to consider the coupling of the atoms with a thermal bath. A common approach to this problem is to consider the reduced density operator [154]. Because of the averaging over the thermal reservoir, an additional term appears in the time-evolution equation for the density matrix elements:

$$\dot{\rho}_{\alpha,\beta} = -\Gamma_{\alpha,\beta}\rho_{\alpha,\beta}, \tag{2.27}$$

where

$$\Gamma_{\alpha,\beta} = \frac{1}{2}(\gamma_\alpha + \gamma_\beta) + \gamma_{\alpha,\beta}\delta_{\alpha,\beta}. \tag{2.28}$$

Here $\gamma_{\alpha,\beta}$ are the inverse lifetimes of the states $|\alpha\rangle$ and $|\beta\rangle$, and $\gamma_{\alpha,\beta}$ is the pure dephasing rate, which is nonzero only for the off-diagonal matrix elements. Adopting the terminology of NMR experiments, γ_i is the decay rate of the atomic population, and $\Gamma_{\alpha,\alpha} = 1/T_1$, where T_1 is the longitudinal relaxation time. The pure dephasing rate $\gamma_{\alpha,\beta}$ is due to the phase relaxation, and $\Gamma_{\alpha,\beta} = 1/T_2$ is the transverse relaxation time.

In reality there are a many physical processes which results in the redistribution of the atomic populations and decoherence [21,161]. Spontaneous emission (radiative decay) [155, 157], destruction of the coherence due to collisions with the wall of an atomic cell [19, 162], the effect of elastic collisions with the buffer gas atoms or molecules (collisional broadening) [163–165], spin-exchange between electrons [166–168], the motion of atoms in inhomogeneous electric and magnetic fields [169, 170], etc., can be incorporated into the description of the interaction of the electromagnetic field with the atoms based on the density matrix elements using the decay rates as they are introduced in Eq.(2.27).

In a three-level Λ system the radiative decay of the excited level causes fast relaxation of atoms to the ground states. At the same time, transitions between the ground states are forbidden, so the coherence between them can be preserved for a relatively long time [23]. Unless the walls of an atomic cell are coated with a special material (e.g. paraffin), which preserve the atomic coherence [133, 134, 171–173], collisions of atoms with the walls cause thermalization of the ground state sublevel populations, and destruction of their mutual coherence. In this case the lifetime of the ground-state coherence is determined by the time-of-flight of atoms through the laser beam. The case of a cell filled with a buffer gas is considered in a subsequent chapter, since the addition of a buffer gas cannot be properly described solely by the change of the decay rate values.

To describe this situation an open relaxation scheme (Fig. 3a) is often used. The relaxation of the excited level population is described by the natural decay rates $\gamma_{1,2}$ from level $|a\rangle$ to level $|b_{1,2}\rangle$. An additional decay channel $\tilde{\gamma}_r$ is introduced to model the population pumping into states that do not interact with the fields (such as another Zeeman or hyperfine levels). The population decay rate γ_0 represents the atoms leaving the interaction region. To model the atoms flying into the laser beam, we introduce the incoherent pump r_i . If $\Delta_{b_1b_2} \ll k_BT$, where T is the reservoir average temperature, and k_B is the Boltzmann constant, the populations of the ground states are completely equalized in the collision with the walls, so the value of the incoherent pump is the same for all levels. Its value $r = \gamma_0/2$ is determined so that the sum of ground level populations is equal to unity in the case of a quasi-closed configuration $\tilde{\gamma}_r = 0$, i.e.

$$\rho_{aa} + \rho_{b_1b_1} + \rho_{b_2b_2} = 1 - \frac{\tilde{\gamma}_r}{\gamma_0}\rho_{aa}. \tag{2.29}$$

When $\tilde{\gamma}_r > 0$, the sum of the populations is less then unity because of optical pumping.

Using Eq.(2.27) we can write the Bloch equations for an open Λ system as follows:

$$\dot{\rho}_{b_{1,2}b_{1,2}} = \gamma_0/2 - \gamma_0\rho_{b_{1,2}b_{1,2}} + \gamma_{1,2}\rho_{aa} + i\Omega^*_{1,2}\rho_{ab_{1,2}} - i\Omega_{1,2}\rho_{b_{1,2}a}; \tag{2.30}$$

$$\dot{\rho}_{ab_{1,2}} = -\Gamma_{ab_{1,2}}\rho_{ab_{1,2}} + i\Omega_{1,2}(\rho_{b_{1,2}b_{1,2}} - \rho_{aa}) + i\Omega_{2,1}\rho_{b_{2,1}b_{1,2}}; \tag{2.31}$$

$$\dot{\rho}_{b_1b_2} = -i\Gamma_{b_1b_2}\rho_{b_1b_2} + i\Omega^*_1\rho_{ab_2} - i\Omega_2\rho_{b_2a}, \tag{2.32}$$

The generalized decay rates are defined as:

$$\Gamma_{ab_{1,2}} \quad = \quad \gamma + i\Delta_{1,2} \tag{2.33}$$

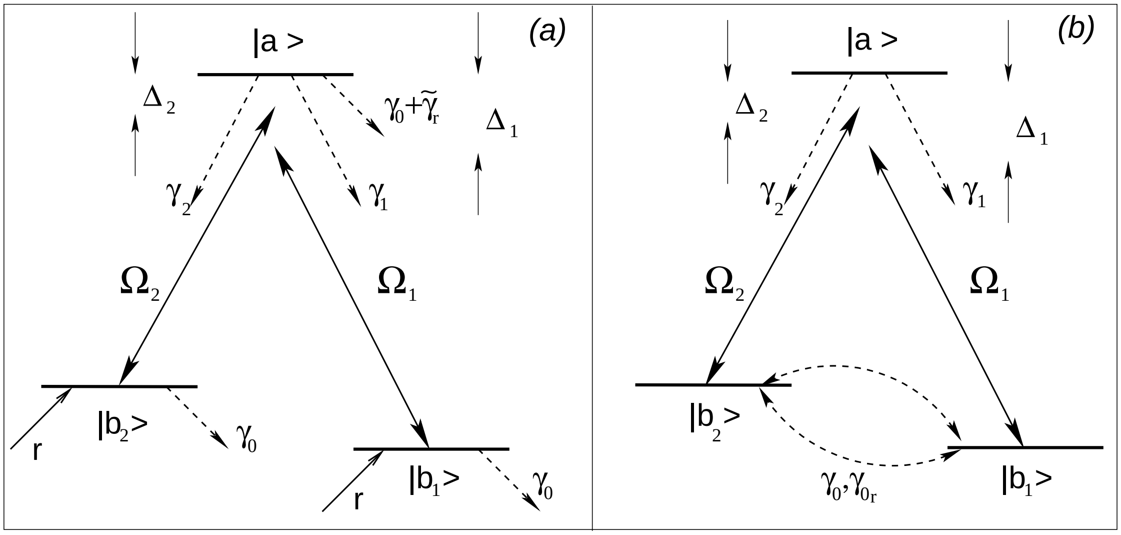
(a)
|a >
Δ_2
Δ_1
$\gamma_0+\tilde{\gamma}_r$
γ_2
γ_1
Ω_2
Ω_1
|b$_2$>
γ_0
r
|b$_1$>
γ_0
r
(b)
|a >
Δ_2
Δ_1
γ_2
γ_1
Ω_2
Ω_1
|b$_2$>
γ_0,γ_{0r}
|b$_1$>

Fig. 3. a) Open Λ scheme ; b) closed Λ scheme.

$$\Gamma_{b_1b_2} \quad = \quad \gamma_0 + i(\Delta_1 - \Delta_2), \tag{2.34}$$

where the polarization decay rate of the excited state is $\gamma = \gamma_0 + (\gamma_1 + \gamma_2 + \tilde{\gamma}_r)/2$.

In many publications the relaxation processes in atoms are described by means of a closed relaxation scheme (Fig.3b). For this system we again assume that the decay rates of the excited transitions are determined by the radiative decay. To describe the evolution of the ground-state populations and coherence we introduce the population exchange rate γ_{0r} and the dephasing rate γ_0. In this scheme all the atomic population is confined within the three levels. Strictly speaking, in the transient regime the closed system cannot be applied. However, the equivalence of the closed and open schemes has been demonstrated under certain conditions [174]. Later we will prove that both of these schemes provide similar results for the description of the nonlinear Faraday effect.

The equations for the off-diagonal matrix elements have the same form as Eqs.(2.31) and (2.32) for the open system, although the decay rates are different:

$$\Gamma_{ab_{1,2}} = \gamma + i\Delta_{1,2}; \quad \gamma = (\gamma_1 + \gamma_2 + \gamma_{0r})/2 + \gamma_{dph} \tag{2.35}$$

$$\Gamma_{b_1 b_2} = \gamma_0 + \gamma_{0r} + i(\Delta_1 - \Delta_2), \tag{2.36}$$

where γ_{dph} is the pure dephasing rate of the radiative transition. Thus, the populations of the ground levels in a closed three-level scheme are defined as:

$$\dot{\rho}_{b_{1,2}b_{1,2}} = -\gamma_{0r}(\rho_{b_{1,2}b_{1,2}} - \rho_{b_{2,1}b_{2,1}}) + \gamma_{1,2}\rho_{aa} + i\Omega^*_{1,2}\rho_{ab_{1,2}} - i\Omega_{1,2}\rho_{b_{1,2}a} \tag{2.37}$$

B. The nonlinear Faraday effect in a three-level Λ system

1. Alkali atoms in the external magnetic field

Let us briefly review the behavior of an atom in an external magnetic field following [156]. We restrict ourselves to the case of a weak magnetic field so that the characteristic energy of the atom in the magnetic field is small compared to the spin-orbit interaction. In this case the total angular momentum $\vec{J} = \vec{L} + \vec{S}$ is a good quantum number. The interaction of an atom with a dc magnetic field $\vec{B}$ is described by the Hamiltonian:

$$H_{magn} = -\vec{\mu}\vec{B} = -\mu_B \mathrm{g}_J \vec{J} \cdot \vec{B}, \tag{2.38}$$

where $\vec{\mu}$ is the magnetic moment of the atom, $\mu_B = \frac{e\hbar}{2mc}$ is a Bohr magneton and g_J is the gyromagnetic ratio (Landé g factor):

$$\mathrm{g}_J = 1 + \frac{J(J+1) - L(L+1) + S(S+1)}{2J(J+1)} \tag{2.39}$$

If we direct the quantization axis along the magnetic field, the Hamiltonian (2.38) is diagonal. The magnetic field lifts the degeneracy of the sublevels with different magnetic quantum number m (corresponding to the quantized z-component of the angular momentum), shifting each sublevel by an amount δ_m, proportional to its magnetic quantum number:

$$\hbar\delta_m = \mathrm{g}_J \mu_B m\ B. \tag{2.40}$$

Thus, in the presence of a magnetic field, the atomic level with angular momentum J is split into $(2J+1)$ equidistant components with $m = \pm J, \pm(J-1), \cdots, 0$. This effect is the well-known Zeeman effect [151, 152, 175].

If we consider hyperfine structure, electronic angular momentum $\vec{J}$ has to be replaced by the total atomic angular momentum $\vec{F}$. In this case the shifts of the magnetic sublevels are determined by the z-components of the total angular momentum $m_F = \pm F, \pm(F-1), \cdots, 0$:

$$\hbar\delta_m = \mathrm{g}_{JF} \mu_B m_F\ B, \tag{2.41}$$

where the factor Landé is now determined as:

$$\mathrm{g}_{JF} = \mathrm{g}_J \frac{F(F+1) + J(J+1) - I(I+1)}{2F(F+1)} \tag{2.42}$$

2. Coherent population trapping in a Λ system

Let us now concentrate on the particular example of the three-level Λ system, the Zeeman sublevels of the same hyperfine atomic level play the role of the ground states in a Λ scheme. The simplest practical realization of such a scheme emerges from an $F = 1 \to F' = 0$ atomic transition. In this case the Λ configuration consists of two circularly polarized components of a single linear or elliptically polarized laser field, which establish a low-frequency coherence between ground-state magnetic sublevels $m = \pm 1$. In the presence of the longitudinal magnetic field, no transitions are allowed between the excited state and the ground-state sublevel with $m = 0$ because of the selection rules.

The interaction Hamiltonian for a Λ system with two circularly polarized electromagnetic fields E_+ and E_- can be written as:

$$\begin{aligned} H_\Lambda &= \hbar\Delta|a\rangle\langle a| - \hbar\delta|b_+\rangle\langle b_+| + \hbar\delta|b_-\rangle\langle b_-| \\ &+ \hbar\left(\Omega_-|a\rangle\langle b_+| + \Omega_+|a\rangle\langle b_-| + H.c.\ \right) \end{aligned} \tag{2.43}$$

where $\Omega_- = \wp_{ab+}E_-/\hbar$, $\Omega_+ = \wp_{ab-}E_+/\hbar$, $\wp_\pm$ are the corresponding dipole moments of the atomic transitions. Due to the symmetry of the problem $\wp_+ = \wp_-$. Δ is the one-photon detuning of the laser frequency from the exact atomic transition, and δ is the Zeeman splitting of the ground-state sublevels $|b_\pm\rangle$.

Let us first find the eigenvalues of this Hamiltonian $H|\lambda\rangle = \hbar\lambda|\lambda\rangle$. An equation for the eigenvalues of the Λ system can be written as:

$$\begin{vmatrix} \delta-\lambda & \Omega_+^* & 0 \\ \Omega_+ & \Delta-\lambda & \Omega_- \\ 0 & \Omega_-^* & -\lambda-\delta \end{vmatrix} = 0 \tag{2.44}$$

or, alternatively

$$-\lambda^3 + \lambda^2\Delta + \lambda(\delta^2 + |\Omega_+|^2 + |\Omega_-|^2) - \delta(\delta\Delta + |\Omega_-|^2 - |\Omega_+|^2) = 0\ . \tag{2.45}$$

Let us first consider the case of no splitting between the Zeeman sublevels (degenerate Λ scheme). Then the eigenvalues and corresponding eigenstates can be easily found:

$$\lambda_D = 0 \tag{2.46}$$

$$|D\rangle = \frac{\Omega_+|b_+\rangle - \Omega_-|b_-\rangle}{\sqrt{|\Omega_+|^2 + |\Omega_-|^2}} \tag{2.47}$$

$$\lambda_{B_{1,2}} = \frac{\Delta}{2} \pm \sqrt{\frac{\Delta^2}{4} + |\Omega_+|^2 + |\Omega_-|^2} \tag{2.48}$$

$$|B_{1,2}\rangle = \sqrt{\frac{|\lambda_{B_{1,2}}|}{\lambda_{B_1} - \lambda_{B_2}}} \left(|a\rangle + \frac{\Omega_+^*}{\lambda_{B_{1,2}}} |b_-\rangle + \frac{\Omega_-^*}{\lambda_{B_{1,2}}} |b_+\rangle \right) . \tag{2.49}$$

The state denoted as $|D\rangle$ is called the "dark state" because an atom in this state does not interact with the light fields and therefore does not fluoresce. Atoms in the other two states, called "bright states", readily absorb light. Therefore, atoms initially prepared in a bright state are optically pumped into the dark state after some finite time comparable with the lifetime of the excited state $|a\rangle$. Thus, in steady-state, the atomic ensemble does not interact with the electro-magnetic fields, which is the essence of CPT. The dispersive properties of the atomic system in the dark state are governed by the coherence between the ground states of the Λ system. The corresponding density matrix element may be found from Eq.(2.46):

$$\rho_{b+b-} = -\frac{\Omega_-^* \Omega_+}{|\Omega_-|^2 + |\Omega_+|^2} . \tag{2.50}$$

The true dark state exists only for $\delta = 0$. As soon as the exact resonant conditions are disturbed, the system starts interacting with light. However, for small detunings ($\sqrt{|\Omega_+|^2 + |\Omega_-|^2} \gg |\delta|, \ \sqrt{|\Delta\delta|}$) the disturbance of the dark state is small, and most of the atomic population is concentrated in the modified dark state $|\tilde{D}\rangle$. In this case the eigenvalue $\tilde{\lambda}_D$ corresponding to this state can be found by solving Eq. (2.45) and keeping only the terms linear in δ:

$$\tilde{\lambda}_D = \delta \frac{|\Omega_-|^2 - |\Omega_+|^2}{|\Omega_+|^2 + |\Omega_-|^2} \tag{2.51}$$

$$|\tilde{D}\rangle \simeq \mathcal{N} \left\{ |D\rangle + 2\delta \frac{\Omega_+ \Omega_-}{(|\Omega_+|^2 + |\Omega_-|^2)^{3/2}} |a\rangle \right\} \tag{2.52}$$

where $\mathcal{N} \simeq 1 + O(\delta^2)$ is a normalization constant. From Eq. (2.52) it is obvious that the population of the excited level $|a\rangle$ is proportional to δ^2.

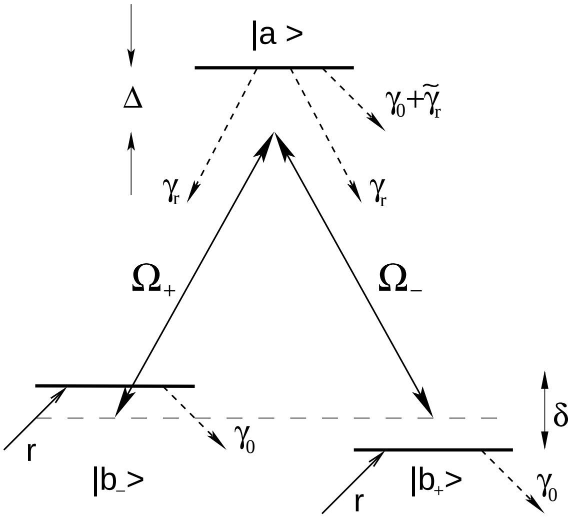

Fig. 4. a) Three-level open Λ system, based on the Zeeman sublevels.

3. The solution for the case of a homogeneously broadened transition

In the following calculations we consider the open atomic configuration shown in Fig. 4. In this case, γ_r is the radiative linewidth of the transitions $|a\rangle \rightarrow |b_\pm\rangle$, $\tilde{\gamma}_r$ is the decay outside the system (for example, to the atomic level $m = 0$), γ_0 is the ground-state population decay rate due to the transient effect.

The time-evolution equations for the atomic populations can be obtained from Eqs.(2.30)-(2.32) with the proper change of notation:

$$\begin{aligned} \dot{\rho}_{b-\,b-} &= \frac{\gamma_0}{2} - \gamma_0 \rho_{b-\,b-} + \gamma_r \rho_{a\,a} + i(\Omega_+^* \rho_{a\,b-} - c.c.), && (2.53) \\ \dot{\rho}_{b+\,b+} &= \frac{\gamma_0}{2} - \gamma_0 \rho_{b+\,b+} + \gamma_r \rho_{a\,a} + i(\Omega_-^* \rho_{a\,b+} - c.c.). && (2.54) \end{aligned}$$

Analogously, for the polarizations we have

$$\begin{aligned} \dot{\rho}_{a\,b\pm} &= -\Gamma_{a\,b\pm} \rho_{a\,b\pm} + i\Omega_{\mp}(\rho_{b\pm\,b\pm} - \rho_{a\,a}) \\ &\quad + i\Omega_{\pm} \rho_{b\mp\,b\pm}, && (2.55) \end{aligned}$$

$$\dot{\rho}_{b-\,b+} = -\Gamma_{b-\,b+}\rho_{b-\,b+} + i\Omega_{+}^{*}\rho_{a\,b_+} - i\Omega_{-}\rho_{b-\,a}, \tag{2.56}$$

where

$$\begin{aligned} \Gamma_{a\,b\pm} &= \gamma + i\left(\Delta \pm \delta\right), && (2.57) \\ \Gamma_{b-\,b+} &= \gamma_0 + i2\delta. && (2.58) \end{aligned}$$

Here the transverse decay rate of the excited level is $\gamma = \gamma_r + (\gamma_0 + \tilde{\gamma}_r)/2$.

In steady state regime, we can solve equations Eqs.(2.55) and (2.56) in terms of atomic populations:

$$\begin{aligned} \rho_{b-\,b+} &= -\frac{\Omega_{+}^{*}\Omega_{-}\left(\dfrac{n_{b-\,a}}{\Gamma_{b_-\,a}} + \dfrac{n_{b+\,a}}{\Gamma_{a\,b_+}}\right)}{\Gamma_{b-\,b+} + \dfrac{|\Omega_+|^2}{\Gamma_{a\,b+}} + \dfrac{|\Omega_-|^2}{\Gamma_{b-\,a}}} && (2.59) \\ \rho_{a\,b\pm} &= \frac{i\Omega_{\mp}}{\Gamma_{a\,b\pm}} \frac{n_{b\pm\,a}\left(\Gamma_{b\mp\,b\pm} + \dfrac{|\Omega_{\mp}|^2}{\Gamma_{b\mp\,a}}\right) - n_{b\mp\,a}\dfrac{|\Omega_{\pm}|^2}{\Gamma_{b\mp\,a}}}{\Gamma_{b\mp\,b\pm} + \dfrac{|\Omega_{\pm}|^2}{\Gamma_{a\,b\pm}} + \dfrac{|\Omega_{\mp}|^2}{\Gamma_{b\mp\,a}}} && (2.60) \end{aligned}$$

where $n_{b\pm\,a} \equiv \rho_{b\pm\,b\pm} - \rho_{aa}$. Inserting these expressions into Eqs.(2.53) and (2.54) we can in principle derive linear equations for the atomic populations. In the general case, however, this solution is very cumbersome.

Let us consider the situation of a strong electro-magnetic field, such that $|\Omega|^2/\gamma_0\gamma \gg 1$. We also assume that $|\delta|, \gamma_0 \ll \gamma, |\Omega|$, and $\Delta = 0$. In the zeroth approximation, the atomic populations are determined by Eq.(2.51):

$$\begin{aligned} \rho^{(0)}_{b\pm\,b\pm} &\simeq \frac{|\Omega_\pm|^2}{|\Omega|^2}, && (2.61) \\ \rho^{(0)}_{a\,a} &\simeq 0, && (2.62) \end{aligned}$$

where $|\Omega|^2 = |\Omega_+|^2 + |\Omega_-|^2$.

Now we can solve for the polarizations $\rho_{a\,b\pm}$, keeping only the terms linear in δ

and γ_0:

$$\rho_{a\,b\pm} = \frac{i\Omega_{\mp}}{\Gamma_{a\,b\pm}} \frac{\gamma(\gamma_0 \pm i\delta)\frac{|\Omega_{\pm}|^2}{|\Omega|^2} + \{|\Omega_{\mp}|^2 n^{(1)}_{b\pm\,a} + |\Omega_{\pm}|^2 n^{(1)}_{b\mp\,a}\}}{\gamma\gamma_0 + |\Omega|^2} \tag{2.63}$$

where $n^{(1)}_{ab}$ is the correction to the atomic population proportional to γ_0.

Substituting this expression to the equation for the ground-state populations Eqs.(2.54),(2.53), we find:

$$|\Omega_{\mp}|^2 n^{(1)}_{b\pm\,a} + |\Omega_{\pm}|^2 n^{(1)}_{b\mp\,a} = -\frac{\gamma_0\gamma}{2}\frac{|\Omega_{\pm}|^2 + |\Omega_{\mp}|^2}{|\Omega|^2}. \tag{2.64}$$

In this case the atomic polarization is:

$$\rho_{a\,b\pm} \simeq \frac{i\Omega_{\mp}}{|\Omega|^4}(\frac{\gamma_0}{2}|\Omega|^2 \pm i\delta|\Omega_{\pm}|^2). \tag{2.65}$$

It is important to note that this expression for the polarization, obtained in an open Λ system coincides with the analogous expression, calculated by Fleischhauer *et al.* [124] for a closed system, if the ground-state coherence dephasing rate and the population exchange rate between ground levels are the same and equal to γ_0. This demonstrates the equivalence of the open and closed models for the description of Λ schemes, which has been previously demonstrated by Lee *et al.* [174] for the particular case of a weak probe field.

The stationary propagation of two circularly polarized components of the laser field through the atomic medium is described by Maxwell-Bloch equations Eq.(2.25):

$$\frac{\partial\Omega_{\pm}}{\partial z} \simeq -\kappa\frac{\Omega_{\pm}}{|\Omega|^4}(\frac{\gamma_0}{2}|\Omega|^2 \mp i\delta|\Omega_{\mp}|^2). \tag{2.66}$$

Separating the real and imaginary parts of this expression and using $\Omega_{\pm} = |\Omega_{\pm}|\ e^{i\phi_{\pm}}$, one can find the propagation equations of the electromagnetic field intensity $|\Omega|^2$ and the rotation of the polarization ellipse $\phi = \phi_+ - \phi_-$:

$$\frac{\partial|\Omega|^2}{\partial z} \quad = \quad -\kappa\gamma_0 \tag{2.67}$$

$$\frac{\partial \phi}{\partial z} = -\frac{\kappa\delta}{|\Omega|^2}. \tag{2.68}$$

After trivial integration, the final expressions for the light transmission $|\Omega(z)|^2$ I_{out} and the polarization rotation angle ϕ are:

$$|\Omega(z)|^2 = |\Omega(0)|^2 \left(1 - \frac{\kappa\gamma_0}{|\Omega(0)|^2}\right); \tag{2.69}$$

$$\phi = -\frac{\delta}{\gamma_0} \ln \frac{|\Omega(z)|^2}{|\Omega(0)|^2}. \tag{2.70}$$

As one can see, the absorption is drastically reduced compared to the incoherent case, which is the usual consequence of CPT. At the same time the polarization rotation increases dramatically.

To compare theoretical expressions with the experimental results it is convenient to rewrite Eq.(2.69) in terms of the laser intensity:

$$I_{\text{out}} = I_{\text{in}} - \frac{2\pi\hbar\nu}{c}\gamma_0 N L \tag{2.71}$$

C. Nonlinear Faraday effect in hot atomic vapor: the influence of Doppler broadening

A moving atom, interacting with an electromagnetic field of frequency ν_0, “sees” it at the shifted frequency $\nu = \nu_0 - \vec{k}\vec{v}$, where $\vec{k}$ is the electromagnetic field wave-vector, and $\vec{v}$ is the velocity of the atom (Doppler effect). Because of this effect, resonant features which appear due to the resonant interaction of light with atoms are the subject of inhomogeneous Doppler broadening, if the atomic velocity distribution is nonuniform [161].

In two-photon processes, the motion of the atoms plays an important role as well, since coherent interaction in a general Λ scheme occurs only if the atom is in resonance with both electromagnetic fields $\omega_{2ph} = (\nu_1 - \vec{k}_1\vec{v}) - (\nu_2 - \vec{k}_2\vec{v})$. For example, in the case of counter-propagating waves, only a group of atoms with specific velocity participates in the coherent interaction (velocity-selective coherent population trappings) This effect has been successfully used for sub-recoil cooling of atoms in a magneto-optic trap [176]. On the other hand, electromagnetically induced transparency observed in a co-propagating geometry is affected only by the residual Doppler effect, caused by the mismatch between the wave-vectors of the two transitions $|k_1 - k_2|$, which is often negligible since $v/c \ll 1$. There are numerous studies of CPT and EIT in Doppler-broadened atomic media in various interaction schemes [174, 177–185]; the modifications of EIT lineshape due to atomic thermal motion are addressed in [186–189].

The problem of residual Doppler broadening is completely eliminated in the nonlinear Faraday effect, since two circularly polarized fields are of the same frequency and perfectly overlapped, being the components of a single laser field. In this case the motion of an atom is equivalent to the detuning of the laser field from the exact transition. It is easy to see that the coherent superposition of Zeeman sublevels, associated with the dark state, Eq.(2.46), is independent of laser detuning; thus, all velocity groups of atoms contribute to the nonlinear Faraday effect.

Although the calculations of nonlinear susceptibility of inhomogeneously broaden coherent media is quite straightforward, it is generally very cumbersome, and analytical expressions are obtained only in specific cases: of strongly asymmetric Λ scheme [189], and the nonlinear Faraday effect under the approximation of infinite Doppler width [127]. Here we derive general expressions for absorption and polarization rotation of arbitrary laser detuning, and then consider some special cases, which allow the analytical integration over the Doppler velocity distribution.

Once again we assume that the electro-magnetic field is strong enough, such that $|\Omega|^2/\gamma_0\gamma \gg 1$, and that $|\delta|, \gamma_0 \ll \gamma, |\Omega|$; at the same time we do not put any constraints on the value of laser detuning Δ, so the terms proportional to $\gamma_0\Delta$ and $\delta\Delta$ cannot be considered small. As in the resonant case, the atomic populations in the zeroth approximation are determined by Eq.(2.51):

$$\begin{aligned} \rho^{(0)}_{b\pm\, b\pm} &\simeq \frac{|\Omega_\pm|^2}{|\Omega|^2}, & (2.72)\\ \rho^{(0)}_{a\, a} &\simeq 0, & (2.73) \end{aligned}$$

With this result, the expression for atomic polarization $\rho_{ab\pm}$ Eq.(2.60) can be rewritten, keeping only terms linear in γ_0 and δ :

$$\rho_{ab\pm} = i\Omega_\mp \frac{\{(\gamma_0\gamma \pm 2\delta\Delta) + i(\pm 2\delta\gamma - \gamma_0\Delta)\}\dfrac{|\Omega_\pm|^2}{|\Omega|^2} + X_\pm}{(\gamma|\Omega|^2 + \gamma_0\Delta^2) + i\left(\pm 2\delta\Delta^2 - \Delta(|\Omega_\pm|^2 - |\Omega_\mp|^2)\right)}, \tag{2.74}$$

where

$$X_\pm \equiv |\Omega_\mp|^2 \Delta n^{(1)}_{b\pm a} - |\Omega_\pm|^2 \Delta n^{(1)}_{b\mp a}. \tag{2.75}$$

The first-order corrections to the ground-state populations $\Delta n^{(1)}_{b\pm a}$ may be found by substituting the expression for atomic polarizations Eq.(2.74) into the equations (2.53) and (2.54), and solving for $X_\pm$:

$$\begin{aligned} X_\pm &= -\gamma_0 \frac{|\Omega_\pm|^2 - |\Omega_\mp|^2}{2|\Omega|^4}(\gamma|\Omega|^2 + \gamma_0\Delta^2) - \frac{\gamma_0\Delta^2}{2}\frac{|\Omega_\pm|^2 - |\Omega_\mp|^2}{\gamma|\Omega|^2 + \gamma_0\Delta^2} \\ &\pm \frac{2\delta\Delta}{|\Omega|^2}\frac{\gamma_0\Delta^2(|\Omega_\pm|^2 - |\Omega_\mp|^2)^2 - 2\gamma|\Omega|^2|\Omega_\pm|^2|\Omega_\mp|^2}{\gamma|\Omega|^2 + \gamma_0\Delta^2}. \end{aligned} \tag{2.76}$$

Substituting this expression into Eq.(2.74), we obtain the density matrix element $\rho_{ab\pm}$ for arbitrary laser detuning Δ. Because of the extreme bulkiness of the final result, further integration of this expression would not lead to any meaningful results. Instead we consider a few special cases.

Let us first find the absorption in the system when no magnetic field is present, and the ground-state sublevels are degenerate. Using Eq.(2.66), we can then write down the propagation equations for the intensities of the circularly polarized components $|\Omega_\pm|^2$:

$$\frac{\partial|\Omega_\pm|^2}{\partial z} = -\kappa|\Omega_\mp|^2 \frac{\gamma_0\gamma(\gamma|\Omega|^2+\gamma_0\Delta^2)+\gamma_0\Delta^2(|\Omega_\pm|^2-|\Omega_\mp|^2)}{(\gamma|\Omega|^2+\gamma_0\Delta^2)^2+\Delta^2(|\Omega_\pm|^2-|\Omega_\mp|^2)^2} \tag{2.77}$$

It is easy to see that the difference between the absorption coefficients for the two circularly polarized waves are due to the second term in the numerator of Eq.(2.77). This difference vanishes if the laser is tuned exactly to the resonant frequency, or if linearly polarized light is used. In the latter case, this means that the linear polarization is preserved during the propagation of the laser field through the resonant medium regardless of frequency detuning. The propagation equation for the intensity of the linearly polarized wave is given by:

$$\frac{\partial|\Omega|^2}{\partial z} = -\kappa\gamma_0 \frac{\gamma|\Omega|^2}{\gamma|\Omega|^2+\gamma_0\Delta^2} \tag{2.78}$$

Let us now find the expression of the propagation equation for the rotation angle of the polarization direction for the linearly polarized laser field, detuned from exact resonance by the detuning Δ. To do that we need to write the expression for the density matrix element $\rho_{ab\pm}$, assuming $|\Omega_\pm|^2 = |\Omega_\mp|^2 = \frac{1}{2}|\Omega|^2$. At this point we are interested only in the limit of small magnetic field, so only the terms linear in δ are retained:

$$\rho_{ab\pm} = i\Omega_\mp \frac{\frac{1}{2}\gamma_0\gamma(\gamma|\Omega|^2+\gamma_0\Delta^2) \pm \delta\gamma|\Omega|^2 - \frac{1}{2}\gamma_0\gamma(\gamma|\Omega|^2+\gamma_0\Delta^2)}{(\gamma|\Omega|^2+\gamma_0\Delta^2)^2} \tag{2.79}$$

From this expression it is easy to see that no circular dichroism arises for any value of Δ to the first order in the magnetic field. Following the same procedure as in the previous section, the propagation equation for the polarization rotation angle $\phi = (\phi_+ - \phi_-)/2$ (where the phases of the circularly polarized components are defined as before $\Omega_\pm = |\Omega|/\sqrt{2}\, e^{i\phi_\pm}$):

$$\frac{\partial \phi}{\partial z} = \kappa\delta \frac{\gamma^2|\Omega|^2}{(\gamma|\Omega|^2 + \gamma_0\Delta^2)^2} \tag{2.80}$$

It is important to mention here that the propagation equations for laser intensity $|\Omega(z)|^2$ and polarization rotation angle $\phi(z)$, obtained above are similar to the analogous equations, obtained in Ref. [127] for the $F = 1 \rightarrow F' = 0$ transition in the limit of strong electromagnetic field.

If the electromagnetic field propagates through hot atomic vapor, the contributions of atoms from different velocity group have to be taken into account. In a Doppler-broadened medium, the laser frequency detuning Δ should be replaced by $(\Delta + kv)$, and Equation (2.25) is written as:

$$\frac{\partial \Omega_\pm}{\partial z} = i\kappa\langle\rho_{ab\mp}\rangle_T, \tag{2.81}$$

where $\langle\cdots\rangle \equiv \int \cdots f(kv)d(kv)$. The velocity distribution of thermal atomic gas at temperature T is described by one-dimensional Doppler function:

$$f(kv) = \frac{1}{\sqrt{\pi}kv_T} \exp\left(-\frac{(kv)^2}{(kv_T)^2}\right), \tag{2.82}$$

where $v_T = \sqrt{2k_BT/M}$ is the most probable speed of atoms (here k_B is Boltzmann constant, and M is the atomic mass). However, it is a well-established practice to use a Lorentzian distribution for the sake of simplicity, since this provides much simpler analytic expressions [174]. For all the calculations below we use the following distribution function $f(kv)$:

$$f(kv) = \frac{1}{\pi}\frac{W_D}{W_D^2 + (kv)^2}, \tag{2.83}$$

where $W_D = \sqrt{\ln 2}kv_T$ is HWHM of the velocity distribution (Doppler width).

Following the prescription given by Eq.(2.81), to calculate the transmitted intensity and polarization rotation angle Eqs.(2.78),(2.80) should be averaged over the Doppler velocity distribution:

$$\frac{\partial|\Omega|^2}{\partial z} = -\kappa\gamma_0\langle\frac{\gamma|\Omega|^2}{\gamma|\Omega|^2+\gamma_0\Delta^2}\rangle_T; \tag{2.84}$$

$$\frac{\partial\phi}{\partial z} = \kappa\delta\langle\frac{\gamma^2|\Omega|^2}{(\gamma|\Omega|^2+\gamma_0\Delta^2)^2}\rangle_T \tag{2.85}$$

After the simple integration we arrive at the following expressions:

$$\frac{\partial|\Omega|^2}{\partial z} = -\kappa\gamma_0\frac{|\Omega|}{|\Omega|+\sqrt{\frac{\gamma_0}{\gamma}}W_D}; \tag{2.86}$$

$$\frac{\partial\phi}{\partial z} = \frac{\kappa\delta}{|\Omega|}\frac{|\Omega|+\frac{1}{2}\sqrt{\frac{\gamma_0}{\gamma}}W_D}{(|\Omega|+\sqrt{\frac{\gamma_0}{\gamma}}W_D)^2} \tag{2.87}$$

Following the same procedure, described in the previous section, the final expression for output Rabi frequency $|\Omega|$ and polarization rotation angle ϕ are obtained:

$$\left(|\Omega(z)|+\sqrt{\frac{\gamma_0}{\gamma}}W_D\right)^2 = \left(|\Omega(0)|+\sqrt{\frac{\gamma_0}{\gamma}}W_D\right)^2 - \kappa\gamma_0 z; \tag{2.88}$$

$$\phi = -\frac{\delta}{\gamma_0}\ln\left(\frac{|\Omega(z)|}{|\Omega(0)|}\frac{|\Omega(z)|+\sqrt{\frac{\gamma_0}{\gamma}}W_D}{|\Omega(0)|+\sqrt{\frac{\gamma_0}{\gamma}}W_D}\right) \tag{2.89}$$

It is easy to see that we regain the expression for the transmission and polarization rotation in a homogeneously broadened medium Eqs.(2.69),(2.70), if the laser intensity is high enough $|\Omega| \gg \sqrt{\frac{\gamma_0}{\gamma}}W_D$. In this case, when CPT conditions are obeyed for all atomic velocity groups, the interaction is effectively independent of Doppler broadening (sometimes this is called the Doppler-free regime).

In a regime when CPT exists only for a group of atoms $\sqrt{\gamma_0\gamma} \ll |\Omega| \ll \sqrt{\frac{\gamma_0}{\gamma}}W_D$, the expressions for both transmission and polarization rotation angle are quite different. Namely, the laser intensity attenuates as a quadratic polynomial of optical path

L instead of the linear dependence in Doppler-free regime.

$$|\Omega(z)| = |\Omega(0)| - \frac{\sqrt{\gamma_0 \gamma}}{2W_D} \kappa L \tag{2.90}$$

Although the form of the equation for the polarization rotation does not vary from the Doppler-free regime, an additional numerical factor appears in the denominator:

$$\phi = -\frac{\delta}{2\gamma_0} \ln \frac{|\Omega(z)|^2}{|\Omega(0)|^2} \tag{2.91}$$

D. Normalization conditions for the $F = 1 \to F = 0$ transitions

The correspondence between the $F = 1 \to F = 0$ transition interaction scheme (Fig. 5a) and the idealized three-level Λ scheme considered above (Fig. 5b) can be obtained if we exchange γ_r by $\gamma_{aa}/3$, where γ_{aa} is the decay rate of the excited state to the ground state. The decay rate $\tilde{\gamma}_r$ should be written as $\tilde{\gamma}_r = \gamma_{aa}/3 + \tilde{\gamma}_{aa}$, where $\tilde{\gamma}_{aa}$ stands for the decay of the excited state outside of the system in Fig. 5a.

We assume that the incoherent pumping rate into each Zeeman ground state is equal to $\gamma_0/3$, to keep the normalization condition similar to Eq.(2.29):

$$\tilde{\rho}_{aa} + \rho_{+1,+1} + \rho_{-1,-1} + \rho_{0,0} = 1 - \frac{\tilde{\gamma}_{aa}}{\gamma_0} \tilde{\rho}_{aa}, \tag{2.92}$$

where $\tilde{\rho}_{aa} = \xi \rho_{aa}$, $\rho_{+1,+1} = \xi \rho_{b+b+}$, and $\rho_{-1,-1} = \xi \rho_{b-b-}$. The normalization parameter ξ can be found from Eqs.(2.29) and (2.92).

Taking in mind that the population of the state $m = 0$ is determined by the decay rate of the excited state $|a\rangle$ and by the decay outside of the system we write the rate equation

$$\dot{\rho}_{0,0} = \frac{\gamma_0}{3} - \gamma_0 \rho_{0,0} + \frac{\gamma_{aa}}{3} \tilde{\rho}_{aa}, \tag{2.93}$$

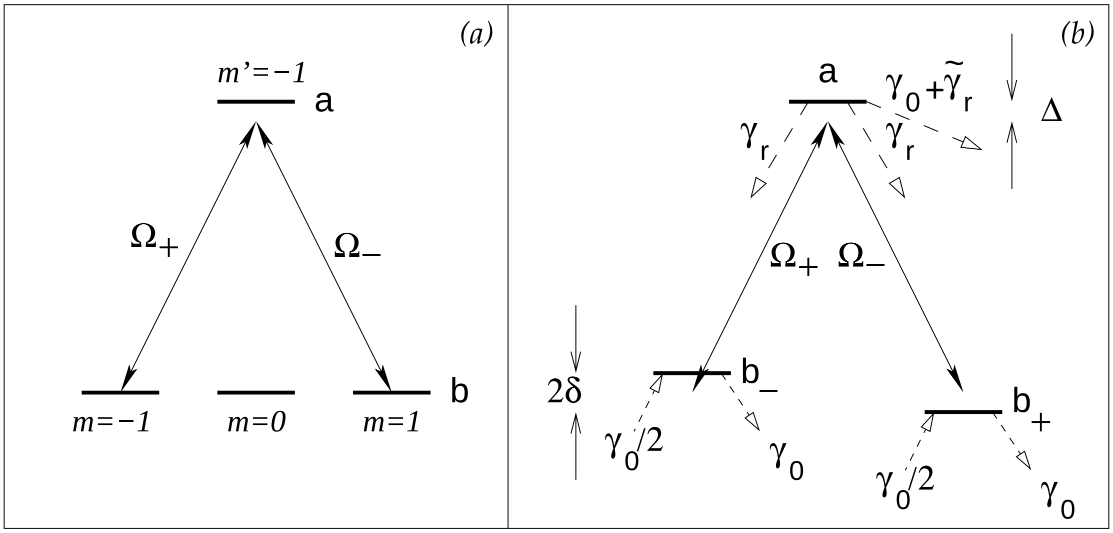

Fig. 5. (a) Scheme of interaction of an electromagnetic wave with atomic transition $|b\rangle,\ F = 1 \rightarrow |a\rangle,\ F' = 0$. (b) Simplification of the scheme (a) to the three-level Λ system

and solve it in the steady state

$$\rho_{0,0} = \frac{1}{3} + \frac{\gamma_{aa}}{3\gamma_0}\tilde{\rho}_{aa}. \tag{2.94}$$

Substituting (2.94) into (2.92) and comparison of this expression with (2.29) allows us to find

$$\xi = \frac{2}{3}. \tag{2.95}$$

Therefore, we can derive elements of density matrix for the level scheme shown in Fig. 5a by simple multiplication of the elements of the density matrix for the Λ scheme by the scaling factor ξ (2.95).

CHAPTER III

NONLINEAR FARADAY EFFECT IN DENSE Rb VAPOR

This chapter is devoted to the experimental study of the nonlinear Faraday rotation[1] in Rb vapor cells. It also includes a detailed description of the experimental apparatus and measurement procedure.

We present the experimental spectra for the laser absorption and the nonlinear Faraday rotation for different transitions of Rb. The data obtained for optically thick vapor exhibits significant enhancement of the polarization rotation simultaneously with the suppression of the residual absorption. The shape of the nonlinear resonances is also analyzed.

The experimental data, presented in this Chapter, are taken in a cell containing only the saturated vapor of Rb; the modifications of NMOR in the cells with an additional buffer gas are described in Chapter V.

A. Experimental setup

1. Diode lasers

Since their invention forty years ago [190, 191], diode lasers have become one of the most common source of coherent radiation; they are widely used in both industry and science. Comprehensive reviews of basic properties and spectroscopic applications of diode lasers can be found, for example, in [192–194]; for that reason we instead provide the specific information concerning the diode laser systems which have been used in the experiments.

---

[1] We use the term "Nonlinear Faraday effect" to describe the rotation of the *linear* polarization in external magnetic field, in analogy with classical Faraday effect. The term "Nonlinear Magneto-Optical Effects" is more general and is used to described the variety of modifications of the optical field polarization in magnetic field.

For the laser field with wavelength $\lambda = 795$nm we use a single mode index guided laser diode (LD) Sharp $LT024$. The diode is thermostabilized to ensure reliable operation and to eliminate the drift of the laser frequency due to temperature fluctuations. Since the spectrum of a free-running diode laser is quite broad ($\Delta\lambda \sim 2$nm), it can be substantially narrowed by using, for example, frequency selective optical feedback from a high-finesse external cavity [195–199]. In our experiments, we use an external cavity in Littman configuration [200, 201], shown in Fig. 6. In this case the laser operates on the resonator formed by the external mirror from one arm, and the one of the LD facets from the other. The second facet of the diode has an anti-reflection coating to increase the effect of the external feedback. A diffraction grating placed inside the resonator ensures that the phase-matching conditions are obeyed only for a small part of the LD gain spectra. Tuning of the generated frequency is realized by rotation of the external mirror, which changes the length of the resonator. Although we have not performed precision measurements of the laser linewidth for our system, its average value for analogous systems is about 1 MHz, which is below the radiative width of the Rb transitions ($\gamma_r = 2\pi \cdot 5$MHz).

A diode laser with a distributed Bragg reflector [194] SDL-DBR3S, operating on the wavelength $\lambda = 780$nm, is used in the experiments on the D_2 line of Rb. In this case, one of the mirrors of the LD is replaced by the refractive index grating, which provides selective Bragg back-scattering of the laser radiation. Although the laser spectral linewidth in this case is usually wider ($1 - 5$MHz) than for the ECDL, the distributed Bragg reflector provides high stability and wide tuning range.

The stability of the free-running lasers in both cases is enough for our experiments, and no additional active stabilization of the laser frequency is requited.

The rest of the laser system is identical for both lasers (Fig. 7). It is a well-

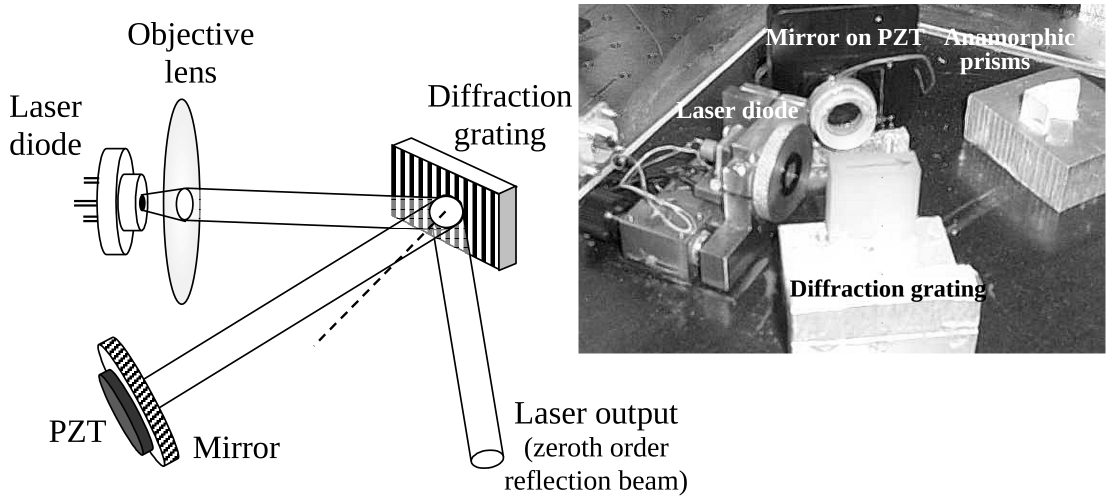
Objective lens
Laser diode
Diffraction grating
PZT
Mirror
Laser output
(zeroth order reflection beam)
Mirror on PZT
Anamorphic prisms
Laser diode
Diffraction grating

Fig. 6. The schematic and the photo of the external cavity diode laser used in the experiments.

known fact that the spacial profile of the diode laser output is a Gaussian beam with substantially different transverse cross-sections. The symmetry of the laser beam may be adjusted by a pair of anamorphic prisms [202, 203]. Any parasite optical feedback results in a disturbance of the laser operation and, therefore, is highly undesirable. To avoid retro-reflections from various surfaces a Faraday isolator [204, 205] is placed after the laser. To obtain an accurate reference of the laser frequency, we separate a small part of the laser beam and perform the saturated-absorption spectroscopy [206] using an independent cell filled with a natural mixture of Rb isotopes. The maximum laser power, available from both laser systems is $P_{max} \simeq 5$ mW, and the laser bean diameter is $d = 2$ mm. If necessary, it can be increased using a beam expander.

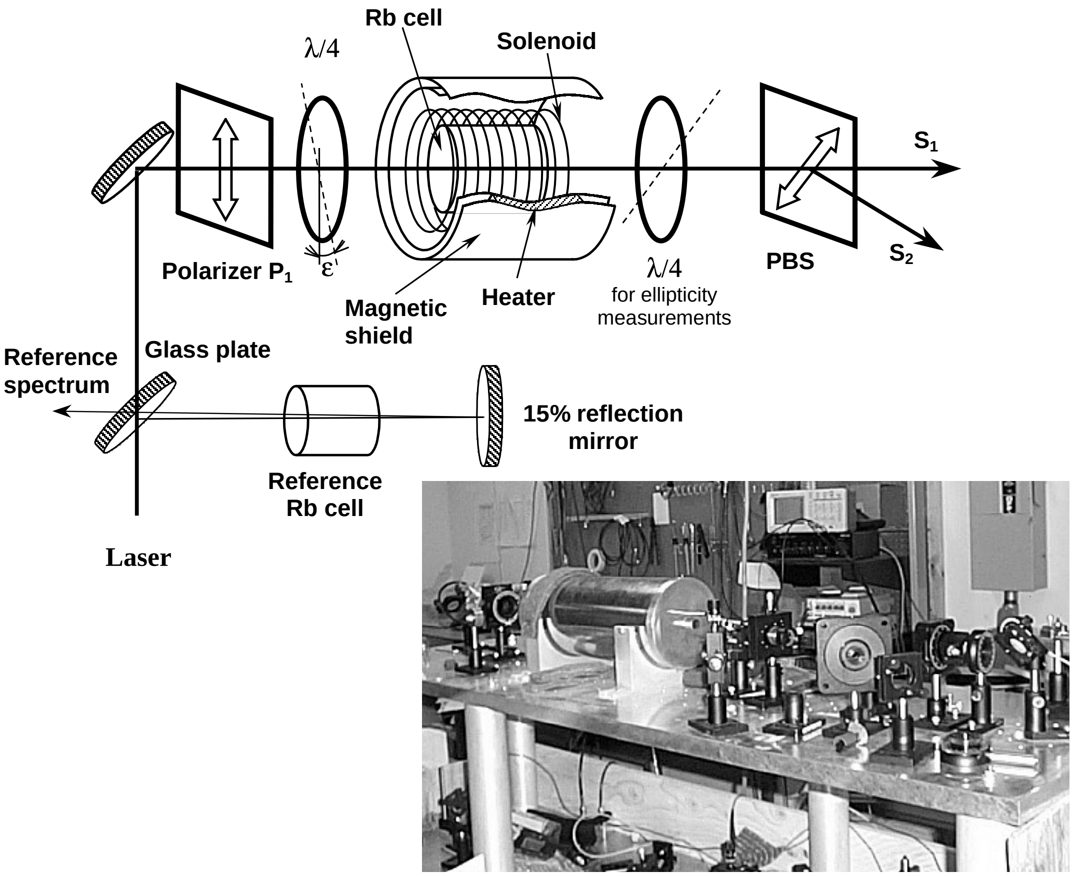
Rb cell
Solenoid
λ/4
S1
S2
Polarizer P1
ε
Magnetic shield
Heater
λ/4
for ellipticity measurements
PBS
Reference spectrum
Glass plate
15% reflection mirror
Reference Rb cell
Laser

Fig. 7. The schematic and photo of the experimental setup used in the experiments.

Table I. Parameters of the atomic cells used in the experiments. Neon is used as a buffer gas for all cells except the one with 0.12Torr of Kr.

Isotope	Buffer gas, Torr	Length, mm	Diameter, mm
^{87}Rb	no	50	25
^{85}Rb	no	25	35
^{87}Rb	0.12	50	30
natural Rb	0.3	60	30
^{87}Rb	1.0	10	10
natural Rb	3.0	40	30
^{87}Rb	10.0	60	30
^{87}Rb	30.0	25	25

2. Polarization rotation measurements

The laser beam passes trough a high quality polarizer P_1 which provides initial linear polarization. A half wave-plate, mounted in front of the polarizer P_1, allows us to attenuate the laser power. To control the diameter of the laser beam a beam expander, consisting of positive and negative lenses, may be used. The absorption cell is placed inside a double layer magnetic shield to suppress the influence of the laboratory magnetic field. In our experiments we use several cylindrical glass cells, filled with Rb vapor; their parameters are listed in Table I. The longitudinal magnetic field is created by a solenoid mounted inside the inner magnetic shield. The atomic density is controlled by a heating element placed between the two shielding layers.

To simultaneously measure the transmitted laser power and the polarization rotation angle a polarization beam splitter (PBS) is placed after the atomic cell.

Signals from the two PBS channels $S_{1,2}$ are collected with PBS axis tilted at 45^o degrees with respect to the main axis of the polarizer P_1. In this configuration the transmitted light power is proportional to the sum of two signals $S_1 + S_2$ and the polarization rotation angle ϕ is given by:

$$\phi = \frac{1}{2} \arcsin \frac{S_1 - S_2}{S_1 + S_2} \tag{3.1}$$

In the experiments with the elliptically polarized light the ellipticity ε is controlled by a quarter wave-plate placed after the polarizer P_1. The rotation angle of the polarization ellipse in this case can be measured using the same technique as for the linear polarization. If the PBS axis is tilted by 45^o with respect to the fast axis of the waveplate, the polarization is rotated by the angle ϕ:

$$\phi = \frac{1}{2} \arcsin \frac{S_1 - S_2}{(S_1 + S_2)\cos 2\varepsilon} \tag{3.2}$$

It is also possible to detect a change in the ellipticity of the outgoing laser beam by placing another quarter-wave plate after the cell and before the PBS. Providing that the fast wave plate axis is aligned with the PBS axis and makes 45^o with the main axis of the initial polarization ellipse, the ellipticity ε_{out} of the outgoing beam can be found similarly to the rotation angle:

$$\varepsilon_{out} = \frac{1}{2} \arcsin \frac{\tilde{S}_1 - \tilde{S}_2}{\tilde{S}_1 + \tilde{S}_2} \tag{3.3}$$

B. Absorption and polarization rotation on various Rb transitions

Using the laser systems described above we are able to study the resonant phenomena on the D_1 line: $5S_{1/2} \rightarrow 5P_{1/2}$ ($\lambda = 795$nm), and the D_2 line: $5S_{1/2} \rightarrow 5P_{3/2}$ ($\lambda = 780$nm) of both isotopes of Rb. The various parameters of the allowed transitions in Rb vapor may be found in Appendix A. Let us just briefly mention that the D_1 line consists of 4 transitions between various hyperfine sublevels: $F = 1, 2 \rightarrow F' = 1, 2$ for ^{87}Rb, and $F = 2, 3 \rightarrow F' = 2, 3$ for ^{85}Rb. The D_2 line has a more complex structure and consists of 6 allowed transitions: $F = 1 \rightarrow F' = 0, 1, 2$ and $F = 2 \rightarrow F' = 1, 2, 3$ for ^{87}Rb, and $F = 2 \rightarrow F' = 1, 2, 3$ and $F = 3 \rightarrow F' = 2, 3, 4$ for ^{85}Rb.

Although the radiative width of all excited levels is rather small ($\simeq 5$ MHz), the thermal motion of the atoms results in the inhomogeneous Doppler broadening of the transitions. The value of the Doppler width for the room temperature is about $\Delta_{\mathrm{Dopp}} \simeq 500$ MHz. This broadening exceeds the hyperfine splitting of all excited levels, so the transitions to these states from the same hyperfine ground state are unresolved within the Doppler contour. The only exception is the state $5P_{1/2}$ of ^{87}Rb, for which the hyperfine levels are split by $\Delta_{\mathrm{hf}} = 812$ MHz, so the corresponding transitions are partially resolved. Since the interaction with other hyperfine level(s) is not taken into account in most theoretical models, we usually study the NMOR effects on the transitions within the D_1 line of ^{87}Rb. The absorption and the polarization rotation spectra as the laser frequency is swept across the D_1 line of Rb are shown in Fig. 8. To illustrate the reduction of the resonant absorption due to coherent population trapping, two transmission spectra are shown: one is for zero magnetic field, when there is no two-photon detuning between the circular components of the laser field, and the conditions for the dark state formation are optimal, and the other is for relatively large magnetic field, when the ground-state coherence is effectively destroyed. The experimental data demonstrate that the EIT is observed for three out of four possible transitions (except $F = 1 \rightarrow F' = 2$), with the maximum contrast for the $F = 2 \rightarrow F' = 1$ transition. Note, that nonlinear magneto-optic rotation is substantially higher on this transition as well.

The rotation and transmission spectra, taken for a particular value of the magnetic fields, sometimes may be deceiving, since resonances of different widths are to

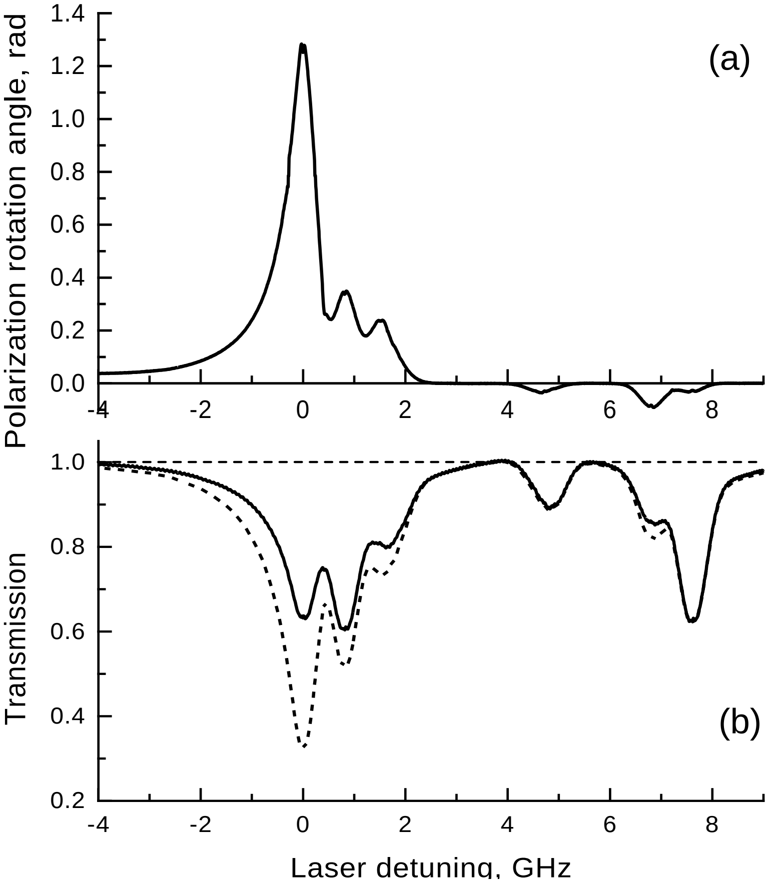

Fig. 8. (a) The polarization rotation angle ϕ at magnetic field $B = 0.2$ G as a function of the laser frequency;(b) transmitted intensity under maximum CPT condition ($B = 0$) (solid line) and for large magnetic field $B = 2.8$ G (dashed line). Zero detuning corresponds to the $F = 2 \rightarrow F' = 1$ transition. Laser power $P = 2$ mW, laser beam diameter $d = 2$ mm, atomic density $N = 5.6 \cdot 10^{11}\text{cm}^{-3}$. The additional peaks are due to contamination of the cell by ^{85}Rb.

be analyzed. To get deeper insight we record the dependencies of the polarization rotation angle and transmitted intensity as a function of applied magnetic field for laser light resonant with all transitions. The experimental data are presented in Fig. 9. These data confirm the earlier conclusion that the best EIT, accompanied by the maximum polarization rotation, is observed for the $F = 2 \rightarrow F' = 1$ transition. The reason is the following: in this case all transitions between the Zeeman sublevels contribute to the creation of the ground-state coherence, forming three Λ links. For the $F = 2 \rightarrow F' = 2$ and the $F = 1 \rightarrow F' = 1$ transitions both Λ and V interaction schemes are equally probable; since CPT is created only in a Λ system, the effectiveness of the optical pumping to a dark state for these transitions is lower. Finally, enhanced absorption is observed for the $F = 1 \rightarrow F' = 2$ transition. In further discussion we consider only the nonlinear magneto-optic rotation due to CPT, particularly on the $F = 2 \rightarrow F' = 1$ transition. The nonlinear properties of the light interacting with the $F = 1 \rightarrow F' = 2$ transition should be considered separately.

The NMOR signal for the D_2 line of ^{87}Rb is shown in Fig. 10. The excited state $5P_{3/2}$ consists of 4 hyperfine sublevels ($F' = 0, 1, 2, 3$), which are significantly closer to each other than for $5P_{1/2}$ state (D_1 line). Thus, the hyperfine structure is completely overlapped by Doppler broadening, which makes it virtually impossible to separate the influence of different transitions. For that reason in our study of the nonlinear Faraday effect the D_1 line is used much more often.

One can also see that EIT for the D_2 line appears to be weaker than for the D_1 line. For example, the strong cycling transition $F = 2 \rightarrow F' = 3$ is mostly responsible for the absorption at the $F = 2 \rightarrow F'$ transition, and there is no dark state formed there. On the contrary, the coherent interaction of the electromagnetic field with this transition is associated with enhanced absorption resonances [35, 66].

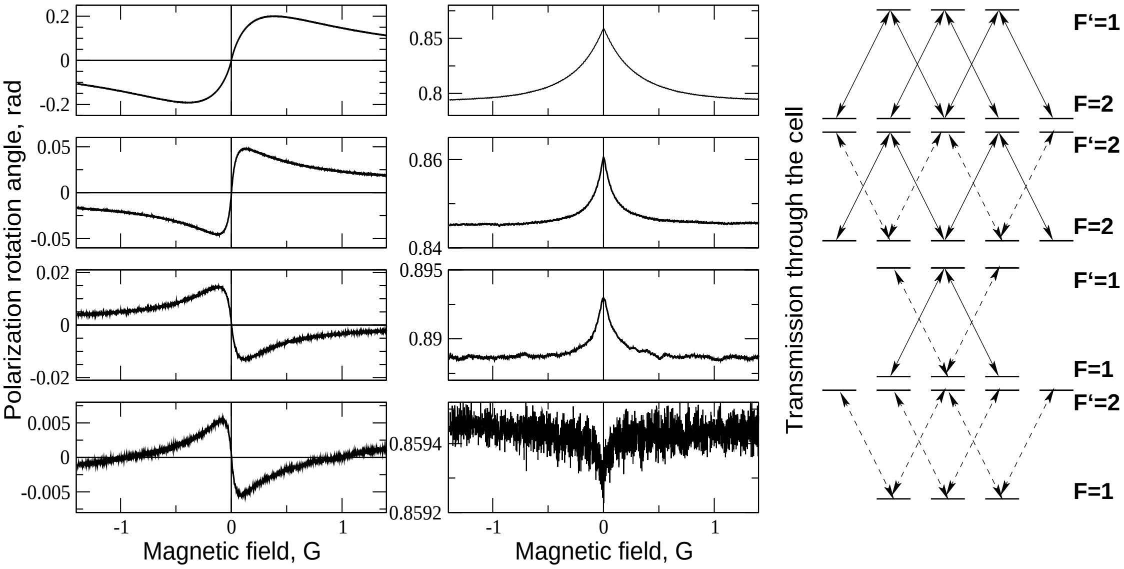

Fig. 9. The polarization rotation angle ϕ (left column) and the transmitted laser intensity (middle column) as a function of the applied magnetic field. The interaction of the linearly polarized laser light with the magnetic sublevels on different transitions are shown in right column. The transitions, drawn in solid lines, contribute to CPT; those drawn in dashed lines do not contribute to a dark state. To avoid the modification of the resonance shapes due to propagation effects, we considered optically thin Rb vapor ($N = 8 \cdot 10^{10}\text{cm}^{-3}$). Laser power $P = 2$ mW, laser beam diameter $d = 2$ mm.

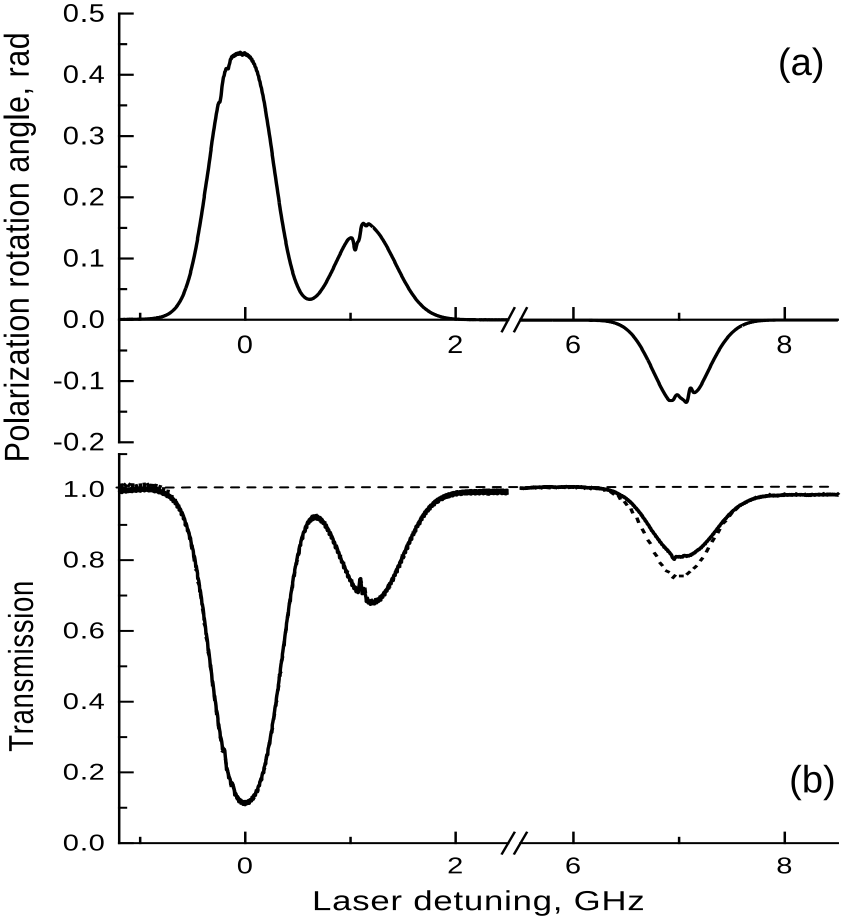

Fig. 10. (a) The polarization rotation angle ϕ at magnetic field $B = 0.2$ G as a function of the laser frequency;(b) transmitted intensity under maximum CPT condition ($B = 0$) (solid line) and for large magnetic field $B = 2.8$ G (dashed line). Zero detuning corresponds to the center of the absorption line of the $F = 2 \rightarrow F'$ transition. Laser power $P = 2$ mW, laser beam diameter $d = 4$ mm, atomic density $N = 5.6 \cdot 10^{10}\text{cm}^{-3}$. The additional peak at 1 GHz is due to contamination of the cell by ^{85}Rb. Sub-Doppler structures observed on both transmission and rotation resonances are due to the redistribution of atomic population by retroreflected light.

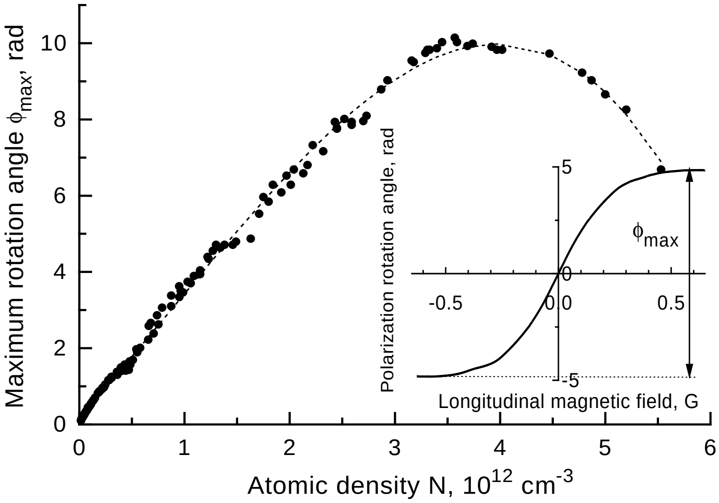

Fig. 11. The experimental dependence of the maximum rotation angle of polarization on atomic density; the dashed line is to guide the eyes.

C. Enhancement of the nonlinear Faraday rotation with atomic density

One of the most important features of coherent phenomena is the strong enhancement of the nonlinearities with the density of resonant atoms. The resonant enhancement of NMOR is demonstrated in Figs. 11 and 12, where the maximum angle of rotation ϕ_{max} and the zero-field rotation slope $d\phi/dB$ are recorded as functions of atomic density N. The maximum angle of rotation is found by adjusting the magnetic field at each density, with $B \sim 0.6$ G for the full data set. The zero-field rotation slope $d\phi/dB$ (shown in Fig. 12) is measured by dithering the field minimally around $B = 0$. Enhancement of the rotation is more than two order of magnitude with respect to its value at room temperature.

The maximum rotation angle observed in the experiment was $\phi_{\text{max}} = 10$ rad. To our knowledge, this is the first experiment where polarization rotation greater than π radians is detected for a sub-Gauss magnetic field. Comparable angles of polarization

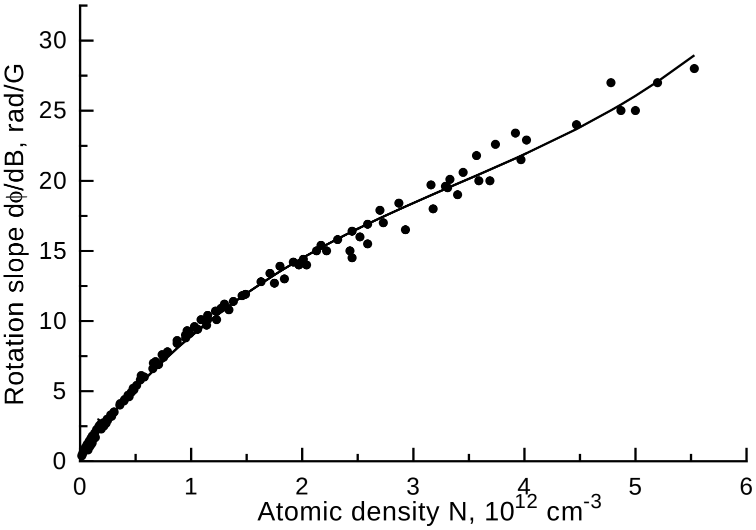

Fig. 12. The experimental dependence of the rotation slope $d\phi/dB$ for $B = 0$ on atomic density (dots); dashed line is to guide the eyes.

rotation were previously observed for much higher magnetic fields and laser intensities [94, 129].

It is interesting to mention here that such large rotation corresponds to a large index of refraction of the medium. The index or refraction for each circular polarization component is about $n = 1 \pm \phi_{\max}\lambda/(4\pi L) \approx 1 \pm 10^{-5}$, where $L = 5.0$ cm is the length of the atomic cell, and $\lambda = 795$ nm is the wavelength of the laser light. Previous enhanced index of refraction obtained in a Λ-type EIT scheme with incoherent pumping [207] was only one order of magnitude more than in our case, whereas the index of refraction of a non-resonant gas at this density is about 10^{-7}.

An analysis of the experimental data shows substantial discrepancy with the predictions of the theory developed in Chapter II for a simplified three-level scheme. For example, the experimentally observed dependence of transmission $I_{\text{out}}/I_{\text{in}}$ and rotation slope $d\phi/dB$ with respect to the atomic density coincide with the calculated

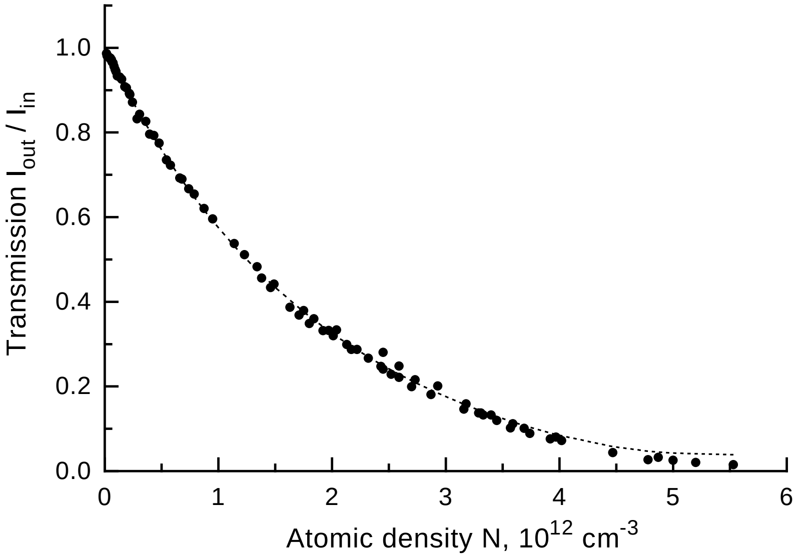

Fig. 13. The experimental dependence of the transmission through the cell on atomic density (dots) for $B = 0$; the dashed line is to guide the eyes.

dependence for optically thin vapor, but disagree for higher density (see Figs. 12 and 13). The observed rotation is much less then predicted by both simplified analytical expressions Eqs.(2.69)and(2.70) and exact numerical simulation, which takes into account the complete Zeeman substructure of the D_1 line of ^{87}Rb and includes Doppler averaging. To explain this behavior it is necessary to assume that the effective decay of Zeeman coherence γ_0 is not determined solely by the time-of-flight of the atom through the laser beam, but also depends on the atomic density. We attribute the origin of this discrepancy to the effect of radiation trapping [208,209] on ground-state coherence.A detailed analysis of this phenomenon is presented in the next Chapter.

D. Experimental study of the NMOR resonance line-shape

The dependence of the polarization rotation angle and transmitted intensity on magnetic field can be found by solving the same equations for the density matrix elements

Eqs.(2.53)-(2.56) keeping all terms proportional to δ. For the laser tuned exactly on resonance $\Delta = 0$, we obtain the following expression for the polarization of the optical transition for the linearly polarized electromagnetic field ($|\Omega_+|^2 = |\Omega_-|^2 = \frac{1}{2}|\Omega|^2$):

$$\rho_{a\,b\pm} = \frac{i\Omega_\mp}{2(\gamma \pm i\delta)} \frac{(\gamma_0 \pm 2i\delta)(\gamma \pm i\delta)}{(\gamma_0 \pm 2i\delta)(\gamma \pm i\delta) + |\Omega|^2}. \tag{3.4}$$

Using Eq.(3.4), the expressions for the polarization rotation angle ϕ and absorption coefficient $\alpha = -\frac{d}{dz}|\Omega|^2$ as functions of magnetic field (more precisely, of magnetic field induced level shift δ) can be derived:

$$\begin{aligned} \phi &= -\kappa \frac{\delta|\Omega|^2 L}{|\Omega|^4 + 4\gamma^2\delta^2} & (3.5) \\ \alpha &= \kappa \frac{\gamma_0|\Omega|^2 + 2\gamma\delta^2}{|\Omega|^4 + 4\gamma^2\delta^2}, & (3.6) \end{aligned}$$

where L is the length of the cell. It is important to mention here that the above expressions are valid only for optically thin media such that the variation of the laser intensity is negligible ($I_{out} \simeq I_{in}$).

In reality the line-shape of the observed resonances is quite far from the Lorentzian functions, shown above. An example of the transmission and rotation resonances are shown in Fig. 14. One can see that there is a relatively large discrepancy between the experimental data and best Lorentzian fit. Note, that this effect has been also observed in EIT resonances in case of hyperfine coherence [210].

Deviations of the resonance line-shape from the prediction of the simple theory in cells without buffer gas is mainly due to inhomogeneous distribution of the laser intensity within a laser beam. This problem is solved analytically for two limiting cases: for low laser power regime [121,211,214], and for the limit of strong laser field [215].

A theoretical description for NMOR in the limit of low laser intensity ($|\Omega| \ll \gamma$)

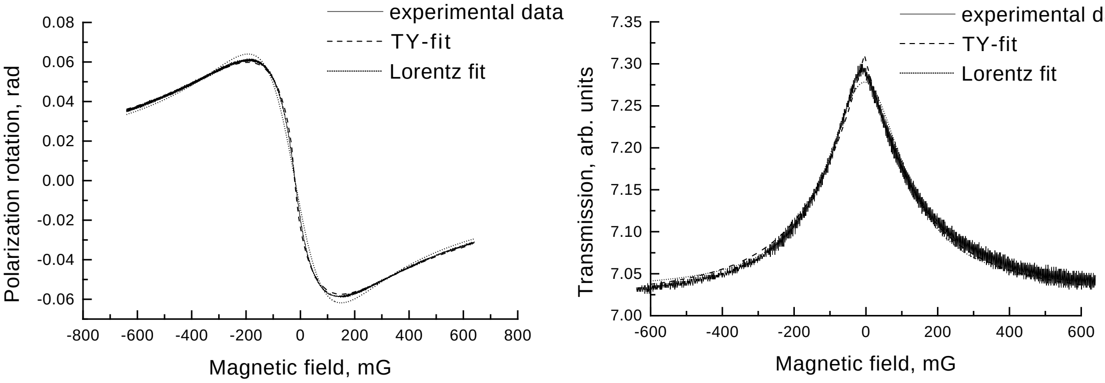

Fig. 14. Polarization rotation and transmission resonances in the ^{87}Rb cell without buffer gas. The laser is tuned at the $F = 2 \rightarrow F' = 1$ resonance of the D_1 line.

has been developed by Weis *et al.* [121, 122]. In this case the nonlinear polarization rotation is treated as three-stage process: first, the interaction of an atom with the laser light creates a ground-state longitudinal alignment; then this alignment precesses with Larmor frequency in the external magnetic field, which produces the time-averaged birefringence in the atomic medium. The polarization rotation is due to the propagation of the light field through such a medium. The transverse inhomogeneity of the laser beam can be taken into account by averaging the alignment over the spatial energy distribution. In the case of a Gaussian distribution function, which is a good approximation for most diode lasers [192], the following expressions for polarization rotation angle and absorption are obtained [211, 212]:

$$\phi \propto \frac{|\Omega|^2}{\gamma}\left[e^{-x}\,\overline{Ei}(x) - e^{x}\,Ei(x)\right]; \tag{3.7}$$

$$\alpha \propto \frac{|\Omega|^2}{\gamma}e^{-|x|}, \tag{3.8}$$

where $Ei(x)$ is the integral exponential function [213], $|\Omega|$ is the Rabi frequency, corresponding to the maximum laser intensity, and $x = \delta/\gamma_0$ is the dimentionless magnetic level shift (or Larmor frequency), $\gamma_0 = v_T/d$, where v_T is the average thermal velocity of Rb atoms, and d is the laser beam diameter. Later Pfleghaar *et al.* conducted similar calculations, taking into account time-of-flight effects [214]. The result of these calculations repeats the expressions Eqs.(3.7,3.8), except for a scaling factor $\sqrt{3}$ in the expression for polarization rotation angle ($x = \sqrt{3}\delta/\gamma_0$), and $\sqrt{2}$ for the laser absorption ($x = \sqrt{2}\delta/\gamma_0$).

The opposite limit of a strong laser field can be treated similarly. In this case the average time-of-flight of atoms through the laser beam is assumed to be much larger than the characteristic times of the other stimulated and relaxation processes, so the motion of atoms in the transverse direction can be neglected. Then, solving the density matrix equations and integrating the result over the Gaussian transverse laser intensity distribution, the following expressions for polarization rotation and absorption are obtained:

$$\begin{aligned} \phi &\propto x \log(1 + \frac{1}{x^2}) && (3.9) \\ \alpha &\propto x \arctan\frac{1}{x}, && (3.10) \end{aligned}$$

where $x = \delta\gamma/|\Omega|^2$. Note, that for the high-power limit the width of the resonances is determined by the Rabi frequency (power broadening) of the laser field rather than the ground-state coherence decay rate γ_0.

Since the experimental NMOR spectra are obtained for conditions closer to the high laser intensity limit, we apply the corresponding fitting functions (3.9,3.10), denoted on the graphs as “YT-fit”. As one can see on Fig.(14), this fit works much better for both polarization rotation and transmission than Lorentzian function. It diverges a little in the vicinity of $B = 0$, where the fit forms a sharp peak whereas

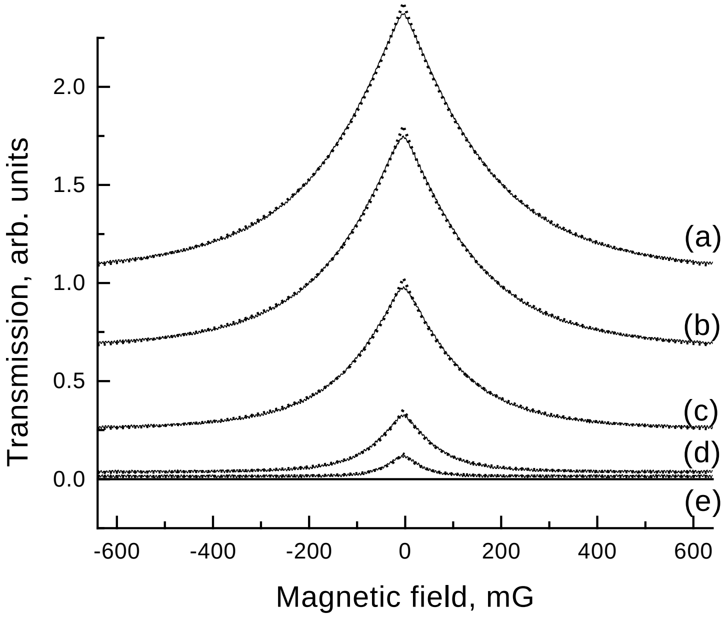

Fig. 15. Experimentally observed dark resonances (solid line) and their best fit (dotted line) using Eq.(3.10). The laser intensity is (a) 2.0 mW; (b) 1.5 mW; (c) 1.0 mW; (d) 0.5 mW; (e) 0.25 mW; laser beam diameter $d = 2$ mm. The laser is tuned to the $F = 2 \rightarrow F' = 1$ resonance of the D_1 line. Atomic density is $5.6 \cdot 10^{11}\text{cm}^{-3}$.

the experimental points lay lower. At the same time, if the laser power increases, the fitting function and the experimental points become closer and closer, as it is shown in Fig. 15. If the maximum relative deviation, calculated as $(I_{exp} - I_{fit})/I_{exp} \times 100\%$, is less than 1 % for laser power $P = 2$ mW, it is reaches 15% for $P = 0.3$ mW. Thus, the reason of divergence between the experiment and theoretical formulae given by Eq.(3.10) may be insufficient laser power.

It is also interesting to note here, that fitting of the experimental spectra with expressions (3.7,3.8) also provides an unexpectedly good agreement. However, the resulting width no longer represents the ground-state coherence decay rate. Although

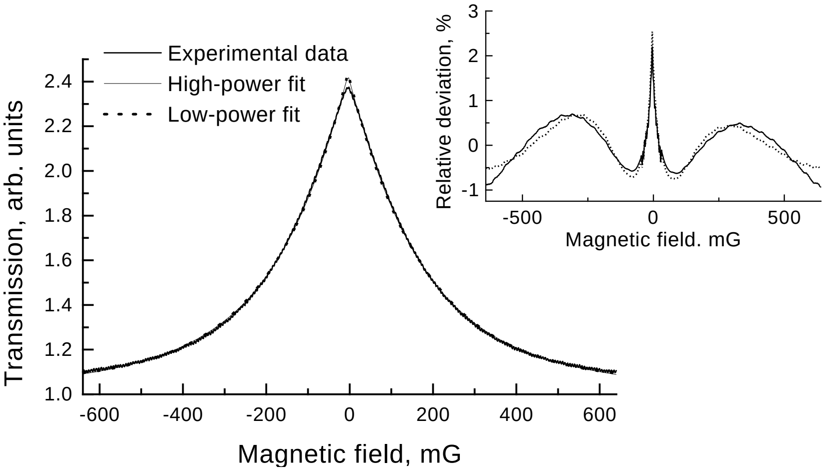

Fig. 16. Experimentally observed dark resonance and its best fit using theoretical lineshape, calculated in high and low laser power limits (Eq.(3.10)and Eq.(3.8) correspondingly). The laser power is 2.0 mW, laser beam diameter $d = 2$ mm. The laser is tuned to the $F = 2 \rightarrow F' = 1$ resonance of the D_1 line. Atomic density is $5.6 \cdot 10^{11}\text{cm}^{-3}$. Inset: the relative deviation of the experimental data from the best fitting functions.

these expressions and Eqs.(3.9,3.10) are obtained for different interaction regimes, the coincidence between the fitting results is practically complete (although both of them can deviate from the experimental data), as shown in Fig. 16.

CHAPTER IV

THE EFFECT OF RADIATION TRAPPING ON ZEEMAN COHERENCE

It is often assumed that atoms interact with an electro-magnetic field independently of each other, and have no influence on each other. This assumption is quite satisfactory for optically thin media. However, if the atomic density increases, collective phenomena such as supperradiance [1, 216–219], local field interactions [220–224], collisions [21, 225–230], etc., become important. Radiation trapping [209] is one of these collective effects and is probably the most sensitive to the density of the atomic medium. To have significant near field interactions or collisional broadening the density of atomic vapor should be more than 10^{14} cm^{-3} [21], while radiation trapping appears for 10^{13} cm^{-3} or even lower densities [209].

Radiation trapping results from the reabsorption of spontaneously emitted photons in optically thick media. This process has been studied extensively in astrophysics, plasma physics, and atomic spectroscopy [209]. Radiation trapping affects high precision metrology experiments [21]. For example, radiation trapping has been predicted and demonstrated to have a destructive effect on the atomic spin orientation produced by optical pumping [21, 231–234], which is important for creation of high quality optical frequency standards.

In this chapter we discuss the influence of radiation trapping on coherent population trapping (CPT) and electromagnetically induced transparency (EIT). Since a common condition for applications of EIT is high optical density of the resonant medium (for example, in experiments demonstrating enhancement of index of refraction [207,235], in EIT-based magnetometers [4,5,158], in experiments with ultraslow slow group velocity of light in hot gases [236]), radiation trapping should be taken into account. The quality of EIT is determined by the residual absorption of electromagnetic field interacting with the atoms. Ideally, when pumped into the "dark" state, the atomic medium does not absorb light. However, there is some residual absorption because of the finite interaction time of atoms and light. Because the spontaneously emitted photons are dephased and depolarized with respect to the coherent fields interacting with the atoms, the effect of radiation trapping can be described as an external incoherent pumping of the atomic transitions [233, 234]. Any incoherent optical pumping also leads to an absorption increase [1]. Under the conditions of EIT, almost all atomic population is in the "dark" state and there are not many atoms undergoing spontaneous emission. However, these spontaneous photons destroy the atomic coherence in the same way incoherent pumping does.

This chapter is organized as follows: first we develop a phenomenological description of radiation trapping effect in two- and three-level systems. We demonstrate, that radiation trapping is equivalent to an incoherent pumping source, and find an expression for its value in terms of atomic density and laser intensity. Using this model we then calculate the modifications of CPT and the nonlinear Faraday effect due to radiation trapping and show that it leads to the deterioration of ground-state coherence.

To verify the predictions of the theory, we conduct an experimental study of the effective decay rate of Zeeman coherence. We create the coherence between ground state magnetic sublevels of the D_1 line of ^{87}Rb vapor, and study the dependence of various NMOR parameters on the vapor density. We observe that the relaxation time of the coherent state is determined not only by the time-of-flight of the atom through the laser beam, but also by the density of the atomic vapor. For atomic densities $N \approx 5 \times 10^{12}\mathrm{cm}^{-3}$ the effective coherence decay rate increases by several times compared with the decay rate for $N \approx 5 \times 10^{10}\mathrm{cm}^{-3}$. We associate this phenomenon with the growing influence of the reabsorbed spontaneous photons.

To double check our conclusions we perform the experiment for two geometrically identical atomic cells, one of which contains buffer gas and the other with atoms in vacuum. Although the absolute value of the ground-state coherence decay rate is different in the cells with and without buffer gas, their dependence on the atomic density perfectly coincides for the both cells. We also compare the results for two laser beams of different sizes and show that the coherence decay rates depends on the geometry in the way predicted by the radiation trapping theory.

A. Radiation trapping in two-level and three-level systems

To understand the origin of radiation trapping we consider of a two-level atom coupled to a radiation reservoir as shown in Fig. 17a and, more specifically, assume that the atom is placed in a bath of thermal photons. The reduced density matrix operator derived in Weisskopf-Wigner approximation [1] has the form

$$\begin{aligned}\dot{\rho}(t) = -\bar{n}_{th}\gamma_r\left[\hat{\sigma}_-\hat{\sigma}_+\rho(t) - \hat{\sigma}_+\rho(t)\hat{\sigma}_-\right] - \\ (\bar{n}_{th}+1)\gamma_r\left[\hat{\sigma}_+\hat{\sigma}_-\rho(t) - \hat{\sigma}_-\rho(t)\hat{\sigma}_+\right] + H.c.,\end{aligned} \tag{4.1}$$

where $\bar{n}_{th}$ is the thermal average photon number in the reservoir, γ_r is the atomic decay rate of the two level system, $\hat{\sigma}_- = |b\rangle\langle a|$ and $\hat{\sigma}_+ = |a\rangle\langle b|$, where $|a\rangle$ and $|b\rangle$ are the excited and ground states of the atom. The equations of motion for the excited state population, obtained from Eq. (4.1), is

$$\dot{\rho}_{aa} = -2\gamma_r(\bar{n}_{th}+1)\rho_{aa} + 2\gamma_r\bar{n}_{th}\rho_{bb}. \tag{4.2}$$

It is convenient to introduce $R = 2\gamma_r\bar{n}_{th}$, the incoherent pumping rate due to thermal photons reabsorption. A spontaneously emitted photon can be absorbed by another similar atom. If we now consider a medium consisting of two-level atoms, a part

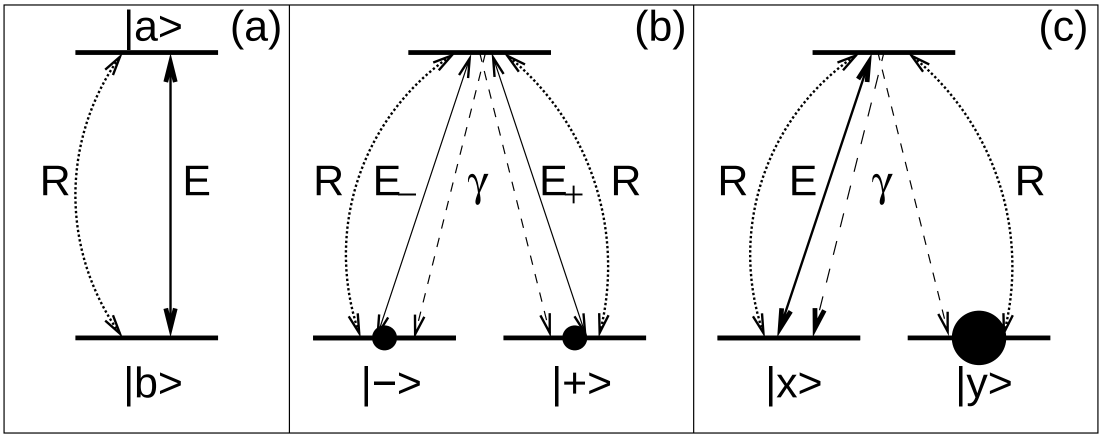

Fig. 17. (a) Two-level atom interacting with a coherent field E and incoherent pump R; (b) Three-level atom interacting with coherent fields E_+ and E_- and incoherent pump $R = 2\gamma_r \bar{n}_{th}$; (c) is the same atom as in (b) shown in the basis of "dark" $|y\rangle = (E_-|+\rangle - E_+|-\rangle)/\sqrt{|E_+|^2 + |E_-|^2}$ and "bright" states $|x\rangle = (E_+|+\rangle + E_-|-\rangle)\ /\sqrt{|E_+|^2 + |E_-|^2}$, and $E = \sqrt{|E_+|^2 + |E_-|^2}$. Incoherent pump leads to transferring of the population from the "dark" state to the "bright" state and, therefore, to absorption of the fields.

of which is initially excited, we see that in an optically thin atomic medium the probability of the photon reabsorption is small and $\bar{n}_{th} = 0$. However, in optically thick media this probability becomes large. Spontaneously emitted photons stay in the medium and diffuse through it due to emission and reabsorption processes. This creates $\bar{n}_{th} \neq 0$. The value of $\bar{n}_{th}$ can be found using the rate equation

$$\dot{\bar{n}}_{th} = -\gamma_R \bar{n}_{th} + r\rho_{aa}, \tag{4.3}$$

where γ_R is the photon escape rate and r is the pumping rate due to the atomic decay. Both γ_R and r are functions of geometric parameters of the system and the atomic density. We have to stress here, that this is an oversimplified approach which only gives a qualitative picture of radiation trapping process. A more rigorous analysis can be found in [209].

Solving Eq.(4.3) in steady state, we get $\bar{n}_{th} = r\rho_{aa}/\gamma_R$. It is convenient to introduce a function $\xi(N) \geq 0$ ($\xi(N=0)=0$) which characterizes radiation trapping: $r/\gamma_R = \xi/(1+\xi)$. The ratio r/γ_R characterizes number of spontaneous photons per excited atom in the medium and can not exceed unity without the system becoming unstable, which is unphysical under present equilibrium conditions. Then, in the case when almost all atoms are in the ground state $\xi\rho_{aa} \ll 1$, we get from (4.2)

$$\dot{\rho}_{aa} \approx -2\gamma_r \frac{\rho_{aa}}{1+\xi(N)}, \tag{4.4}$$

and

$$R = 2\gamma_r \frac{\xi(N)}{\xi(N)+1} \rho_{aa}. \tag{4.5}$$

Eq. (4.4) shows how fast an excited atom decays in an optically thick atomic vapor. It was found from rigorous analysis [209] that for an unsaturated Doppler broadened gas with high opacity the trapping factor $\xi \gg 1$ can be approximated as

$\xi(N) \approx \alpha_0 L\sqrt{\alpha_0 L}$, where α_0 describes the linear absorption of the medium ($1/\alpha_0$ is Beer's absorption length), and L is a characteristic size of the medium.

When radiation trapping is weak enough so that $\gamma_r \gg R$, the incoherent pump R can be written in terms of light absorption in the medium. This is clear because the number of spontaneously emitted photons directly depends on the number of scattered photons from the coherent electromagnetic wave propagating through the medium, i.e. the absorption of the wave. Let us focus on the problem of excitation of the two-level atom by resonant cw light. In the approximation of unsaturated propagation of the light and weak radiation trapping $1 \gg \bar{n}_{th}$ the light absorption obeys the equation $d|\Omega|^2/dz \simeq -3\gamma_r^2 N\lambda^2\rho_{aa}/(4\pi)$, where $\Omega = \wp E/\hbar$ is the Rabi frequency of the light, λ is the wavelength, $\wp$ is the dipole moment of the atomic transition, N is the atomic density, and z is the space coordinate. In this case, the population of the excited state is $\rho_{aa} \simeq |\Omega|^2/\gamma_r^2$. It is useful to repeat here that we consider unsaturated interaction so that $\rho_{aa} \ll 1$. To describe atomic excitation by the incoherent radiation in the reservoir, an incoherent pumping rate (4.5) can be introduced. This rate can be rewritten as

$$R = -\frac{8\pi}{3N\lambda^2\gamma_r}\frac{\xi(N)}{1+\xi(N)}\frac{\mathrm{d}}{\mathrm{d}z}|\Omega|^2 \,. \tag{4.6}$$

This result is rather obvious. Radiation trapping can exist only if the coherent radiation is absorbed by the system and is scattered due to spontaneous emission.

Keeping the incoherent pumping as in (4.6) we return to the problem of light propagation in the three level medium (Fig. 17b). Two cw electromagnetic waves E_+ and E_- propagating in the medium create a coherent superposition of ground state levels that does not interact with the field $|Y\rangle = (E_-|+\rangle - E_+|-\rangle)/\sqrt{|E_+|^2 + |E_-|^2}$ (Fig. 17c). If there is no decay of the coherence between ground state levels $|+\rangle$ and $|-\rangle$, there is no absorption in the medium. The incoherent pump destroys the "dark"

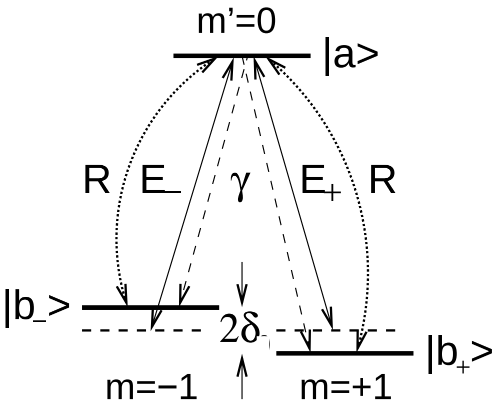

Fig. 18. Idealized three-level system used for analytical theoretical calculations.

state. Therefore, radiation trapping should influence on EIT in an optically thick medium. Below we discuss this phenomenon for the example of nonlinear magneto-optic rotation in optically thick ^{87}Rb atomic vapor.

B. Radiation trapping and nonlinear magneto-optic rotation: theory

As it has been shown in previous sections, the nonlinear Faraday effect in Rb atoms may be successfully described using three-level Λ interaction scheme. Here we will use this scheme again (Fig. 18). Later, to prove the validity of our analytical calculations we will compare their results with numerical simulations for the exact problem including consideration of Zeeman substructure of $5S_{1/2}$, $F = 2 \to 5P_{1/2}$, $F' = 1$ of ^{87}Rb atoms.

We consider the linearly polarized light as two circular components E_+ and E_- which generate a coherent superposition of the Zeeman substates $|b_+\rangle$ and $|b_-\rangle$ with $m = \pm 1$ (a “dark” state). The main difference of this scheme from the one we used previously in Chapter II is the additional incoherent field R which acts on both transitions. As before, this field is equivalent to the reabsorption of spontaneous photons in the medium.

Following the procedure, described in Chapter II, we can write the Bloch equations for the atomic populations and polarizations for the interaction scheme, shown in Fig. 18:

$$\dot{\rho}_{b-\,b-} = -R(\rho_{b-\,b-} - \rho_{a\,a}) + \gamma_{\rm r}\rho_{a\,a} + i(\Omega_-^*\rho_{a\,b-} - \text{c.c.}) \tag{4.7}$$

$$\dot{\rho}_{b+\,b+} = -R(\rho_{b+\,b+} - \rho_{a\,a}) + \gamma_{\rm r}\rho_{a\,a} + i(\Omega_+^*\rho_{a\,b+} - \text{c.c.}) \tag{4.8}$$

$$\dot{\rho}_{a\,b\pm} = -\Gamma_{a\,b\pm}\rho_{a\,b\pm} + i\Omega_\pm(\rho_{b\pm\,b\pm} - \rho_{a\,a}) + i\Omega_\mp\rho_{b\mp\,b\pm}, \tag{4.9}$$

$$\dot{\rho}_{b-\,b+} = -\Gamma_{b-\,b+}\rho_{b-\,b+} + i\Omega_-^*\rho_{a\,b_+} - i\Omega_+\rho_{b-\,a}, \tag{4.10}$$

where

$$\Gamma_{a\,b\pm} \equiv \gamma + \frac{3}{2}R + i\,(\Delta \mp \delta) \tag{4.11}$$

$$\Gamma_{b-\,b+} \equiv \gamma_0 + R - 2i\delta\ . \tag{4.12}$$

In this expression $\gamma_{\rm r}$ is the radiative linewidth of the transitions $|a\rangle \to |b_\pm\rangle$, and γ is the homogeneous transverse linewidth of the optical transitions $|a\rangle \to |b_\pm\rangle$, $\Delta = \Delta_0 + kv$, where Δ_0 is the one photon detuning, k is the wave vector of the field, 2δ is the Zeeman splitting between the ground-state magnetic sublevels. The incoherent pumping R, appearing due to radiation trapping, does not depend on time because we solve the problem in the stationary limit.

We calculate the stationary solutions of the Bloch-equations by considering only the lowest order in γ_0, R and δ, assuming $\Delta_0 = 0$, $|\Omega_-(z)|^2 \approx |\Omega_+(z)|^2$, and $|\Omega(z)|^2 = |\Omega_-(z)|^2 + |\Omega_+(z)|^2 \gg W_d(\gamma_0 + R) \gg \gamma(\gamma_0 + R)$, where W_d is the Doppler half-width of the thermal distribution. In this limit we find

$$\rho_{ab_\pm} \simeq \frac{i\,\Omega_\pm}{2}\frac{[\gamma + i(kv)]\,[\gamma_0 + R \mp 2i\delta]}{[\gamma_0 + R \mp 2i\delta]\,(kv)^2 + \gamma|\Omega|^2}\,. \tag{4.13}$$

Because the Doppler distribution depends on the atomic density (temperature), to study the effect of radiation trapping it is convenient to consider the Doppler-free case of EIT, that is, when the absorption and the dispersion do not depend on the width of the Doppler distribution W_d. Doppler averaging of Eq. (4.13) shows that this condition is fulfilled for comparably large light intensities ($|\Omega(z)| \gg W_d\sqrt{\gamma_0/\gamma}$ for any z). With this assumption we have

$$\langle\rho_{ab_\pm}\rangle_v = \frac{i\,\Omega_\pm}{2|\Omega|^2}\,[\gamma_0 + R \mp 2i\delta]\ . \tag{4.14}$$

It is convenient to separately consider the spatial evolution of amplitudes and phases of the complex Rabi-frequencies $\Omega_\pm(z) = |\Omega_\pm(z)|\mathrm{e}^{i\phi_\pm(z)}$. Using Eq.(2.81) we find the propagation equations for the circular components. The intensities of the two fields are attenuated in the same way:

$$\frac{\mathrm{d}}{\mathrm{d}z}|\Omega_\pm|^2 = -\kappa(\gamma_0 + R)\frac{|\Omega_\pm|^2}{|\Omega|^2}\,, \tag{4.15}$$

where $\kappa = (3/8\pi)N\lambda^2\gamma_r$. However, the phases of the two fields change with opposite sign

$$\frac{\mathrm{d}}{\mathrm{d}z}\phi_\pm = \mp\delta\frac{\kappa}{|\Omega|^2}\,. \tag{4.16}$$

From Eqs. (4.15) and (4.16) we derive expressions for the relative phase $\phi = (\phi_- - \phi_+)/2$ and the total intensity $|\Omega|^2$

$$\frac{\mathrm{d}}{\mathrm{d}z}|\Omega|^2 = -\kappa(\gamma_0 + R), \tag{4.17}$$

$$\frac{\mathrm{d}}{\mathrm{d}z}\phi = \delta\frac{\kappa}{|\Omega|^2}\,. \tag{4.18}$$

To solve these equations we must specify the functional form of the incoherent pumping rate R that results from radiation trapping. From the general properties of radiation trapping [209] and from the results from radiation trapping in a two-level system we assume that in the case of Doppler-free EIT the incoherent pumping can be modelled by (4.6), where $\xi(N)$ is a function of the atomic density that depends on the shape and size of the atomic cell and the diameter of the atomic beam. As we shall see, this model works very well.

With this form for R, Eq. (4.17) can be easily solved and we arrive at

$$\left|\frac{\Omega(z)}{\Omega(0)}\right|^2 = 1 - \frac{\gamma_0 \kappa z}{|\Omega(0)|^2}\left(1+\xi(N)\right) \tag{4.19}$$

so from Eq. (4.6) we have $R = \xi(N)\gamma_0$. Integration of Eq. (4.18) for the phase yields

$$\left.\frac{d\phi(z)}{dB}\right|_{B\to 0} = \frac{\mu_b}{\hbar\left(\gamma_0 + R\right)} \ln\left|\frac{\Omega(0)}{\Omega(z)}\right|^2 . \tag{4.20}$$

Detection of $|\Omega(L)/\Omega(0)|^2$ and $d\phi(L)/dB$, where L is the length of atomic cell, allows us to infer the value of the coherence decay rate as a function of the atomic density and estimate radiation trapping effect. Thus we see that for optically thick media the coherence decay rate increases with the density.

For smaller intensities $W_d\sqrt{\gamma_0/\gamma} \gg |\Omega(z)|$, Doppler-free EIT is not established, so the approximation Eq. (4.6) is not valid and we do not discuss this regime here.

C. Radiation trapping and nonlinear magneto-optic rotation: experiment

The form of Eqs. (2.70) and (4.20) describing the polarization rotation and the transmitted intensity suggests that the most convenient way to study the effect of radiation trapping is to analyze the dependence of the polarization rotation rate on the absorption in the system. Both these values are measured experimentally; it is

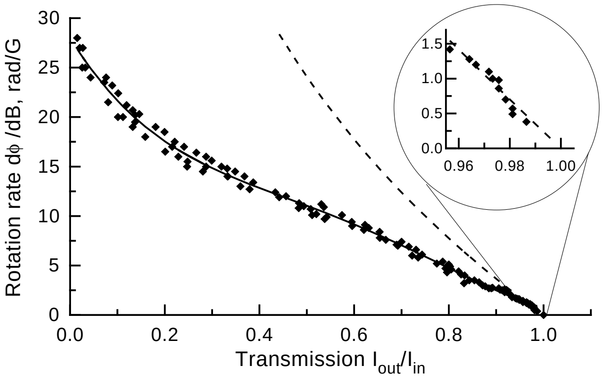

Fig. 19. The dependence of rotation rate $d\phi/dB$ on transmission through the system $I_{\text{out}}/I_{\text{in}}$ for the beam with diameter $d = 2$ mm: experimental (dots), prior theory with $\gamma_0 = 0.004\gamma_r$ (dashed line), and obtained by numerical simulation including radiation trapping (solid line).

also important that there is no atomic density-dependent parameters other than the ground-state coherence decay rate. The typical shape of this dependence is presented in Fig. 19. The individual points on this plot correspond to different atomic densities. The experimental data can be described by the Eq.(2.70) only for the small region in the vicinity of $I_{\text{out}}/I_{\text{in}} \approx 1$ (See Fig. 19 inset); this region corresponds to an optically thin sample, so there is no reabsorption of spontaneous photons. For higher atomic densities, the experimental data cannot be fit either by the simple theory developed in Chapter II or by the numerical simulation of actual Rb atoms, unless we suppose that the coherence decay rate increases with atomic density.

To check the validity of our theoretical approach we use two similar atomic cells (Fig. 20). One cell contains only Rb vapor and the other also contain 0.12 Torr of Kr as a buffer gas. In a cell with buffer gas, atoms do not fly through the beam but rather diffuse through it due to coherence preserving collisions with the buffer gas atoms. The coherence decay rate depends on the interaction time of atoms with the laser radiation and buffer gas effectively increases this time, therefore γ_0 in a cell with buffer gas is less than in a vacuum cell. At the same time radiation trapping process is determined by the geometry of the beam and the cell, and does not depend on the presence of any buffer gas other than through γ_0. Thus, according to our simple theory, the ratio R/γ_0 should be identical for both cells with or without buffer gas. We also measure the transmission and the polarization rotation in the vacuum cell using two laser beams of different diameters but approximately the same intensity. In this case since the geometry of the problem changes, we would expect different behavior for R/γ_0 for different beams.

The value of the coherence decay rate γ_0 may be determined for an optically thin medium using Eqs.(2.69) and (2.70), since radiation trapping is negligible then ($R = 0$). In our case we found $\gamma_0 \approx 0.0033\gamma_r$ for the vacuum cell and the beam diameter $d = 2$ mm, $\gamma_0 \approx 0.0014\gamma_r$ for the cell with buffer gas and the beam diameter $d = 2$ mm, and $\gamma_0 \approx 0.001\gamma_r$ for the vacuum cell and the beam diameter $d = 5$ mm. Using these values, the incoherent pumping rate due to radiation trapping R may be obtained from the experimental data for the rotation rate and transmission, using Eq. (4.20). The ratio R/γ_0, obtained this way is shown in Fig. 21 and Fig. 22. As one can see, it does not depend on the addition of the buffer gas, as expected basing on our understanding of radiation trapping.

The peculiar dependence of the effective pumping rate on the atomic density may be explained using the following reasoning. The probability of photon reabsorption becomes significant when the medium becomes optically thick on the length scale of the atomic cell size D [209] (under the Doppler-free EIT condition almost all atomic population is in the ground state), or

$$\frac{3}{8\pi} N \lambda^2 D \frac{\gamma_r}{W_d} > 1 \,. \tag{4.21}$$

For our experiment $\gamma_r/W_d \approx 0.01$, so Eq. (4.21) is fulfilled for $N > 5 \times 10^{10}$ cm^{-3}.

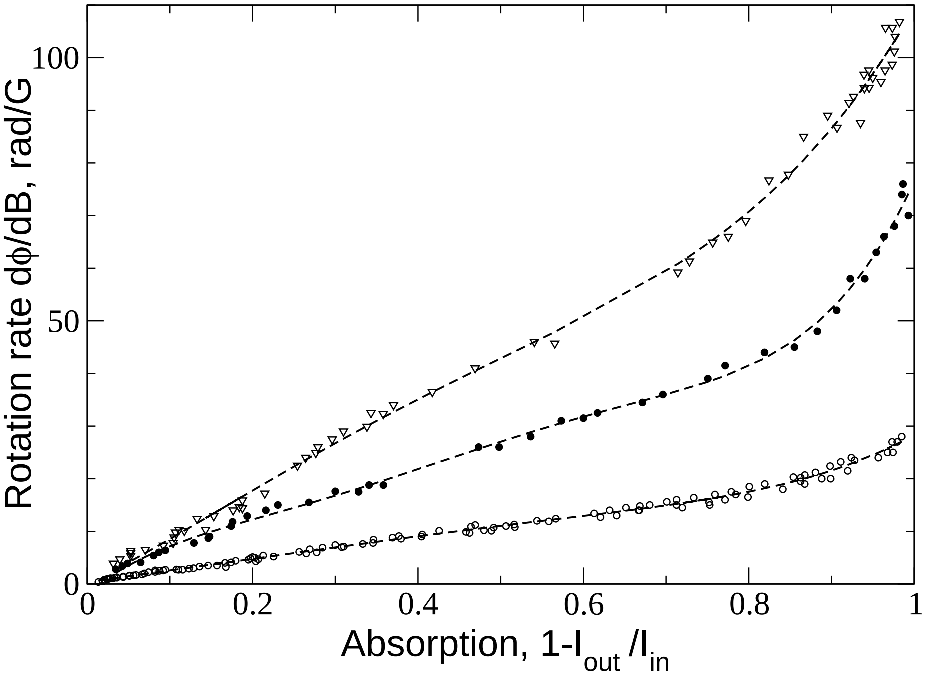

Fig. 20. The dependence of rotation rate $d\phi/dB$ on the absorption $1 - I_{out}/I_{in}$: for the laser beam diameter $d = 2$ mm and the cell without buffer gas (empty circles) and with buffer gas (filled circles); for the laser beam diameter $d = 5$ mm and the cell without buffer gas (empty triangles). Solid lines are to guide the eyes. The laser is tuned on the $F = 2 \rightarrow F' = 1$ transition of the ^{87}Rb D$_1$ line. As it follows from Eq. (4.20) the rotation rate plotted as a function of the absorption characterizes the EIT dephasing rate γ_0. The bigger $d\phi/dB$ for a fixed absorption, the less γ_0. The absorption serves as a measure of the vapor pressure via optical density (see Eq. (4.19)).

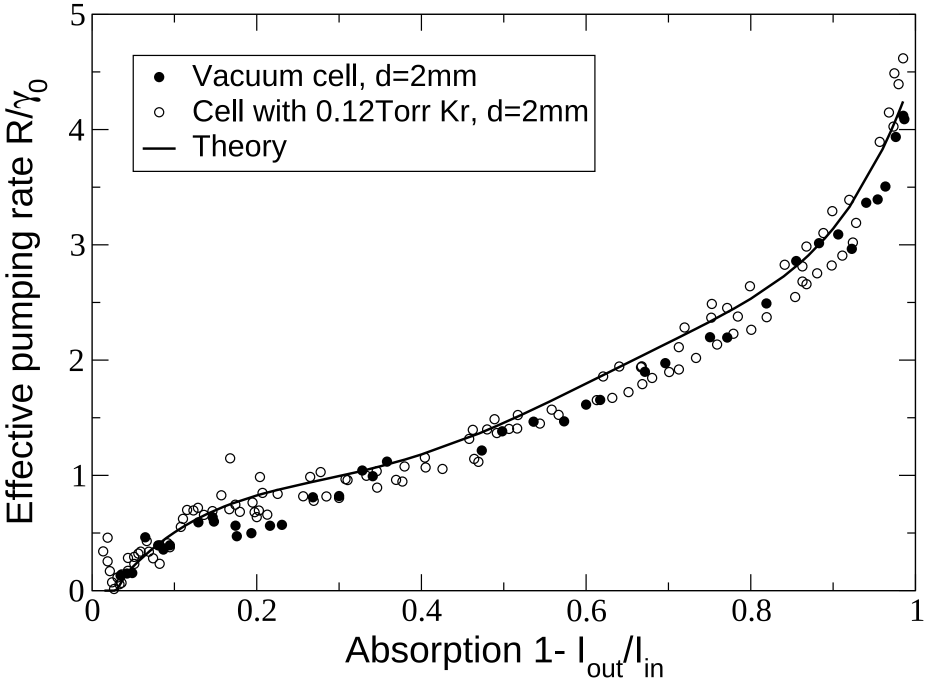

Fig. 21. The incoherent pumping rate R/γ_0 due to radiation trapping as a function of absorption $1 - I_{out}/I_{in}$: calculated by applying Eq. (4.20) to the experimental data: for the cell without buffer gas (empty circles) and with buffer gas (filled circles), and obtained by numerical simulation for the laser beam diameter $d = 2$ mm and the cell without buffer gas (solid line).

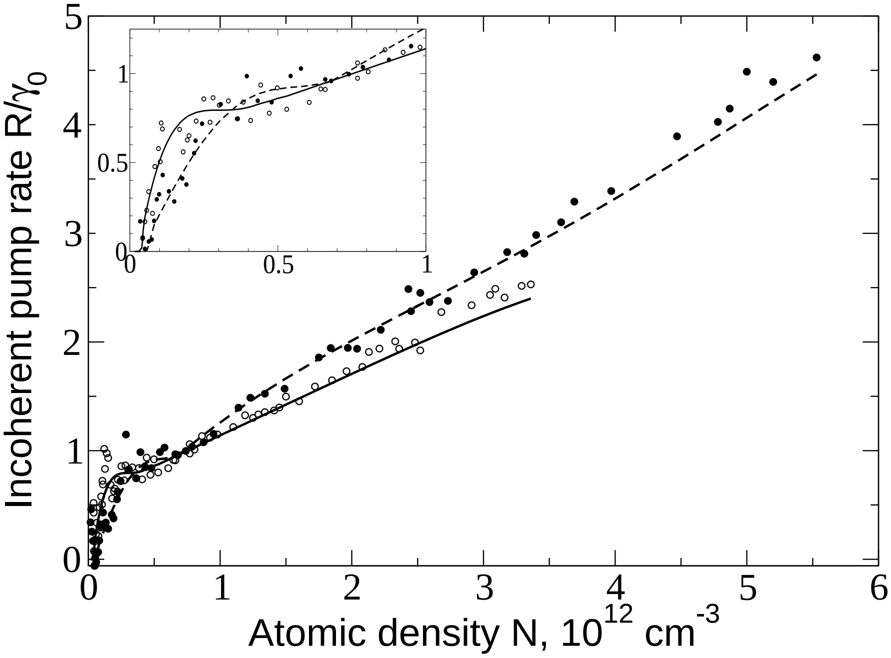

Fig. 22. The incoherent pumping rate R/γ_0 due to radiation trapping as a function of atomic density N: calculated by applying Eq. (4.20) to the data (dots) and obtained by numerical simulation (solid and dashed lines) for the laser beams with diameters $d = 2$ mm (dashed line) and $d = 5$ mm (solid line).

For densities less than this, radiation trapping is negligible and we have $R \approx 0$. Above this value there are two distinct regimes of behavior, with both seen in Fig. 22. At low density we have that R increases linearly with density due to photon absorption and emission within the cell. If the atomic beam is narrower than the radius of the atomic cell, as we have in our experiment ($d \sim 0.1D$), the next regime occurs for densities when photon reabsorption becomes significant inside the laser beam. In our case this is $N > 5 \times 10^{11}$ cm^{-3} for the narrow beam and $N > 2 \times 10^{11}$ cm^{-3} for wide beam (see Fig. 22).

In general, the functional form of R is not an "absolute", and it may change if the cell geometry or laser beam size changes. The results shown in Fig. 22 demonstrate that for high atomic densities, when radiation trapping takes place on the length scales comparable with the laser beam diameter, the functional form of R does not depend on the beam diameter. This appears because the distribution of the "trapped" photons is nearly homogeneous for the atomic cell with dense atomic vapor and an increase in the beam diameter does not change the distribution significantly. In turn, for the lower atomic densities (less absorption) radiation trapping for the laser beam with diameter $d = 5$ mm exceeds radiation trapping for the laser beam with diameter $d = 2$ mm, as can be seen in Fig. 22. Because one would not expect such behavior from other mechanisms than radiation trapping, we take this as a further confirmation that radiation trapping is the correct explanation.

To confirm our simple analytical calculations we have also made detailed numerical simulations of the experiment. We have considered light propagation in a thirteen-level Doppler broadened system corresponding to the $F = 2 \rightarrow F' = 1, 2$ transitions in ^{87}Rb. The decay of atomic coherence is modelled by finite time of flight through the laser beam (an open system). We have solved density matrix equations in steady state using the coherence decay rate as a fit parameter. In other words, we choose the effective coherence decay rate $\gamma_0 + R$ in such a way that our theoretical points for the dispersion $d\phi/dB$ and intensity $I_{\rm out}/I_{\rm in}$ corresponds to the experimental results. The dependence for R/γ_0 obtained this way for the laser beam diameters $d = 2$ mm and $d = 5$ mm and the cell without buffer gas is shown in the solid line in Fig 22.

We see that the simple analytical analysis of the data coincides with the simulations for low atomic densities and diverges slightly for high densities. We explain this difference by inadequate intensity of the laser light. The maximum intensity of our laser ($\sim$ 100mW/cm^2) corresponds to a Rabi frequency $|\Omega_0| \sim 3.6\gamma_r$ which lies on the edge of Doppler-free region which is determined by $|\Omega_0| \geq W_d\sqrt{\gamma_0/\gamma} \approx 6\gamma_r$. The absorption further decreases the intensity and, as a result, the Doppler broadening becomes important, unlike in our simplified calculations.

Finally, we note that the observations reported here cannot be explained by spin exchange collisions between the atoms. The collisional cross section for Rb atoms is approximately 2×10^{-14} cm^2 [21] which results in a coherence decay rate $\gamma_0 \approx 2 \times 10^{-5}\gamma_r$ for the densities reported here. This is approximately two orders of magnitude less than the time-of-flight limited coherence decay rate $\gamma_0 \approx 4 \times 10^{-3}\gamma_r$ that we measured for the vacuum cell.

In conclusion, we have studied the atomic density dependence of the decay rate of the atomic coherence established by linearly polarized laser radiation between Zeeman sublevels of the ground state of Rb atoms. We have demonstrated that the experimentally observed enhancement of the decay rate may be explained by reabsorption of spontaneously emitted photons. We have developed a simplified theory of non-linear magneto-optic rotation which takes into account the destructive effect of radiation trapping. The predictions of this theory are in a good agreement with exact numerical simulations performed for the actual sublevel system. That means that the effect of radiation trapping plays an important role and should be taken into consideration in the CPT experiments in optically thick media.

CHAPTER V

MODIFICATION OF THE NONLINEAR FARADAY ROTATION IN THE PRESENCE OF BUFFER GAS

The thermal velocity distribution of atoms often results in Doppler broadening of the resonant features observed in atomic cells. It has been known for a long time that the restriction of the atomic motion leads to substantial narrowing of the resonant linewidth [237]. In practice this restriction is often achieved by diluting the resonant atoms in a gas of weakly interacting neutral atoms or molecules, usually called a buffer gas [238, 239]. The inert gases (Ne, Ar, Kr) as well as some simple diatomic (N_2, H_2) and organic (CH_4, C_2H_6) gases are commonly used as buffer gases in alkali vapor cells. Since the intrinsic spin of a buffer gas atom or molecule is zero, its collisions with alkali atoms does not change their population distribution. At the same time dephasing due to collisions produces small shifts of the atomic levels (pressure shifts) and additional homogeneous broadening of the atomic resonances (collisional broadening) proportional to the buffer gas pressure [21, 161, 163, 240].

The influence of Doppler broadening may be substantially reduced in multi-photon processes, such as coherent population trapping. Due to the two-photon nature of this process, CPT is possible only for very small values of the two-photon detuning, determined by the relaxation rate of the ground-state coherence. Thus, the width of the EIT resonances is not limited by either the Doppler broadening or the natural decay rate of the excited state.

The relaxation of the ground-state coherence is determined by many factors [21, 161]. If the density of atoms is not very high, so that the depolarization of the ground-state because of the spin-exchange collisions can be neglected, the main ground state relaxation mechanism is due to the destruction of the coherence by collisions with the walls of the cell [162]. For this reason, in hot atomic gases the ground-state coherence lifetime is normally determined by the interaction time of the moving atoms with the electromagnetic fields; once an atom has left the interaction region, it cannot return back without a collision with the wall. The time-of-flight is inversely proportional to the thermal velocity of the atoms and directly proportional to the laser beam diameter. For example, in the case of a 1 cm beam the width of an EIT resonance in Rb vapor at room temperature is limited to a few tens of kHz.

There are several methods to reduce the resonance width. The expansion of the laser beam is limited by the geometry of the experimental setup and/or the laser intensity. The relaxation of the ground-state coherence on the walls can be avoided by anti-relaxation coatings, such as paraffin [171, 172, 241, 242]. Extremely narrow resonances are reported in experiments on optical pumping [172,243,244] and Zeeman coherence [45, 133, 134]. At the same time manufacturing of the wall-coated cells is a complicated and technically challenging process which vastly limits their availability.

Filling an atomic cell with additional buffer gas is a quite simple and effective way to obtain the narrow EIT resonances. The interaction time can be reduced by several orders of magnitude, since now atoms diffuse rather than fly through the laser beam. There is a large number of publications devoted to the study of the relaxation processes of the atomic populations and coherences in various buffer gases in optical pumping experiments [20, 21, 161] and the CPT- and EIT-related experiments [165, 245, 246]. In general, the ground-state coherence decay rate γ_0 in the buffered cells is determined by the diffusion time of the atom through the laser beam and the dephasing due to the collisions with the buffer gas atoms. Under the approximation of small laser beam diameter ($d \ll D$, where d and D are the diameters of the laser beam and the atomic cell) γ_0 can be written as [21, 165]:

$$\gamma_0 = 2.405^2 \frac{D}{a^2} \frac{1}{1 + 6.8\lambda/a} + 2\sigma_{\mathrm{dph}} v_T n_b, \tag{5.1}$$

where $a = d/2$ is the laser beam radius, D is the diffusion coefficient, $\lambda = 3D/v_T$ is the mean free path, σ_{dph} is the ground-state relaxation cross-section, $v_T = \sqrt{2k_B T/M}$ is the average thermal velocity of the Rb atoms (k_B is the Boltzmann constant, T is the temperature of the cell, and M is the mass of a Rb atom), n_b is the density of the buffer gas atoms. The first term describes the escape of the atom from the interaction region, its dependence of the buffer gas pressure p is determined by the diffusion coefficient $D = D_0(760/p[\mathrm{Torr}])$, where D_0 is the diffusion coefficient for the buffer gas pressure equal to 1 atmosphere. The second term is due to the collisional dephasing, and it grows linearly with buffer gas pressure ($p = 2/3 n_b k_B T$). Thus, there exists an optimal value of the buffer gas pressure corresponding to the minimum relaxation rate which has been observed experimentally [245]. The minimum ground-state coherence decay rate for hot Rb atoms ($T = 400$K), diluted in Ne buffer gas ($D_0 = 0.5$ cm$^2/s$, $\sigma_{\mathrm{dph}} = 5.2\ 10^{-23}$ cm^{-2} [21]) is estimated to be $\gamma_{0\min} \sim 11/[a]$ Hz (a is in centimeters), providing the optimal buffer gas pressure is $p \sim 400[a]$ Torr. Thus, for a 2 mm laser beam the relaxation rate $\gamma_0 \sim 100$ Hz is expected for the buffer gas pressure $p = 40$ Torr.

Velocity-changing collisions with the buffer gas atoms should be also taken into account for an accurate description of the light-atom interaction. If a collision happens much faster than the characteristic times of the atomic relaxation processes, the velocity change is equivalent to an instantaneous detuning of the laser field without change in the atomic state. There have been a number of theoretical [162, 165] and experimental [246–248] studies of the effect of velocity changing collisions on coherent population trapping which demonstrated that the ground-state coherence survives up to 1000 Torr buffer gas pressure. Moreover, Dicke narrowing is responsible for the elimination of the residual Doppler broadening [246].

In this Chapter we experimentally study the effect of the buffer gas addition on the coherence formed between Zeeman sublevels of the same hyperfine level using nonlinear magneto-optic rotation in optically dense Rb vapor. Although the restriction of the atomic motion due to the buffer gas results in the expected narrowing of the resonance linewidth, we also observe a reduction of the polarization rotation and EIT contrast as buffer gas pressure increases. We attribute this to the influence of the hyperfine structure of the excited state. We also demonstrate that the narrow features in both rotation and transmission appear due to the atoms which temporarily leave the interaction region (or change their velocity so that they do not interact with the light), allowing the coherence to evolve for a time significantly longer than the transient time.

A. The effect of velocity-changing collisions on Zeeman coherence

The simple theory developed in Chapter II for the nonlinear Faraday effect in a three-level system predicts that the polarization rotation angle for small magnetic field is inversely proportional to the decay rate of the ground-state coherence (Eq.(2.70)). So one would expect a dramatic enhancement of polarization rotation in case of buffered cells due to the longer coherence lifetime. This prediction, however, is not supported by the experimental data for polarization rotation in Rb atoms.

To study the effect of the addition of buffer gas, we observe the spectral dependence of the rotation rate $d\phi/dB$ for several glass cells filled with ^{87}Rb vapor and various amount of a buffer gas. Since the lengths of the cells differ, the temperature is adjusted in each case so that the total minimum transmission is $I_{out}/I_{in} \approx 0.8$. The observed spectra are shown in Fig. 23. For the cell without buffer gas, the rotation rate as a function of laser frequency consists of two partially resolved peaks corresponding to transitions of the two hyperfine sublevels ($F' = 1$ and $F' = 2$) of the excited state. The width of both peaks is determined by Doppler broadening, and their shape is well fit by the sum of two Gaussian functions.

The situation is quite different for the atomic cells with buffer gas. First, we do not observe the predicted enhancement of the polarization rotation. Although for small amounts of buffer gas the value of the rotation rate increases significantly (compare results for the cell without buffer gas and cells with 0.12 Torr or 1 Torr of Ne in Fig. 23). Higher buffer gas pressure actually causes a reduction of the rotation rate which cannot be explained by increasing of γ_0 due to collisional dephasing of ground state coherence [21]. At the same time, one can see that the rotation spectra as a function of laser frequency are broadened far beyond the predicted collisional broadening [163]. Simultaneously, the linear absorption line does not exhibit such behavior.

Another unexpected feature is observed if the laser is tuned between the transitions. Even for small amounts of buffer gas, the rotation goes to zero and even becomes negative. A similar effect is reported in experiments with alkali vapor cells with anti-relaxation coatings [249]. At the same time the maximum rotation rate is no longer observed at the frequency of atomic transitions, but shifted away.

We believe that the effects listed above occur because of the internal structure of the alkali atoms and the diffusion in coordinate and velocity space associated with collisions with buffer gas atoms or coated walls. To account for these factors, we must solve a modified time-evolution equation for the density matrix operator $\hat{\rho}$, which

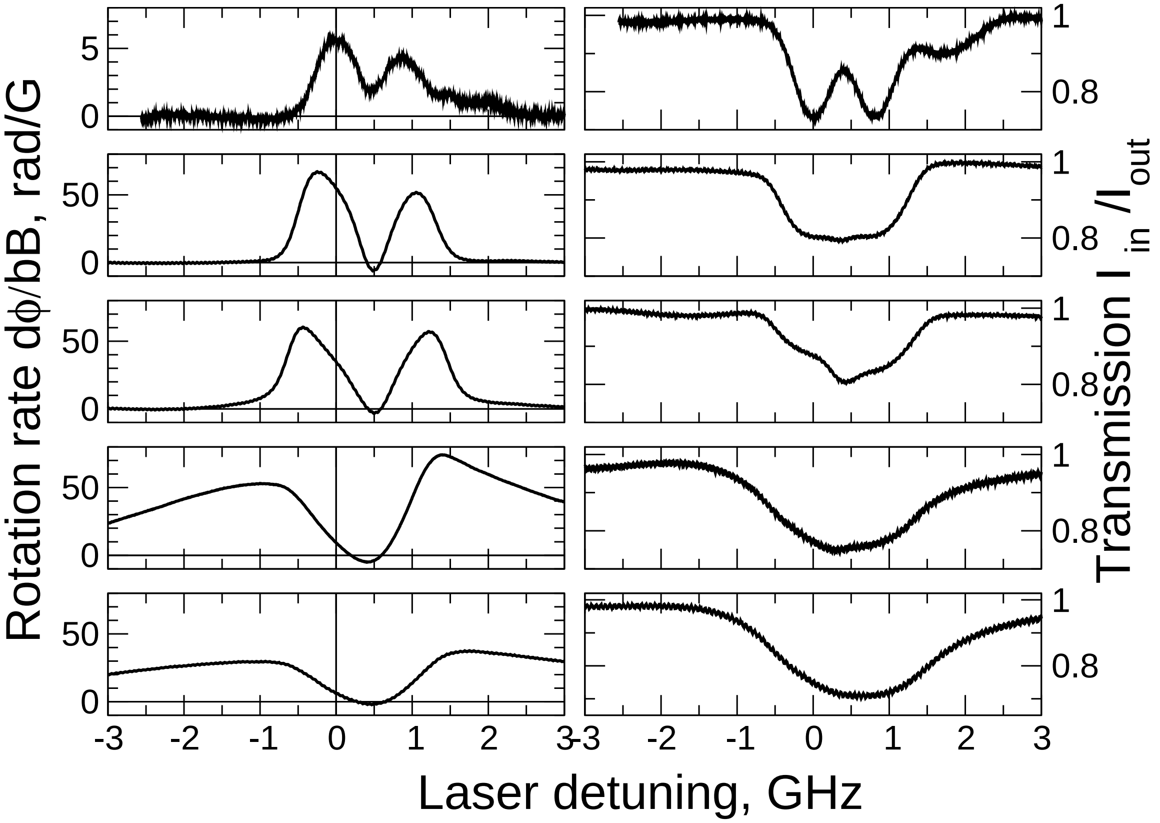

Fig. 23. Polarization rotation rate $d\phi/dB$ and transmission I_{out}/I_{in} of linearly polarized coherent laser radiation through an atomic cell as a function of laser detuning from the ^{87}Rb $F = 2 \rightarrow F' = 1$ transition. Data are presented for cells with (from top to bottom) 0 Torr, 0.12 Torr, 1 Torr, 10 Torr, and 30 Torr of buffer gas. For each nonzero buffer gas pressure, some frequency may be found such that zero polarization rotation is observed.

includes a kinetic term to describe atomic interaction with the buffer gas [251, 252]:

$$\frac{d\hat{\rho}}{dt} = -\frac{i}{\hbar}[\hat{H}, \hat{\rho}] - \frac{1}{2}\{\hat{\Gamma}, \hat{\rho}\} + \hat{L}\hat{\rho} + R, \tag{5.2}$$

where $\hat{H}$ is the interaction Hamiltonian for the light and atoms, $\hat{\Gamma}$ is the relaxation matrix, $\hat{L}$ is the collisional operator, and R is the pumping term. The exact solution, however, is extremely complicated, and cannot be obtained even numerically. Instead we experimentally study the modification of the nonlinear Faraday rotation and transmission spectra in two limiting cases: when the mean free path of Rb atom is much smaller than the laser beam diameter (high buffer gas pressure), and when they are comparable (low buffer gas pressure).

1. Low buffer gas pressure

First, we study the nonlinear Faraday rotation in a glass cell filled with ^{87}Rb vapor and 0.12Torr of Kr as a buffer gas. The mean free pass of Rb atoms in this case is $\lambda \approx 1.5$ mm, which is very close to the laser beam diameter $d = 2$ mm.

To investigate the effect of buffer gas addition on the nonlinear Faraday effect more closely, we scan the laser frequency across all four possible transitions of the Rb D_1 line and monitor three parameters. First one (Fig. 24a) is the contrast of the EIT peak:

$$C = \frac{I_{EIT} - I_{one-photon}}{I_{EIT} + I_{one-photon}}, \tag{5.3}$$

where $I_{EIT} = I_{out}(B = 0)$ is the transmission through the cell under EIT conditions, and $I_{one-photon}$ corresponds to one-photon transmission when the coherence is destroyed by large magnetic field ($B \approx 1G$). We also measure the polarization rotation rate $d\phi/dB$ for zero magnetic field (Fig. 24b)and the polarization rotation angle ϕ for the magnetic field close to the rotation resonance width $B = 0.1G$ (Fig. 24c).

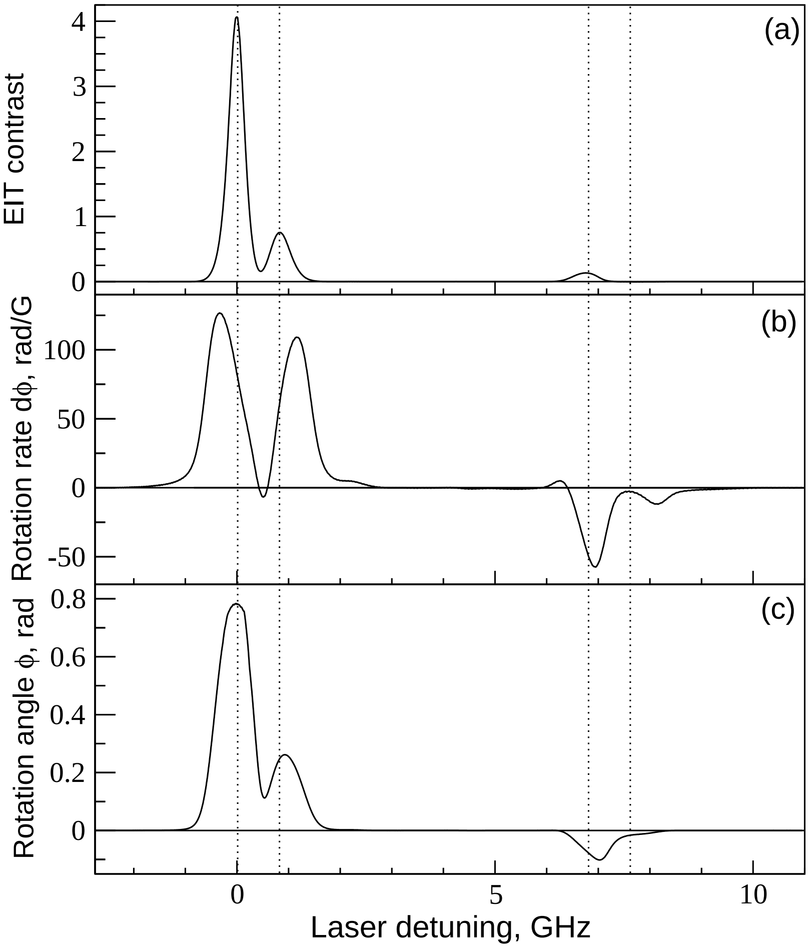

Fig. 24. (a) The EIT contrast, (b) the rotation rate $\frac{d\phi}{dB}\Big|_{B=0}$, and (c) the polarization rotation angle ϕ for $B = 100$mG as functions of the laser frequency in the ^{87}Rb cell with 0.12 Torr Kr buffer gas. Zero detuning corresponds to the $F = 2 \rightarrow F' = 1$ transition. The atomic density is $N = 5.2 \cdot 10^{11}\mathrm{cm}^{-3}$.

Comparison between these data and the analogous set for the cell without buffer gas (Fig. 8) immediately shows that the EIT contrast and the polarization rotation angle spectra are quite similar: they are still very well fit by the sum of gaussian-shaped peaks, corresponding to Doppler-broadened partially-resolved transitions. The main difference appears in the rotation rate $d\phi/dB$. Let us recall that this parameter is very sensitive to the value of the coherence decay rate, and any processes which affect the ground-state coherence should have a strong influence on the polarization rotation in the vicinity of zero magnetic field.

For a more comprehensive analysis we now record the transmission and polarization rotation angle as a function of magnetic field as the laser frequency is tuned across the $F = 2 \rightarrow F' = 1, 2$ transition. These transitions are more interesting for the present study, since they both form dark states, and the NMOR may be explained from the point of view of CPT on Zeeman sublevels. Fig. 25 clearly shows that the polarization rotation and transmission spectra consist of two resonances of the different widths. The properties of the wide resonance are very similar to those of the NMOR spectra in bufferless cell, and its width is defined by the time-of-flight of the atoms through the laser beam. The narrow feature, however, is quite different: if the laser is resonant or red-detuned from the $F = 2 \rightarrow F' = 1$ transition, it leads to the enhancement of polarization rotation, whereas for the laser tuned between two excited states ($\Delta \sim 400$ MHz) the sign of this rotation is reversed, which is responsible for the negative polarization rotation rate here. [1]

---

[1] We assume that when the magnetic field is much smaller than the width of the narrowest resonance, the polarization rotation is a linear function of the magnetic field. In this case the rotation rate may be experimentally measured by subtracting two rotation spectra for $B = \pm 1mG$, and dividing them by the variation of the magnetic field. The polarization rotation rate $d\phi/dB(B = 0)$ provides the information primarily on the narrow feature in the vicinity of zero magnetic field, and the polarization rotation for nonzero magnetic field reflects the properties of the wider resonances.

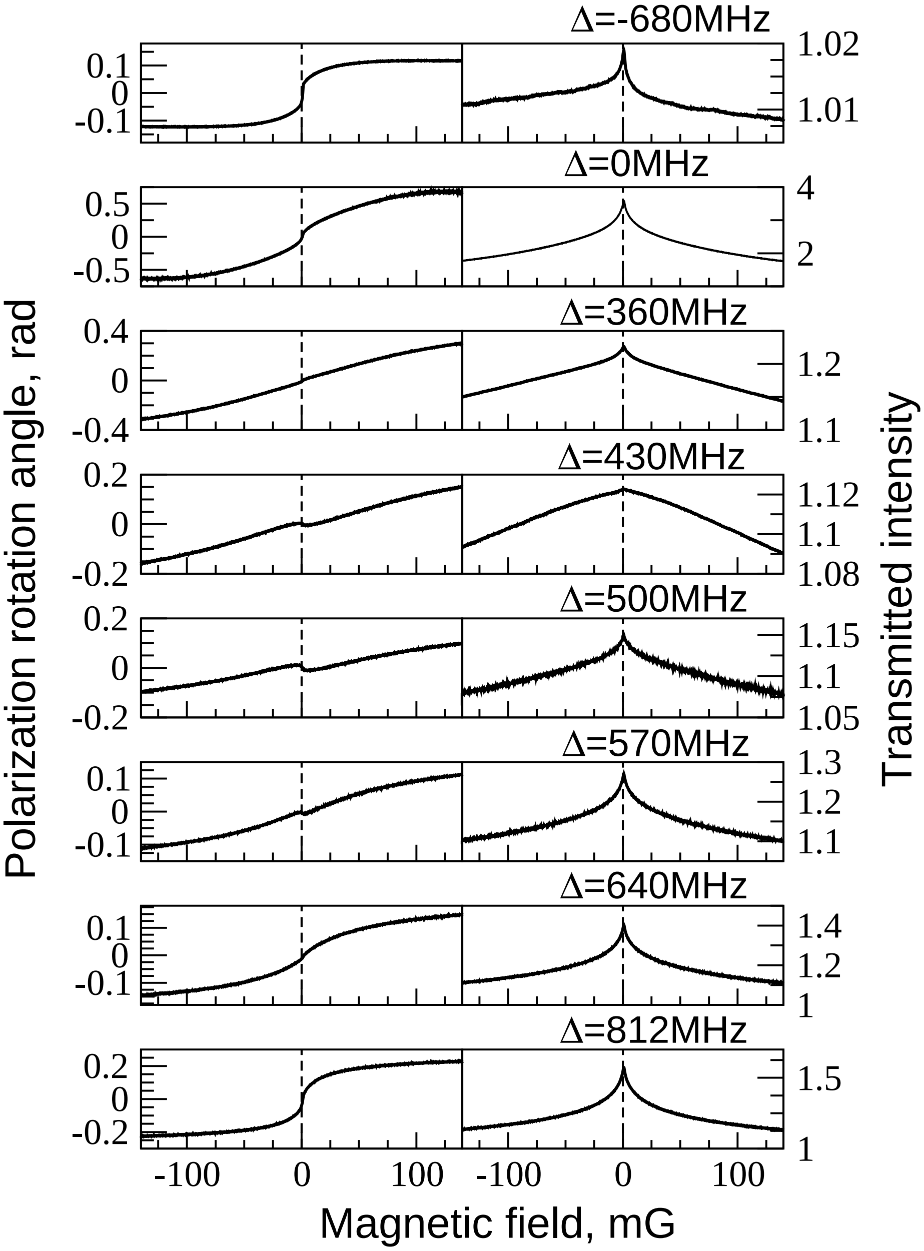

Fig. 25. The polarization rotation (left column) and transmitted intensity (right column) as functions of the applied magnetic field for different laser detunings in ^{87}Rb cell with 0.1 Torr Kr buffer gas. The transmitted intensity is normalized to the transmission without EIT (for large magnetic field). Zero detuning corresponds to the $F = 2 \rightarrow F' = 1$ transition. Note the scale difference for each graph. The atomic density $N = 5.2 \cdot 10^{11}\mathrm{cm}^{-3}$.

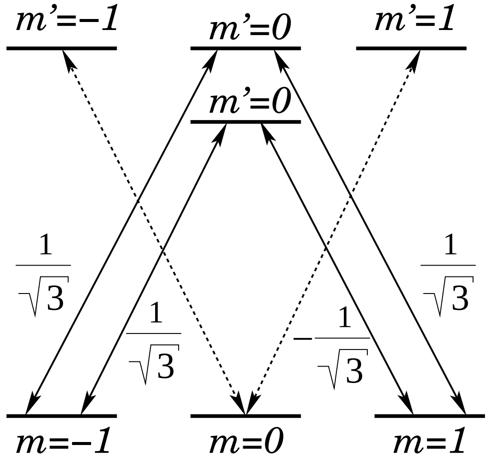

Fig. 26. Dipole moments for the transitions the $F = 1 \rightarrow F' = 0, 1$; solid arrows show the transition which take part in the dark states formation; dotted arrows are used for the other transitions.

The existence of resonances of two different widths suggests that there are two distinctive relaxation mechanisms for the Zeeman coherence. In the limit of low buffer gas pressure the properties of NMOR, determined by the transient effect, (wide resonance) should not depend much on the presence of buffer gas, since the probability of collision between a Rb atom and a buffer gas atom is low. However, there is a nonzero probability, that an atom, prepared in dark state during the interaction with the laser beam, will return to the interaction region as a result of collisions with buffer gas atoms before its coherence is destroyed [136,137]. Since the coherence lifetime for these atoms is much longer than the time-of-flight, this process results in narrower resonances in polarization rotation, observed in the vicinity of the magnetic field. This phenomenon is very similar to ultra-narrow features observed in paraffin-coated cells by Budker *et al.* (compare NMOR spectra shown in Fig. 25 with those reported in Ref. [134]).

To explain sign change of the narrow polarization rotation resonance, we need to look closely at the values of the transition dipole moments within the allowed transitions. Since the $F = 2 \rightarrow F'$ level structure is complicated, we use the simpler $F = 1 \rightarrow F' = 0, 1$ transitions instead. In this system, the dark state can be formed among $m = \pm 1$ sublevels of the ground state either through excited state $F' = 0, m' = 0$ or $F' = 1, m' = 0$, depending on the laser detuning. As shown in Fig. 26, the dipole moments for all four transition have the same absolute value, but one of them $\wp_{F=1,m=1 \rightarrow F=0,m=0}$ is negative. Thus, the dark states $|D_{10}\rangle$, formed on the $F = 1 \rightarrow F' = 0$, and $|D_{11}\rangle$, formed on the $F = 1 \rightarrow F' = 1$ transition, are different and, in the case of linearly polarized light, orthogonal:

$$|D_{10}\rangle = \frac{\Omega_+|b_+\rangle + \Omega_-|b_-\rangle}{\sqrt{|\Omega_+|^2 + |\Omega_-|^2}}; \tag{5.4}$$

$$|D_{11}\rangle = \frac{\Omega_+|b_+\rangle - \Omega_-|b_-\rangle}{\sqrt{|\Omega_+|^2 + |\Omega_-|^2}}. \tag{5.5}$$

In the case of Rb atoms, the hyperfine splitting between excited levels is big enough ($\Delta_{hfs} \gg \gamma$), so if the electromagnetic field is resonant with one of the atomic transitions, the influence of the other is negligible. The relative phase of the dark state does not matter for a bufferless Rb cell, since the velocity of an atom does not change during the interaction process, and each atom interacts with the light field on only one transition.

The situation is very different, however, if a buffer gas is added, and velocity-changing collisions become possible. Now a Rb atom, pumped into dark state on one transition, may be suddenly "switched" to the other one as a result of a collision. In this case the state of the atom with respect to this transition is a bright state, and the ground-state coherence is rapidly destroyed. Thus, in an ideally symmetric scheme one would expect the complete cancellation of EIT and the nonlinear Faraday rotation for a laser tuned exactly halfway between the transitions to the excited hyperfine sublevels, when the probabilities of interaction of atoms with either transition are equal. In reality, however, the complicated magnetic structure should be taken into account, which results in a difference in the transition strengths (i.e. the polarization rotation on the $F = 2 \rightarrow F' = 2$ transition is noticeably weaker). This imbalance leads to the reverse of the sign of the polarization rotation and enhancement of the light absorption.

It is also clear that for small buffer gas pressure the change of sign of the rotation angle occurs only for the narrow structure, which appears due to the contribution of the atoms returning into the beam after some spatial diffusion. Indeed, the atoms responsible for the wide resonance (determined by the diffusion time of the atom through the laser beam) are not likely to change their velocity while passing the interaction region. Therefore, the properties of the corresponding rotation and absorption resonances are not differ from the case of a cell without buffer gas. On the contrary, the returning atoms have a Doppler velocity distribution after several collisions with the buffer gas atoms, effectively mixing the dark states formed on different transitions, as we see in our experiment.

For this reason the polarization rotation on the D_2 line of Rb (on which the splitting between excited hyperfine levels are almost an order of magnitude smaller) deteriorates very rapidly with addition of a buffer gas, and almost completely disappears for buffer gas pressure more than 1 Torr, as shown in Fig. 27.

2. High buffer gas pressure

As the buffer gas pressure grows, the changes in the rotation rate become more profound: the central drop between transitions $F = 2 \rightarrow F' = 1, 2$ becomes wider and the rotation maxima move farther away from the resonance frequencies (Fig. 28b). At the same time, since mean free pass is much smaller than the laser beam diameter ($\lambda \approx$

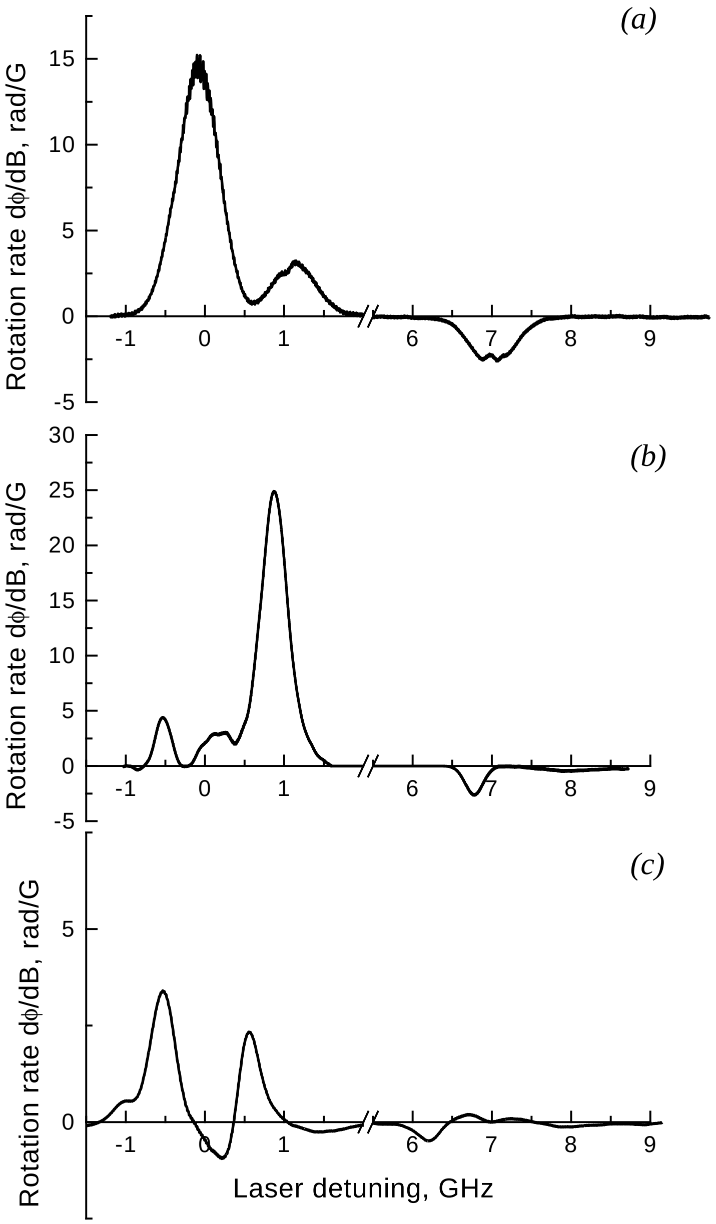

Fig. 27. Polarization rotation rate $d\phi/dB$ ($B = 0$) for the D_2 line of ^{87}Rb in an atomic cell with (a) no buffer gas (the additional rotation peak at a detuning about 1 GHz is due to residual ^{85}Rb); (b) 0.12 Torr of Kr; and (c) 1 Torr of Ne. Laser power is 2.5 mW, the temperature is adjusted for each cell so that the total transmission on the $F = 2 \rightarrow F'$ transition is about 80%. Zero laser detuning is chosen to coincide with the center of the absorption peak of the $F = 2 \rightarrow F'$ transition.

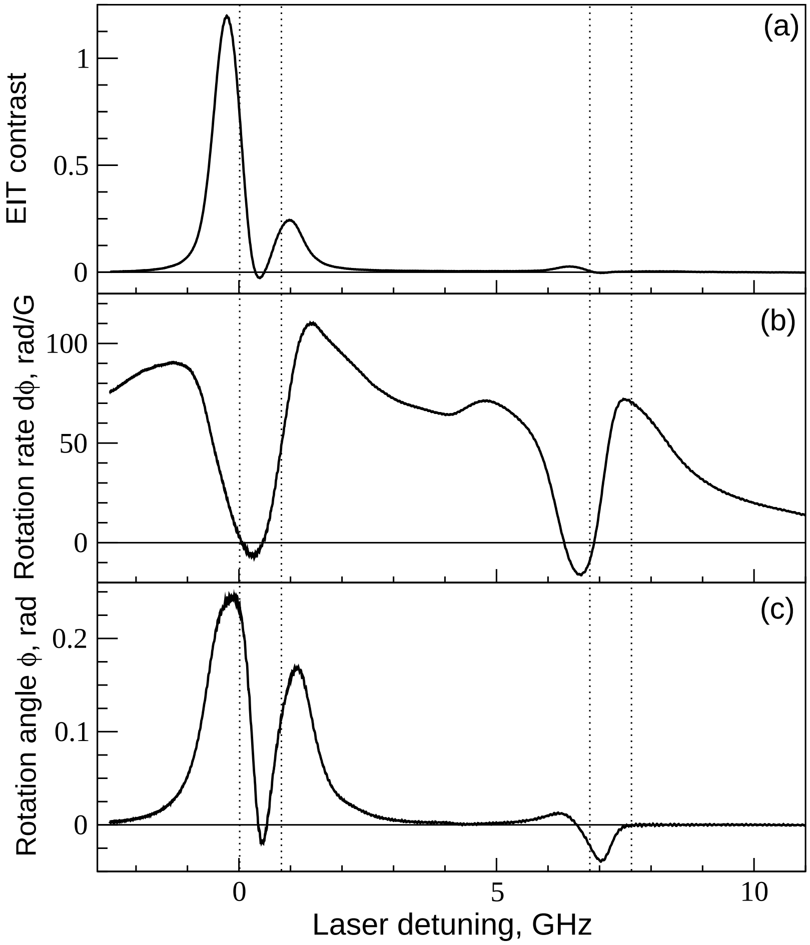

Fig. 28. Same as for Fig. 24 in ^{87}Rb cell with 10 Torr Ne buffer gas. The atomic density $N = 2.1 \cdot 10^{12}\mathrm{cm}^{-3}$.

$3 \cdot 10^{-2}$ mm), similar modifications occur for the wide resonance as well. Enhanced absorption is observed when the laser tuned between two atomic transitions. This is accompanied by a negative polarization rotation (Fig. 28a and c, Fig. 29). It is also important to note that efficient mixing of all velocity groups results in a reduction of both EIT contrast (1.4 for 10 Torr vs. 4.2 for 0.12 Torr) and maximum polarization rotation angle (0.8 rad vs. 0.25). However, for the same reason the range of laser frequencies where the polarization rotation occurs is extended significantly for the high buffer gas pressure cells: even if the laser detuned quite far from the atomic transition, and only a tiny fraction of all atoms in the Doppler distribution "sees" the laser field, each atom changes its velocity many times while travelling through the laser beam and its probability to have a resonant velocity at least for some time increases. One can see that for the Rb cell with 10 Torr of buffer gas the rotation peaks, corresponding to the transition from the different ground hyperfine levels (split by 6.8 Ghz) are not resolved.

B. The shape of NMOR resonances in the presence of buffer gas

Now let us study the dependence of the width and the maximum rotation angle for both narrow and wide rotation resonances on laser power. For this purpose we use the cell with 10 Torr of Ne and fix the laser frequency to be exactly between the $F = 2 \rightarrow F' = 1, 2$ transitions (i.e. detuned 400MHz from either of them). In this case two resonant features are resolved, and the width of both narrow and wide resonance may be measured accurately. At this frequency, both rotation curves are inverted with respect to the direction of the polarization rotation without buffer gas at the same magnetic field which corresponds to enhanced absorption resonances of the same widths. The atomic density of Rb vapor is $N = 6 \cdot 10^{11}\text{cm}^{-3}$, so that the

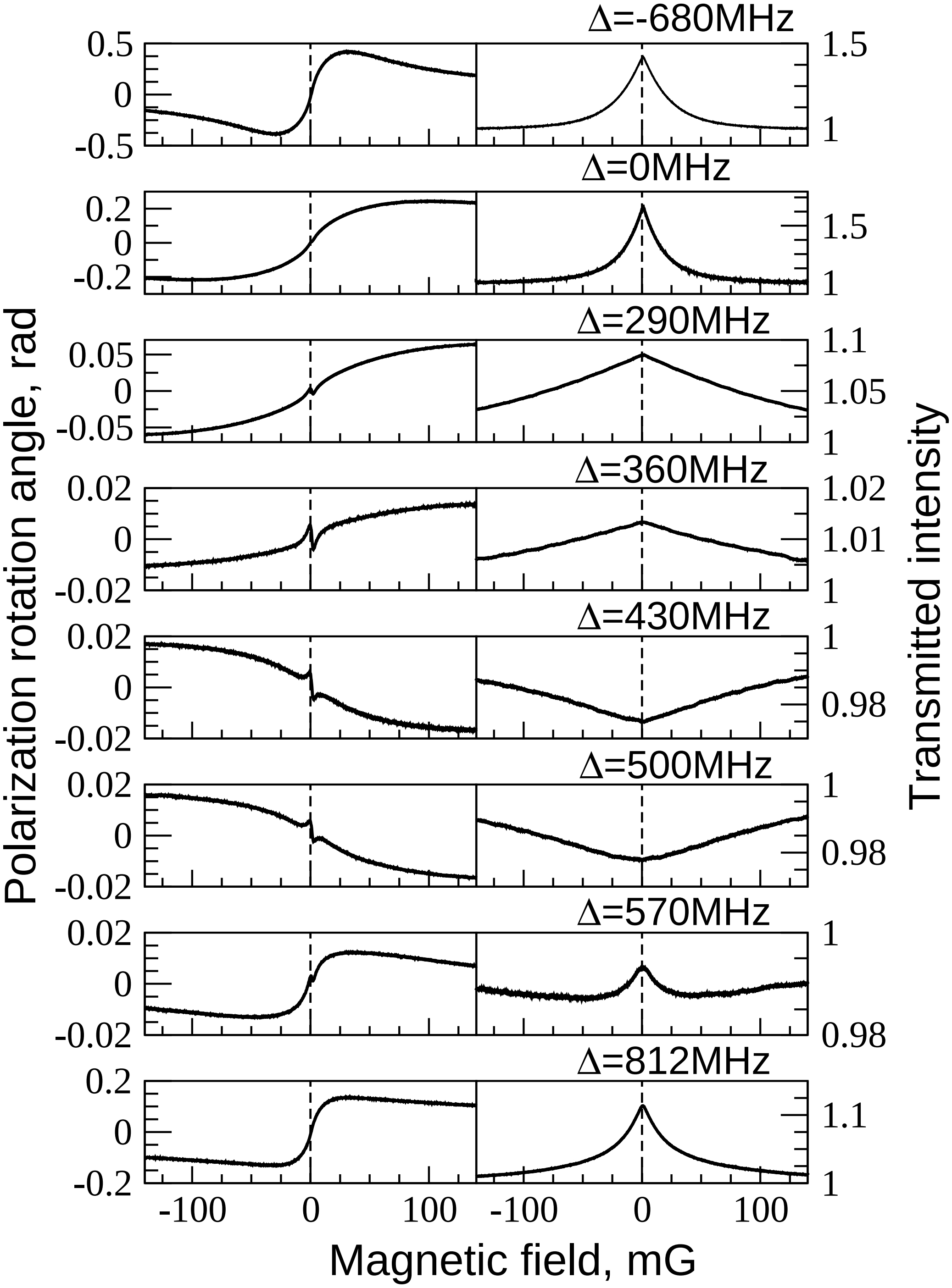

Fig. 29. Same as for Fig. 25 in ^{87}Rb cell with 10 Torr Ne buffer gas. The atomic density $N = 2.1 \cdot 10^{12}\text{cm}^{-3}$.

transmission for laser power $P = 2mW$ is about 90%.

The presence of buffer gas has little affect on the shape of the wide resonance. The enhanced absorption resonance corresponding to the wide rotation also resembles the triangular-shaped EIT resonance in a bufferless cell (compare with Fig. 16). In this case the width of the rotation resonance is defined as the distance between opposite rotation maxima. At the same time, the shape of the narrow rotation resonances is well-described by a Lorenzian function (Fig. 30a inset):

$$\phi(B) = \phi_{\max} \frac{wB}{w^2 + B^2}, \tag{5.6}$$

where $\phi_{\max}$ is the maximum rotation angle, and w is the width of the resonance.

The data for the width of both narrow and wide resonances as well as the maximum polarization rotation angle for different laser intensities are presented in Fig. 31. Note that the behavior of either of them is quite different for narrow and wide resonances. For the wide resonance the maximum polarization rotation angle is practically constant, whereas the width of the resonance falls linearly with laser power. This kind of behavior is expected from the power-broadened EIT-related resonance in the Doppler-free interaction regime ($|\Omega| \gg W_D\sqrt{\gamma_0/\gamma}$) [188]. On the other hand, since the narrow rotation resonance is due to the atoms which spend most of the coherence evolution time outside the laser beam, the narrow resonances are practically insensitive to power broadening (Fig. 31b), and the corresponding value of the maximum rotation exhibits the square-root dependence on laser power.

C. Detection on non-resonant impurities using the nonlinear Faraday effect

Atomic cells containing alkali vapors are a basic element in atomic clocks, frequency standards, optical magnetometers and many other high precision spectroscopic de-

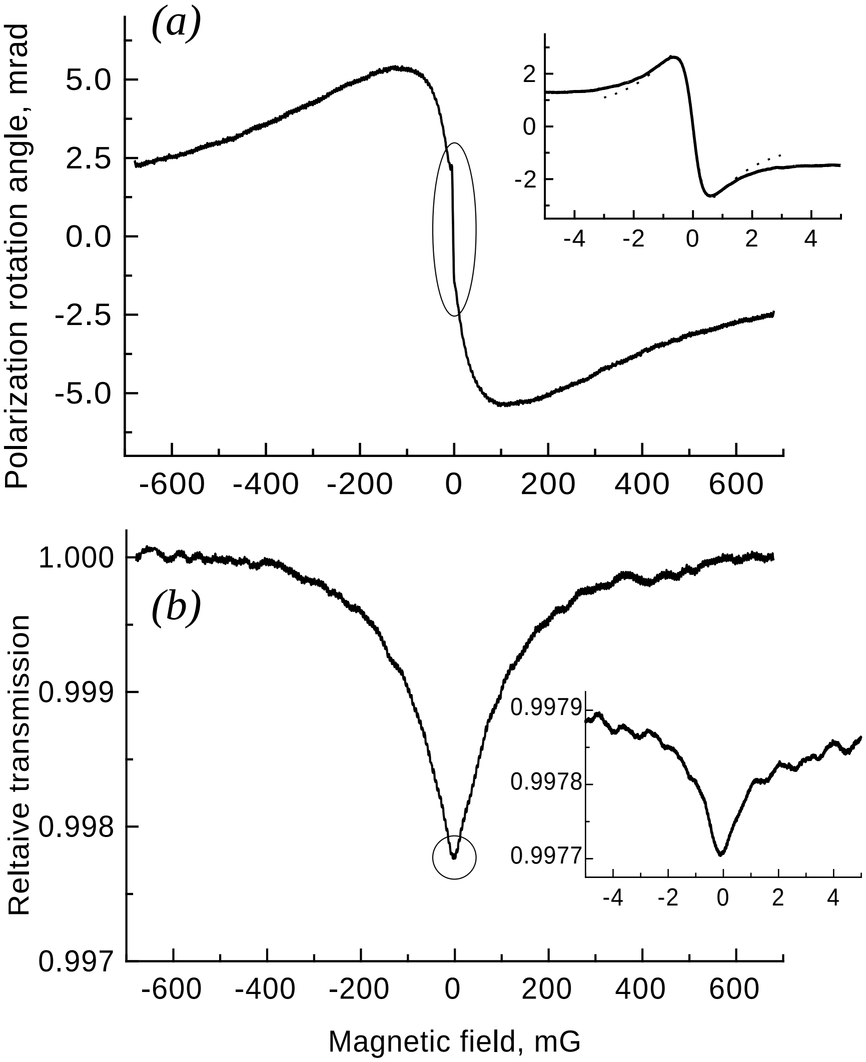

Fig. 30. (a) The polarization rotation angle as a function of magnetic field. Inset: central narrow resonance; dotted line - lorentzian fit. (b) The transmission of the laser field through the cell. Inset: central narrow absorption resonance, corresponding to the narrow rotation.

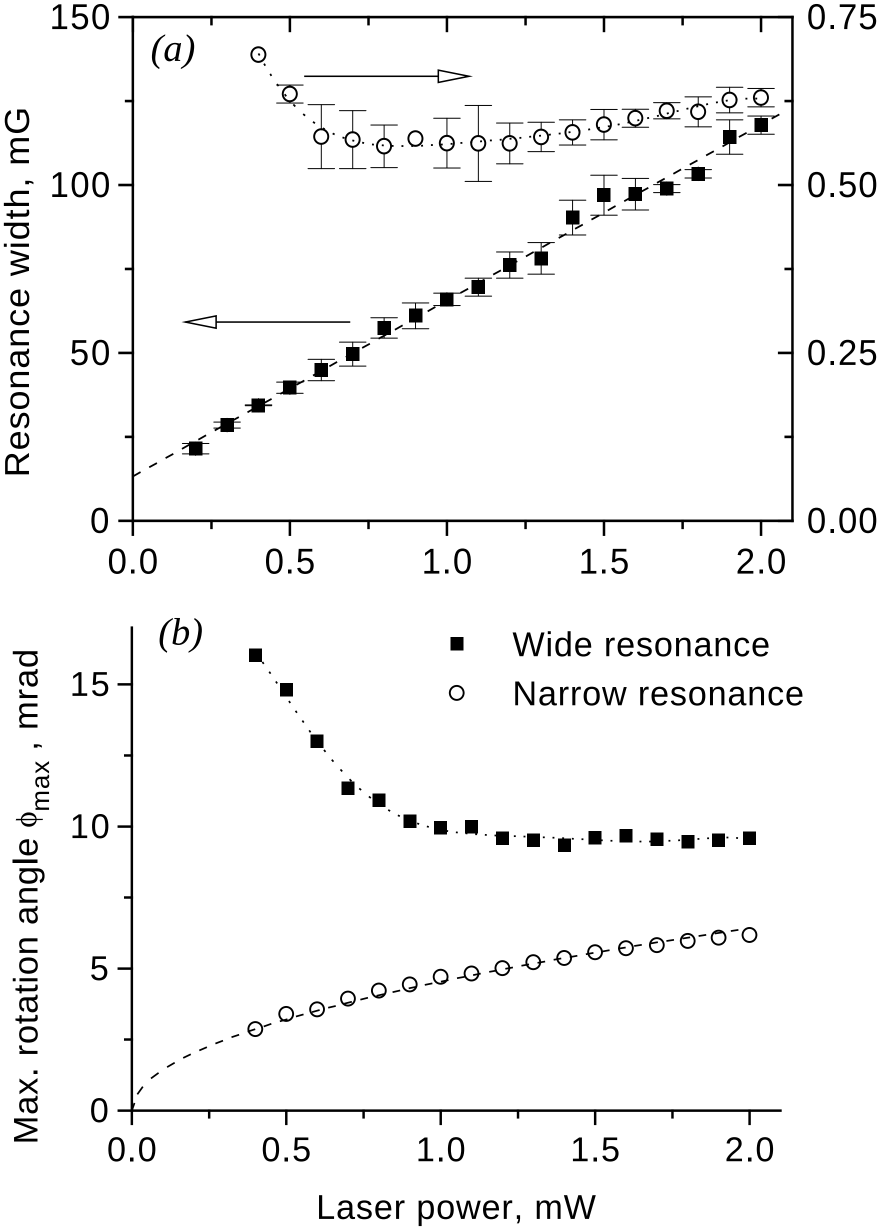

Fig. 31. (a) The maximum polarization rotation angle and (b) the width of the rotation resonance for both narrow and wide structures. On (a) the dashed line represents the square-root fit, the dotted line is to guide the eyes. On (b) the best linear fits are shown for both curves.

vices. Impurities in the cells, for example, due to atmosphere leakage or improper cell fabrication may cause serious changes in the performance of these devices.

Although it is always possible in principle to detect any gas in an atomic cell using broad-band spectroscopic techniques, this may not always be convenient. In many situations, the only spectroscopic sources present may be narrow band lasers tuned to the atomic transitions interesting for experiments to be performed on the alkali atoms. If the impurity resonance frequencies lie outside the tunable range of these lasers, the only way to detect the impurity must be based on measurements of parameters of the atoms of interest. The question is: what property of alkali atomic vapor is both sensitive to the presence of an impurity and convenient for precise measurements?

Photon echoes can be used for buffer gas detection. It was recently shown that coherence among ground state Zeeman sublevels of Rb atoms can be used for detection of a perturber (Ar) in an atomic cell [253]. In this experiment, the cross-section for Rb-Ar velocity changing collisions was inferred from properties of coherence grating echoes [254]. However, photon echoes are essentially transient phenomena with a complicated experimental implementation.

Our experiments demonstrate that the nonlinear Faraday rotation may be used as a sensitive detector of a buffer gas in an atomic cell. The existence of the "hole" between resonances is a clear indication of the presence of a buffer gas in the cell, and it may be used for a leak control [2]. The effect is even more dramatic for the D_2 line of Rb, since the excited sublevels are closer to each other. In this case the polarization rotation almost completely vanishes for buffer gas pressure as low as 1Torr.

For precision measurements there are several parameters to consider: the position and the value of the maximum rotation, the value of the rotation versus laser detuning, etc. We suggest measurement of the value of the rotation rate $d\phi/dB$ at the resonance frequency for given transmission as the best compromise between experimental complexity and sensitivity to the presence of buffer gas. Our experimental results show that the maximum rotation rate is of the same order of magnitude for a wide region of buffer gas pressures ($0.1 \div 10$ Torr). However, the rotation rate at resonance decreases because of the shift of the rotation maximum. The value of rotation may be easily measured, and the amount of buffer gas is found from these data.

---

[2] A discovery of a leaky cell in our lab gave rise to this study.

Certainly, there are existing experimental techniques with greater sensitivity to various gas atoms, with perhaps the most notable being residual gas analysis mass spectroscopy. However, the method described here has several advantages, most notably that it is completely non-invasive, provides reliable information for any kind of buffer gas, and uses only a single stabilized diode laser that may already be present in spectroscopy experiments.

In conclusion, we demonstrated the profound effect of a buffer gas on the Zeeman coherence. The diffusion of atoms in a buffer gas gives rise to an additional narrow feature in nonlinear Faraday rotation. At the same time velocity-changing collisions produce effective mixing of the dark states created on different hyperfine transitions, resulting in enhanced absorption between transitions and an inversion of the sign of the polarization rotation. A possible application of this effects is leak detection and buffer gas measurements in atomic cells.

CHAPTER VI

ELLIPTICITY-DEPENDENT MAGNETO-OPTICAL ROTATION VIA MULTI-PHOTON COHERENCE

As we demonstrated in the previous chapters, an accurate description of NMOR signals is obtained from an analysis of density matrix equations for the atomic polarizations and populations along with Maxwell equations describing propagation of the electromagnetic fields in the atomic medium. Even for the simplest interaction schemes (which consists of three or four energy levels), an analytical solution of these equations is not always available in a relatively simple form. For more elaborated systems the exact solution is very complicated, and in general may be obtained only numerically. Thus, to recover any analytical results the problem should be somehow simplified .

The traditional approach to a solution of the problem is based on the approximation of weak electromagnetic fields and low atomic vapor densities [86, 105, 109, 122], conditions found in early experiments involving incoherent radiation from atomic discharge lamps. In this case one can use perturbation theory, and the atomic susceptibility may be decomposed in a series of the electromagnetic fields involved. Magnetic field dependent terms of the susceptibility decomposition which are nonlinear in the electromagnetic fields are responsible for NMOR. It can be demonstrated that only two-photon processes are important in this approximation, and therefore complicated multilevel systems may be reduced to systems with small level number (such as Λ, V, or X–schemes) [92, 109, 255]. In this approximation, NMOR is a consequence of low frequency ground-state coherence formed by two-photon processes between Zeeman sublevels with difference in magnetic quantum numbers equal to $\Delta m = \pm 2$. In some cases it is convenient to describe the atom-light interaction from the point of view of light-induced multipole moments of the atomic electron distribution. Conventionally this is done in terms of an irreducible tensor representation of the density matrix [15, 256, 257]. In this case, the ground-state coherence is equivalent to the quadrupole moment, or alignment. It has been suggested that NMOR is a consequence of the alignment to orientation conversion [123], where the orientation is equivalent to the population difference between nearest Zeeman sublevels with $\Delta m = \pm 2$.

The simplified theoretical approaches used for weak electromagnetic fields generally fail for strong ones. The question that arises here is whether or not the interaction with strong fields bring new physics, e.g. if the higher order atomic coherences influence NMOR. Alkali atoms have a level structure which allows for a formation of the coherent superposition of the magnetic sublevels with $\Delta m = \pm 4$ (hexadecapole moment in the multipole decomposition of the interaction process) and even higher. Such coherences should be excited by multiphoton processes that include four or more photons. Gawlik *et al.* [85] observed strong narrow features in a forward scattering experiment with free sodium atoms, which were attributed to a hexadecapole moment. However, subsequent work of Giraud-Cotton *et al.* [86] and other groups [92, 109, 255] demonstrated that these features may be explained using third-order perturbation theory which includes only quadrupole moments.

There have been a number of publications where observation of hexadecapole and higher order moments is reported for the case where the magnetic field is perpendicular to the light propagation direction [30, 258]. At the same time, the question of their influence on forward scattering and NMOR signals in Faraday configuration is still open (see, for example, [93] and references therein). Generally, the interpretation of the experimental results in the case of strong laser fields and large multipole moments is very complicated. The high-order coherence causes only slight modifications of the rotation caused by the quadrupole moment, which hinders a convincing demonstration of these high-order effects.

We solve here both analytically and numerically the problem of the propagation of strong elliptically polarized electro-magnetic fields through resonant atomic media in the presence of a magnetic field. We particularly investigate the properties of the light which interacts with the magnetic sublevels in an M-like level configuration and, therefore, forms coherence with $\Delta m = 4$. We demonstrate that this coherence is responsible for a new type of polarization rotation which depends on both the light ellipticity and the applied magnetic field. We observe this effect in hot vapor of rubidium atoms. Since such rotation does not appear for an isolated Λ scheme, our experiment may be treated as a clear demonstration of the hexadecapole moment of atoms.

Another interesting and important feature of the system under consideration is connected with a large Kerr nonlinearity associated with NMOR. We analyze Kerr nonlinearity in the M level configuration and show that the ratio between the nonlinearity and the absorption may be large. Moreover, we show that by increasing the number of Zeeman sublevels (e.g. by using another Rb isotope or different alkali atom with higher ground-state angular momentum) it is possible to realize higher orders of nonlinearities. Our method of creation of the highly nonlinear medium with small absorption has prospects in fundamental as well as applied physics. It can be used for construction of nonclassical states of light as well as coherent processing of quantum information [259].

To bridge between this and previous studies we remind that NMOR may be attributed to coherent population trapping, and both EIT and CPT are able to suppress linear absorption of resonant multilevel media while preserving a high level of nonlinear susceptibility [260–262]. Previous theoretical studies of coherent media with large optical Kerr nonlinearities have described nonlinearities resulting from the effective self-action of an electromagnetic field at a single photon energy level, such as a photon blockade [263–266], or an effective interaction between two electromagnetic fields due to refractive [261,262,267,268] and absorptive [269] Kerr nonlinearities. The absorptive $\chi^{(3)}$ nonlinearities were studied experimentally for quasiclassical cases [270, 271]. It was shown quite recently, that a similar approach may lead to achievement of even higher orders of nonlinearity [272].

A method of producing Kerr nonlinearity with vanishing absorption is based on the coherent properties of a three-level Λ configuration (see Fig. 32a). In such a scheme the effect of EIT can be observed. Two optical fields, α_1 and Ω_1, resonant with the transitions of the Λ system, propagates through the medium without absorption. However, because an ideal EIT medium does not interact with the light, it also can not lead to any nonlinear effects at the point of exact transparency [1]. To get a nonlinear interaction in the coherent medium one needs to “disturb” the EIT regime by introducing, for example, additional off-resonant level(s) (level a_2 in Fig. 32b). In the following we refer to the resultant level configuration an N-type scheme. Such a scheme has been used in previous works [261–266, 268]. If the disturbance of EIT is small, i.e., the detuning Δ is large, the absorption does not increase significantly. At the same time, the nonlinearity can be as strong as the nonlinearity in a near-resonant two level system. Unlike the early ideas of Kerr nonlinearity enhancement, we propose to use not a single Λ scheme, but several coupled Λ schemes. In particular, we consider the M-type configuration as shown in Fig. 32c. Coherent population trapping exists in such a scheme, like in a Λ-type level system.

By introducing a small detuning, δ, we may disturb this CPT and produce a strong nonlinear coupling among the electromagnetic fields interacting with the atomic system, while having small absorption of the fields [273]. The dispersion of the M level media and associated group velocity of light propagating in the media

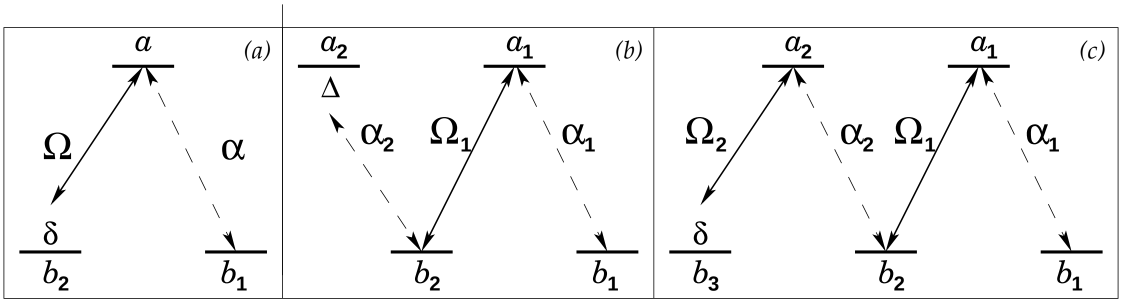

Fig. 32. Energy level schemes for (a) Λ-system; (b) N-system; (c) M-system.

are intensity dependent due to the nonlinearity, as was theoretically predicted by A. Greentree *et al.* [274]. Finally, in the case discussed below, energy levels of the M configuration correspond to Zeeman sublevels of alkali atoms. The multi-photon detuning is introduced by a magnetic field, resulting in the intensity dependent polarization rotation.

A. Analysis of NMOR in M interaction scheme

Let us concentrate first a $F = 2 \rightarrow F' = 1$ transition, which occurs in the ^{87}Rb D$_1$ line. The case of higher angular momenta is discussed in the next section. Interaction of elliptically polarized light with the $F = 2 \rightarrow F' = 1$ transition may be decomposed into a Λ scheme with $m = -1 \leftrightarrow m' = 0 \leftrightarrow m = +1$, and an M scheme $m = -2 \leftrightarrow m' = -1 \leftrightarrow m = 0 \leftrightarrow m' = +1 \leftrightarrow m = +2$, as shown in Fig. 33a. The distinguishing difference between an M scheme and a Λ scheme is that the higher order coherence ($\Delta m = 4$) becomes important. Since the Λ system had been studied in detail in Chapter II, we primarily concentrate on the M scheme here.

The M scheme is described by a set of twelve density matrix equations. The only straightforward way to solve this system is with numerical methods. However,

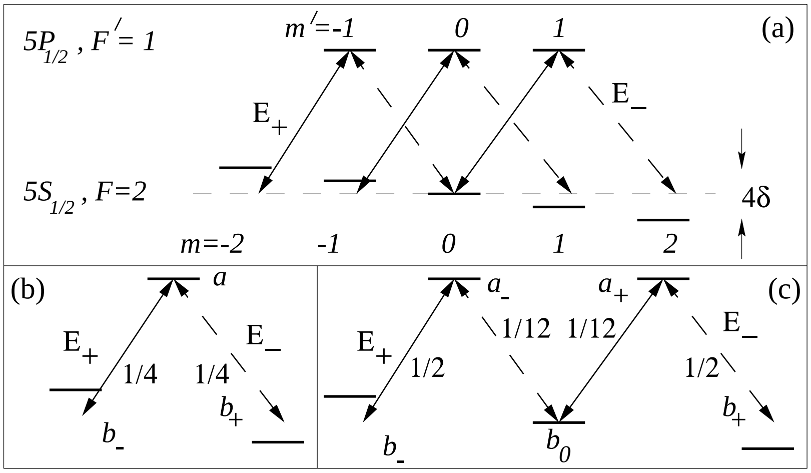

Fig. 33. a) Energy level scheme for ^{87}Rb atoms. This scheme may be decomposed into a superposition of b) Λ-system and c) M-system. Transition probabilities are shown for each individual transition.

if we study the atomic interactions with weak magnetic fields, the decay processes and polarization rotation processes are independent, and the polarization rotation may be found in analytical form under the condition of zero relaxation using the Hamiltonian diagonalization procedure. The modified Schrödinger equation model is suited for this as well. The optical losses may be found separately by considering optical pumping into the dark state with zero magnetic field.

1. Coherent population trapping in an M level scheme

It has been shown that the dark state exists even for atoms with complicated Zeeman substructure interacting with elliptically polarized light [276–281]. Here we recall the analytical expressions for this dark state and the corresponding eigenvalues. Using an effective interaction Hamiltonian, we derive propagation equations for the electromagnetic fields. We restrict our consideration to the case relevant to the M configuration consisting of Zeeman energy sublevels in the magnetic field. That is, we assume that the atomic transition frequencies are such that $\omega_{a_-b_0} = \omega_{a_+b_0} = \omega$, $\omega_{a_-b_-} = \omega - 2\delta$, and $\omega_{a_+b_+} = \omega + 2\delta$, where the detuning δ is due to a Zeeman shift, and the laser frequency ν is resonant with the atomic transition. The interaction Hamiltonians for M systems is

$$\begin{aligned} H_M &= -2\hbar\delta|b_+\rangle\langle b_+| + 2\hbar\delta|b_-\rangle\langle b_-| + \hbar(\Omega_{1-}|a_+\rangle\langle b_+| + \Omega_{2-}|a_-\rangle\langle b_0| \\ &+ \Omega_{1+}|a_+\rangle\langle b_0| + \Omega_{2+}|a_-\rangle\langle b_-| + H.c.), \end{aligned} \tag{6.1}$$

where $\Omega_{1-} = E_-\wp_{a+b+}/\hbar$, $\Omega_{1+} = E_+\wp_{a+b0}/\hbar$, $\Omega_{2-} = E_-\wp_{a-b0}/\hbar$, $\Omega_{2+} = E_+\wp_{a-b-}/\hbar$ (see Fig. 33c).

As in the Λ system, the eigenvalues of the interaction Hamiltonian can be determined from:

$$\begin{vmatrix} 2\delta-\lambda & \Omega_{2+}^* & 0 & 0 & 0 \\ \Omega_{2+} & -\lambda & \Omega_{2-} & 0 & 0 \\ 0 & \Omega_{2-}^* & -\lambda & \Omega_{1+}^* & 0 \\ 0 & 0 & \Omega_{1+} & -\lambda & \Omega_{1-} \\ 0 & 0 & 0 & \Omega_{1-}^* & -\lambda-2\delta \end{vmatrix} = 0 \tag{6.2}$$

Also, as in the Λ scheme, the eigenvalue $\lambda = 0$ and corresponding “dark state” exists only for $\delta = 0$:

$$|D\rangle = \frac{\Omega_{1+}\Omega_{2+}|b_+\rangle - \Omega_{1-}\Omega_{2+}|b_0\rangle + \Omega_{1-}\Omega_{2-}|b_-\rangle}{\sqrt{|\Omega_{1-}|^2|\Omega_{2+}|^2 + |\Omega_{1+}|^2|\Omega_{2+}|^2 + |\Omega_{1-}|^2|\Omega_{2-}|^2}} \tag{6.3}$$

It is worth noting that, similar to the Λ system, the non-vanishing low frequency coherences ρ_{b+b0} and ρ_{b0b-} are important here. The major difference in the dispersive properties of the M and Λ schemes arises from the existence of the four-photon coherence ρ_{b+b-}:

$$\rho_{b+b-} = \frac{\Omega_{1-}^*\Omega_{2-}^*\Omega_{1+}\Omega_{2+}}{|\Omega_{1-}|^2|\Omega_{2+}|^2 + |\Omega_{1+}|^2|\Omega_{2+}|^2 + |\Omega_{1-}|^2|\Omega_{2-}|^2} \ . \tag{6.4}$$

For small δ we can again find the eigenvalue for the quasi-dark state, taking into account only the linear terms in δ:

$$\tilde{\lambda}_M = 2\delta \frac{|\Omega_{2-}|^2|\Omega_{1-}|^2 - |\Omega_{2+}|^2|\Omega_{1+}|^2}{|\Omega_{2+}|^2|\Omega_{1+}|^2 + |\Omega_{2-}|^2|\Omega_{1-}|^2 + |\Omega_{2+}|^2|\Omega_{1-}|^2} \ . \tag{6.5}$$

2. Equations of motion

It is possible to obtain the equation of motion for the electro-magnetic fields, using the method reported in Ref. [272, 273]. If we assume a small disturbance of CPT, almost all atomic population remains in a dark state during the interaction process, and we can rewrite the interaction Hamiltonian as

$$H \simeq \hbar\tilde{\lambda}_D \hat{I}. \tag{6.6}$$

In this case we can exclude the atomic degrees of freedom from the interaction picture, and write the quasi-classical analogue of the interaction Hamiltonian with respect to the atomic degrees of freedom: $H \simeq \hbar\tilde{\lambda}_D$. This Hamiltonian may be further rewritten in the Heisenberg picture, so that $\Omega \propto \hat{a}$, where $\hat{a}$ is the annihilation operator for the electromagnetic field [272]. The quantum mechanical equation for the electromagnetic creation and annihilation operators may be presented in the following form:

$$\frac{d\hat{a}}{dt} = -\frac{i}{\hbar}\frac{\partial H}{\partial \hat{a}^\dagger} \ . \tag{6.7}$$

Strictly speaking, the right-hand side of this equation should involve functional derivative, rather than a partial one. However, in this case the two give the same result. The propagation equation for the electromagnetic field amplitude E can be obtained from Eq. (2.51) as a quasi-classical analogue of Eq. (6.7) [275]:

$$\frac{\partial E}{\partial z} = 2\pi i N \frac{\nu}{c}\frac{\partial H}{\partial E^*} \tag{6.8}$$

where N is the density of the atoms in the cell, and ν is a carrier frequency of the electromagnetic wave. Using Eq. (6.8) we derive equations of motion for the electromagnetic field amplitudes. For example,

$$\frac{\partial\Omega_{2-}}{\partial z} = 2i\kappa\delta\Omega_{2-}\frac{\wp^2_{a-b0}}{\wp^2}\frac{2|\Omega_{1+}|^2|\Omega_{1-}|^2|\Omega_{2+}|^2 + |\Omega_{2+}|^2|\Omega_{1-}|^4}{(|\Omega_{1-}|^2|\Omega_{2+}|^2 + |\Omega_{1+}|^2|\Omega_{2+}|^2 + |\Omega_{1-}|^2|\Omega_{2-}|^2)^2} \tag{6.9}$$

where κ is the coupling constant with respect to the transition as a whole (i.e., γ_r in Eq. (2.26) is now the total natural decay rate of the excited state $F' = 1$), and $\wp^2 = 4\nu^3\gamma_r/(3\hbar c^3)$ is the dipole moment of the transition.

The further calculations can be considerably simplified if the numerical values of the transition probabilities are used. Let us now consider the particular case of the M part of the $F = 2 \to F = 1$ transition. According to the transition probabilities, shown in Fig. 33c, we get $|\Omega_{2+}|^2/|\Omega_{2-}|^2 = 6|E_+|^2/|E_-|^2$ and $|\Omega_{1+}|^2/|\Omega_{1-}|^2 = |E_+|^2/6|E_-|^2$. The interaction Hamiltonian ($H_M \simeq \hbar\tilde{\lambda}_M$) for the elliptically polarized laser field can therefore be rewritten as

$$H_M \simeq 2\hbar\delta\frac{|E_-|^4 - |E_+|^4}{|E_+|^4 + |E_-|^4 + 6|E_+|^2|E_-|^2} \tag{6.10}$$

and therefore

$$\frac{\partial E_\pm}{\partial z} = \mp 8i\pi\hbar\delta N\frac{\nu}{c}E_\pm|E_\mp|^2\frac{3(|E_+|^4 + |E_-|^4) + 2|E_+|^2|E_-|^2}{(|E_+|^4 + |E_-|^4 + 6|E_+|^2|E_-|^2)^2}\,. \tag{6.11}$$

In what follows we derive the same equation using the more rigorous modified Schrödinger formalism [282].

3. Solution based on the modified Schrödinger equations

The interaction described above of the four electromagnetic fields with the M energy level configuration may be also studied using Schrödinger equations. This approach enables us to find exact expressions for all the atomic observables when we can ignore spontaneous emission. The state vector of the atom can be written as:

$$|\Psi\rangle = a_+ e^{-i\nu t}|a_+\rangle + a_- e^{-i\nu t}|a_-\rangle + b_0|b_0\rangle + b_+|b_+\rangle + b_-|b_-\rangle\,. \tag{6.12}$$

Solving the Schrödinger equation

$$|\dot{\Psi}\rangle = -\frac{i}{\hbar}\hat{H}|\Psi\rangle$$

for the interaction Hamiltonian Eq. (6.1), we obtain the following equations of motion for the slowly-varying state amplitudes:

$$\dot{a}_+ = i\Omega_{1+}b_0 + i\Omega_{1-}b_+ \tag{6.13}$$

$$\dot{a}_- = i\Omega_{2+}b_- + i\Omega_{2-}b_0 \tag{6.14}$$

$$\dot{b}_+ = 2i\delta b_+ + i\Omega^*_{1-}a_+ \tag{6.15}$$

$$\dot{b}_- = -2i\delta b_- + i\Omega^*_{2+}a_- \tag{6.16}$$

$$\dot{b}_0 = i\Omega^*_{1+}a_+ + i\Omega^*_{2-}a_-\ . \tag{6.17}$$

In the steady state regime, this system has a nontrivial solution only for $\delta = 0$. The solutions for nonzero detunings correspond to zero amplitudes for all parameters. Thus, to sustain steady state in the open system, external pumping is necessary. For a small splitting between ground state levels $\hbar\delta \ll kT$, where T is the temperature of the vapor, we assume that in thermal equilibrium, i.e., in the absence of all fields, all lower states $|b_\pm\rangle$ and $|b_0\rangle$ are equally populated. And, therefore, within the open-system approach, we assume that the atoms are pumped into states $|b_+\rangle$, $|b_-\rangle$, or $|b_0\rangle$ with equal probability from outside of the system. The corresponding rate can be determined by the requirement that the total probability to find an atom in any of the states is unity.

Unlike the density matrix approach, a straightforward introduction of incoherent pumping into the ground states of the system is impossible. It was shown by Fleischhauer [282] in an elegant way that the effective density matrix equations for open systems with injection rates into states and decays out of states can be written in terms of stochastic complex state amplitudes.

Let us consider an effective density matrix equation for an atomic ensemble undergoing a unitary interaction with some external fields or potentials. In addition, decay out of atomic states $|j\rangle$ is taken into account with rates γ_j. Also injection into certain states is considered with injection rates R_{ij}. In our case the injection occurs only into energy eigenstates of the atoms or incoherent mixtures of them, so only diagonal elements of the matrix R_{ij} are nonzero. If injection in a coherent superposition states is considered, non-diagonal elements are also required to be taken into account.

An effective density matrix equation has the following structure:

$$\dot{\rho}_{ij}(t) = R_{ij} - \frac{\gamma_i + \gamma_j}{2}\rho_{jj} - \frac{i}{\hbar}\big[H, \rho\big]_{ij} \tag{6.18}$$

where γ_i are decay rates out of the system, which can in general be different for individual states. Generally, the pump rates R_{ij} are time dependent, but for the sake of simplicity we assume in the following that the rates R_{ij} are constant.

Density matrix elements may be represented in terms of state amplitudes $\rho_{ji} = c_i^* c_j$. In order to put the pump term R_{ij} in a similar form, we introduce a formal Gaussian stochastic variable r_i with the following properties:

$$\langle r_i \rangle = 0 \tag{6.19}$$

$$\langle r_i r_j \rangle = 0 \tag{6.20}$$

$$\langle r_i^* r_j \rangle = R_{ij} \; . \tag{6.21}$$

This yields a set of amplitude equations with stochastic pump terms:

$$\dot{c}_i = r_i - \frac{\gamma_i}{2}\, c_i + \frac{i}{\hbar} H_{ij}\, c_j \ . \tag{6.22}$$

Since the amplitude equations are linear, their solution will be a linear functional of the stochastic pump rates r_i. Thus the averaging of bilinear quantities such as $c_i^* c_j$ required to obtain the density matrix elements can easily be performed. Generally, solution c_j of Eq. (6.22) no longer makes sense as the amplitude for the atomic wave function. It only determines density matrix elements of the system.

To apply the above technique to our problem, we rewrite Eqs. (6.13)–(6.17) (with time derivatives set equal to zero)

$$i\Omega_{1+} b_0 + i\Omega_{1-} b_+ = 0 \tag{6.23}$$

$$i\Omega_{2+} b_- + i\Omega_{2-} b_0 = 0 \tag{6.24}$$

$$2i\delta b_+ + i\Omega_{1-}^* a_+ = ir_+ \tag{6.25}$$

$$-2i\delta b_- + i\Omega_{2+}^* a_- = ir_- \tag{6.26}$$

$$i\Omega_{1+}^* a_+ + i\Omega_{2-}^* a_- = ir_0 \tag{6.27}$$

where the stochastic "pumping" is introduced

$$\langle r_\pm \rangle = \langle r_0 \rangle = 0 \tag{6.28}$$

$$\langle r_\pm r_\mp \rangle = \langle r_\pm r_0 \rangle = 0 \tag{6.29}$$

$$\langle r_\pm^* r_\mp \rangle = \langle r_\pm^* r_0 \rangle = 0 \tag{6.30}$$

$$\langle r_\pm^* r_\pm \rangle = \langle r_0^* r_0 \rangle = r^2 \ . \tag{6.31}$$

Solving Eqs. (6.23)–(6.27) with respect to a_1, a_2, $b_\pm$, and b_0 we get

$$b_+ = -b_0\frac{\Omega_{1+}}{\Omega_{1-}}\ , \quad b_- = -b_0\frac{\Omega_{2-}}{\Omega_{2+}} \tag{6.32}$$

$$b_0 = \frac{r_+|\Omega_{2+}|^2\Omega_{1-}\Omega^*_{1+} + r_-|\Omega_{1-}|^2\Omega_{2+}\Omega^*_{2-} - r_0|\Omega_{1-}|^2|\Omega_{2+}|^2}{2\delta\left(|\Omega_{1+}|^2|\Omega_{2+}|^2 - |\Omega_{1-}|^2|\Omega_{2-}|^2\right)} \tag{6.33}$$

$$a_- = \frac{r_+\Omega^*_{1+}\Omega_{1-}\Omega_{2-} + r_-|\Omega_{1+}|^2\Omega_{2+} - r_0|\Omega_{1-}|^2\Omega_{2-}}{|\Omega_{1+}|^2|\Omega_{2+}|^2 - |\Omega_{1-}|^2|\Omega_{2-}|^2} \tag{6.34}$$

$$a_+ = -\frac{r_+|\Omega_{2-}|^2\Omega_{1-} + r_-\Omega^*_{2-}\Omega_{1+}\Omega_{2+} - r_0|\Omega_{2+}|^2\Omega_{1+}}{|\Omega_{1+}|^2|\Omega_{2+}|^2 - |\Omega_{1-}|^2|\Omega_{2-}|^2}\ . \tag{6.35}$$

Utilizing the normalization condition

$$\langle a^*_- a_-\rangle + \langle a^*_+ a_+\rangle + \langle b^*_+ b_+\rangle + \langle b^*_- b_-\rangle + \langle b^*_0 b_0\rangle = 1 \tag{6.36}$$

we get

$$\begin{aligned}
& r = 2\delta\left(|\Omega_{1+}|^2|\Omega_{2+}|^2 - |\Omega_{1-}|^2|\Omega_{2-}|^2\right)/ \\
& \Big\{(|\Omega_{1-}|^2|\Omega_{2+}|^2 + |\Omega_{1+}|^2|\Omega_{2+}|^2 + |\Omega_{1-}|^2|\Omega_{2-}|^2)^2 + \\
& 4\delta^2\Big[|\Omega_{1+}|^2|\Omega_{1-}|^2(|\Omega_{1+}|^2 + |\Omega_{2+}|^2) + \\
& 2(|\Omega_{1+}|^4|\Omega_{2+}|^2 + |\Omega_{1-}|^4|\Omega_{2-}|^2)\Big]\Big\}^{1/2}\ .
\end{aligned} \tag{6.37}$$

Using Eq. (6.37) we arrive at the complete solution of the problem which takes into account all orders in δ. For $\delta = 0$ the system is in a dark state and the density matrix elements correspond to the elements generated by Eq. (6.3). For a nonzero small two-photon detuning the populations and coherences for the ground state stay approximately unchanged. The solution for the populations of the excited states are

$$\rho_{a-a-} = 4\delta^2\frac{|\Omega_{1+}|^2|\Omega_{1-}|^2|\Omega_{2-}|^2 + |\Omega_{1+}|^4|\Omega_{2+}|^2 + |\Omega_{1-}|^4|\Omega_{2-}|^2}{(|\Omega_{1-}|^2|\Omega_{2+}|^2 + |\Omega_{1+}|^2|\Omega_{2+}|^2 + |\Omega_{1-}|^2|\Omega_{2-}|^2)^2} \tag{6.38}$$

$$\rho_{a+a+} = 4\delta^2\frac{|\Omega_{2+}|^2|\Omega_{2-}|^2|\Omega_{1+}|^2 + |\Omega_{2+}|^4|\Omega_{1+}|^2 + |\Omega_{2-}|^4|\Omega_{1-}|^2}{(|\Omega_{1-}|^2|\Omega_{2+}|^2 + |\Omega_{1+}|^2|\Omega_{2+}|^2 + |\Omega_{1-}|^2|\Omega_{2-}|^2)^2} \tag{6.39}$$

and for the atomic polarizations are

$$\begin{aligned}
\rho_{a-b0} &= \frac{2\delta\Omega_{2-}(2|\Omega_{1+}|^2|\Omega_{1-}|^2|\Omega_{2+}|^2 + |\Omega_{2+}|^2|\Omega_{1-}|^4)}{(|\Omega_{1-}|^2|\Omega_{2+}|^2 + |\Omega_{1+}|^2|\Omega_{2+}|^2 + |\Omega_{1-}|^2|\Omega_{2-}|^2)^2} \qquad (6.40)\\
\rho_{a+b0} &= -\frac{2\delta\Omega_{1+}(2|\Omega_{1-}|^2|\Omega_{2+}|^2|\Omega_{2-}|^2 + |\Omega_{1-}|^2|\Omega_{2+}|^4)}{(|\Omega_{1-}|^2|\Omega_{2+}|^2 + |\Omega_{1+}|^2|\Omega_{2+}|^2 + |\Omega_{1-}|^2|\Omega_{2-}|^2)^2} \qquad (6.41)\\
\rho_{a-b-} &= -\frac{2\delta\Omega_{2+}(2|\Omega_{1+}|^2|\Omega_{1-}|^2|\Omega_{2-}|^2 + |\Omega_{2-}|^2|\Omega_{1-}|^4)}{(|\Omega_{1-}|^2|\Omega_{2+}|^2 + |\Omega_{1+}|^2|\Omega_{2+}|^2 + |\Omega_{1-}|^2|\Omega_{2-}|^2)^2} \qquad (6.42)\\
\rho_{a+b+} &= \frac{2\delta\Omega_{1-}(2|\Omega_{1+}|^2|\Omega_{2+}|^2|\Omega_{2-}|^2 + |\Omega_{1+}|^2|\Omega_{2+}|^4)}{(|\Omega_{1-}|^2|\Omega_{2+}|^2 + |\Omega_{1+}|^2|\Omega_{2+}|^2 + |\Omega_{1-}|^2|\Omega_{2-}|^2)^2}\ . \qquad (6.43)
\end{aligned}$$

Here we kept only the lowest order terms in δ. In the expressions for the atomic polarizations, the first term, containing the amplitude of all four optical fields (for example, $\Omega_{1+}|\Omega_{1-}|^2|\Omega_{2+}|^2|\Omega_{2-}|^2$ in the equation for ρ_{a+b0}), is due to the four-photon coherence (hexadecapole moment), whereas the second term represents the effect of optical pumping.

The propagation equation for the fields is

$$\frac{\partial\Omega_{ij}}{\partial z} = i\frac{2\pi\nu}{c}N\frac{\wp_{ij}^2}{\hbar}\rho_{ij} \qquad (6.44)$$

where the indexes ij show that the values are related to the same transition $|i\rangle \rightarrow |j\rangle$. It is easy to see, for example, that the matrix element in Eq. (6.40) results in the propagation equation in Eq. (6.9). The two approaches are therefore equivalent. The equation of motion for the circularly polarized electromagnetic fields in $E_\pm$ are given by the following expressions:

$$\begin{aligned}
\frac{\partial E_+}{\partial z} &= i\frac{2\pi\nu}{c}N\left(\wp_{a-b-}\rho_{a-b-} + \wp_{a+b0}\rho_{a+b0}\right) \qquad (6.45)\\
\frac{\partial E_-}{\partial z} &= i\frac{2\pi\nu}{c}N\left(\wp_{a+b+}\rho_{a+b+} + \wp_{a-b0}\rho_{a-b0}\right)\ . \qquad (6.46)
\end{aligned}$$

Substituting the expressions for atomic polarizations Eqs. (6.40)–(6.43) and using the proper dipole moments for each transition (for the ^{87}Rb they are equal 1/2 for

$|b_{\pm}\rangle \rightarrow |a_{\pm}\rangle$, and 1/12 for $|b_0\rangle \rightarrow |a_{\pm}\rangle$ (Fig. 33c)), we obtain Eqs. (6.11).

So far we have made no assumption concerning the losses in the system. Generally, this requires solving the Bloch equations for the atomic populations and polarizations as is done for the Λ system. For the M scheme, however, this process is rather involved even for the degenerate system ($\delta = 0$). Since the dark state exists for any value of Rabi frequency Ω_{ij} (Eq.(6.3)), it is always possible to transform the basis of the atomic states so that there is one atomic level uncoupled from the laser field. The M system can be represented as two independent open two-level systems, connected only via relaxation processes [283]. The absorption in this systems has properties similar to those of the Λ system: it is proportional to decay rate γ_0 and inversely proportional to the light intensity. The exact analytical expression for this absorption is rather lengthy and is not given here.

B. Polarization rotation for the $F = 2 \rightarrow F' = 1$ transition

To describe the polarization rotation on the $F = 2 \rightarrow F' = 1$ transition we write the interaction Hamiltonian as a balanced sum of the Hamiltonians for the M and Λ systems, taking into account the branching ratio for the atomic transitions

$$H_{2\rightarrow 1} = \zeta_1 H_{\Lambda} + \zeta_2 H_M = \zeta_1 \hbar \tilde{\lambda}_{\Lambda} + \zeta_2 \hbar \tilde{\lambda}_M \tag{6.47}$$

where ζ_1 and ζ_2 are weighting coefficients ($\zeta_1 + \zeta_2 = 1$) that describe the population redistribution between the Λ and M schemes. Using the numerical simulation of this system, we find them to be equal with very good accuracy. Using Eq. (6.8) we now derive the equation of motion for this system:

$$\begin{aligned}\frac{\partial E_\pm}{\partial z} &= \mp 4i\pi\hbar\delta N\frac{\nu}{c}E_\pm\frac{|E_\mp|^2}{(|E_+|^2+|E_-|^2)^2}\left[1+\right.\\ &\left. 2(|E_+|^2+|E_-|^2)^2\frac{3(|E_+|^4+|E_-|^4)+2|E_+|^2|E_-|^2}{(|E_+|^4+|E_-|^4+6|E_+|^2|E_-|^2)^2}\right]. \qquad (6.48)\end{aligned}$$

It is interesting to note that for linearly polarized light ($|\Omega_+| = |\Omega_-|$) the contributions from Λ and M system are identical, and Eq. (6.48) coincides with Eq. (2.66) under condition of zero coherence decay rate. This proves that a single Λ system may be used for accurate description of the dispersive properties of more complicated level configurations.

Let us introduce the electromagnetic field ellipticity parameter q such that the amplitudes of the circularly polarized components are $E_\pm = |E|\sqrt{(1\pm q)}\exp(i\phi_\pm)/\sqrt{2}$. Then Eq. (6.48) transforms to

$$\frac{\partial E_\pm}{\partial z} = \mp 2i\pi\hbar\delta N\frac{\nu}{c}\frac{E_\pm(1\mp q)}{|E|^2}\left[1+2\frac{2+q^2}{(2-q)^2}\right]. \qquad (6.49)$$

Based of the results of our numerical simulation, we conclude that absorption of light that interacts with the $F=2\rightarrow F'=1$ transition does not depend on the ellipticity of the light. The light transmission through the cell can be described by an equation similar to Eq.(2.71):

$$I_{\text{out}} = I_{\text{in}}\left(1-\frac{2\pi\hbar\gamma_0 NL}{|E(0)|^2}\frac{\nu}{c}\right). \qquad (6.50)$$

The rotation angle for the light polarization is then given by

$$\phi = \frac{\delta}{\gamma_0}\left[1+2\frac{2+q^2}{(2-q^2)^2}\right]\ln\frac{I_{\text{in}}}{I_{\text{out}}} \qquad (6.51)$$

where I_{in} and I_{out} are the intensities of the electromagnetic field at the entrance and exit of the medium. The value of polarization rotation increases with the light ellipticity by the factor

$$\frac{\phi_{M+\Lambda}}{\phi_\Lambda} = \frac{1}{2}\left(1 + 2\frac{2+q^2}{(2-q^2)^2}\right) \tag{6.52}$$

compared to Λ system. Therefore NMOR on the $F=2 \rightarrow F'=1$ transition may only be properly described by a Λ configuration for linearly polarized light. The difference between the M and Λ systems results from the hexadecapole moment induced in M configuration.

C. NMOR in atoms with large values of angular momentum

Higher order coherence can be excited among Zeeman sublevels of alkali atoms with $F > 2$. Here we find a perturbed dark state for the generalized M scheme consisting of an arbitrary number of Λ-links, using the method described above. Then we apply these results to evaluate the nonlinear Faraday rotation in the ^{85}Rb $F=3 \rightarrow F=2$ transition. We consider the scheme in Fig. 34. The interaction Hamiltonian for this scheme is

$$\begin{aligned} H_{n\times\Lambda} &= -\hbar\delta\sum_{k=0}^{n}(n-2k)|b_{k+1}\rangle\langle b_{k+1}| \\ &+ \hbar\sum_{k=1}^{n}\left(\Omega_{k-}|a_k\rangle\langle b_k| + \Omega_{k+}|a_k\rangle\langle b_{k+1}| + H.c.\right) \end{aligned} \tag{6.53}$$

Here n is the number of Λ links, which connects $n+1$ ground-state levels via n excited states. There exists a dark state for this system for exact resonance (δ=0):

$$|D\rangle = \frac{\sum_{k=0}^{n}(-1)^k \prod_{j=1}^{k}\Omega_{j-} \prod_{l=k+1}^{n}\Omega_{l+}\ |b_{k+1}\rangle}{\sqrt{\sum_{k=0}^{n}\prod_{j=1}^{k}|\Omega_{j-}|^2 \prod_{l=k+1}^{n}|\Omega_{l+}|^2}} \tag{6.54}$$

where we use a convention that $\prod_{j=1}^{0} \equiv \prod_{j=n+1}^{n} \equiv 1$. We deduce the perturbed "dark

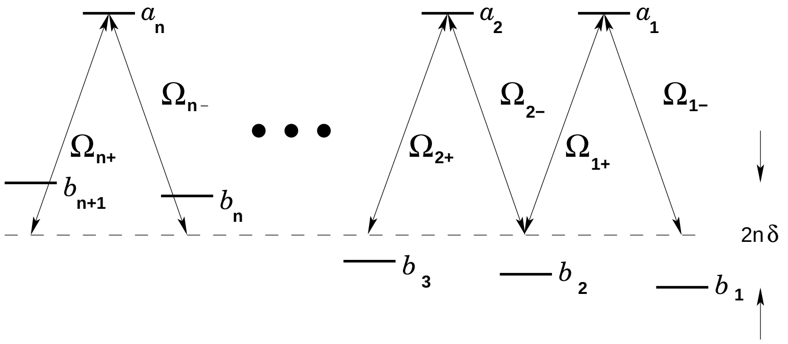

Fig. 34. Generalized M interaction scheme. Here $\Omega_{i-} = E_- \wp_{a_i b_i}/\hbar$, $\Omega_{i+} = E_+ \wp_{a_i b_{i-1}}/\hbar$.

state" eigenvalue for the Hamiltonian using the same procedure as we used before in Eq. (6.54)

$$\tilde{\lambda}_{n\times\Lambda} \simeq \delta \frac{\sum_{k=0}^{n} (2k-n) \prod_{i=1}^{k} |\Omega_{i-}|^2 \prod_{j=k+1}^{n} |\Omega_{j+}|^2}{\sum_{k=0}^{n} \prod_{i=1}^{k} |\Omega_{i-}|^2 \prod_{j=k+1}^{n} |\Omega_{j+}|^2} \,. \tag{6.55}$$

The equation of motion for the circularly polarized electromagnetic fields can be found from Eq. (6.8). As an example, let us calculate the interaction Hamiltonian for light interacting with the $5S_{1/2}F = 3 \rightarrow 5P_{1/2}F' = 2$ transition of ^{85}Rb (Fig. 35). The circularly polarized components of the resonant electromagnetic field form an M scheme and a triple-Λ scheme. Using the proper values of the transition probabilities, shown in the same Figure, we derive

$$H_{3\rightarrow 2} = 3\hbar\delta \left[2\zeta_1 \frac{|E_-|^4 - |E_+|^4}{3|E_+|^4 + 3|E_-|^4 + 10|E_+|^2|E_-|^2} + \right.$$

$$\left. \zeta_2 \frac{|E_-|^6 + 5|E_+|^2|E_-|^4 - 5|E_+|^4|E_-|^2 - |E_+|^6}{|E_+|^6 + 15|E_-|^2|E_+|^4 + 15|E_-|^4|E_+|^2 + |E_-|^6} \right] \tag{6.56}$$

(6.57)

Here again $\zeta_{1,2}$ are the coefficients reflecting the population distribution between the schemes. By differentiating the Hamiltonian it is easy to find the polarization rotation in the system

$$\frac{\partial \phi}{\partial z} = -6i\pi N \frac{\nu}{c} \frac{\hbar\delta}{|E|^2} \left[2\zeta_1 \frac{4+q^2}{(4-q^2)^2} + \zeta_2 \frac{8-6q^2+3q^4}{(4-3q^2)^2} \right]. \qquad (6.58)$$

It is obvious that both interaction chains contribute to the elliptically dependent NMOR. At the same time different orders of the nonlinear susceptibility are responsible for the polarization rotation: if in the case of the M scheme it is $\chi^{(3)}$ nonlinearity, for the triple-Λ scheme it is $\chi^{(5)}$ nonlinearity, since there are 7 photons involved in the creation of the ground-state coherence. This might be the reason why the triple-Λ scheme shows more enhancement of the polarization rotation for nearly circular polarization compared to the rotation of linear polarization than does the M scheme (10 vs 20/9 times for the $F = 3 \rightarrow F' = 2$ transition).

D. Experimental study of ellipticity-dependent MNOR in Rb vapor

There are two factors contributing to the rotation of the elliptical polarization of light propagating through the Rb vapor: the nonlinear Faraday rotation, caused by the shifts of the magnetic sublevels in an external magnetic field, and the self-rotation caused by the ac-Stark shifts due to the off-resonant interaction of the electromagnetic field with far-detuned levels (see Chapter VII). Since the latter effect does not depend on the magnetic field, we eliminate it from the experimental data either by our measurement procedure or by direct subtraction. In all further discussions we consider NMOR signals only.

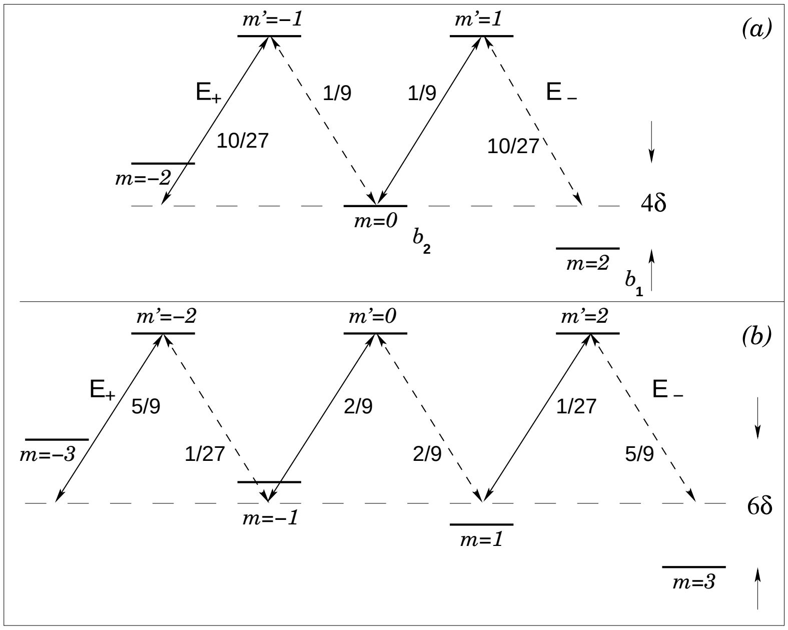
(a)
m'=−1
m'=1
E+
1/9
1/9
E−
10/27
10/27
m=−2
m=0
4δ
b2
m=2
b1
(b)
m'=−2
m'=0
m'=2
E+
5/9
2/9
1/27
E−
m=−3
1/27
2/9
5/9
m=−1
6δ
m=1
m=3

Fig. 35. Energy level scheme for ^{85}Rb atoms. This scheme may be decomposed into a superposition of a) M-system and b) triple-Λ system. Transition probabilities are shown for each individual transition.

1. The experiments with ^{87} Rb vapor

Let us first study the modification of the polarization rotation by measuring the rotation rate $\frac{d\phi}{dB}(B = 0)$ as a function of light ellipticity. We find the rotation rate by modulating the magnetic field by a small amount and dividing the difference of two rotation signals corresponding to the small variation of the magnetic field by the magnitude of this variation. This way we detect only the rotation which depends on the external magnetic field.

The rotation rate as a function light ellipticity is shown in Fig. 36. We observe a polarization rotation enhancement as predicted theoretically. At the same time, the experimental data cannot be fitted using Eq. (6.52) because of the Doppler broadening of the transition and the ac-Stark of the magnetic sublevels. However, an exact numerical simulation based on steady state solution of Maxwell-Bloch equations for the $F = 2 \rightarrow F' = 1$ transition, which takes into account these effects, is in excellent agreement with the experimental data.

It is also possible to verify that there is no polarization rotation enhancement in an isolated Λ system. To do that we tune the laser to the $F = 1 \rightarrow F' = 1$ transition of the ^{87}Rb D_1 line. In this case, the ground-state coherence is formed by only one Λ link. The relative rotation rate for $F = 1, 2 \rightarrow F' = 1$ transitions are presented in Fig. 37. Although there is a slight dependence of the rotation angle on the light ellipticity for the $F = 1 \rightarrow F' = 1$ transition, this deterioration may be determined by Doppler broadening, ac-Stark shifts, etc.

It is important to point out that even though the theoretical expression for the relative rotation rate (Eq. (6.52)) does not fit the experimental data precisely, it correctly predict some of the rotation properties. For example, our experiments confirm that the relative rotation rate does not depend on the sign of the ellipticity

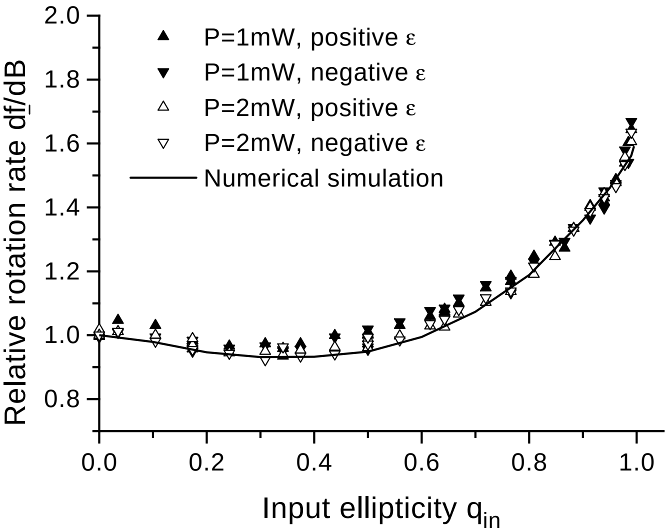

Fig. 36. The normalized slope of the nonlinear magneto-optic rotation as a function of the ellipticity of the incident light. Experimental data are shown for opposite values of ellipticity and two different values of laser power: P=2 mW (hollow up triangles for positive ellipticity and hollow down triangles for negative ellipticity) and P=1 mW (solid up triangles for positive ellipticity and solid down triangles for negative ellipticity). The results of the numerical simulations for the case of 2 mW laser power are shown by a solid line. Absolute values of the nonlinear Faraday rotation for the linear polarization were $d\phi/dB(B=0) = 4.5$ rad/G and 6 rad/G for P=2 mW and P=1 mW respectively.

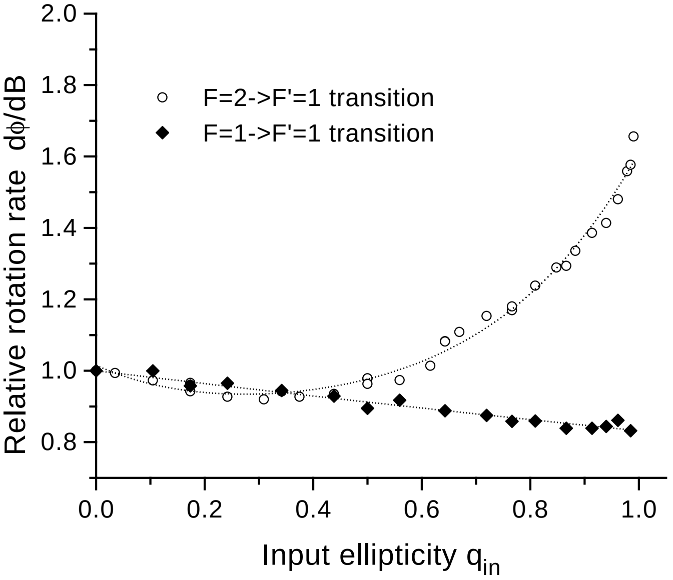

Fig. 37. The normalized slope of nonlinear magneto-optic rotation as a function of the ellipticity of the incident light for the Λ scheme (transition $F = 1 \rightarrow F' = 1$) and $M + \Lambda$ scheme (transition $F = 2 \rightarrow F' = 1$). Dotted lines are to guide the eyes. Input laser power is P=2 mW, the atomic densities are chosen to provide 85% absorption on each transition. The absolute value of the nonlinear Faraday rotation of linear polarization were $d\phi/dB(B = 0) = 1.8$ rad/G and 4.5 rad/G for the $F = 1, 2 \rightarrow F' = 1$ transitions respectively.

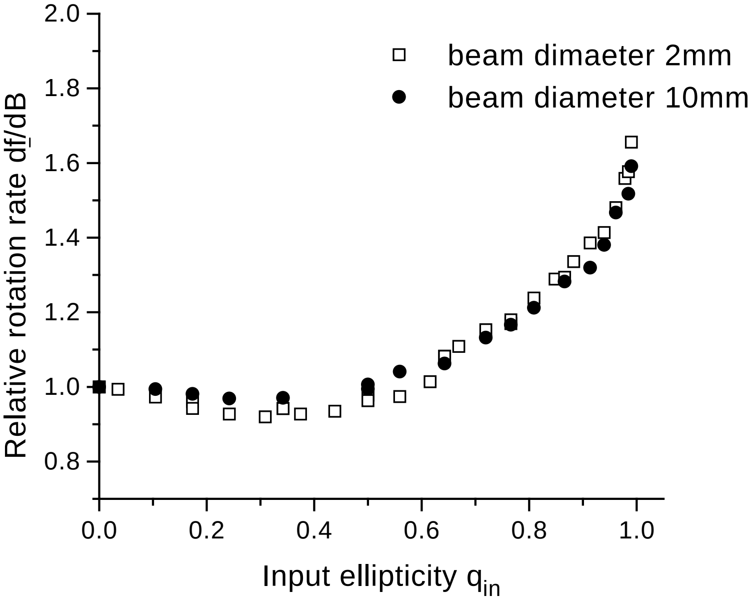

Fig. 38. The normalized slope of nonlinear magneto-optic rotation as a function of the ellipticity of the incident light for two different beam diameters: $d = 2$ mm (squares) and $d = 10$ mm (diamonds). In both cases the laser power is kept at 2 mW. Absolute values of the nonlinear Faraday rotation for the linear polarization were $d\phi/dB(B = 0) = 4.5$ rad/G and 30 rad/G respectively.

(Fig. 36). If we vary the total laser power or the coherence decay rate γ_0 (by varying the laser beam diameter), the absolute value of the rotation changes according to Eq. (6.51); its dependence on the light ellipticity is the same within the experimental uncertainty (Figs. 36 and 38).

All previous data were obtained for optically thin Rb vapor (transmission is about 85%). The dependence of the relative rotation rate on the ellipticity for higher atomic densities is shown in Fig. 39. It is easy to see that for nearly circular polarization the rotation decreases as atomic density is increased. This may be caused by optical pumping to the other ground state hyperfine levels, as well as by the destruction of atomic coherence by radiation trapping.

The precise value of the output ellipticity of the laser polarization is required for accurate polarization rotation measurements (see Eq. (3.2)). The experimental observations demonstrate that for optically thin media the ellipticity of the light does not noticeably change due to propagation effects if the magnetic field is small. As the atomic density increases, however, the ellipticity increases (Fig. 39b). Although this change is relatively small ($< 15\%$), the associated error in the calculated rotation is very significant.

2. Polarization rotation of elliptically polarized light for large magnetic fields

Now let us consider the case of large magnetic fields. If the laser frequency is swept across the atomic transition, the following effects contribute to the polarization rotation: the nonlinear Faraday rotation due to the Λ-scheme (experimentally measured for linear polarization), self-rotation of elliptical polarization due to ac-Stark shifts, and the magneto-optic rotation of elliptical polarization due to M-scheme induced coherence. All these components are shown in Fig. 40. It is important to point out that this “new” rotation is comparable with the polarization rotation for the linear polarization and the self-rotation, even though this effect is due to higher order nonlinearity. This proves the effectiveness of the M level scheme for the enhancement of nonlinear susceptibility in atomic media.

The magnetic field dependence of the rotation due to the M-scheme ground-state coherence reveals a very peculiar behavior. Although the polarization rotation is independent of the sign of the ellipticity in the vicinity of zero magnetic field (as it was demonstrated earlier), for larger magnetic fields the it becomes asymmetric with respect to both magnetic field and ellipticity. To invert the sign of the rotation, both the ellipticity and the magnetic field should change their signs (Fig. 41a). The

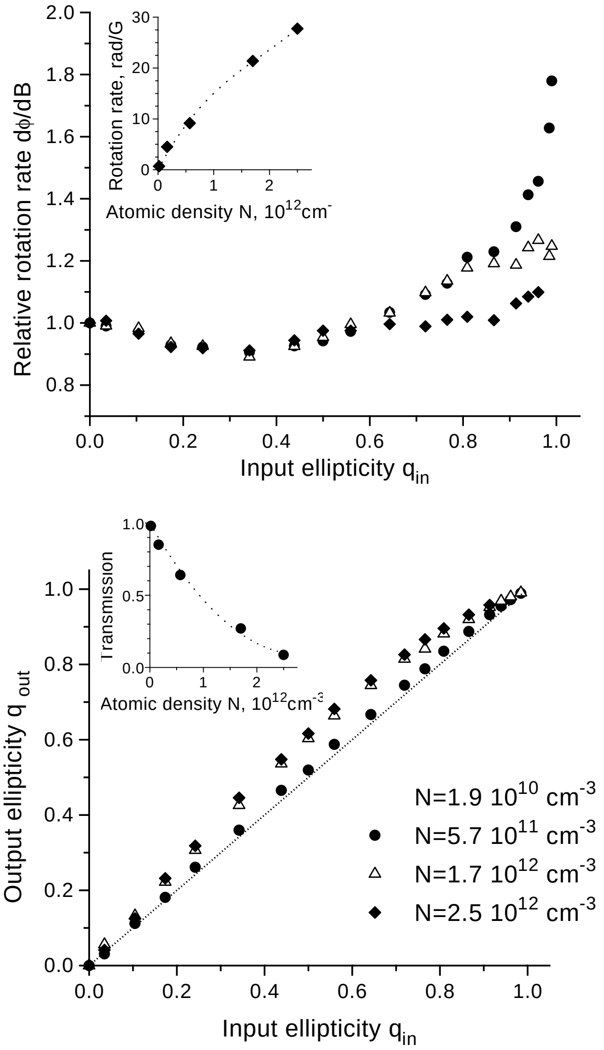

Fig. 39. (a) The normalized slope of nonlinear magneto-optic rotation as a function of the ellipticity of the incident light for various atomic densities. Laser power is 2 mW, beam diameter $d = 2$ mm. Inset: Absolute value of the nonlinear Faraday rotation of linear polarization as a function of atomic density. (b) The output ellipticity ϵ as a function of the ellipticity of the incident light for various atomic densities. Dotted line is for unchanged ellipticity. Inset: Transmission $I_{\text{out}}/I_{\text{in}}$ of linear polarization as a function of atomic density.

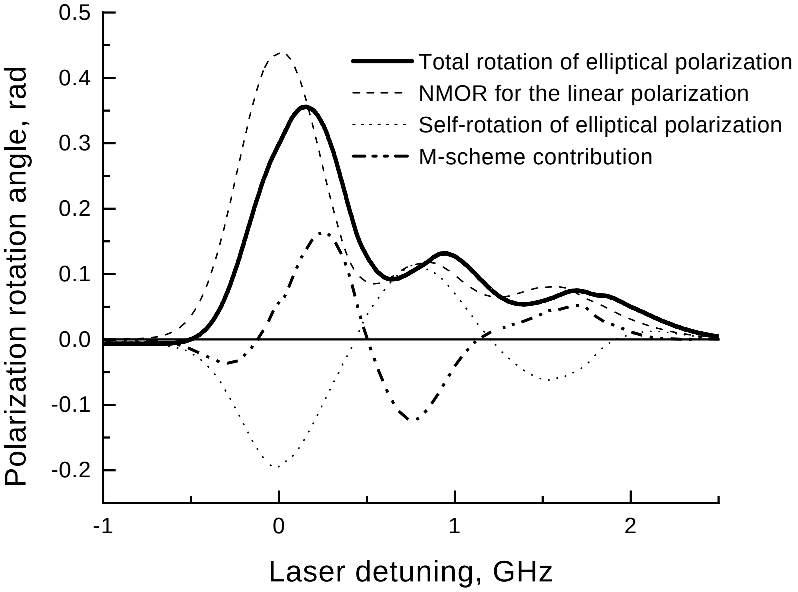

Fig. 40. The polarization rotation angle as a function of laser detuning for ellipticity $\epsilon = 25^o$ and magnetic field $B = 0.35$ G. The components of the rotation due to various processes are also shown. Zero detuning corresponds to the $F = 2 \rightarrow F' = 1$ transition. The small peak on the right is due to contamination of the cell with ^{85}Rb isotope.

ellipticity of the outgoing light also changes with the magnetic field; although it is equal to the initial ellipticity for small magnetic fields (at least for optically thin samples), it grows symmetrically when the magnetic field becomes larger (Fig. 41a). These changes must to be taken into account when the polarization rotation angle is measured.

3. NMOR for atoms with higher angular momentum

As discussed in Sec. II, higher orders of nonlinear susceptibility may be enhanced in multi-Λ systems. In practice this means that atoms with larger ground state angular momentum are required. The most convenient candidate for the study of the higher orders of Zeeman coherence is the ^{85}Rb isotope, since the same laser may be used as for our previous study of ^{87}Rb. In our experiments we use the $5S_{5/2}F = 3 \rightarrow 5P_{3/2}F' = 2$ of ^{85}Rb. The interaction scheme of elliptically polarized light with this transition consists of an M scheme and a triple-Λ scheme.

The relative rotation rate for this transition as a function of the light ellipticity is shown in Fig. 42. The polarization rotation enhancement, observed in this case is noticeably smaller than for ^{87}Rb. The reason for this may be the smaller hyperfine splitting of the excited state (362 MHz vs 812 MHz for ^{87}Rb), which is completely overlapped by the Doppler broadening ($\Delta_{Doppler} \approx 500$ MHz). This overlap results in efficient “mixing” of the coherences induced through different excited states, which may significantly change the properties of the system. That is why it would be very interesting to measure the rotation due to high order coherence, discussed above, in a cloud of cold atoms. In this case we expect to see a much stronger effect (Eq. (6.58)), since all problems caused by the overlapping transitions due to the motion of the atoms would be eliminated in cold gas.

The spectral dependence of the rotation of the elliptical polarization on laser

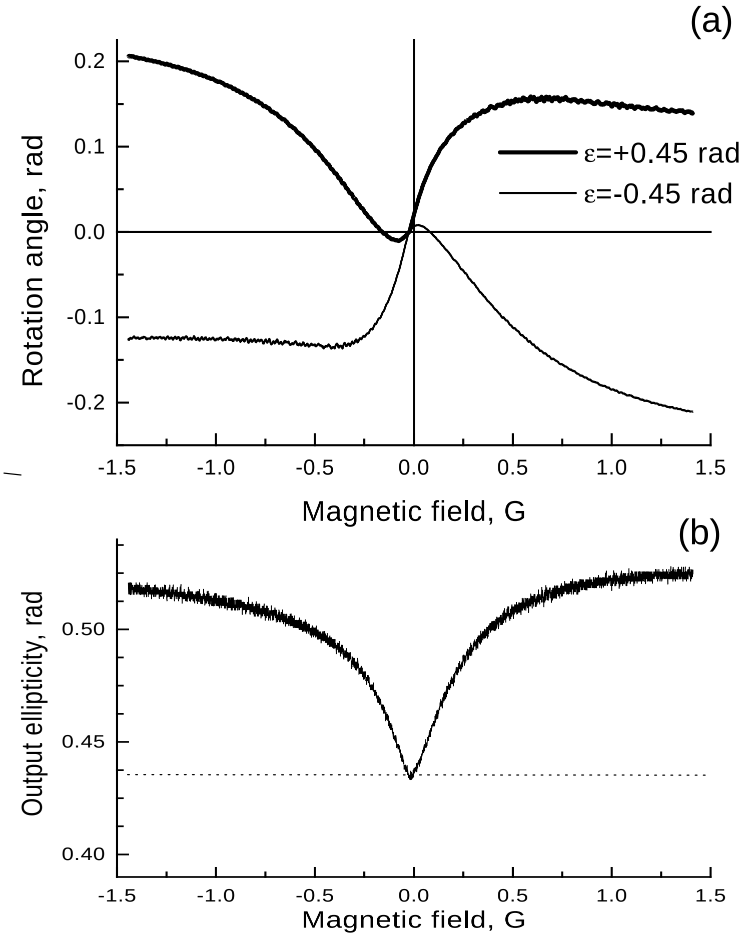

Fig. 41. (a) The polarization rotation angle as a function of magnetic field for opposite values of ellipticity. (b) The ellipticity of the transmitted light as a function of magnetic field. Input ellipticity is shown as a dashed line.

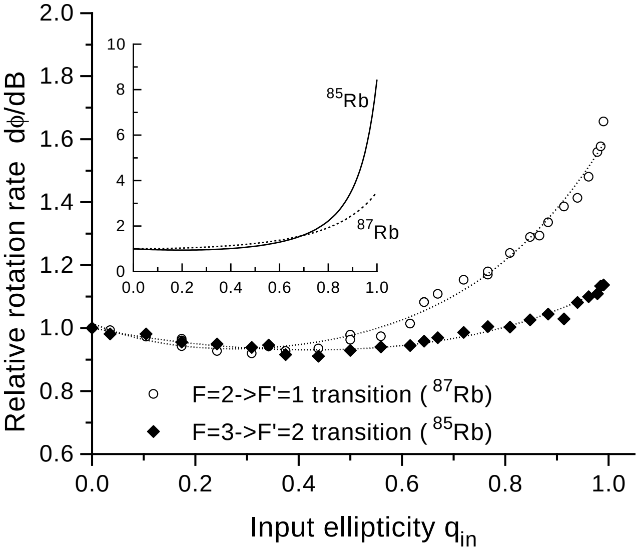

Fig. 42. The normalized slope of nonlinear magneto-optic rotation as a function of the ellipticity of the incident light for the $F = 3 \rightarrow F' = 2$ transition of ^{85}Rb (diamonds), and for the $F = 2 \rightarrow F' = 1$ transition of ^{87}Rb (circles). Input laser power is P=2 mW, the atomic densities are chosen to provide 85% absorption on each transition. Absolute values of the nonlinear Faraday rotation for linear polarization were $d\phi/dB(B = 0) = 2.9$ rad/G and 4.5 rad/G respectively. Inset: the theoretical dependences for naturally broadened Rb isotopes, from Eqs. (6.51) and (6.58).

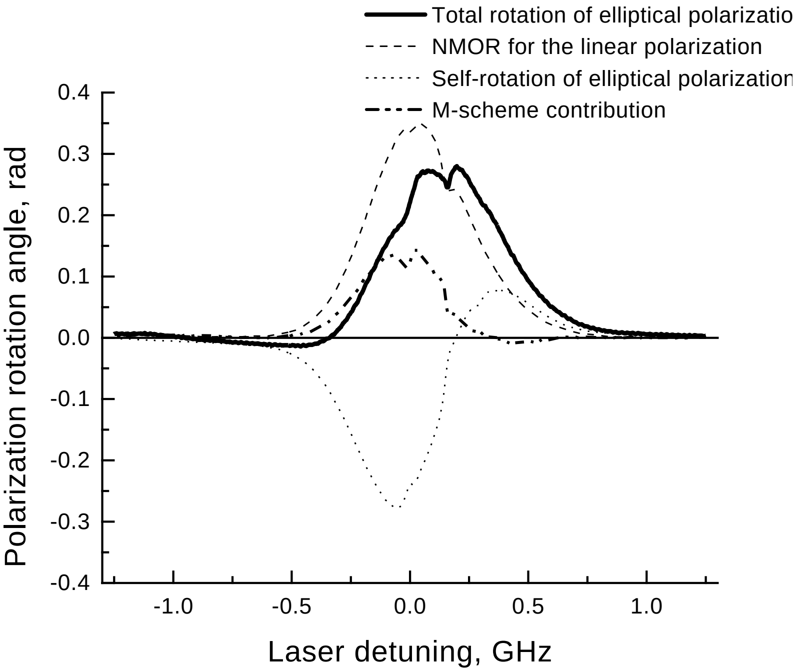

Fig. 43. The polarization rotation angle in ^{85}Rb as a function of laser detuning for ellipticity $\epsilon = 25^o$ and magnetic field $B = 0.35G$. The components of the rotation due to various processes are also shown. Zero detuning corresponds to the cross-resonance $F = 3 \rightarrow F' = 2.3$ transition. The distortions of the resonances are due to reflected light beam.

frequency for the case of large magnetic field is shown in Fig. 43. Similarly to the ^{87}Rb, the high-order Zeeman coherence significantly modifies the rotation spectra, and the contribution of the nonlinear rotation is comparable with the rotation of the linear polarization and self-rotation.

One can see additional sub-Doppler structure on top of the rotation resonances. These peaks appears due to the retro-reflection of the laser beam inside the atomic cell. This additional beam interacts with atoms and causes the redistribution of the atomic population similar to Doppler-free saturation spectroscopy.

As a conclusion, we have studied the nonlinear magneto-optic rotation of elliptically polarized light interacting with various transitions of rubidium atoms. We have shown that this rotation can be described by means of Λ, M, and higher chain Λ schemes. For the simple three-level Λ scheme, the rotation does not depend on the light ellipticity. For more complicated systems, multi-photon processes are responsible for the creation of high-order ground-state coherence resulting in a new type of ellipticity-dependent nonlinear magneto-optical rotation. We have derived simple analytical expressions for this rotation for the M interaction scheme (Eq. (6.51)) and we showed that this effect results from the coherently induced hexadecapole moment.

To verify our theoretical calculations, we have studied the polarization rotation of elliptically polarized laser light propagating through Rb vapor. The M interaction scheme is realized on the $F = 2 \rightarrow F' = 1$ transition of ^{87}Rb, and the triple-Λ scheme is observed on the $F = 3 \rightarrow F' = 2$ transition of ^{87}Rb. Although the experimental points cannot be fit perfectly by the theoretical expressions (Eqs. (2.70) and (6.51)), the basic properties of the new rotation are confirmed.

CHAPTER VII

SELF-ROTATION OF THE ELLIPTICAL POLARIZATION AND ITS APPLICATION FOR THE GENERATION OF SQUEEZED VACUUM

Self-rotation of elliptically polarized light is a well-known nonlinear optical phenomena [21, 285–287]. This effect can be caused by Kerr nonlinearity in solids and liquids [288, 289], optical pumping and ac-Stark shifts in atomic vapors [124, 290–294], and other mechanisms.

Polarization self-rotation in coherent atomic media may be explained as follows. Two circular components of an elliptically polarized electromagnetic wave optically pump the atoms into a coherent superposition of ground-state magnetic sublevels. Since this superposition state is associated with steep dispersion, even small shifts of the magnetic sublevels result in a large shift in the refractive indices for the two circular components. Another manifestation of this effect results in large rotation of linear polarization in the presence of an external magnetic field, discussed earlier. However, the degeneracy of the ground-state magnetic sublevels may be lifted even in the absence of the external magnetic field because of the ac-Stark shifts. Since the value of the shift is proportional to the intensity of the electromagnetic field, the difference in the intensities of the circularly polarized components of the elliptically polarized laser field result in the different light shifts of the different magnetic sublevels, proportional to the light ellipticity, and, therefor, in the different refractive indices for these components. Thus, after traversing the atomic cell the polarization ellipse is rotated at an angle, proportional to its ellipticity.

It should be emphasized that the self-rotation of the elliptical polarization is completely different from the ellipticity-dependent NMOR, considered in Chapter VI. This effect is determined solely by the ellipticity of the electromagnetic field, and exists without any external magnetic or electric fields.

In this Chapter we first develop the phenomenological description of the self-rotation in two interaction pictures, corresponding to the Rb atoms for different interaction regimes. If the laser intensity is relatively low, so that the Rabi frequency is much smaller than the hyperfine splitting of the excited levels, the rotation of the elliptical polarization is well described by double-Λ scheme, whereas the X scheme corresponds to the case then the hyperfine structure is completely overlapped by power broadening.

Then we present the results of the experimental study of the ac-Stark shifts and self-rotation in hot Rb vapor. First, we measure the modification of the EIT resonance observed in elliptically polarized light. These measurements allow us to include the information about actual level structure of the Rb atoms to the simplified theory. Then we study the self-rotation of elliptically polarized light in both Rb isotopes for different experimental conditions, such as laser frequency and intensity, atomic density, etc.

Finally, we demonstrate that the large self-rotation can be used for effective generation of nonclassical states of light, such as squeezed vacuum. The exact numerical simulation, made for Rb atoms, supports this idea.

A. Theory of self-rotation of the elliptical polarization

1. Double-Λ level configuration

Let us study the propagation of an elliptically polarized electromagnetic wave in a medium consisting of double-Λ atoms (see Fig. 44). We treat the wave as a superposition of two circularly polarized components. These left- and right-circularly polarized components interact with transitions $|b_-\rangle \rightarrow |a_{1,2}\rangle$ and $|b_+\rangle \rightarrow |a_{1,2}\rangle$ respectively, and

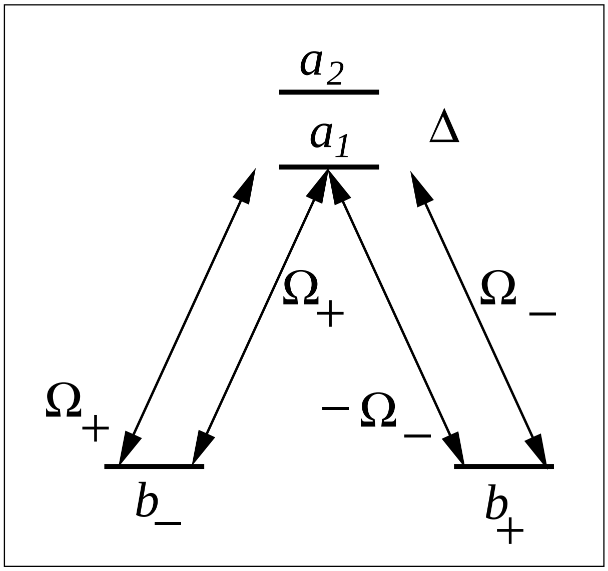

Fig. 44. Atoms in a double-Λ configuration interacting with two circularly polarized fields E_+ and E_-. Field $E_\pm$ is resonant with transitions $a_1 \rightarrow b_\mp$ and off-resonant with transitions $a_2 \rightarrow b_\mp$. The splitting between a_1 and a_2 is Δ. We assume that the angular matrix elements, and consequently the Rabi frequencies, of the $a_2 \rightarrow b_+$ and $a_2 \rightarrow b_-$ transitions have opposite sign, as for the ^{87}Rb D_1 line.

has Rabi frequencies $\Omega_{1-} = \Omega_{2-} = \Omega_+$ and $-\Omega_{1+} = \Omega_{2+} = \Omega_-$[1]. We assume that the electromagnetic wave is resonant with transitions $|b_\pm\rangle \leftrightarrow |a_1\rangle$ and has large detuning Δ from transitions $|b_\pm\rangle \leftrightarrow |a_2\rangle$. Then the coherence between ground state levels $|b_+\rangle$ and $|b_-\rangle$ is mainly determined by the resonant interaction. The off-resonant interaction introduces a slight change in the coherence only. We also assume that the ground state levels are nearly degenerate so that the circularly-polarized components of the electromagnetic wave are nearly two-photon resonant with transitions $|b_+\rangle \leftrightarrow |a_{1,2}\rangle \leftrightarrow |b_-\rangle$.

---

[1] Here and in all following equations we use the notation ± referring to the levels $|b_\pm\rangle$, and $1, 2$ referring to the levels $|a_{1,2}\rangle$.

To describe the interaction of the atoms and the electromagnetic wave we use Bloch equations. Equations for the atomic polarizations are:

$$\begin{aligned}
\dot{\rho}_{1+} &= -\Gamma_{1+}\rho_{1+} + i\Omega_-(\rho_{++} - \rho_{11}) - i\Omega_+\rho_{-+} + i\Omega_-\rho_{12}, && (7.1)\\
\dot{\rho}_{2+} &= -\Gamma_{2+}\rho_{2+} - i\Omega_-(\rho_{++} - \rho_{22}) - i\Omega_+\rho_{-+} - i\Omega_-\rho_{21}, && (7.2)\\
\dot{\rho}_{1-} &= -\Gamma_{1-}\rho_{1-} - i\Omega_+(\rho_{--} - \rho_{11}) + i\Omega_-\rho_{+-} + i\Omega_+\rho_{12}, && (7.3)\\
\dot{\rho}_{2-} &= -\Gamma_{2-}\rho_{2-} - i\Omega_+(\rho_{--} - \rho_{22}) - i\Omega_-\rho_{+-} + i\Omega_+\rho_{21}, && (7.4)
\end{aligned}$$

where

$$\Gamma_{1+} = \Gamma_{1-} = \gamma, \;\; \Gamma_{2+} = \Gamma_{2-} = \gamma + i\Delta, \tag{7.5}$$

where γ is the natural decay rate, and γ_0 is the decay rate of the ground-state coherence. We assume here that there is no radiative decay of the ground state, but only a decay without population exchange.

The populations of the ground-state levels and low-frequency atomic coherences obey the equations:

$$\begin{aligned}
\dot{\rho}_{--} &= \gamma(\rho_{11} + \rho_{22}) + i\left[\Omega_+(\rho_{-1} + \rho_{-2}) - c.c.\right], && (7.6)\\
\dot{\rho}_{++} &= \gamma(\rho_{11} + \rho_{22}) + i\left[\Omega_-(\rho_{+2} - \rho_{+1}) - c.c.\right], && (7.7)\\
\dot{\rho}_{11} &= -2\gamma\rho_{11} + i(\Omega_-\rho_{+1} - \Omega_+\rho_{-1} - c.c.), && (7.8)\\
\dot{\rho}_{22} &= -2\gamma\rho_{22} - i(\Omega_-\rho_{+2} + \Omega_+\rho_{-2} - c.c.), && (7.9)\\
\rho_{11} + \rho_{22} &+ \rho_{++} + \rho_{--} = 1; && (7.10)
\end{aligned}$$

and

$$\dot{\rho}_{-+} = -\Gamma_{-+}\rho_{-+} - i\Omega_+^*(\rho_{1+} + \rho_{2+}) - i\Omega_-(\rho_{-1} - \rho_{-2}), \tag{7.11}$$

$$\dot{\rho}_{12} = -\Gamma_{12}\rho_{12} - i(\Omega_+\rho_{-2} - \Omega_-\rho_{+2} - \Omega_-^*\rho_{1+} - \Omega_+^*\rho_{1-}), \tag{7.12}$$

respectively. Here

$$\Gamma_{+-} = 2\gamma_0 - i\delta, \;\; \Gamma_{12} = 2\gamma - i\Delta. \tag{7.13}$$

δ is the two-photon detuning caused by small shifts of the ground-state levels (for example, due to an external magnetic field).

The equations for the atomic polarizations can be rewritten in the steady state, assuming $\rho_{11} = \rho_{22} = \rho_{12} = 0$,

$$\begin{aligned}
\rho_{1+} &\approx i\frac{\Omega_-}{\Gamma_{1+}}\rho_{++} - i\frac{\Omega_+}{\Gamma_{1+}}\rho_{-+}, &(7.14)\\
\rho_{2+} &\approx -i\frac{\Omega_-}{\Gamma_{2+}}\rho_{++} - i\frac{\Omega_+}{\Gamma_{2+}}\rho_{-+}, &(7.15)\\
\rho_{1-} &\approx -i\frac{\Omega_+}{\Gamma_{1-}}\rho_{--} + i\frac{\Omega_-}{\Gamma_{1-}}\rho_{+-}, &(7.16)\\
\rho_{2-} &\approx -i\frac{\Omega_+}{\Gamma_{2-}}\rho_{--} - i\frac{\Omega_-}{\Gamma_{2-}}\rho_{+-}. &(7.17)
\end{aligned}$$

Then for the low frequency ground state atomic coherence we derive

$$\rho_{-+} = \frac{\Omega_+^*\Omega_-}{\gamma(2\gamma_0 - i\delta) + |\Omega|^2} - 2i\frac{\gamma}{\Delta}\frac{\Omega_+^*\Omega_-}{|\Omega|^2}\frac{|\Omega_+|^2 - |\Omega_-|^2}{|\Omega|^2} \tag{7.18}$$

where $|\Omega|^2 = |\Omega_+|^2 + |\Omega_-|^2$. We assume here that $\rho_{\pm\pm} \approx \rho_{\pm\pm}^{(\Lambda)} = |\Omega_\pm|^2/|\Omega|^2$ (this directly follows from the equations for the populations). Here the first r.h.s. term describes the dark state coherence which appears due to the resonant fields, and the second term appears due to AC-Stark shifts which serve to modify the coherence.

Using the expressions for ground state populations and the coherence, we can calculate the polarizations

$$\begin{aligned}
\rho_{1-} &\approx \frac{\Omega_-|\Omega_+|^2}{|\Omega|^4}\left(2i\gamma_0 + \delta + 2\frac{|\Omega_+|^2 - |\Omega_-|^2}{\Delta}\right), &(7.19)\\
\rho_{1+} &\approx -\frac{\Omega_+|\Omega_-|^2}{|\Omega|^4}\left(2i\gamma_0 - \delta + 2\frac{|\Omega_+|^2 - |\Omega_-|^2}{\Delta}\right), &(7.20)
\end{aligned}$$

$$\rho_{2-} \approx -\frac{2\Omega_-|\Omega_+|^2}{\Delta|\Omega|^2}, \tag{7.21}$$

$$\rho_{2+} \approx -\frac{2\Omega_+|\Omega_-|^2}{\Delta|\Omega|^2}, \tag{7.22}$$

The stationary propagation of the right and left circularly polarized electric field components through the atomic vapor is described by Eq.(2.12). Using the above expressions for the atomic polarizations we derive equations describing the circularly polarized electromagnetic fields propagation through the cell:

$$\frac{\partial}{\partial z}\Omega_+ \approx -2\kappa\Omega_+\frac{|\Omega_-|^2}{|\Omega|^4}\left(\gamma_0 + 2i\frac{|\Omega_-|^2}{\Delta}\right) \tag{7.23}$$

$$\frac{\partial}{\partial z}\Omega_- \approx -2\kappa\Omega_-\frac{|\Omega_+|^2}{|\Omega|^4}\left(\gamma_0 + 2i\frac{|\Omega_+|^2}{\Delta}\right). \tag{7.24}$$

where $|\Omega|^2 = |\Omega_+|^2 + |\Omega_-|^2$, and κ is the coupling constant, given by Eq.(2.26).

In order to evaluate the absorption and self-rotation parameters, we need to separate the real and imaginary parts of the circular components. Using $\Omega_\pm = |\Omega_\pm|\, e^{i\phi_\pm}$, we can rewrite Eqs. (7.23) and (7.24) for the total Rabi frequency $|\Omega|^2$ and the self-rotation angle $\phi_{sr} = \frac{1}{2}\left(\phi_+ - \phi_-\right)$

$$\frac{\partial}{\partial z}|\Omega|^2 = -8\kappa\gamma_0\frac{|\Omega_+|^2|\Omega_-|^2}{|\Omega|^4} \approx -2\kappa\gamma_0 \tag{7.25}$$

$$\frac{\partial}{\partial z}\phi_{sr} = \frac{\kappa}{\Delta}\frac{|\Omega_+|^4 - |\Omega_-|^4}{|\Omega|^4} \approx \frac{2\kappa}{\Delta}\epsilon \tag{7.26}$$

where we used the definition for the ellipticity ϵ

$$\epsilon = \frac{1}{2}\arcsin\frac{|E_+|^2 - |E_-|^2}{|E_+|^2 + |E_-|^2} \approx \frac{1}{2}\left(\frac{|\Omega_+|^2 - |\Omega_-|^2}{|\Omega|^2}\right). \tag{7.27}$$

In this, we have assumed that the light is nearly linearly polarized ($1 \gg \epsilon$), and that its ellipticity does not change while propagating through the medium. Equations (7.25) and (7.26) have the simple solution:

$$|\Omega(z)|^2 \simeq |\Omega(0)|^2 \left(1 - \frac{2\kappa\gamma_0}{|\Omega(0)|^2} z\right) \tag{7.28}$$

$$\phi_{sr} \simeq \frac{2\kappa}{\Delta}\epsilon z \tag{7.29}$$

where $\Omega(0)$ is the total Rabi frequency at the entrance of the medium. One can easily see that the expression for the transmitted light coincide with the analogous expression Eq.(2.69) for a single Λ scheme. This directly follows from the assumption that the off-resonance interaction with level a_2 does not disturb the dark state and causes no additional absorption. At the same time it is easy to see that the self-rotation appears only because of the additional level, and it is disappears for $\Delta \rightarrow \infty$.

For the further analysis it is convenient to introduce the self-rotation coefficient g defined as $\phi_{sr} = \mathrm{g}\epsilon L$, and the absorption coefficient α such as $I_{out} = I_{in}(1 - \alpha L)$. These parameters for the double-Λ interaction scheme can be estimated using Eqs. (7.28) and (7.29)

$$\mathrm{g} = 2\frac{\kappa}{\Delta} \tag{7.30}$$

$$\alpha = 2\frac{\kappa\gamma_0}{|\Omega(0)|^2}\ . \tag{7.31}$$

2. *X* level configuration

In the previous section we restricted ourselves to the case of a far-detuned sublevel of the excited state. The analysis of Eq.(7.31) shows that higher laser power leads to smaller optical losses, which is obviously beneficial for any practical application of self-rotation. At the same time, as the laser power grows, the interaction with both hyperfine sublevels becomes equally important, and the previously developed model cannot be applied anymore.

Now let us consider the case when the hyperfine structure of atoms can be ne-

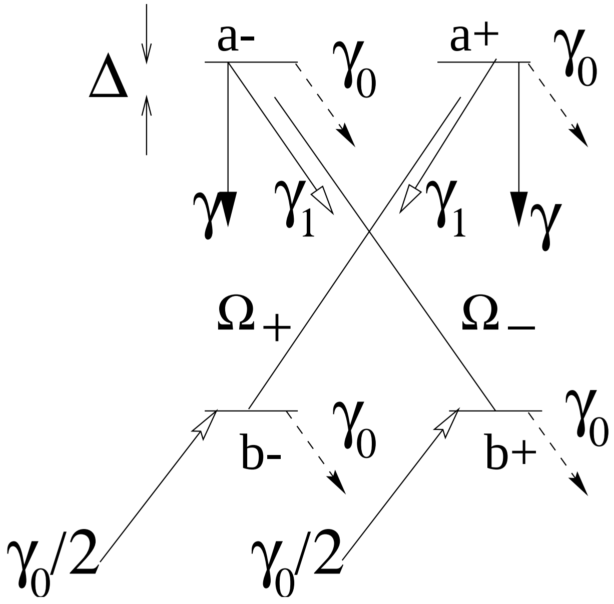

Fig. 45. Atoms in an X configuration interacting with two circularly polarized fields E_+ and E_-.

glected. This situation may be realized, for example, in atomic cells with high buffer gas pressure, where the collisional broadening surpasses the hyperfine splitting [290]. This regime can also be achieved for very high laser intensity, so that $|\Omega| \gg \Delta_{hf}$.

Let us consider open system as shown in Fig. 45. This scheme consists of two independent two-level systems coupled by the population decay. The Bloch equations for non-zero density matrix elements for this system are:

$$\dot\rho_{a\pm a\pm} = -(\gamma+\gamma_1)\rho_{a\pm a\pm} + i\left(\Omega_\pm\rho_{b\mp a\pm} - \Omega_\pm^*\rho_{a\pm b\mp}\right) \tag{7.32}$$

$$\dot\rho_{b\pm b\pm} = -\gamma_0(\rho_{b\pm b\pm} - \frac{1}{2}) + \gamma\rho_{a\pm a\pm} + \gamma_1\rho_{a\mp a\mp} + i\left(\Omega_\mp^*\rho_{a\mp b\pm} - \Omega_\mp\rho_{b\pm a\mp}\right) \tag{7.33}$$

$$\dot\rho_{a\pm b\mp} = -\left(\frac{\gamma+\gamma_1}{2} + \gamma_0 + i\Delta\right)\rho_{a\pm b\mp} - i\Omega_\pm(\rho_{a\pm a\pm} - \rho_{b\mp b\mp}), \tag{7.34}$$

where γ and γ_1 are the decay rates of the excited states (correspondingly $a_\pm \rightarrow b_\pm$ and $a_\pm \rightarrow b_\mp$), and γ_0 is the ground-state population decay rate. It is easy to see that if $\sum \rho_{ii}(t=0) = 1$ than $\sum \rho_{ii}(t) = 1$ for this open system. For simplicity let us introduce the following notation:

$$\Gamma_{ab} = \frac{\gamma + \gamma_1}{2} + \gamma_0 \tag{7.35}$$

$$\Gamma_a = \gamma + \gamma_1 \tag{7.36}$$

Solving Eqs.(7.32)-(7.34) for the steady state regime one can obtain expressions for $\rho_{a\pm a\pm}$, $\rho_{a\pm b\mp}$ and $\rho_{b\pm b\pm}$:

$$\rho_{a\pm a\pm} = \frac{2\Gamma_{ab}|\Omega_\pm|^2}{\Gamma_a(\Gamma_{ab}^2 + \Delta^2) + 2\Gamma_{ab}|\Omega_\pm|^2}\rho_{b\mp b\mp} \tag{7.37}$$

$$\rho_{a\pm b\mp} = i\Omega_\pm \frac{\Gamma_a(\Gamma_{ab} - i\Delta)}{\Gamma_a(\Gamma_{ab}^2 + \Delta^2) + 2\Gamma_{ab}|\Omega_\pm|^2}\rho_{b\mp b\mp} \tag{7.38}$$

$$\rho_{b\pm b\pm} = \frac{1}{2}\frac{(\gamma_0\Gamma_a\Delta^2 + 2\Gamma(2\gamma_0+\gamma)|\Omega_\pm|^2)(\Gamma_a(\Gamma_{ab}^2+\Delta^2) + 2\Gamma_{ab}|\Omega_\mp|^2)}{\Gamma_a\Delta^2(\gamma_0\Gamma_a\Delta^2 + 2\Gamma(2\gamma_0+\gamma)|\Omega|^2) + 4\Gamma_{ab}^2(\gamma_0+\gamma)|\Omega|^4} \tag{7.39}$$

where $|\Omega|^2 = |\Omega_+|^2 + |\Omega_-|^2$. These expressions can be significantly simplified under some realistic assumptions. First, we assume that the decay rates of the excited levels is the same for all channels, i.e. $\gamma = \gamma_1 = \Gamma_a/2$. Second, we consider the case of strong electro-magnetic field, so that $|\Omega| \gg \Gamma_a$. We also consider the usual experimental conditions $\gamma_0 \ll \Gamma_a$, so $\Gamma_{ab} \simeq \Gamma_a/2$. In this case we can write the propagation equations for circular components of the electromagnetic field in the following form:

$$\frac{\partial}{\partial z}\Omega_\pm = i\kappa\rho_{a\pm b\mp} = -\frac{1}{2}\kappa\Omega_\pm(\frac{\Gamma_a}{2} - i\Delta)\frac{\gamma_0\Delta^2 + 2\Gamma_a|\Omega_\pm|^2}{(\Delta^2 + |\Omega|^2)(\gamma_0\Delta^2 + \Gamma_a|\Omega|^2)} \tag{7.40}$$

Using this equation we can find the absorption and self-rotation coefficients by presenting the complex Rabi frequencies as $\Omega_\pm = |\Omega_\pm|e^{i\phi_\pm}$. We also restrict ourselves to the case of nearly linearly polarized light, i.e. $|\Omega_\pm|^2 = |\Omega|^2(1 \pm 2\epsilon)/2$, $\epsilon \ll 1$. In this case the field intensity and the polarization rotation angle are

$$\frac{\partial}{\partial z}|\Omega|^2 = -\frac{1}{2}\kappa|\Omega|^2\frac{\Gamma_a}{\Delta^2+|\Omega|^2} \tag{7.41}$$

$$\frac{\partial}{\partial z}\phi_{sr} = 2\kappa q\frac{\Gamma_a\Delta|\Omega|^2}{(\Delta^2+|\Omega|^2)(\gamma_0\Delta^2+\Gamma_a|\Omega|^2)} \tag{7.42}$$

where the rotation angle of elliptical polarization is $\phi_{sr} = (\phi_+ - \phi_-)/2$. Using our definitions for the absorption and self-rotation coefficients we find:

$$\mathrm{g} = \kappa\frac{\Gamma_a\Delta|\Omega|^2}{(\Delta^2+|\Omega|^2)(\gamma_0\Delta^2+\Gamma_a|\Omega|^2)}. \tag{7.43}$$

$$\alpha = \kappa\frac{\Gamma_a}{\Delta^2+|\Omega|^2} \tag{7.44}$$

B. The influence of ac-Stark shifts on EIT resonance

We already demonstrated in the previous Chapter that the more complicated magnetic structure of Rb atoms lead to the modification of the polarization rotation compare to a simple Λ scheme. This raises the question of the applicability of any simplified interaction pictures for the explanation of the polarization self-rotation. For example, the $5S_{1/2}F = 2 \rightarrow 5P_{1/2}F' = 1,2$ transition of ^{87}Rb consists of 14 transitions between different Zeeman sublevels with different probabilities. The situation is even worse in ^{85}Rb which has higher ground-state angular momentum and richer magnetic structure. The exact solution of the problem of the propagation of elliptically polarized light through such an atomic medium is practically impossible.

However, there is a simple way to study how the Zeeman structure can be taken into account for the ac-Stark effect. Early studies of the interaction of the circularly or elliptically polarized electro-magnetic field with far-detuned transitions [21, 286, 287] demonstrated, that above all the light shifts lift the degeneracy of the Zeeman sublevels the same way as a magnetic field does. This means that the maximum transmission, which corresponds to the zero two-photon detuning between the circularly polarized components, is observed for the value of magnetic field which cancels the level splitting caused by the ac-Stark shifts.

Assuming that the absorption in the system and the polarization ellipticity are small, the two-photon detuning due to the ac-Stark shifts in the case of a four-level scheme, as shown in Fig. 44, is [124, 292]:

$$\delta_{EIT} = \frac{|\Omega_+(0)|^2 - |\Omega_-(0)|^2}{\Delta}. \tag{7.45}$$

For more complicated atomic systems we need to replace the actual hyperfine splitting between upper levels by some effective detuning Δ_0, which depends on the dipole momenta of the driven and perturbing transitions as well as on the structure of the atomic levels. It is important to stress, that in any case the value of two-photon detuning, induced by the light shifts, depends only on the initial intensities of two circular components, which makes it ideal for the experimental measurement of Δ_0.

As shown below, the validity of Eq.(7.45) directly follows from numerical simulations as well as from the experiment. To measure δ_{EIT} the absorption of elliptically polarized light in the atomic cell is detected, and the value of magnetic field corresponding to the maximum of transmitted intensity is recorded. In these experiments we use the cell containing isotopically pure ^{87}Rb and 30 torr of Ne. We use the cell with maximum available buffer gas pressure in order to obtain the narrowest EIT resonances, since the value of the level shift is much smaller than the width of the EIT peak. We also perform a detailed numerical simulation of the modification of the EIT signal. The stationary propagation of the right and left circular polarized electric field components through the atomic vapor is described by Maxwell-Bloch equations in the slowly-varying amplitude and phase approximation. We then solve these equations for the thirteen-level scheme corresponding to the Zeeman structure of

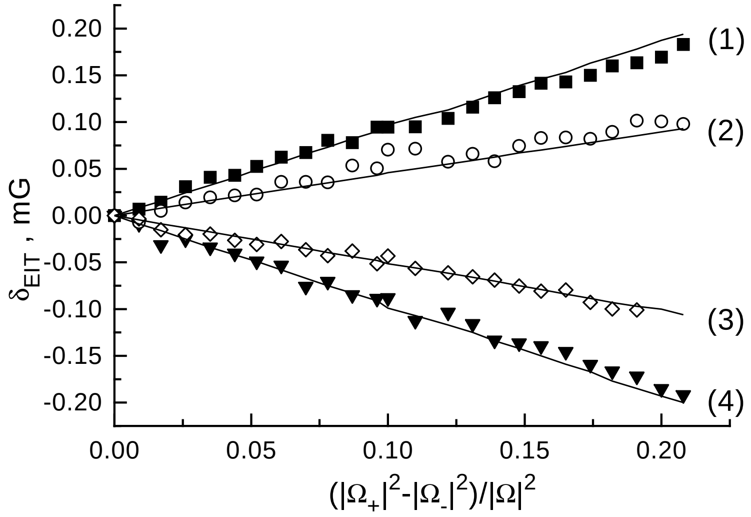

Fig. 46. Position of the EIT resonance (in terms of longitudinal magnetic field B) as a function of the degree of the incoming light ellipticity. Experimental data are shown as dots and theoretical results are shown as lines. Curves (1) and (4) correspond to the transitions $F = 2 \to F' = 1'$ and $F = 2 \to F' = 2'$, with intensity 1.1 mW/cm^2; curves (2) and (3) correspond to the same transitions and intensity 0.54 mW/cm^2. The measured values of the intensities are 1.2 and 0.6 mW/cm^2.

the $5S_{1/2}F = 2 \to 5P_{1/2}F' = 1, 2$ Rb transition, taking into account the propagation effects and Doppler averaging. We find that the results of the numerical simulation are well modelled by Eq.(7.45).

The results of the measurement and numerical simulation are shown in Fig. 46. The dependence of the position of the dark resonance is almost linear for small values of ellipticity. The slopes of the curves are proportional to the light intensity and the sign of their slope depends on the tuning of the laser. This allows us to conclude that Eq.(7.45) gives a correct description of the effect for the real atomic system in the case when laser is tuned near resonance with one of the hyperfine transitions.

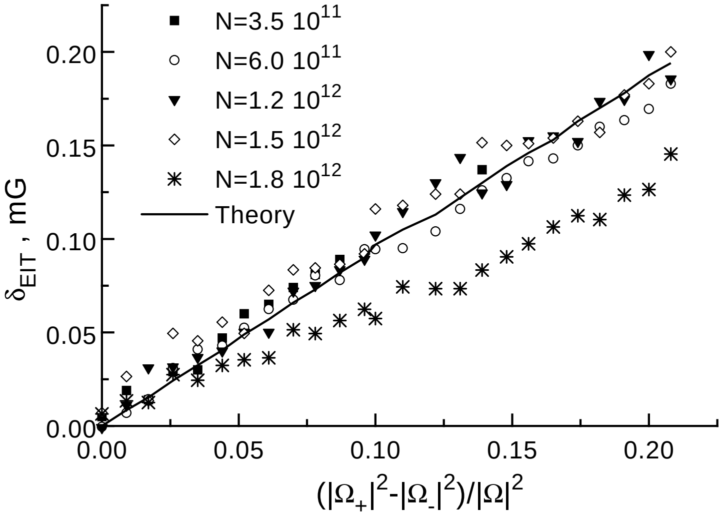

Fig. 47. Position of the EIT resonance (in terms of longitudinal magnetic field B) for the transition $F = 2 \rightarrow F' = 1'$ for various densities N of Rb vapor. Laser intensity is $1.1\,\mathrm{mW/cm^2}$.

The numerical model is in good agreement with the experiment. Possible systematic errors can appear due to imperfections in the quality of the laser beam which prevents an exact knowledge of the Rabi frequencies.

We also verify Eq.(7.45) by detecting δ_{EIT} for different atomic densities. The theory predicts that there should be no dependence of the resonance position. The experimental data, presented in Fig. 47 support this fact. The shift is quite constant for comparable low densities and starts to decrease for higher densities. A “threshold” density, when the deviation from the theory becomes clear, corresponds to the low transmission for which the validity of our approximations is doubtful. For the particular cell this threshold is about $1.7 \times 10^{12}\,\mathrm{cm}^{-3}$.

Since the ac-Stark effect is not a coherent phenomena, the induced two-photon detuning should not depend on the coherent properties of the medium. To check this,

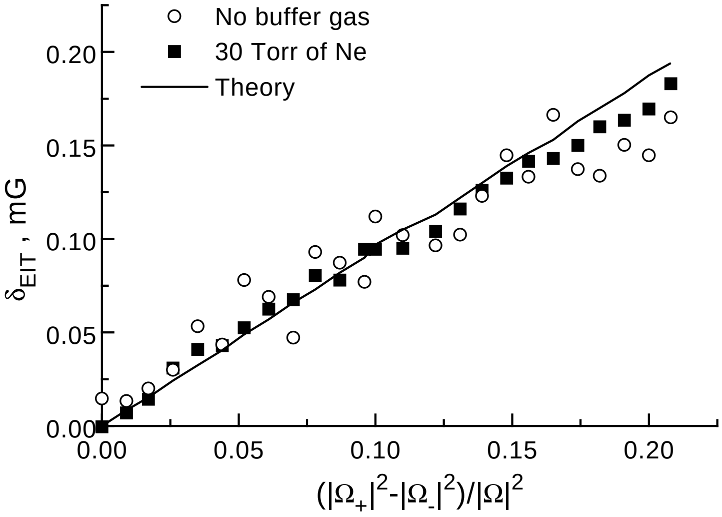

Fig. 48. Position of the EIT resonance (in terms of longitudinal magnetic field B) for the transition $F = 2 \rightarrow F' = 1'$ for the Rb cell with 30 Torr of Ne buffer gas and the one without buffer gas. Laser intensity is $1.1\,\mathrm{mW/cm^2}$.

we make an additional measurements of the EIT resonance position in a cell without buffer gas. Although the coherence decay rates for these two cells are several order of magnitude different, the dependence of the δ_{EIT} on the light ellipticity parameter $(|\Omega_+|^2 - |\Omega_-|^2)/|\Omega|^2$ are essentially the same (see Fig. 48).

It is important to mention that the effective detuning Δ_0 calculated using the experimental data is about 5 GHz, which is almost seven times larger than the actual hyperfine splitting of the $5^2P_{1/2}$ state (Δ_{hf} = 812MHz). The numerical simulation shows that this difference results from the complex structure of the Zeeman sublevels of the system.

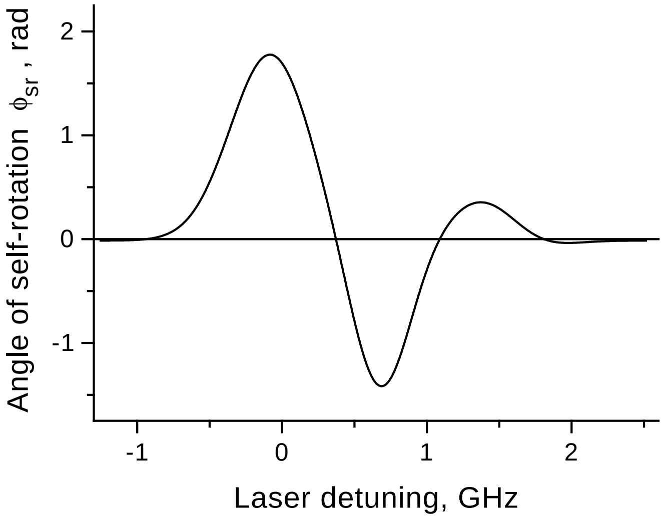

Fig. 49. Large self-rotation of elliptical polarization of the light propagating through vapor of ^{87}Rb vs laser detuning. Zero detuning corresponds to the $F = 2 \rightarrow F' = 1$ transition. Two small peaks on the right are due to the contamination of the cell with small amount of ^{85}Rb.

C. Experimental results

1. Large self-rotation

As in the case of the nonlinear Faraday rotation, the self-rotation of elliptical polarization should be enhanced with the density of atomic vapor. We are able to measure maximum polarization self-rotation of almost two radians in ^{87}Rb (see in Fig. 49). For this measurement, the laser power is 2 mW and the laser was tuned to the $5S_{1/2}, F = 2 \rightarrow 5P_{1/2}, F' = 1, 2$ atomic transition (D_1 line). The ellipticity of the incident light was about $\epsilon = 0.5$ rad. It is interesting to note that this value of SR is comparable with the large nonlinear Faraday rotation detected in similar experimental conditions (Fig. 11, [126]). One would expect to observe even higher value of the self-rotation for the D_2 line; unfortunately, an appropriate laser was not available on the time of these measurements.

2. Self-rotation on the Rb D_1 line

We first study the self-rotation on the D_1 line of ^{87}Rb. Although this line consists of two pairs of partially resolved resonant transitions, we focus our attention on the $F = 2 \rightarrow F' = 1, 2$ transition, since there is no ground-state coherence formed for the $F = 1 \rightarrow F' = 2$ transition [34, 35]. For the $F = 2 \rightarrow F' = 1, 2$ transition, the magnetic sublevels of the ground state are connected with Λ-like links formed by the two circularly polarized components of the elliptically polarized laser field. If the laser frequency is resonant with one transition, for example $F = 2 \rightarrow F' = 1$, the self-rotation of the polarization ellipse is determined by the interaction of the laser with the other transition formed by the same ground state hyperfine level $F = 2$ and the other hyperfine level of the excited state $F' = 2$. Furthermore, the polarization is rotated in opposite directions for light tuned to the $F = 2 \rightarrow F' = 1$ and $F = 2 \rightarrow F' = 2$ transitions (Fig. 50). Since the oscillator strengths of both these transitions are almost equal, the amplitudes of the self-rotation are nearly the same.

From Figs. 49 and 50 it is obvious that the self-rotation angle increases significantly in optically thick media. The value of the self-rotation coefficient g is nearly proportional to the density of atomic vapor, (shown in Fig. 51) which is consistent with the theory Eq.(7.30). At the same time the absorption is a linear function of atomic density, as is expected for the regime of electromagnetically induced transparency considered here (Eq.(7.28)). There is, however, a deviation from the linear behavior. For very high atomic density, we see a "saturation" of the self-rotation. This is because the intensity of the laser beam changes along the cell. As the absorption increases, the intensity of the light near the end of the cell may diminish to the

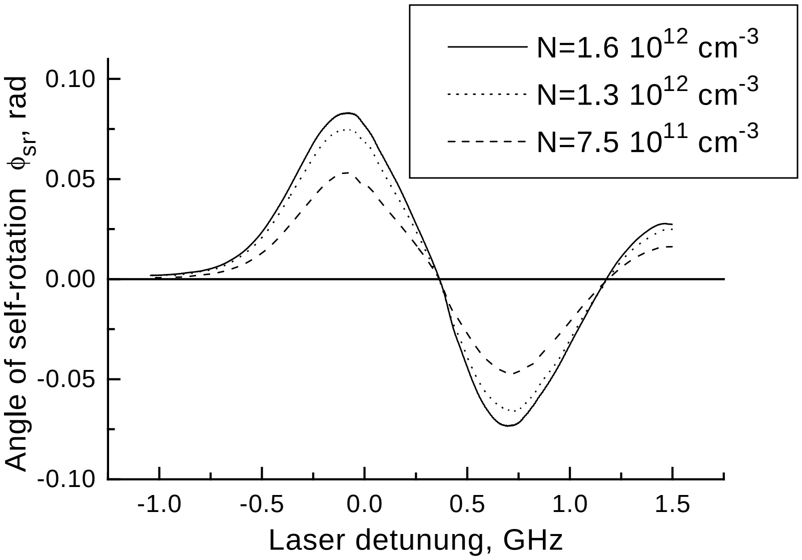

Fig. 50. The self-rotation angle for the $F = 2 \rightarrow F'$ transition of the ^{87}Rb D_1 line of as a function of laser frequency for different atomic densities. Zero detuning corresponds to the $F = 2 \rightarrow F' = 1$ transition. Laser power is $P = 5$ mW. Ellipticity of the beam is $\epsilon = 0.035$ rad.

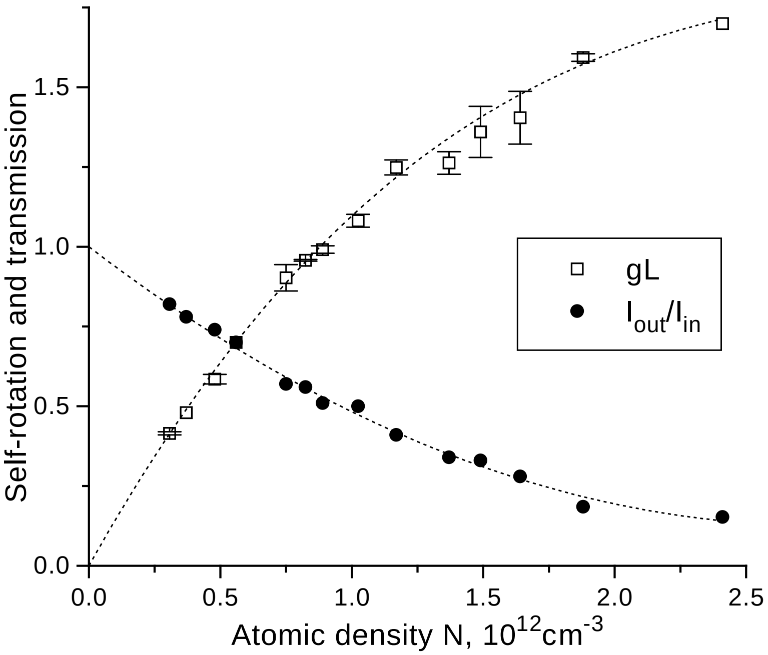

Fig. 51. Self-rotation parameter gL and transmission I_{out}/I_{in} measured as functions of atomic density for the ^{87}Rb D_1 line. Laser power is 5 mW. Ellipticity of the beam is $\epsilon = 0.035$ rad.

point where it is no longer enough to provide optical pumping into the dark state, meaning we no longer reach the regime of electromagnetically induced transparency.

To decrease losses in optically dense media, we must use enough laser power to provide efficient optical pumping into a dark state. Fig. 52 shows how the self-rotation and absorption depend on laser power. This behavior of the self-rotation is not described by Eq.(7.30). In fact, the double-Λ configuration predicts the self-rotation to be independent of the laser intensity. In our experiment, though, higher power leads to smaller absorption and higher self-rotation. At the same time, the power dependence of g is not linear, and it is plausible that it becomes flat for higher laser

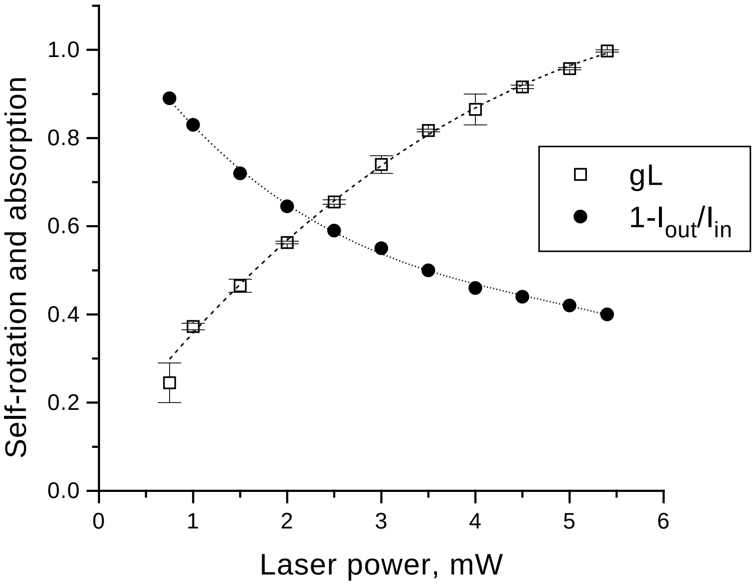

Fig. 52. Self-rotation parameter gL and absorption coefficient $\alpha L = 1 - I_{out}/I_{in}$ measured as functions of laser intensity for the ^{87}Rb D_1 line. Atomic density is $N = 8.2{\times}10^{11}\mathrm{cm}^{-3}$. Ellipticity of the beam is $\epsilon = 0.035$ rad.

power, where the conditions for EIT are obeyed for all Doppler-broadened spectra.

We now consider self-rotation in ^{85}Rb. A simple picture of self-rotation leads one to the conclusion that the effect should be stronger in ^{85}Rb than in ^{87}Rb. Indeed, the ac-Stark shift of Zeeman sublevels that results in polarization self-rotation is inversely proportional to the detuning from the corresponding off-resonant atomic transitions (Eq.(7.30)). The hyperfine splitting of the excited level for ^{85}Rb is, in turn, almost twice as small as the splitting for ^{87}Rb. Therefore, it seems that ^{85}Rb should demonstrate stronger self-rotation than ^{87}Rb.

Our experiment shows that this simple picture is incomplete. By comparing the self-rotation parameters for both ^{85}Rb and ^{87}Rb D_1 lines, (see Figs. 51 and 53), we

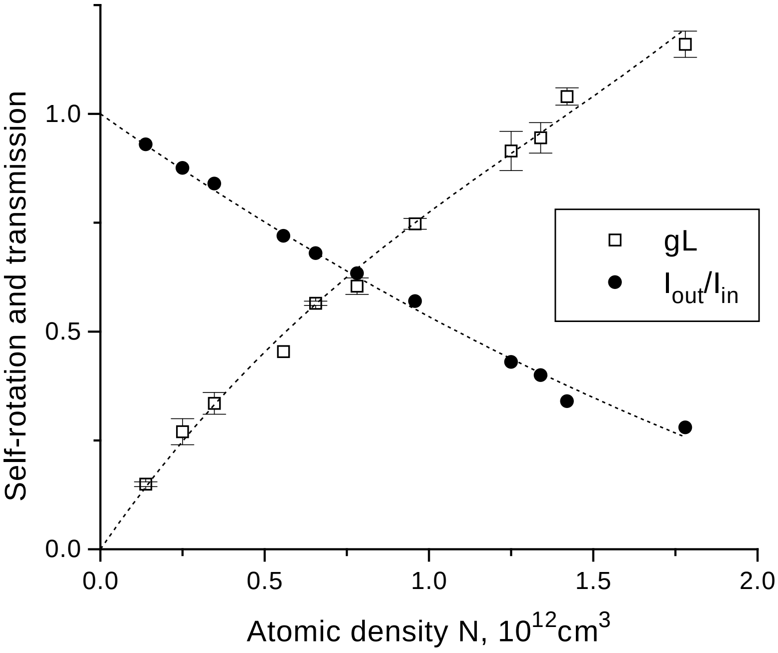

Fig. 53. Self-rotation parameter gL and transmission I_{out}/I_{in} for the ^{85}Rb D_1 line as functions of atomic density. The laser power is 5 mW.

see higher self-rotation in ^{87}Rb. The absorption, however, is almost the same for both isotopes. We can understand this result by noting that the transitions between different magnetic sublevels have different strengths that have to be taken into account, as discussed in the previous Section. Our experiments suggest that the more complicated sublevel structure an atom has, the more important is the dependence of the self-rotation effect on the structure, and this effect is usually destructive.

3. Self-rotation on the Rb D_2 line

Previous studies have shown [293, 294] that the self-rotation of light tuned to the Rb D_2 line is stronger than when tuned to the D_1 line.

We first discuss the experimental results for ^{87}Rb. Results for measurement of the angle of self-rotation on the transition $F = 1 \rightarrow F'$ are shown in Fig. 54. As one can see, the shape of the rotation curve is different from the D_1 line, since the excited state $5P_{3/2}$ consists of four hyperfine sublevels. In this case the laser interacts with three allowed transitions $F = 1 \rightarrow F' = 0, 1, 2$ of different strengths, which results in the highly asymmetric dependence of the self-rotation angle on the laser detuning. Maximum self-rotation is observed for laser tuning about half way between the $F = 1 \rightarrow F' = 0$ and $F = 1 \rightarrow F' = 2$ transitions. The important feature of the effect is that the optimum frequency does not change with laser power or/and atomic density. With this in mind, the laser is tuned to this frequency for further studies of the self-rotation on this line. [2]

The dependence of the self-rotation parameter g on atomic density is shown in

---

[2] The sub-Doppler structure observed for the self-rotation angle (Figs. 54 and 57) is apparently caused by reflections of the laser beam from the inner walls of the atomic cell. This reflected light redistributes the population of the sublevels, resulting in Doppler-free resonances and thus changes the self-rotation. This effect must be taken into account for all cells, since it is very difficult to avoid the retro-reflection.

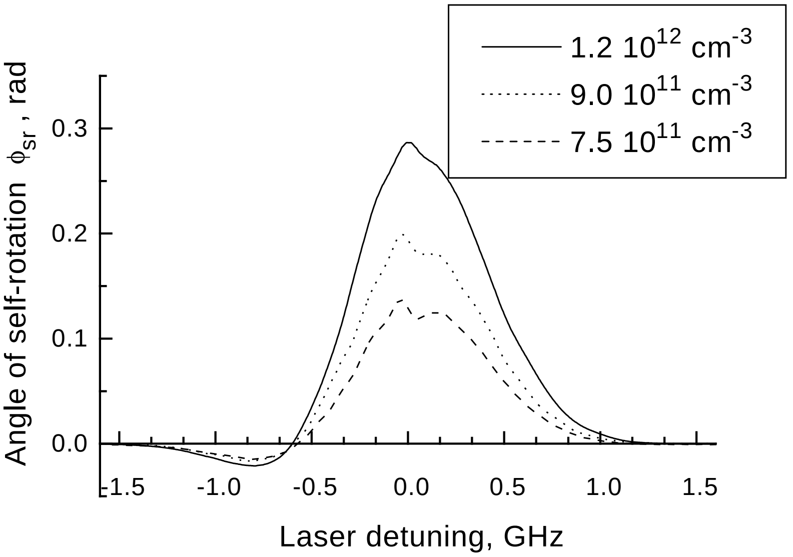

Fig. 54. The angle of self-rotation measured on the $F = 1 \rightarrow F'$ transition of the ^{87}Rb D_2 line as a function of laser detuning. Zero detuning is chosen to coincide with the center of absorption line. Laser power is $P = 5$ mW, ellipticity of the beam is $\epsilon = 0.035$ rad.

Fig. 55. The experimental points are very well fit by a straight line except at very high optical density. At the same time, our experimental results demonstrate that the nonlinearity increases with laser intensity for fixed value of absorption (Fig. 56). This gives us hope that the optical losses may be reduced with significantly higher laser intensity while keeping nonlinearity will at a high level. However, unlike the case for the D_1 line, increasing laser intensity results in a reduction of the self-rotation. There are several reasons for this: first, atoms are optically pumped to the other hyperfine component of the ground state, which corresponds to an effective decrease in the number of atoms interacting with the light. This problem can be solved experimentally by adding an incoherent re-pumping laser from the ground level $F = 2$. Another reason may be the influence of the $F = 1 \rightarrow F' = 2$ transition, for which no ground-state coherence is created.

In previous studies [294] we have measured the angle of self-rotation for the $F = 2 \ \rightarrow \ F'$ transition of the ^{87}Rb D_2 line. The average angle of self-rotation for the $F = 2 \ \rightarrow \ F'$ transition is about 3 times less than for transition the $F = 1 \ \rightarrow \ F'$ transition for the same amount of optical losses. A reason for this may be "trapping" of atoms in the strong non-rotating cycling transition $F = 2 \ \rightarrow \ F' = 3$.

The polarization self-rotation effect for the D_2 line of ^{85}Rb does not exceed that of ^{87}Rb. Moreover, the complicated level structure (arising from the higher nuclear spin) makes the behavior of the self-rotation to be quite unpredictable for the D_2 line, similar to the results for the D_1 line of ^{85}Rb.

Nonetheless, we observe that the self-rotation on the D_2 line of ^{85}Rb depends strongly on the intensity of the laser beam (Fig. 57). Note, that the approximations of our model are not valid here anymore: because of the small hyperfine splitting between excited states the electromagnetic field interacts with all transitions equally, and none of the transitions can be treated as "off-resonant" or independent. Thus, the

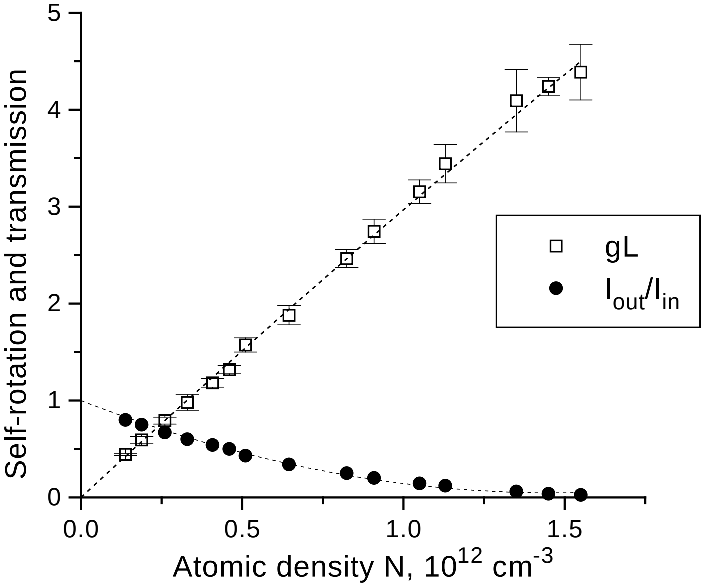

Fig. 55. The nonlinearity parameter gL measured as a function of ^{87}Rb density. Laser power is $P = 5.0$ mW.

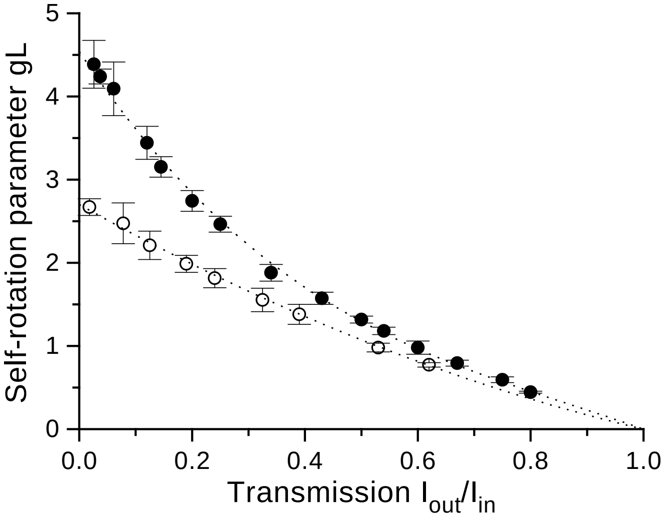

Fig. 56. The self-rotation parameter gL measured as a function of light transmission through the cell. Solid circles are for laser power $P = 5.0$ mW and open circles correspond to power $P = 1.3$ mW. Each point of the graph represents a different value of atomic density.

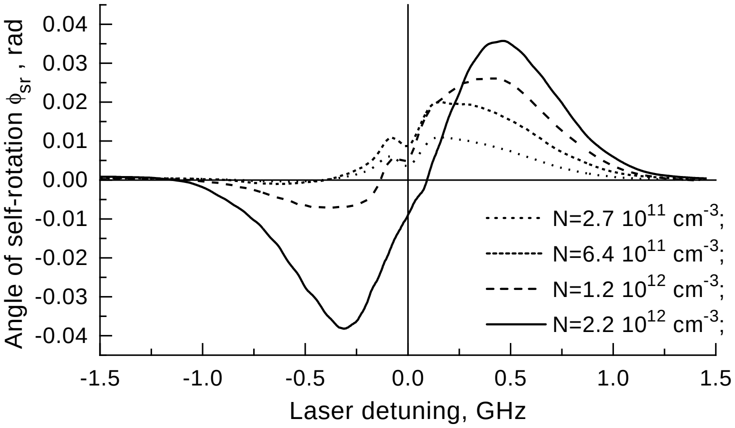

Fig. 57. The angle of self-rotation measured for the $F = 2 \to F'$ transition of the ^{85}Rb D_2 line as a function of laser detuning. Data are shown for different values of the laser power. Zero detuning is chosen to coincide with the center of absorption line. The atomic density is $N = 2 \times 10^{11}$ cm^{-3}. Ellipticity of the beam is $\epsilon = 0.035$ rad.

population of any Zeeman sublevel strongly depends on the laser intensity, causing the change of the self-rotation spectra.

The dependence of the self-rotation on laser intensity is directly reflected on its dependence on atomic density. Because optical losses grow with atomic density, at high density the intensity of the laser field is quite different at the entrance and the exit of the cell. This means that different atoms interact with a laser field of different strength, producing different rotations as shown in Fig. 57. This also explains the change of the shape of the self-rotation angle with increasing of density (Fig. 58). Such behavior makes it hard to predict if the combination of higher laser power and higher atomic density will further increase the nonlinearity and decrease the absorption.

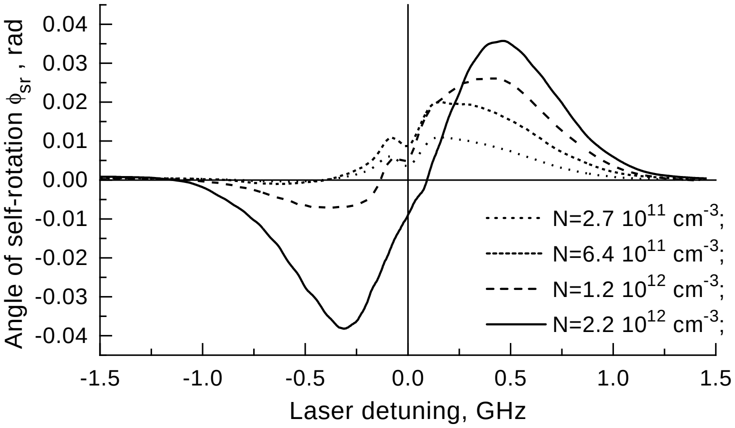

Fig. 58. The angle of self-rotation measured for the $F = 2 \rightarrow F'$ transition of the ^{85}Rb D_2 line a function of laser detuning. Data are shown for different atomic densities. Zero detuning is chosen to coincide with the center of absorption line. The laser power is $P = 5$ mW. Ellipticity of the beam is $\epsilon = 0.035$ rad.

4. Self-rotation in cells with buffer gas

The longer coherence lifetime in the presence of buffer gas results in smaller absorption of the light compared to the cell without buffer gas under the same experimental conditions. The theory for the double-Λ configuration predicts no dependence of the polarization self-rotation on the coherence decay rate; however, the use of buffer gas may be still beneficial to reduce the optical losses in the system.

To study the benefits of the presence of a buffer gas on self-rotation effects we use a cell filled with isotopically enhanced ^{87}Rb and 1 Torr of Ne as a buffer gas.

Fig. 59 shows the self-rotation parameter measured for cells with and without buffer gas. The dependencies versus transmission rather than atomic density are used to correctly compare atomic cells with different lengths. For small absorption, g is much higher for the cell with buffer gas, which agrees nicely with the prediction of

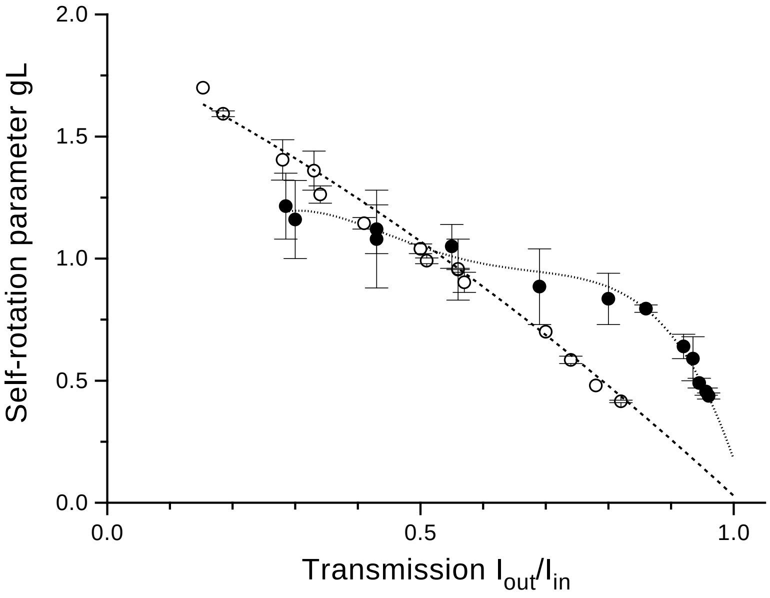

Fig. 59. The self-rotation parameter measured as a function of light transmission through the cell. Solid circles correspond to the cell without buffer gas and open circles correspond to the cell with 1 Torr of Ne. Laser power is $P = 5.0$ mW. Each point of the graph represents a different value of atomic density.

the theory (Eqs.(7.31),(7.30)). However, for higher optical density the self-rotation becomes smaller than that in the vacuum cell for the same level of absorption. Although there are several possible explanations for such behavior, the most obvious reason is the modification of the atomic coherence due to the velocity-changing collisions, described in Chapter V.

D. Application of self-rotation to generation of squeezed vacuum

Quantum fluctuations will soon be the basic source of quality restrictions in precise measurements and optical communications very soon. This calls for new methods which allow us to lift or ease these quantum limits. One of the well known solutions of the problem is based on usage of nonclassical states of light [1, 295]: for example, squeezed light and squeezed electromagnetic vacuum. The technology for producing squeezed vacuum via nonlinear optics is rather well developed [296] and has even been used to enhance the performance of interferometers [297, 298].

However, the efforts to widely exploit the potentialities of nonlinear optical phenomena to change the statistics of quantum fluctuations are hindered, either by the small value of nonlinearity or by absorption losses and the associated noises. When one is working with squeezed light, it is well known that any source of optical loss destroys the squeezed state. This appears because wherever the squeezed light leaves an optical system, the vacuum field necessarily enters the system; and the entering vacuum field is generally unsqueezed [299].

Although a large number of the attempts to generate squeezed light has been made, the level of -10 dB for generated and detected squeezing is still unbeaten. Up to our knowledge, the best result of squeezing generation was achieved in [300]. The detected degree of squeezing there was only -4.3 dB, but the inferred degree of squeezing was much larger. After making an absolute accounting for passive linear losses, these authors inferred a degree of squeezing corresponding to approximately -12 dB, which shows how well the basic nonlinear optical process of parametric down conversion conforms to simple theoretical models [299]. More recently, quantum noise reductions of -6 dB have been recorded directly in the observed homodyne current [301]. In this case the degree of squeezing was limited not by passive linear losses, but instead by nonlinear light induced absorption in potassium niobate crystals used for parametric down conversion. Quite recently, -6.5 dB of vacuum squeezing from a below-threshold optical parametric oscillator have been reported [302], with comparable levels reported in [303].

It has been recently demonstrated that efficient squeezing of vacuum fluctuations can be achieved in nonlinear self-rotating media [304]. When linearly polarized light traverses a medium that causes self-rotation of elliptical polarization, the vacuum field in the orthogonal polarization may be squeezed under optimum conditions. This squeezing was previously demonstrated in optical fibers [305, 306]. In that work, it was shown that if an incoming light pulse, linearly polarized along the X axis, is coupled into a single mode fiber, then the nonlinearity of the fiber transforms the state of the Y polarized mode from its initial coherent vacuum state into a state of squeezed vacuum at the output of the fiber.

The large self-rotation, observed in atomic vapor, may also be used for vacuum squeezing [304]. Although the experimental data, reported in previous Section, as well as many other studies of self-rotation in various experimental arrangements, published earlier [290, 293, 294] do not provide the level of self-rotation required to observe any significant vacuum squeezing, the situation is still optimistic. Here we propose to take advantages of the high laser power and high atomic density regime, which produces large nonlinearity accompanied by the suppression of light absorption.

1. Squeezing of vacuum fluctuations in general self-rotating medium

Let us first describe the propagation of a classical elliptically polarized electromagnetic field through the self-rotating medium. This field can be described by two complex X- and Y-polarized components (E_x and E_y). In this case the ellipticity ϵ of the light field can be written as:

$$\epsilon = \arcsin \frac{i(E_x^* E_y - E_y^* E_x)}{E_x^* E_x + E_y^* E_y}. \tag{7.46}$$

Note that for the particular case of nearly linearly polarized light ($E_y \gg E_x$, $E_y \approx E_y^*$) the expression for the ellipticity may be simplified:

$$\epsilon \approx -i \frac{E_x - E_x^*}{E_y}, \tag{7.47}$$

When this field propagates through a medium, self-rotation causes the principal axis of the ellipse to rotate by an angle $\varphi = \mathrm{g}\epsilon L$:

$$\begin{bmatrix} E_x(L) \\ E_y(L) \end{bmatrix} = \begin{bmatrix} \cos\varphi & \sin\varphi \\ -\sin\varphi & \cos\varphi \end{bmatrix} \begin{bmatrix} E_x(0) \\ E_y(0) \end{bmatrix}. \tag{7.48}$$

Using Eq.(7.47), we arrive to the following simple equation for the output fields $E_x(L)$ and $E_x(L)$:

$$E_x(L) = -i\mathrm{g}L(E_x(0) - E_x^*(0)) + E_x(0), \tag{7.49}$$

$$E_y(L) = E_y(0). \tag{7.50}$$

To describe the fluctuations of the electromagnetic fields, the quantum properties of light have to be taken into account. To find quantum fluctuations after the medium we present the parameters of the system as a sum of expectation and fluctuation parts. We denote expectation values by $\langle \ldots \rangle$. Hence, we have $\hat{E}_\pm = \langle E_\pm \rangle + \delta \hat{E}_\pm$, where $\langle E_\pm \rangle \gg \delta \hat{E}_\pm$ and $\langle \delta \hat{E}_\pm \rangle = 0$.

We describe quantum fluctuations of the fields using creation $\hat{a}_\pm^\dagger$ and annihilation $\hat{a}_\pm$ operators introduced by

$$\delta \hat{E}_\pm = \int_{-\infty}^{\infty} \sqrt{\frac{\hbar\omega_0}{\mathcal{A}c}} \hat{a}_\pm e^{-i\omega t}\, d\omega, \tag{7.51}$$

where $\mathcal{A}$ is the beam cross-section area, ω_0 is the carrier frequency, $\left[\hat{a}_\pm(z),\ \hat{a}_\pm^\dagger(z)\right] = \delta(\omega-\omega')$ and $\left[\hat{a}_\pm(z=0),\ \hat{a}_\mp^\dagger(z=0)\right] = 0$, z changes from 0 to L.

Using the analogy with classical theory we can formally change the classical value of ellipticity ϵ by the quantum operator of the ellipticity $\hat{\epsilon}$

$$\hat{\epsilon} = \arcsin \frac{\hat{E}_+^\dagger \hat{E}_+ - \hat{E}_-^\dagger \hat{E}_-}{\hat{E}_+^\dagger \hat{E}_+ + \hat{E}_-^\dagger \hat{E}_-}, \tag{7.52}$$

where $\hat{E}_x$ and $\hat{E}_y$ are the quantized fields.

If initially light is linearly polarized, it does not change the polarization in terms of the expectation values, i.e. if $\langle E_x(0)\rangle = 0$, then $\langle E_x(z)\rangle = 0$ and $\langle E_y(z)\rangle = \langle E_y(0)\rangle$. However, the calculation analogous to one for the propagation of classical fields demonstrates that the statistics of the light changes according to:

$$\begin{aligned} \hat{a}_x(z) &= \hat{a}_x(0) - igz(\hat{a}_x(0) - \hat{a}_x^\dagger(0)), \qquad (7.53)\\ \hat{a}_y(z) &= \hat{a}_y(0). \qquad (7.54) \end{aligned}$$

It is easy to see that commutation relations between the operators are fulfilled

$$\begin{aligned} &\left[\hat{a}_x(z), \hat{a}_x^\dagger(z)\right] = \left[\hat{a}_y(z), \hat{a}_y^\dagger(z)\right] = \left[\hat{a}_y(0), \hat{a}_y^\dagger(0)\right] = \qquad (7.55)\\ &\left[\hat{a}_x(0), \hat{a}_x^\dagger(0)\right] = \delta(\omega-\omega'). \end{aligned}$$

To adequately describe the quantum properties of the X polarized light component, the quadrature operator is introduced [1]:

$$\begin{aligned} B(z) &= \hat{a}_x(z)\exp(i\theta) + \hat{a}_x^\dagger(z)\exp(-i\theta) = \\ & \left[a_x(0) + a_x^\dagger(0)\right]\cos\ \theta + i\left[a_x(0) - a_x^\dagger(0)\right](\sin\ \theta - 2\mathrm{g}z\cos\ \theta). \end{aligned} \tag{7.56}$$

The amount of vacuum squeezing is characterized by the quadratic deviation of the quadrature component $\langle B^2(z)\rangle$. For the initial vacuum field this value is $\langle B^2(0)\rangle = 1$; it is possible to say that the squeezed vacuum is observed if the vacuum fluctuations are below this limit. According to Eq.(7.56) the quadratic deviation $\langle B^2(z)\rangle$ changes as the light travels through the medium:

$$\langle B^2(z)\rangle = \cos^2\ \theta + (\sin\ \theta - 2gg\cos\ \theta)^2 \tag{7.57}$$

This expression can be minimized under the condition $\mathrm{g}z \gg 1$, which corresponds to strong self-rotation for ctan $2\theta = -gz$:

$$\langle B^2(z)_{min}\rangle \approx (2gz)^{-2} \to 0, \tag{7.58}$$

that means that the vacuum field is squeezed. However, the dispersion of photo-counts in the dark port, proportional to $\hat{a}_x^\dagger(z)\hat{a}_x(z)$, increases compared with the coherent state:

$$(\Delta\hat{n})^2 = (gz)^2\,. \tag{7.59}$$

So far no consideration has been given to the optical losses in the system. We can model a thin medium with a small absorption coefficient in the following way: we assume that we have an ideal, transparent medium that produces self-rotation. After passing through this medium, a beam-splitter reflects a small fraction of the light away. At the same time, vacuum fluctuations enter through the dark port. Thus the squeezed vacuum is attenuated by an amount $e^{-\alpha z} \approx 1 - \alpha z$ while $1 - e^{-\alpha z} \approx \alpha z$ of noise is added to the field: $\hat{a}_\pm \to \hat{a}_\pm\sqrt{1-\alpha z} + \hat{b}_\pm\sqrt{\alpha z}$, where $\hat{b}_\pm$ are the quantum fluctuations leaking into the system due to the absorption. In this case the squeezing is determined by

$$\langle B^2(z)_{min}\rangle \to (2gz)^{-2} + \alpha z. \tag{7.60}$$

For the optimum number of absorption lengths

$$\alpha z_{opt} = \left(\frac{\alpha}{g}\right)^{2/3}, \tag{7.61}$$

the minimum achievable quadratic deviation of the quadrature amplitude is

$$\langle B^2_{opt}\rangle = 3\left(\frac{\alpha}{g}\right)^{2/3}. \tag{7.62}$$

2. The perspectives of squeezed vacuum generation in Rb vapor

Using the general expression Eq.(7.62), it is easy now to calculate the squeezing in case of the simplified interaction schemes considered earlier. Using the expression for self-rotation and absorption coefficients, derived earlier Eqs.(7.30, 7.31) the maximum squeezing, obtained in a double-Λ scheme is:

$$\langle B^2_{opt}\rangle_\Lambda = 3\left(\frac{\gamma_0\Delta}{|\Omega(0)|^2}\right)^{2/3}. \tag{7.63}$$

This means that under the condition of slightly perturbed CPT the squeezing is improving rapidly with growing laser intensity. The coherence is also playing an important role: the squeezing may be almost unlimited under the condition of small γ_0. However, the application of this model for the high laser power regime is limited by the assumption that the hyperfine splitting of the excited state is large. As the laser intensity becomes bigger, the electromagnetic field, resonant with one transition, starts to interact with all allowed transitions equally. To describe this situation, the X interaction scheme is more appropriate. In this case the squeezing of vacuum fluctuations is described by the following expression:

$$\langle B^2 \rangle_X = 3 \left(\frac{2\Delta |\Omega(0)|^2}{\gamma_0 \Delta^2 + \gamma |\Omega(0)|^2} \right)^{2/3} . \tag{7.64}$$

It is easy to see that for a strong laser field $|\Omega(0)|^2 \gg \Delta$ the value of squeezing is independent of laser intensity, and defined by the ratio of one-photon detuning to the radiative decay rate of the excited state . We must note here that this result is rather unsurprising, since Δ/γ describes the ratio of dispersion and absorption for an unsaturated two-level system. This result may be somewhat improved by the optimization of laser detuning for each laser intensity. In this case under conditions of $\Delta_{opt} = (\gamma/\gamma_0)^{1/2} |\Omega(0)|$ the maximum achievable squeezing is:

$$\langle B^2_{opt} \rangle_X = 3 \left(\frac{|\Omega(0)|^2}{\gamma_0 \gamma} \right)^{1/3} . \tag{7.65}$$

To verify the above statements for the real atoms, we perform exact numerical simulations of the vacuum squeezing generated on the $F = 2 \rightarrow F' = 1, 2$ transition of the D_1 line of ^{87}Rb. The value of the squeezing $\langle B^2 \rangle$, given by Eq.(7.62) is shown as a function of laser power in Fig. 60. For each laser power, the density and laser frequency that optimizes the squeezing is shown.

We note that significant squeezing (about -7 dB) is predicted for a laser intensity $\sim$10 W/cm^2. The form of this dependence may be nicely described by the theoretical results for two different interaction schemes. One can see that initially the value of squeezing grows rapidly with the laser intensity, as described by Eq.(7.63). For higher intensities it saturates, approaching a constant value, as predicted by Eq.(7.64).

The low laser power available in the experiments (≤ 5mW) cannot produce vacuum squeezing greater than -1dB, which makes any direct observation virtually impossible. However, we can extrapolate the experimental data for the self-rotation and absorption to the high intensity regime. As it has been shown earlier, the self-

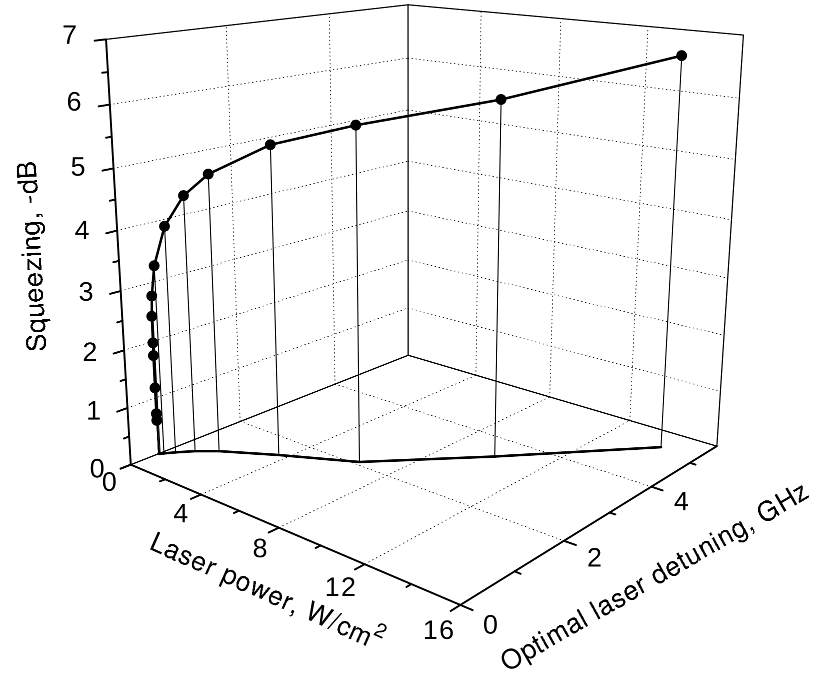

Fig. 60. The squeezing of vacuum fluctuations, as defined in Eq.(7.62), as a function of laser intensity. For each value of laser intensity, the squeezing is calculated for the optimum value of laser detuning and atomic density.

rotation for the D_1 line can be greatly improved by using higher laser power, and at the same time the absorption becomes smaller (Fig. 52). This is very promising for generation of squeezing.

It has been also demonstrated that the self-rotation, measured for the D_2 line, is higher. The maximum observed value of the self-rotation coefficient is $\mathrm{g}L = 5$, which corresponds to the squeezing of ≈ -10dB in a lossless medium as per Eq.(7.58). At the same time, increasing laser power is less effective, since both absorption and self-rotation become smaller (Fig. 56).

In conclusion, we have experimentally and theoretically studied the effect of self-rotation of the polarization ellipse of the electromagnetic field propagating through the atomic medium. Two interaction schemes are proposed to describe self-rotation and absorption of elliptically polarized light in Rb vapor. The experimental data, collected for various transition of both Rb isotopes satisfactorily agree with predictions of the theory. We also demonstrate that the effect of self-rotation can be used for efficient squeezing of vacuum fluctuations. Both theory and numerical simulations predict squeezing up to -10 dB under realistic experimental conditions.

CHAPTER VIII

APPLICATION OF THE NONLINEAR FARADAY EFFECT FOR HIGH-PRECISION MAGNETOMETRY

In this chapter we discuss the prospects of using the nonlinear Faraday effect for the precision measurements of a magnetic field. We first give a brief overview of the existing optical magnetometers. Then we present results for measurements of this rotation for resonant light in optically dense Rb vapor under various conditions, with and without buffer gas. And finally, we propose a method of in-principle improvement of the Faraday magnetometer by cancelling the ac-Stark shifts, which limit the sensitivity for the high power regime.

A. Optical methods of magnetic field measurements

The problem of sensitive measurement of small magnetic fields is very important, and optical techniques have proven very successful and competitive in this field. Magnetic sensors based on the Faraday effect (rotation of the linear polarization of the light propagating through a magnetic crystal placed in a longitudinal magnetic field) and the magneto-optical Kerr effect (change of polarization and intensity of light reflected from a magnetic sample) have found many applications due to their contactlessness, high stability with respect to electromagnetic interference, and wide frequency and dynamic ranges [307]. However, the sensitivity of these devices is limited by the relatively weak response of the system to changes in the magnetic field. For example, the value of the Verdet constant (the proportionality coefficient between the polarization rotation angle and applied magnetic field per unit length) for a diamagnetic sensor glass $SF-57$ is as low as 4×10^{-6}rad/(G cm) [308]. The situation may be improved by using transparent ferromagnetics (such as ytterbium iron garnets), which provide much higher Faraday rotation ($V = 10^{-2}$rad/(G cm)) [307, 309, 310]. At the same time, the polarization rotation in these crystals is not always a linear function of the applied magnetic field.

Much better sensitivity is achieved in optical magnetometers based of resonant phenomena. For example, optically pumped magnetometers (OPM) are based on the change of light absorption in a glass cell with He^4 or alkali vapor in the presence of a dc magnetic field (which resolve the electronic Zeeman structure) and a tunable rf magnetic field [244,311–313]. If the frequency of the rf field is resonant with the Zeeman splitting, a narrow dip in the absorption is observed which is used for accurate dc field measurements. OPMs already provide a realistic alternative to SQUID (superconducting quantum interference device) magnetometers [307,314]. The sensitivity of commercial OPMs is typically 10^{-9} G/$\sqrt{\mathrm{Hz}}$ [244, 307], and can reach 10^{-11} G/$\sqrt{\mathrm{Hz}}$ under laboratory conditions [315].

Another absorption-based method of magnetic field detection is based on CPT in Cs vapor [316–318]. In this method two phased-locked lasers (or two modes of a single laser) are used to create coherent superpositions between the ground-state hyperfine levels of Cs atoms in a Λ configuration. If the Zeeman structure is resolved, the EIT is observed every time the laser fields are in resonance with particular magnetic sublevels. So, if a laser is swept across the atomic transition, the comb of transmission peaks is observed, and the value of the magnetic field may be calculated by measuring their relative shifts.

The usual arrangement for the absorption-based measurements is to use low laser power to avoid power broadening and light shifts, and low atomic density to keep the sample optically thin. It was pointed out by Scully and Fleischhauer that in coherent media the power broadening can be completely compensated by increasing the atomic density, if phase -sensitive measurements are performed [4,5,158]. The estimates show that in this case substantial improvement over an OPM is possible. Unfortunately, in traditional EIT experiments the light shifts of the hyperfine-levels give rise to a bias phase shift, which becomes the major source of systematic error. This problem can be eliminated, however, in magnetometers, based on Zeeman ground-state coherence [124]. In this case only one laser field of linear (or elliptical) polarization may be used, and the change of the refractive indexes caused by CPT leads to the relative phase shift between the two circularly polarized components.

One possible application of this effect, proposed by Bretenaker *et al.* [319], is a so-called mean-field magnetometer. If the atomic medium is placed inside a resonator, then the phase difference of the two circular polarizations results in a difference in their frequencies of generation. In this case the beat-note frequency provides the information about the applied magnetic field.

The information about magnetic field may also be obtained from direct measurement of the polarization rotation (a magnetometer based on the nonlinear Faraday effect). Recently, several studies have shown the possibility of using NMOR for magnetometry under different conditions: in optically thin Rb vapor in the cells with anti-relaxation coating [249, 320], in optically thick vapor in uncoated cells with or without buffer gas [124,127,321], and in cold Rb atoms [322]. Although no practical realizations of such magnetometers has been reported so far, the estimations of the possible sensitivity of this method predict almost an order of magnitude better value than for the best optical pumping magnetometers.

B. Magnetometer based on the nonlinear Faraday effect in optically dense Rb vapor

1. Factors limiting the sensitivity of the magnetic field detection

A detailed theoretical study of a magnetometer based on NMOR is presented by Fleischhauer *et al.* [124]. They demonstrate that the sensitivity of magnetic field measurements is limited by two fundamental restrictions: vacuum fluctuations of the laser field (shot noise of a photodetector) and coupling of the laser field to non-resonant levels (ac-Stark shifts). The shot noise is crucial for low laser power, whereas the ac-Stark effect is dominant for higher laser fields. It was shown in that the minimum detectable level shift is given by:

$$\delta_0 = \gamma_0 \sqrt{\frac{1 + \frac{|\Omega|^4}{\gamma_0^2 \Delta_0^2} \eta (1-\eta) \ln(\eta^{-1})}{\langle n \rangle_{\text{out}} \ln(\eta^{-1})}} \tag{8.1}$$

where $\eta = I_{\text{out}}/I_{\text{in}}$ is the transmission through the medium, $\langle n \rangle_{\text{out}}$ is the average number of photons on the photodetector, and Δ_0 is the detuning of non-resonant sublevels. The value of Δ_0 taking into account the real sublevel system in ^{87}Rb was found in Chapter VII to be $\Delta_0 \approx 5$ GHz. The first term in the numerator comes from the shot-noise of the photodector while the second one is due to non-resonant coupling with upper levels. Because of the opposite dependence of these terms on laser intensity, the sensitivity may be optimized. Reference [124] showed that the sensitivity reaches its optimum value if the laser intensity is:

$$|\Omega|^2 = \sqrt{\frac{\gamma_0^2 \Delta_0^2}{\eta (1-\eta) \ln(\eta^{-1})}} \approx \gamma_0 \Delta_0 \tag{8.2}$$

For this optimal laser intensity the transmission should be $\eta \approx 6\%$, and the minimum detectable frequency shift of the levels is given by:

$$\delta_0^{\text{SQL}} = f \left(\frac{\gamma_r}{\Delta_0} \frac{3}{2\pi} \frac{\lambda^2}{\pi d^2} \frac{\gamma_0}{t_m} \right)^{1/2}, \tag{8.3}$$

where $f = ((1-\eta)/(\eta \ln^3(\eta^{-1})))^{1/4}$ is a numerical factor which varies between 1 and 2 for light transmission ratios from 0.01 to 0.8, d is the laser beam diameter, and t_m is the measurement time.

2. Estimation of the sensitivity for Rb vapor

Let us first consider the case of the cell without buffer gas. In our experiments we use a cylindrical uncoated glass cell 5 cm in length and 2.5 cm in diameter filled with isotopically enhanced ^{87}Rb.

One of the possible advantages of a Faraday magnetometer over the other devices is the possibility to separate a small region where the magnetic field is measured from the rest of the setup by delivering input and output laser radiation to the atomic cell via polarization-preserving optical fiber. Thus, if the atomic cell with geometrical sizes in sub-millimeter region is fabricated, the detector head may be made extremely small. In this case the following question rises: since the minimization of the interaction region leads to shorter interaction time, is it possible to maintain the sensitivity of the magnetic field measurements at a competitive level if the coherence decay rate increases significantly?

To investigate this problem experimentally, we study the effect of the laser beam diameter on the polarization rotation angle and the transmission in the system. If the intensity of the beam is constant, but the diameter is decreased by placing an iris diaphragm before the cell, rapid deterioration of sensitivity is observed as shown in Fig. 61. This effect supports the fact that the ground state coherence decay rate γ_0 in a vacuum cell is determined by time-of-flight of the atoms through the laser beam: it is inversely proportional to the beam diameter. Increasing γ_0 leads to a decrease of both rotation and transmission, according to Eqs. (2.69) and (2.70), which results in the observed behavior of the sensitivity.

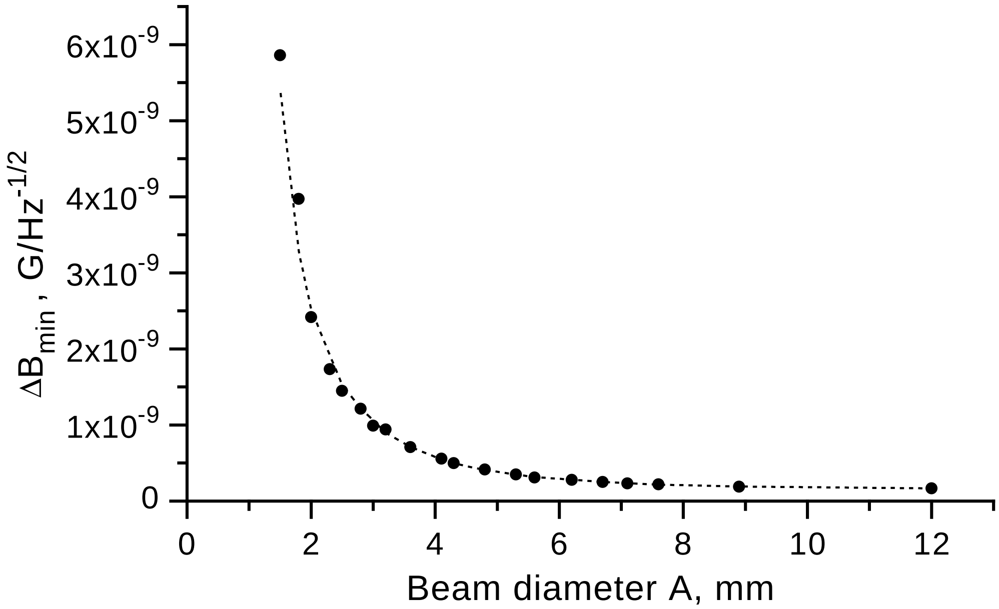

Fig. 61. Estimated sensitivity of magnetic field measurements ΔB_{min} as a function of laser beam diameter. Laser intensity $I_{\text{in}} \approx 2$ mW/cm^2, atomic density $N \approx 10^{12}$ cm^{-3}.

If the size of the laser beam is controlled with a beam expander, so the total laser power does not change, the result is not so obvious. In this case, decreasing the beam diameter leads to a simultaneous increase of the laser intensity. We show here the result for two different beam diameters $d_1 = 2$ mm and $d_2 = 12$ mm. The laser power for both cases is $P = 2.5$ mW, giving peak laser intensities $I_1 \approx 80$ mW/cm^2 and $I_2 \approx 2$ mW/cm^2 respectively. Since the optimum atomic density depends on intensity, we study the sensitivity versus density for each of these intensities. The rotation rate $d\phi/dB$ and absorption $I_{\mathrm{out}}/I_{\mathrm{in}}$ as functions of atomic density are shown in Figs. 62a and b. Higher intensity can potentially lead to a higher rotation rate, but for these parameters it is not adequate to compensate the increased effect of power broadening and increased coherence decay rate (transit-time effect), so the rotation slope for the smaller beam is significantly lower than for the larger beam (Fig. 62a). Hence, for the larger beam, we observe about a ten-fold increase of the estimated sensitivity of magnetic field measurements $\Delta B_{\min}$ (Fig. 62c). However, it worth mentioning here that even though the sensitivity for the small beam is lower, it can be partially compensated by using higher laser power.

To understand the dependence of the minimum detectable magnetic field $\Delta B_{\min}$ on atomic density we have found that reabsorption of spontaneously emitted photons, called radiation trapping, considered in Chapter IV, may be an important factor. For low atomic density ($N \leq 10^{11}$ cm^{-3}) the behavior of the system can be described by the theoretical approach of Fleischhauer *et al.* [124], which predicts that the sensitivity increases rapidly with atomic density . However, as the atomic vapor becomes optically thick, the destructive effect of radiation trapping leads to the deterioration of the ground-state coherence decay rate γ_0, as demonstrated in Chapter IV. This increase in γ_0 leads to a linear increase of the optimal power (Eq. (8.2)) and a square root decrease of the sensitivity (Eq. (8.3)).

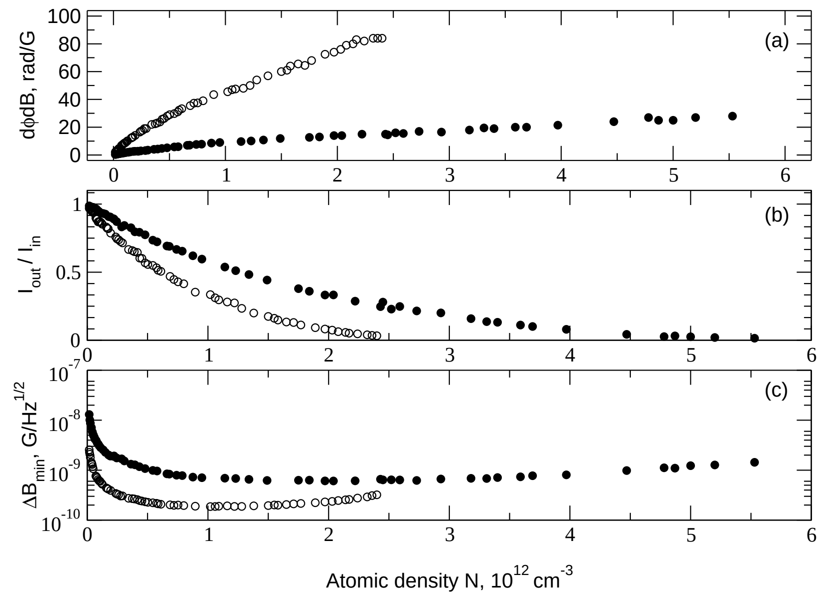

Fig. 62. (a) Rotation rate $d\phi/dB$ as a function of atomic density in the cell without buffer gas; (b) Transmission through the cell; (c) estimated minimum detectable magnetic field $\Delta B_{\rm min}$. Solid dots are for laser beam diameter $d = 2$ mm, open dots are for $d = 12$ mm.

It is important to remember that the width of the NMOR signals in the high laser power regime is determined by power broadening. Although this becomes a serious problem for some detection schemes (like OPM, or dark-state magnetometer), in the magnetometer based on the nonlinear Faraday effect this broadening is compensated by the enhancement of the polarization rotation. Moreover, it may be useful to overcome the main problem of such devices: the limited region of the measurable magnetic fields to the vicinity of zero field. Since large linewidth means that even a relatively strong magnetic field does not destroy the sensitivity, power-broadened NMOR can be very useful for measurements of small changes in a background magnetic field (for example, the Earth's magnetic field). As demonstrated in Fig. 11, the width of the resonances in the cell without buffer gas may be quite large, but the rotation angle is very large too. In our experiments the characteristic width of rotation is already comparable with the Earth's magnetic field ($B \sim 0.5$ G), and the sensitivity of magnetic field measurements is still quite high: $\Delta B_{\mathrm{min}} = 7 \times 10^{-10}$ G/$\sqrt{\mathrm{Hz}}$.

The rotation slope and the sensitivity as a function of laser frequency is shown in Fig. 63. For these data, the laser power is $P = 2.5$ mW, the beam diameter is $d = 12$ mm, and the atomic density $N \approx 10^{12}$ cm^{-3} is chosen to have optimal sensitivity according to Fig. 62c. The rotation slope is calculated by measuring the difference in the rotation angle for two magnetic fields $B = \pm 0.1$ mG to exclude any possible background rotation. In the case of no buffer gas, (dashed lines) the rotation rate $d\phi/dB$ appears as the sum of two peaks centered at the $F = 2 \rightarrow F' = 1$ and the $F = 2 \rightarrow F' = 2$ transitions. The sensitivity is also best at these points and is not very different for frequencies between the two transitions (since both the rotation and absorption are smaller there.)

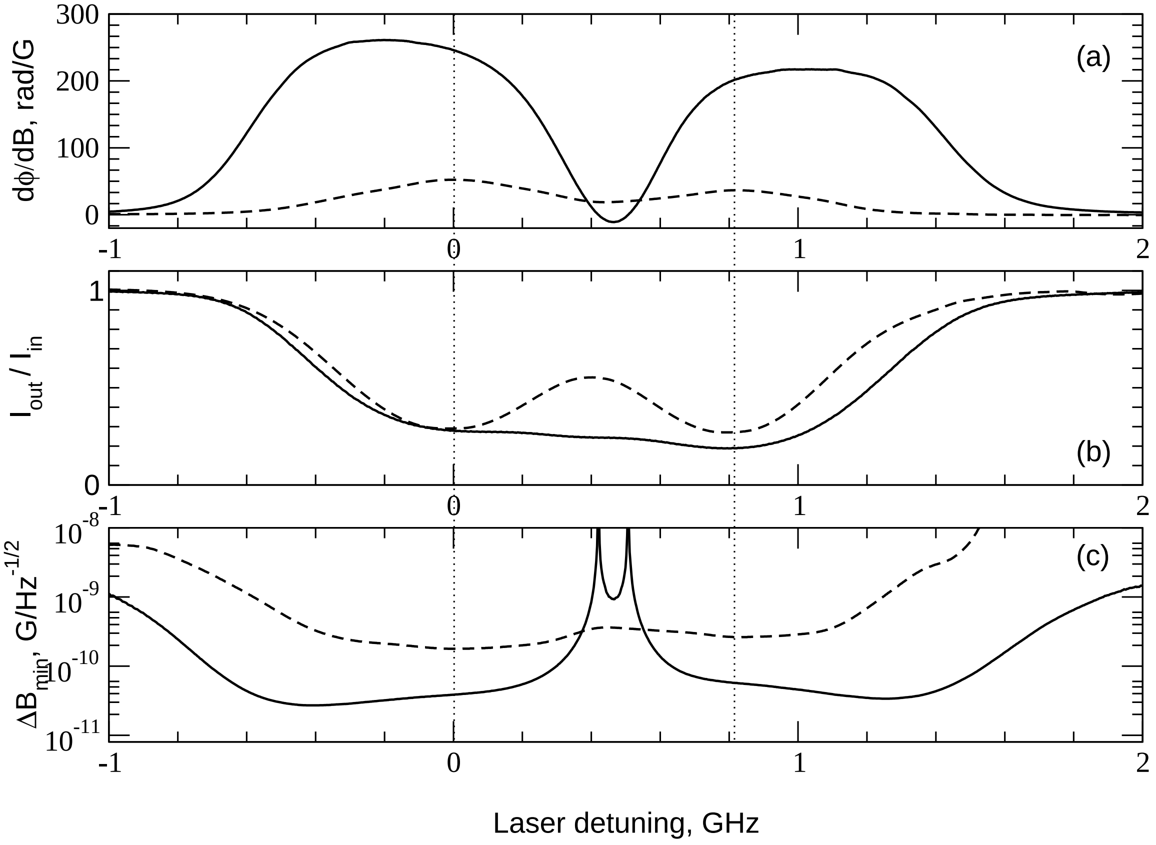

Fig. 63. (a) Rotation rate $d\phi/dB$ as a function of laser frequency in the cell without buffer gas (dashed line) and with 0.12 torr Kr (solid line); (b) Transmission through the cell; (c) estimated minimum detectable magnetic field ΔB_{min}. Laser power $P_{\text{in}} = 2.5$ mW, beam diameter $d = 12$ mm. Atomic density is $N = 2 \times 10^{12}$ cm^{-3} for vacuum cell and $N = 10^{12}$ for the cell with buffer gas. The frequency of the transition $F = 2 \rightarrow F' = 1$ is chosen as zero detuning. The vertical dotted lines show the positions of the transitions $F = 2 \rightarrow F' = 1, 2$.

3. Experiments with buffered cells

In Chapter V we have demonstrated that the reduction of the coherence decay rate associated with the buffer gas addition leads to the narrowing of the NMOR and increasing of the rotation rate $d\phi/dB$, similar to that caused by the beam expansion. At the same time, the modification of the rotation spectra due to velocity changing collisions, described in the same Chapter, causes the important differences between the sensitivity curves as functions of laser frequency for the cells with and without buffer gas. Fig. 63 shows the rotation rate $d\phi/dB$, transmission and the estimated sensitivity for the cell with 0.12 torr Kr (the dimensions of the cell are the same as for the vacuum one, described above). As one can see, the “dip” between transitions $F = 2 \rightarrow F' = 1, 2$ observed in the rotation rate and caused by the destructive interference of the coherences created on each transition, results in very poor sensitivity for the laser frequencies between the two transitions. Even if the laser is tuned directly in resonance with one of the transitions, the influence of the other is quite remarkable, so the maximum of the rotation rate $d\phi/dB$ is displaced “outside” the exact transition frequency (see Fig. 63a). The result is that the best sensitivity is reached when the laser frequency is detuned from exact transition,and the value of the optimal detuning depends on atomic density and the amount of buffer gas. It is also important to note that the dependence of the sensitivity shown in Fig. 63c and that found for cells with anti-reflection coatings [249] is remarkably similar.

Estimates of the sensitivity for different cells (vacuum cell, cell with 0.12 torr Kr, and 0.3 torr Ne) are shown in Fig. 64. To compare these with theoretical predictions, we use Eq. (8.1). The values of γ_0 may be found from the asymptotics for rotation slope $d\phi/dB$ and transmission $I_{\mathrm{out}}/I_{\mathrm{in}}$ using Eqs. (2.69) and (2.70) for low atomic densities, where radiation trapping does not play any significant role. The

Table II. Comparison between theoretical prediction and experimental estimation for minimum detectable magnetic fields for different cells and laser beam diameters.

Cell	γ_0 (kHz)	I_{opt} (mW)	$\Delta B_{\min}$ (G/$\sqrt{\text{Hz}}$) theory	$\Delta B_{\min}$ (G/$\sqrt{\text{Hz}}$) experiment
No buffer gas, $d = 2$ mm	20	63	3×10^{-10}	7×10^{-10}
No buffer gas, $d = 12$ mm	8.3	26	4×10^{-11}	2×10^{-10}
0.12 torr Kr, $d = 2$ mm	7.8	25	2×10^{-10}	5×10^{-10}
0.12 torr Kr, $d = 12$ mm	2.2	7	2×10^{-11}	5×10^{-11}
0.3 torr Ne, $d = 2$ mm	2.5	8	10^{-10}	3×10^{-10}

values of optimized intensity I_{opt} from Eq. (8.2), Zeeman coherence decay rate γ_0 estimated from our experimental results, the sensitivity $\Delta B_{\min}$ predicted theoretically by Eq. (8.3), and the sensitivity $\Delta B_{\min}$ using Eq. (8.1) for different cells and laser beam diameters are shown in Table II.

C. Compensation of ac-Stark shifts

As shown above, the coupling between the circularly polarized electromagnetic fields due to the ac-Stark effect is the main limitation for the sensitivity of the magnetic field measurements for high laser power. Ac-Stark shifts become a serious problem in other precision measurements, like atomic clocks and frequency standards [323–325]. There are a number of methods to scale down the negative effect of the light shifts: laser detuning [326], electronic self-tuning [327], coherent light modulation [325,328], etc.

The studies of the ac-Stark shifts for the D_1 line of ^{87}Rb, presented in Chapter

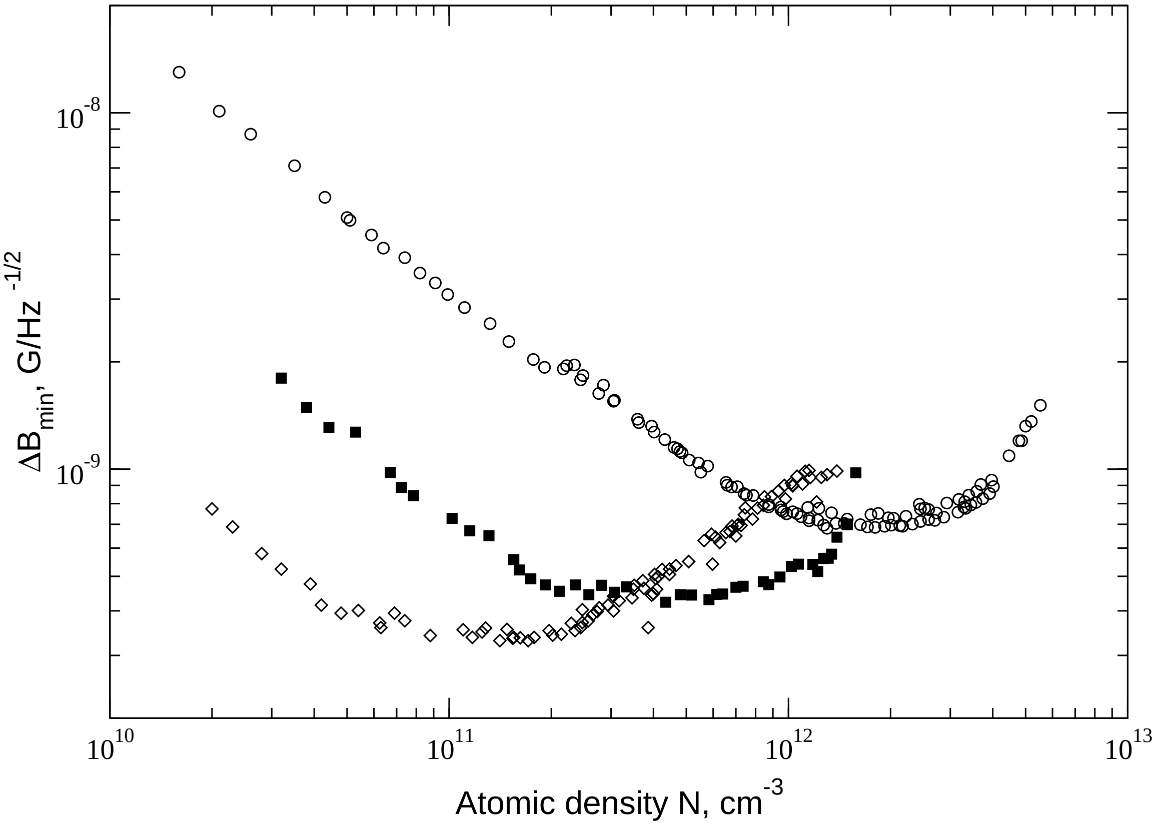

Fig. 64. (a) Estimated sensitivity of magnetic field measurements $\Delta B_{\rm min}$ as a function of atomic density for different cells: without buffer gas (open circles), with 0.12 torr Kr (squares) and with 0.3 torr Ne (diamonds). Laser power $P_{\rm in} \approx 2.5$ mW, laser beam diameter $d = 2$ mm. The dimensions of all cells are the same (length ≈ 5 cm, diameter ≈ 2.5 cm).

VII showed experimentally that the ac-Stark shift depends inversely on the detuning from non-resonant atomic hyperfine sub-levels. Further, we show that there is some laser frequency between the resonant transitions where the light shifts cancel. At this point the non-correlated intensity fluctuations of each circular component have no effect on their relative phase, and the direction of the output polarization is not affected by the medium. Therefore, at this frequency the sensitivity of an NMOE magnetometer is limited only by photon shot-noise, allowing the use of higher laser power to achieve better signal to noise ratio.

To find the laser frequency corresponding to the ac-Stark shift compensation, we study the spectra of self-rotation of the light polarization ellipse for the different degree of ellipticity. Obviously, at the point of interest there should be no self-rotation for any ellipticity value. At the same time we have to remember that the absence noise associated with light shifts does not guarantee the best sensitivity, since the sensitivity is also proportional to the slope of the polarization rotation with magnetic field, $d\phi/dB$. To maintain high sensitivity, this parameter should be large enough at the point of ac-Stark suppression.

Experimental spectra for both the angle of self-rotation ϕ_{AC} and magnetic rotation slope $d\phi/dB$ are shown for the D_1 line in Fig. 65a and b and the D_2 line in Fig. 66. For each case the rotation angle at zero magnetic field (self-rotation) has been recorded for three different degrees of ellipticity of the laser beam (Figs. 65a and 66a).

In both cases there exists a value of the detuning where the ellipticity of the laser beam does not lead to any rotation. This compensation point is also independent of the laser intensity. For the D_1 line this is a point midway between the transitions to the two upper state hyperfine levels. The rotation peaks are partially resolved, and in the middle point the value of rotation slope ($d\phi/dB$) is about 40% of its

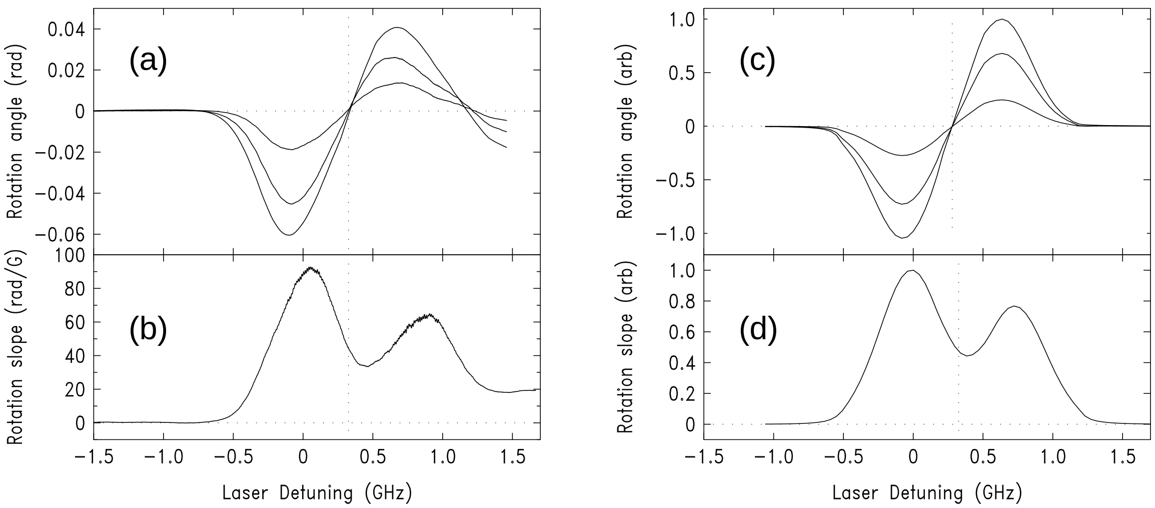

Fig. 65. (a) Measured rotation angle ϕ_{AC} for elliptical polarizations of 2°, 4° and 6° degrees. (b) Measured Faraday rotation slope, $\frac{d\phi}{dB}$ with linearly polarized light. Both (a) and (b) are for the ^{87}Rb D_1 line, with no buffer gas and atomic density $N = 1.5 \times 10^{12}\text{cm}^{-3}$. (c) Calculated rotation angle ϕ_{AC} for D_1 line. (d) Calculated Faraday rotation slope, $\frac{d\phi}{dB}$.

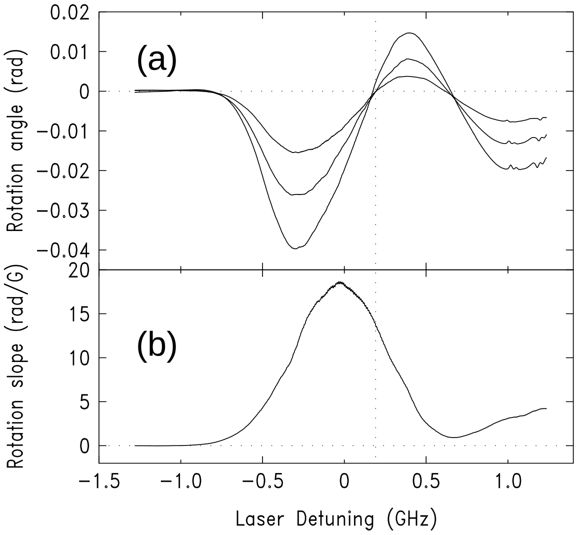

Fig. 66. Same as Fig. 65a and b for the D_2 line and atomic density $N = 8 \times 10^{10}\mathrm{cm}^{-3}$. Zero detuning corresponds to the resonance with transition $5s_{1/2}F = 2 \rightarrow 5p_{1/2}F' = 1$ for the D_1 line and to the center of the absorption on the transition $5s_{1/2}F = 2 \rightarrow 5p_{3/2}$ for the D_2 line.

maximum value. For the D_2 lines, the point of compensation is near the center of the upper hyperfine manifold. It is important to note the compensation in the D_2 case, which occurs for an upper manifold consisting of three levels instead of two. In both of these pictures, there is another point on the high-frequency side where an extra compensation point appears. This is due to contamination of the cell by ^{85}Rb and demonstrates the interesting possibility to eliminate ac-Stark shifts by tuning the laser between the transition for two different isotopes.

To understand these results, we first analyze the simple case of motionless atoms by performing numerical simulations for the density matrix propagation for the thirteen levels of the D_1 line. The calculated rotation angle is shown in Fig. 67a. We see that if the atoms are motionless there are two points where ac-Stark shifts from different levels cancel each other very close to each resonance. Figure 67b shows the

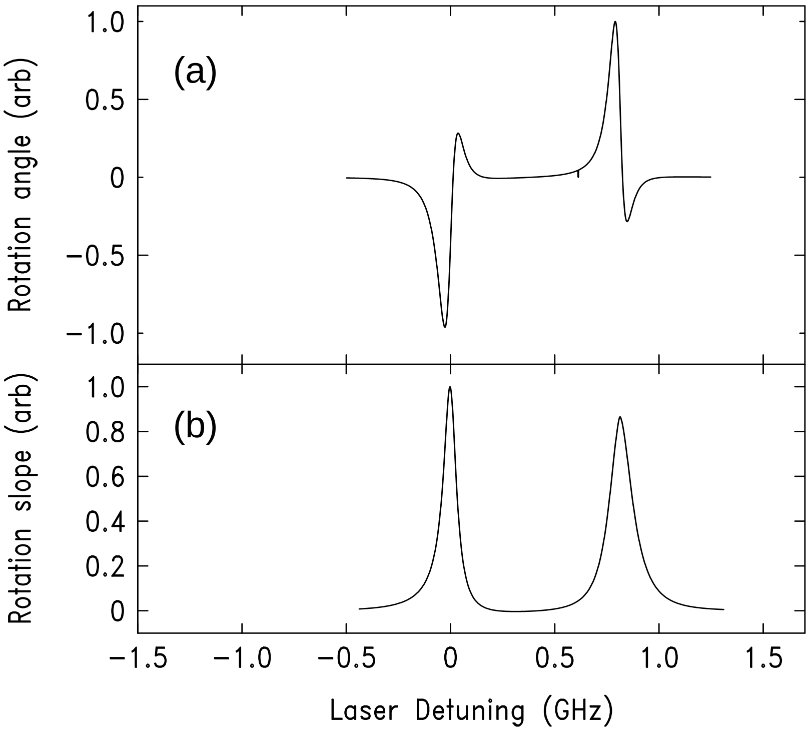

Fig. 67. (a) Calculated rotation angle ϕ_{AC} and (b) calculated Faraday rotation slope $d\phi/dB$ for motionless atoms.

calculated rotation slope which predicts two sharp resonant peaks. This means that for motionless atoms a very small detuning can eliminate the effect of ac-Stark shift completely without loss of sensitivity. However, the use of cold atoms is a complicated process that may not be well suited to practical magnetometry.

For atoms in a vapor, Doppler averaging causes the cancellation points near the resonances to disappear. Thus, the shifts are compensated only at the point exactly between the two transitions where the rotation slope is somewhat smaller than its maximum value. However, Fig. 63c shows that the sensitivity at this frequency is only a factor of two worse than the optimal one. Taking into account that the rotation rate increases significantly with atomic density and laser power, this frequency may be quite promising to avoid the limitation imposed by ac-Stark broadening if high laser power is used.

Unfortunately, this method cannot by successfully applied for the cells with the buffer gas. The cancellation of the nonlinear Faraday rotation for the laser field tuned between hyperfine transitions, makes it impossible to achieve the required sensitivity in the point of ac-Stark shift compensation. To study this effect, we have used a cell with 0.12 torr of Kr buffer gas. The results are shown for the D_1 line in Fig. 68a and b. We see that the ac-Stark effect is eliminated by detuning between the resonances as before. However, in this case the rotation slope is also strongly suppressed in the same frequency region, being almost exactly zero at the point of compensation. In the case of the D_2 line Fig. 68c and d the rotation slope, while not zero, is much smaller at the point of compensation.

In conclusion, we have studied the application of NMOR to magnetometry for the regime of high laser power and high atomic density for different parameters of the system: laser intensity, laser frequency, laser beam diameter, atomic density, presence of buffer gas, etc. We have shown that the zero-field sensitivity of such measurements is not as as high as expected for anti-relaxation coated cells [249], but is comparable with the sensitivity of optical pumping magnetometers [244]. Furthermore we have shown that strong power broadening of the line makes it feasible to use this effect for earth-field measurements.

We also expect in-principle improvement of the sensitivity of the magnetic field detection in high laser power regime by compensation of ac-Stark shifts. We have studied the dependence of the ac-Stark shift versus frequency of the probing laser for the D_1 and D_2 lines of ^{87}Rb, and have shown that there exists a frequency where the shifts from different hyperfine components of the upper level cancel each other.

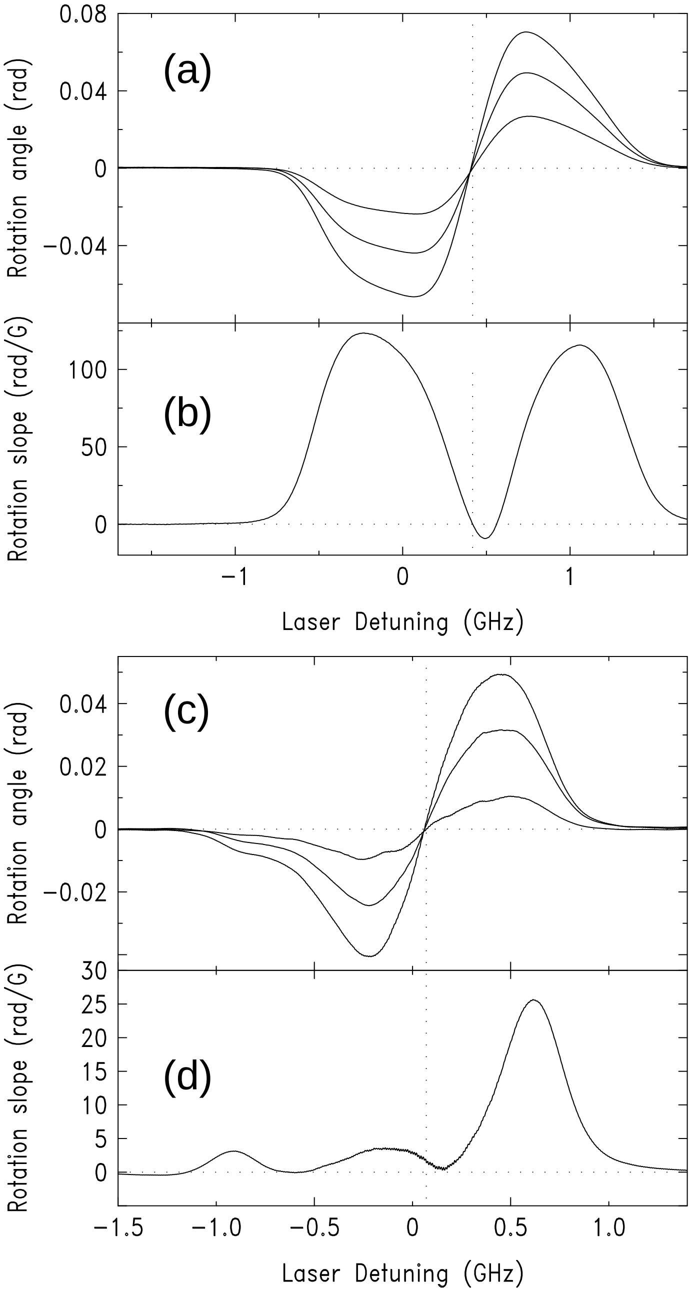

Fig. 68. (a) and (c) Measured rotation angle ϕ_{AC} for elliptical polarizations of 2°, 4° and 6° degrees. (b) and (d) Measured Faraday rotation slope, $\frac{d\phi}{dB}$ with linearly polarized light. Both (a) and (b) are for the ^{87}Rb D_1 line, (c) and (d) are for the ^{87}Rb D_2 line, in the cell with 0.12 torr of Kr buffer gas and atomic density $N = 1.5 \times 10^{12}\text{cm}^{-3}$.

CHAPTER IX

SUMMARY AND CONCLUSIONS

The main results of this work are the following:

1. Quantum interference of the ground-state Zeeman sublevels leads to a wide variety of nonlinear magneto-optical effects, such as the nonlinear Faraday effect. At the same time, the analysis of both polarization rotation and laser absorption provide an excellent tool to study the fundamental properties of coherent media.

2. We observed several orders of magnitude enhancement of the nonlinear Faraday rotation in optically thick Rb vapor. Polarization rotation angle higher than 10 rad has been demonstrated for the first time for sub-Gauss magnetic field.

3. A theoretical and experimental study of the effect of reabsorption of spontaneous radiation on the atomic coherence was developed. We have demonstrated that the radiation trapping leads to deterioration of atomic coherence, and has to be taken into account for high atomic densities.

4. The presence of a buffer gas has a profound effect on the nonlinear Faraday effect. We have observed an additional narrow feature in both absorption and polarization rotation spectra, which can be explained by the spatial diffusion of Rb atoms in a buffer gas. At the same time, velocity-changing collisions produce effective "mixing" of the dark states created on different hyperfine transitions, resulting in the inversion of the polarization rotation signal and an enhanced absorption resonance between transitions.

5. An analysis of the ellipticity-dependent magneto-optical rotation allows to sep-

arate the influence of the multi-photon coherence. An analytical treatment of this problem was developed.

6. High nonlinearity, associated with coherent media, leads to large self-rotation of the elliptically polarized light, which is caused by the off-resonant interaction of the laser field with far-detuned atomic levels. We demonstrated the enhancement of self-rotation for elliptically polarized light in optically thick Rb vapor. Our theoretical models predict that this effect can be used for effective squeezing of vacuum fluctuations. Squeezing up to -7dB is estimated for ^{87}Rb vapor under realistic conditions.

7. The nonlinear Faraday effect is a promising tool for precision metrology. We have estimated the sensitivity of a magnetometer based on nonlinear polarization rotation, and demonstrated that higher atomic density leads to better sensitivity, and that optimal operation conditions are reached for optically thick Rb vapor. At the same time the dynamic range of the measured magnetic fields may be controlled by power broadening of the resonance.

REFERENCES

[1] M. O. Scully, and M. S. Zubairy, *Quantum Optics* (Cambridge University Press, Cambridge, UK, 1997).

[2] W. Gawlik, in *Modern Nonlinear Optics*, edited by M. Evans and S. Kielich, Advances in Chemical Physics Series (Wiley, New York, 1994), Vol. LXXXV, pp. 733-845.

[3] D. Budker, W. Gawlik, D. F. Kimball, S. M. Rochester, V. V. Yashchuk, and A. Weis, Rev. Mod. Phys. **74**, 1153 (2002).

[4] M. O. Scully, and M. Fleischhauer, Phys. Rev. Lett. **69**, 1360 (1992).

[5] M. Fleischhauer, and M. O. Scully, Phys. Rev. A **49**, 1973 (1994).

[6] W. Hanle, Z. Phys. **30**, 93 (1924).

[7] N. Bohr, Naturwissenschaften **12**, 1115 (1924).

[8] W. Heisenberg, Z. Phys. **31**, 617 (1925).

[9] R. Oppenheimer, Z. Phys. **43**, 27 (1927).

[10] V. Weisskopf, Ann. Phys. **9**, 23 (1931).

[11] G. Breit, Rev. Mod. Phys. **5**, 91 (1936).

[12] R. W. Wood and A. Ellett, Proc. R. Soc. London, Ser. A **102**, 190 (1923); Phys. Rev. **24** 243 (1924).

[13] E. B. Aleksandrov, Opt. Spectr. **17**, 522 (1964).

[14] J. N. Dodd, R. D. Kaul, and D. M, Warrington, Proc. Phys. Soc. London **84**, 176 (1964).

[15] E. B. Alexandrov, M, P. Chaika, and G. I. Khvostenko, *Interference of Atomic States*, (Springer-Verlag, New York 1993).

[16] *The Hanle Effect and Level-crossing Spectroscopy*, edited by G. Moruzzi and F. Strumia (Plenum Press, New York 1991).

[17] F. D. Colegrove, P. A. Franken, R. R. Lewis, and R. H. Sands, Phys. Rev. Lett. **3**, 420 (1959).

[18] P. A. Franken, Phys. Rev. **121**, 508 (1961).

[19] R. Bernheim, *Optical Pumping*, (W. A. Benjamin, Inc., New York, 1965).

[20] C. Cohen-Tannoudji, and A. Kastler, in *Progress in Optics* edited by E. Wolf, (Elsevier Science, Amsterdam, 1966), Vol. V, Chap. I, pp. 3-84 .

[21] W. Happer, Rev. Mod. Phys. **44**, 169 (1972).

[22] B. D. Agapyev, M. B. Gornyi, B. G. Matisov, and Y. V. Rozhdestvenskii, Usp. Fiz. Nauk **163** 1 (1993).

[23] E. Arimondo, in *Progress in Optics*, edited by E. Wolf, (Elsevier Science, Amsterdam, 1996), Vol. XXXV, Chap. V, pp. 259-354.

[24] S. E. Harris, Phys. Today, **50**(7), 36 (1997).

[25] J. P. Marangos, J. Mod. Opt. **45**, 471 (1998).

[26] E. Arimondo, and G. Orriols, Nuovo Cimento Lett. **17**, 333 (1976).

[27] H. R. Gray, R. M. Whitley, and C. R. Stroud, Opt. Lett. **3**, 218 (1978).

[28] H. I. Yoo, and J. H. Eberly, Phys. Reports **118**, 239 (1985).

[29] G. Borghs, P. Debisschop, M. Vanhove, and R. E. Silverance, Phys. Rev. Lett. **52**, 2030 (1984).

[30] G. Théobald, N. Dimarcq, V. Giordano, and P. Cérez, Opt. Commun. **71**, 256 (1989).

[31] E. G. Saprykin, V. P. Soldatov, and V. A. Sorokin, Sov. J. Quantum. Electron. **13**, 2057 (1986).

[32] T. Mishina, Y. Fukuda, and T. Hashi, Opt. Commun. **66**, 25 (1988).

[33] F. Renzoni, W. Maichen, L. Windholz, and E. Arimondo, Phys. Rev. A **55**, 3718 (1997).

[34] Y. Dancheva, G. Alzetta, S. Cartaleva, M. Taslakov, and C. Andreeva, Opt. Commun. **178**, 103 (2000).

[35] G. Alzetta, S. Cartaleva, Y. Dancheva, C. Andreeva, S. Gozzini, L. Botti, and A. Rossi, J. of Opt. B **3**, 181 (2001).

[36] S. A. Hopkins, E. Usadi, H. X. Chen, and A. V. Durrant, Opt. Commun. **138**, 185 (1997).

[37] D. J. Fulton, R. P. Moseley, S. Shepherd, B. D. Sinclair, and M. H. Dunn, Opt. Commun. **116**, 231 (1995).

[38] H. Y. Ling, Y. Q. Li, and M. Xiao, Phys. Rev. A **53**, 1014 (1996).

[39] R. Holler, F. Renzoni, L. Windholz, and J. H. Xu, J. Opt. Soc. Am. B **14**, 2221 (1997).

[40] R. Wynands, A. Nagel, S. Brandt, D. Meschede, and A. Weis, Phys. Rev. A **58**, 196 (1998).

[41] Y. C. Chen, C. W. Lin, and I. A. Yu, Phys. Rev. A **61**, 053805 (2000).

[42] A. Nottelmann, C. Peters, and W. Lange, Phys. Rev. Lett. **70**, 1783 (1993); W. Lange, A. Nottelmann, and C. Peters, Quantum. Opt. **6**, 273 (1994).

[43] A. V. Durrant, H. X. Chen, S. A. Hopkins, and J. A. Vaccaro, Opt. Commun. **151**, 136 (1998).

[44] X. W. Xia, D. Hsiung, P. S. Bhatia, M. S. Shahriar, T. T. Grove, and P. R. Hemmer, Opt. Commun. **191**, 347 (2001).

[45] D. Budker, D. F. Kimball, S. M. Rochester, and V. V. Yashchuk, Phys. Rev. Lett. **83**, 1767 (1999).

[46] I. V. Zelensky, V. A. Mironov, J. Exp. Theor. Phys. **94**, 916 (2002).

[47] J. Martin, B. W. Shore, and K. Bergmann, Phys. Rev. A **52**, 566 (1995); **52**, 583 (1995), **54**, 1556 (1996).

[48] K. Bergmann, H. Theuer, and B. W. Shore, Rev. Mod. Phys. **70**, 1003 (1998).

[49] N. V. Vitanov, M. Fleischhauer, B. W. Shore, and K. Bergmann, in *Advances in Atomic, Molecular, and Optical Physics* edited by B. Bederson, and H. Walter, (Academic Press, San Diego, 2001), Vol. 46, pp. 55-190.

[50] P. Marte, P. Zoller, and J. L. Hall, Phys. Rev. A **44**, R4118 (1991).

[51] J. Lawall, and M. Prentiss, Phys. Rev. Lett. **72**, 993 (1994).

[52] L. S. Goldner, C. Gerz, R. J. C. Spreeuw, S. L. Rolston, C. I. Westbrook, W. D. Phillips, P. Marte and P. Zoller, Phys. Rev. Lett. **72**, 997 (1994).

[53] H. Theuer, and K. Bergmann, Eur. Phys. J. D **2** 279 (1998).

[54] E. Marechal, R. Long, T. Miossec, J. L. Bossennec, R. Barbe, J. C. Keller, and O. Gorceix, Phys. Rev. A **62**, 053603 (2000).

[55] A. S. Parkins, P. Marte, P. Zoller, and H. J. Kimble, Phys. Rev. Lett. **71**, 3095 (1993).

[56] M. D. Lukin, S. F. Yelin, and M. Fleischhauer, Phys. Rev. Lett. **84**, 4232 (2000).

[57] A. E. Kozhekin, K. Mølmer, and E. Polzik, Phys. Rev. A **62**, 033809 (2000).

[58] D. F. Phillips, A. Fleischhauer, A. Mair, R. L. Walsworth, and M. D. Lukin, Phys. Rev. Lett. **86**, 783 (2001).

[59] A. Mair, J. Hager, D. F. Phillips, R. L. Walsworth, and M. D. Lukin, Phys. Rev. A **65**, 031802 (2002).

[60] A. S. Zibrov, A. B. Matsko, O. Kocharovskaya, Y. V. Rostovtsev, G. R. Welch, and M. O. Scully, Phys. Rev. Lett. **88**, 103601 (2002).

[61] A. M. Akulshin, S. Barreiro, and A. Lazema, Phys. Rev. A **57**, 2996 (1998); A. Lazema, S. Barreiro, and A. M. Akulshin, Phys. Rev. A **59**, 4732 (1999).

[62] A. Lipsich, S. Barreiro, A. M. Akulshin, and A. Lazema, Phys. Rev. A **61**, 053803 (2000).

[63] M. Kwon, K. Kim, H. S. Moon, H. D. Park, and J. B. Kim, J. Phys. B **34**, 2951 (2001); K. Kim, M. Kwon, H. D. Park, H. S. Moon, H. S. Rawat, K. An, and J. B. Kim, J. Phys. B **34**, 4801 (2001).

[64] C. Y. Ye, Y. V. Rostovtsev, A. S. Zibrov, and Y. M. Golubev, Opt. Commun. **207**, 227 (2002).

[65] F. Renzoni, C. Zimmermann, P. Verkerk, and E. Arimondo, J. Opt. B – Quant. Semiclass. Opt. **3**, S7 (2001); F. Renzoni, S. Cartaleva, G. Alzetta, and E. Arimondo, Phys. Rev. A **63**, 065401 (2001).

[66] C. Andreeva, S. Cartaleva, Y. Dancheva, V. Biancalana, A. Burchianti, C. Marinelli, E. Mariotti, L. Moi, and K. Nasyrov, Phys. Rev. A **66**, 012502 (2002).

[67] S. G. Rautian, J. Exp. Theor. Phys. **88**, 6 (1999).

[68] A. V. Taichenachev, A. M. Tumaikin, and V. I. Yudin, JETP Lett. **69**, 819 (1999); A. V. Taichenachev, A. M. Tumaikin, and V. I. Yudin, Phys. Rev. A **60**, 011802 (2000).

[69] A. M. Akulshin, S. Barreiro, and A. Lezama, Phys. Rev. Lett. **83**, 4277 (1999).

[70] A. M. Akulshin, A. Cimmino, and G. I. Opat, Quantum Electron. **32**, 567 (2002).

[71] A. M. Akulshin, S. Barreiro, and A. Lezama, Quantum Electron. **30**, 189 (2000).

[72] A. Lipsich, S. Barreiro, P. Valente, and A. Lazema, Opt. Commun. **190**, 185 (2001).

[73] D. Macaluso, and O. Corbino, Nuovo Cim. **8**, 257 (1898); D. Macaluso, and O. Corbino, Nuovo Cim. **9**, 384 (1899).

[74] W. Voigt, Göttingen Nachr. **1898**, 349 (1898).

[75] W. Voigt, *Magneto-und Elektrooptik* (Teubner, Leipzig, 1908).

[76] L. Rosenfeld, Zeits. f. Physik **57**, 835 (1930).

[77] R. Serber, Phys. Rev. **41**, 489 (1932).

[78] R. Fork, and L. Bradley III, Appl. Opt. **3**, 137 (1964).

[79] W. Demtröder, *Laser Spectroscopy* (Springer, Berlin, 1996).

[80] M. Faraday, *Experimental Research in Electricity*, (London, 1855), Vol. III.

[81] W. Voigt, Ann. Der Phys. **4**, 197 (1901).

[82] A. Cotton, and H. Mouton, J. Phys. **1**, 5 (1911).

[83] A. Corney, B. P. K. Kibble, and G. W. Series, Proc. R. Soc. London Ser. A **293**, 70 (1996).

[84] A. V. Durrant, and B. Landheer, J. Phys. B **4**, 1200 (1971).

[85] W. Gawlik, J. Kowalski, R. Newmann, and F. Trager, Phys. Lett. A **48**, 283 (1974); W. Gawlik, J. Kowalski, R. Newmann, and F. Trager, Opt. Commun. **12**, 400 (1974).

[86] S. Giraud-Cotton, V. P. Kaftandjian, and L. Klein, Phys. Lett. A **88**, 453 (1982).

[87] A. M. Badalyan, V. I. Kovalevskii, M. K. Makarov, E. G. Saprykin, G. I. Smirnov, and V. A. Sorokin, Sov. J. Quantum. Electron. **11**, 1802 (1984).

[88] S. Giraud-Cotton, V. P. Kaftandjian, and L. Klein, Phys. Rev. A **32**, 2211 (1985); S. Giraud-Cotton, V. P. Kaftandjian, and L. Klein, Phys. Rev. A **32**, 2223 (1985).

[89] W. Gawlik, and J. Zachorowski, J. Phys. B **20**, 5939 (1987).

[90] P. Jungner, T. Fellman, B. Stahlberg, and M. Lindberg, Opt. Commun. **73**, 38 (1989).

[91] I. Hirano, Phys. Rev. A **50**, 4650 (1994); I. Hirano, Phys. Rev. A **52**, 3594 (1995).

[92] B. W. Holmes, and J. A. R. Griffith, J. Phys. B: At. Mol. Opt. Phys. **28**, 2829 (1995).

[93] B. Lobodzinski, and W. Gawlik, Phys. Rev. A **54**, 2238 (1996); B. Lobodzinski, and W. Gawlik, Phys. Scripta **T70**, 138 (1997).

[94] W. Gawlik, J. Kowalski, R. Neumann, H. B. Weigemann, and K. Winkler, J. Phys. B **12**, 3873 (1979).

[95] W. R. C. Garton, J. P. Connerade, M. A. Baig, J. Holmes, and B. Alexa, J. Phys. B **16**, 389 (1983).

[96] M. C. E. Huber, and R. J. Sandeman, Rep. Progr. Phys. **49**, 397 (1986).

[97] D. A. Church, and D. Hadeishi, Appl. Phys. Lett. **24**, 185 (1974).

[98] M. Ito, S. Murayama, K. Kayama, and M. Yamamoto, Spectrochim. Acta B **32B**, 327 (1977).

[99] W. Hanle, A. Scharmann, and P. Wirz, Phys. Lett. A **69**, 12 (1978).

[100] M. Yamamoto, and S. Murayama, J. Opt. Soc. Am. **69**, 781 (1979).

[101] J. P. Woerdman, and M. F. H. Schuurmans, Opt. Commun. **14**, 248 (1975); M. F. H. Schuurmans, J. Phys. **37**, 469 (1975).

[102] A. M. Akulshin, V. L. Velichanskii, A. S. Zibrov, V. V. Nikitin, V. A. Sautenkov, E. K. Yurkin and N. V. Senkov, JETP Lett. **36**, 303 (1982).

[103] A. Weis, V. A. Sautenkov, and T. W. Hnsch, Phys. Rev. A **45**, 7991 (1992); J. Phys. **3**, 263 (1993).

[104] R. Schlesser, and A. Weis, Opt. Lett. **17**, 1015 (1992).

[105] K. H. Drake, W. Lange, and J. Mlynek, Opt. Commun. **66**, 315 (1988).

[106] L. M. Barkov, D. A. Melik-Pashaev, and M. S. Zolotorev, Opt. Commun. **70**, 467 (1989).

[107] P. E. G. Baird, M. Irie, and T. D. Wolfenden, J. Phys. B **22**,1733 (1989).

[108] X. Chen, V. L. Telegdi, and A. Weis, Opt. Commun. **78**, 337 (1990).

[109] X. Chen, V. L. Telegdi, and A. Weis, Opt. Commun. **74**, 301 (1990).

[110] I. Hirano, J. Phys. B **26**, 3497 (1994).

[111] F. Schuller, M. J. D. Macpherson, and D. N. Stacey, Opt. Commun. **71**, 61 (1989).

[112] A. C. Izmailov, Opt. Spectr. **66**, 784 (1989).

[113] T. Y. Karagodova, V. A. Makarov, and A. I. Karagodov, Opt. Spectr. **69**, 389 (1990); T. Y. Karagodova, A. A. Zakharov, and A. V. Kolpakov, Izv. Akad. Nauk SSSR Fiz. **56**, 209 (1992).

[114] S. V. Fomichev, J. Phys. B **24**, 4695 (1991).

[115] K. P. Zetie, R. B. Warrington, M. J. D. Macpherson, and D. N. Stacey, Opt. Commun. **91**, 210 (1992).

[116] F. Schuller, M. J. D. Macpherson, D. N. Stacey, R. B. Warrington, and K. P. Zetie, Opt. Commun. **86**, 123 (1991).

[117] F. Schuller, R. B. Warrington, K. P. Zetie, M. J. D. Macpherson, and D. N. Stacey, Opt. Commun. **93**, 169 (1992).

[118] K. Muroo, T. Matsunobe, Y. Tukubo, and M. Yamamoto, J. Opt. Soc. Am. B **11**, 409 (1994).

[119] F. Schuller, and D. N. Stacey, Phys. Rev. A **60**, 973 (1999).

[120] X. Chen, L. V. Telegdi, and A. Weis, J. Phys. B **20**, 5653 (1989).

[121] A. Weis, J. Wurster, and S. I. Kanorsky, J. Opt. Soc. Am. B **10**, 716 (1993).

[122] S. I. Kanorsky, A. Weis, J. Wurster, and T. W. Hansch, Phys. Rev. A **47**, 1220 (1993).

[123] D. Budker, D. F. Kimball. S. M. Rochester, and V. V. Yashchuk, Phys. Rev. Lett. **85**, 2088 (2000).

[124] M. Fleischhauer, A. B. Matsko, and M. O. Scully, Phys. Rev. A **62**, 013808 (2000).

[125] V. A. Sautenkov, M. D. Lukin, C. J. Bednar, I. Novikova, E. Mikhailov, M. Fleischhauer, V. I. Velichansky, G. R. Welch, and M. O. Scully, Phys. Rev. A **62**, 023810 (2000).

[126] I. Novikova,A. B. Matsko, and G. R. Welch, Opt. Lett. **26**, 1311-1313 (2000).

[127] S. M. Rochester, and D. Budker, J. Mod. Opt. **49**, 2543 (2002)

[128] R. A. Ahmedzhanov, and I. V. Zelensky, JETP Lett. **76**, 419 (2002).

[129] G. S. Agarwal, P. A. Lakshmi, J. P. Connerade, and S. West, J. Phys. B **30**, 5971 (1997).

[130] S. Franke-Arnold, M. Ardntm and A. Zeilinger, J. Phys. B **34**, 2527 (2001).

[131] G. Labeyrie, C. Miniatura, R. Kaiser, Phys. Rev. A **64**, 033402 (2001).

[132] B. Schuh, S. I. Kanorsky, A. Weis, and T. W. Hansch, Opt. Commun. **100**, 451 (1993).

[133] S. I. Kanorsky, A. Weis, and J. Skalla, Appl. Phys. B **60**, S165 (1995).

[134] D. Budker, V. Yashchuk, and M. Zolotorev, Phys. Rev. Lett. **81**, 5788 (1998).

[135] D. Budker, D. J. Orlando, and V. Yashchuk, Am. J. Phys. **67**, 584 (1999).

[136] A. S. Zibrov, I. Novikova, and A. B. Matsko, Opt. Lett. **26**, 1311 (2001).

[137] A. S. Zibrov, and A. B. Matsko, Phys. Rev. A **65**, 013814 (2002).

[138] A. M. Badalyan, B. A. Glushko, and M. E. Movsesyan, Opt. Spectr. **68**, 1266 (1990).

[139] D. M. Lukas, R. B. Warrington, C. D. Thompson, and D. N. Stacey, J. Phys. B **27**, 5497 (1994).

[140] M. Kristensen, M. A. van Eijkelenborg, and J. P. Woerdman, Phys. Rev. Lett. **72**, 2155 (1994); M. Kristensen, F. J. Blok, M. A. van Eijkelenborg, G. Nienhuis, and J. P. Woerdman, Phys. Rev. A **51**, 1085 (1995).

[141] J. P. Woerdman, F. J. Blok, M. Kristensen, and C. A. Schrama, Phys. Rev. A **53**, 1183 (1996).

[142] P. Bicchi, L. Moi, and B. Zambon, Nuovo Cim. **49**, 9 (1978).

[143] H. Brand, K. H. Drake, W. Lange, and J. Mlynek, Phys. Lett. A **75**, 345 (1980).

[144] G. G. Adints, E. G. Kanetsyan, and M. V. Slobodskoi, Opt. Spectr. **64**, 258 (1988).

[145] M. G. Kozlov, Opt. Spectr. **67**, 1342 (1989).

[146] A. K. Patnaik, and G. S. Agarwal, Opt. Commun. **179**, 97 (2000).

[147] A. K. Patnaik, and G. S. Agarwal, Opt. Commun. **199**, 127 (2001).

[148] W. F. Buell, and M. Fink, Appl. Phys. B **60**, S227 (1995).

[149] V. M. Entin, I. I. Ryabtsev, A. E. Boguslavsky, and Yu. V. Brzhazovsky, Opt. Commun. **207**, 201 (2002).

[150] V. V. Yashchuk, E. Mikhailov, I. Novikova, and D. Budker, preprint LBNL-44762 (1999).

[151] L. D. Landau, and E. M. Lifshitz, *The Classical Theory of Fields* (Pergamon Press, Oxford, 1975).

[152] J. D. Jackson, *Classical Electrodynamics* (Wiley, New York, 1975).

[153] K. Blum, *Density Matrix Theory and Applications* (Plenum Press, New York, 1981).

[154] S. Mukamel, *Principles of Nonlinear Optical Spectroscopy* (University Press, Oxford, 1995).

[155] B. W. Shore, and D. H. Menzel, *Principles of Atomic Spectra* (Wiley, New York 1968).

[156] I. I. Sobel'man, *Introduction to the Theory of Atomic Spectra* (Pergamon Press, Oxford, 1972).

[157] I. I. Sobel'man, *Atomic Spectra and Radiative Transitions* (Springer-Verlag, Berlin, 1992).

[158] H. Lee, M. Fleischhauer, and M. O. Scully, Phys. Rev. A **58**, 2587 (1998).

[159] S. Stenholm, *Foundations of Laser Spectroscopy* (Wiley, New York, 1984).

[160] C. Cohen-Tannoudji, J. Dupont-Roc, and G. Grynberg, *Photons and Atoms : Introduction to Quantum Electrodynamics*(Wiley, New York, 1989).

[161] J. Vanier, and C. Audoin, *The Quantum Phisics of Atomic Frequency Standards*, (Hilger, Bristol, 1989), Vol. I.

[162] M. Graf, E. Arimondo, E. S. Fry, D. E. Nikonov, G. G. Padmabandu, M. O. Scully, and S. Zhu, Phys. Rev. A **51**, 4030 (1995).

[163] Ch. Ottinger, R. Scheps, G. W. York, and A. Gallagher, Phys. Rev. A **11**, 1815 (1975).

[164] N. Allard, and J. Kielkopf, Rev. Mod. Phys. **54**, 1103 (1982).

[165] E. Arimondo, Phys. Rev. A **54**, 2216 (1996).

[166] N. W. Ressler, R. H. Sands, and T. E. Stark, Phys. Rev. **184**, 102 (1969).

[167] V. A. Kartoshkin, Opt. Spectr. **79**, 26 (1995).

[168] S. Kadlecek, L. W. Anderson, and T. G. Walker, Phys. Rev. Lett. **80**, 5512 (1998).

[169] R. L. Gamblin, and T. R. Carver, Phys. Rev. **138**, A946 (1965).

[170] L. D. Schearer, and G. K. Walters, Phys. Rev. **139**, A1398 (1965).

[171] H. G. Robinson, E. S. Ensberg, and H. G. Dehmelt, Bull. Am. Phys. Soc. **3**, 9 (1958).

[172] M. A. Bouchiat, and J. Brossel, Phys. Rev. **147**, 41 (1966).

[173] E. B. Alexandrov, M. V. Balabas, A. S. Pasgalev, A. K. Vershovskii, and N. N. Yakobson, Laser Phys. **6**, 244(1996).

[174] H. Lee, Y. Rostovtsev, C. J. Bednar, and A. Javan, Appl. Phys. B **76**, 33 (2002).

[175] H. P. Zeeman, Phil. Mag. **43**, 226 (1897).

[176] A. Aspect, E. Arimondo, R. Kaiser, N. Vansteenkiste, and C. Cohen-Tannoudji, Phys. Rev. Lett. **61**, 826 (1988).

[177] J. Gea-Banacloche, Y. Q. Li, S. Z. Jin, and M. Xiao, Phys. Rev. A **51**, 576 (1995).

[178] A. Karawajczyk, and J. Zakrzewski, Phys. Rev. A **51**, 830 (1995).

[179] D. Wang, and J. Gao, Phys. Rev. A **52**, 3201 (1995).

[180] G. Vemuri, and G. S. Agarwal, Phys. Rev. A **53**, 1060 (1996); G. Vemuri, G. S. Agarwal, and B. D. N. Rao, Phys. Rev. A **53**, 2842 (1996).

[181] Y. F. Zhu, and T. N. Wasserlauf, Phys. Rev. A **54**, 33653 (1996); Y. F. Zhu, S. J. Wang, N. M. Mulchan, Phys. Rev. A **59**, 4005 (1999); S. Wang, D. G. Ducreay, R. Pina, M. Yan, and Y. F. Zhu, Phys. Rev. A **61**, 033805 (2000).

[182] S. Shepherd, D. J. Fulton, and M. H. Dunn, Phys. Rev. A **54**, 5394 (1996).

[183] J. R. Boon, E. Zekou, D. McGloin, and M. H. Dunn, Phys. Rev. A **58**, 2560 (1998).

[184] N. Mulchan, D. G. Ducreay, R. Pina, M. Yan, and Y. F. Zhu, J. Opt. Soc. Am. B **17**, 820 (2000).

[185] C. Y. Ye, A. S. Zibrov, and Y. V. Rostovtsev, J. Mod. Opt. **49**, 391 (2002).

[186] A. V. Taichenachev, A. M. Tumaikin, and V. I. Yudin, JETP Lett. **72**, 119 (2000).

[187] C. Y. Ye, and A. S. Zibrov, Phys. Rev. A **65**, 023806 (2002).

[188] A. Javan, O. Kocharovskaya, H. Lee, and M. O. Scully, Phys. Rev. A **66**, 013805 (2002).

[189] Y. Rostovtsev, I. Protsenko, H. Lee, and A. Javan, J. Mod. Opt. **49**, 2501 (2002).

[190] N. G. Basov, O. N. Krokhin, and Y. M. Popov, JETP **40**, 1320 (1961).

[191] R. N. Hall, G. E. Fenner, J. D. Kingsley, T. J. Soltys, and R. O. Carlson, Phys. Rev. Lett. **9**, 366 (1962).

[192] C. E. Wieman, and L. Hollberg, Rev. Sci. Instrum. **62**, 1 (1991).

[193] M. Ohtsu, *Highly Coherent Semiconductor Lasers* (Artech House, Boston, 1992).

[194] M.-C. Amann, and J. Buus, *Tunable Laser Diodes* (Artech House, Boston, 1998).

[195] M. W. Fleming, and A. Mooradian, Appl. Phys. Lett. **38**, 511 (1981).

[196] L. Goldberg, H. F. Taylor, and J. F. Weller, Electron. Lett. **18**, 353 (1982).

[197] E. M. Belenov, V. L. Velichansky, A. S. Zibrov, V. V. Nikitin, V. A. Sautenkov, and A. V. Uskov, Sov. J. Quantum. Electron. **13**, 792 (1983).

[198] R. Wyatt, and W. J. Delvin, Electron. Lett. **19**, 110 (1983).

[199] B. Dahmani, L. Hollberg, and R. Drullinger, Opt. Lett. **12**, 876 (1987).

[200] M. G. Littman, Opt. Lett. **3**, 138 (1978).

[201] K. C. Harvey, and C. J. Myatt, Opt. Lett. **16**, 910 (1991).

[202] G. J. Escandon, Y. Liu, G. J. Sonek, and M. W. Berns, IEEE Photonics Tech. Lett. **6**, 597 (1994).

[203] Y. S. Cheng YS, and R. C. Chang, Opt. Eng. **37**, 2717 (1998).

[204] L. G. Deshazer, and E. A. Maunders, Rev. Sci. Instrum. **38**, 248 (1967).

[205] D. J. Gauthier, P. Narim, and R. W. Boyd, Opt. Lett. **11**, 623 (1986).

[206] S. Haroche, and F. Hartmann, Phys. Rev. A **6**, 1280 (1972).

[207] A. S. Zibrov, M. D. Lukin, L. Hollberg, D. E. Nikonov, M. O. Scully, H. G. Robinson, V. L. Velichansky, Phys. Rev. Lett. **76**, 3935 (1996).

[208] T. Holstein, Phys. Rev. **72**, 1212 (1947); D. Alpert, A. O. Mccoubrey, and T. Holstein, Phys. Rev. **76**, 1257 (1949).

[209] A. F. Molisch, and B. P. Oehry, *Radiation Trapping in Atomic Vapours* (Clarendon Press, Oxford,1995).

[210] V. A. Sautenkov, M. M. Kash, V. L. Velichansky, and G. R. Welch, Laser Phys. **9**, 889 (1999).

[211] M. V. Krasheninnikov, V. S. Smirnov, M. V. Sultanov, A. M. Tumaikin, and V. I. Yudin, Sov. Phys. JETP **67**, 113 (1988).

[212] A. Weis, J. Wurster, S. I. Kanorsky, and T. W. Hänsch, in *Spectral Line Shapes*, edited by R. Stamm and B. Talin (Nova Science, New York, 1993), Vol.7, pp.234-236.

[213] G. E. Andrews, R. Askey, and R. Roy, *Special functions* (Cambridge University Press, Cambridge, UK, 1999).

[214] E. Pfleghaar, J. Wurster, S. I. Kanorsky, and A. Weis, Opt. Commun. **99**, 303 (1993).

[215] A. V. Taichenachev, V. I. Yudin, M. Stahler, J. Kitching, R. Wynands, and L. Hollberg, *Technical Digest of International Quantum Electronics Conference*, 337 (2002);

[216] R. H. Dicke, Phys. Rev. **93**, 99 (1954).

[217] M. F. H. Schuurmans, Q. H. Vrehen, D. Polder, and H. M. Gibbs, in *Advances in Atomic and Molecular Physics*, edited by D. Bates and B. Bederson, (Academic, New York, 1981), pp. 167-228.

[218] G. Benedict, A. M. Ermolaev, V. A. Malyshev, I. V. Sokolov, and E. D. Trifonov, *Superradiance, Multiatomic Coherent Emission* (IOP, Bristol, 1996).

[219] L. Mandel, and E. Wolf, *Optical Coherence and Quantum Optics*, (Univ. Press, Cambridge, 1995).

[220] C. M. Bowden, and J. P. Dowling, Phys. Rev. A **47**, 1247 (1993).

[221] A. S. Manka, J. P. Dowling, C. M. Bowden, and M. Fleischhauer, Phys. Rev. Lett. **73**, 1789 (1994).

[222] A. S. Manka, J. P. Dowling, C. M. Bowden, and M. Fleischhauer, Phys. Rev. Lett. **74**, 4965 (1995).

[223] H. van Kampen, V. A. Sautenkov, C. J. C. Smeets, E. R. Eliel, and J. P. Woerdman, Phys. Rev. A **59** 271 (1999).

[224] M. E. Crenshaw, and C. M. Bowden, Phys. Rev. A **63**, 013801 (2001).

[225] J. P. Wittke, and R. H. Dicke, Phys. Rev. **103**, 620 (1956).

[226] L. W. Anderson, and A. T. Ramsey , Phys. Rev. **132**, 712 (1963).

[227] N. W. Ressler, R. H. Sands, and T. E. Stark, Phys. Rev. **184**, 102 (1969).

[228] S. Kadlecek, L. W. Anderson, and T. G. Walker, Phys. Rev. Lett. **80**, 5512 (1998).

[229] H. van Kampen, A. V. Papoyan, V. A. Sautenkov, P. H. Castermans, E. R. Eliel, and J. P. Woerdman, Phys. Rev. A **56**, 310 (1997).

[230] H. van Kampen, V. A. Sautenkov, A. M. Shalagin, E. R. Eliel, J. P. Woerdman, Phys. Rev. A **56**, 3569 (1997).

[231] D. Peterson, and L. W. Anderson, Phys. Rev. A **43**, 4883 (1991).

[232] T. Scholz, M. Schiffer, J. Welzel, D. Cysarz, and W. Lange, Phys. Rev. Lett. **53**, 2169 (1996).

[233] G. Ankerhold, M. Schiffer, D. Mutschall, T. Scholz, and W. Lange, Phys. Rev. A **48**, R4031 (1993).

[234] M. Fleischhauer, Europhys. Lett. **45**, 659 (1999).

[235] M. O. Scully, Phys. Rev. Lett. **67**, 1855 (1991).

[236] M. M. Kash, V. A. Sautenkov, A. S. Zibrov, L. Hollberg, G. R. Welch, M. D. Lukin, Y. Rostovtsev, E. S. Fry, and M. O. Scully, Phys. Rev. Lett. **82**, 5229 (1999).

[237] R. H. Dicke, Phys. Rev. **89**, 472 (1953).

[238] C. Cohen-Tannoudji, J. Brossel, and A. Kastler, C. R. Ac. Sci. **245**, 1027 (1957).

[239] M. Rambosson, J. Brossel, and A. Kastler, C. R. Ac. Sci. **246**, 1522 (1958).

[240] I. I. Sobel'man, L. A. Vainshtein, and E. A. Yukov, *Excitation of Atoms and Broadening of Spectral Lines* (Springer-Verlag, Berlin, 1981).

[241] J. C. Camparo, J. Chem. Phys. **86**, 1533 (1987).

[242] E. B. Alexandrov, M. V. Balabas, D. Budker, D. S. English, D. F. Kimball, C.-H. Li, and V. V. Yashchuk, Phys. Rev. Lett. **66**, 042903 (2002).

[243] H. G. Robinson, and C. E. Johnson, Appl. Phys. Lett. **40**, 771 (1982).

[244] E. B. Alexandrov, and V. A. Bonch-Bruevich, Opt. Eng. **31**, 711 (1992).

[245] S. Brandt, A. Nagel, R. Wynands, and D. Meschede, Phys. Rev. A **56**, R1063 (1997); R. Wynands, and A. Nagel, Appl. Phys. B **68**, 1 (1998).

[246] M. Erhard, S. Nußmann, and H. Helm, Phys. Rev. A **62**, 061802(R) (2000); M. Erhard, and H. Helm, Phys. Rev. A **63**, 043813 (2001).

[247] J. H. Xu, and G. Alzetta, Phys. Lett. A **248**, 80 (1998).

[248] S. Gozzini, P. Sartini, C. Gabbanini, A. Lucchesini, C. Marinelli, L. Moi, J. H. Xu, and G. Alzetta, Eur. Phys. J. D **6**, 127 (1999).

[249] D. Budker, D. F. Kimball, S. M. Rochester, V. V. Yashchuk, and R. Zolotorev, Phys. Rev. A **62**, 043403 (2000).

[250] I. Novikova, A. B. Matsko, and G. R. Welch, Appl. Phys. Lett. **81**, 193 (2002).

[251] P. R. Berman, Adv. Atom. Mol. Phys. **13**, 57 (1977); ed. by D. R. Bates and B. Bederson.

[252] A. G. Kofman, Phys. Rev. A **58**, 3012 (1998).

[253] A. Kumarakrishnan, U. Shim, S. B. Cahn, and T. Sleator, Phys. Rev. A **58**, 3868 (1998).

[254] B. Dubetsky and P. R. Berman, Appl. Phys. B: Laser Opt. **59**, 147 (1994).

[255] B. Stahlberg, P. Jungner, T. Fellman, and A. Lindberg, Appl. Phys. B **50**, 547 (1990).

[256] M. I. D'yakonov, Soviet Phys. JETP **20**, 1484 (1965).

[257] D. A. Varshalovich, A. N. Moskalev, and V. K. Khersonskii, *Quantum Theory of Angular Momentum* (World Scientific, Singapore) 1988.

[258] D. Suter, and T. Marty, Opt. Commun. **100**, 443 (1993); D. Suter, and T. Marty, J. Opt. Soc. Am. B **11**, 242 (1994).

[259] A. Ekert, R. Jozsa, Rev. Mod. Phys. **68**, 733 (1996); A. Steane, Rep. Prog. Phys. **61**, 117 (1998).

[260] S. E. Harris, J. E. Field, and A. Imamoglu, Phys. Rev. Lett. **64**, 1107 (1990).

[261] H. Schmidt and A. Imamoglu, Opt. Lett. **21**, 1936 (1996).

[262] M. D. Lukin and A. Imamoglu, Nature **413**, 273 (2001).

[263] A. Imamoglu, H. Schmidt, G. Woods, and M. Deutsch, Phys. Rev. Lett. **79**, 1467 (1997).

[264] S. Rebic, S. M. Tan, A. S. Parkins, and D. F. Walls, J. Opt. B – Quant. Semiclass. Opt. **1**, 490 (1999).

[265] K. M. Gheri, W. Alge, and P. Grangier, Phys. Rev. A **60**, R2673 (1999).

[266] A. D. Greentree, J. A. Vaccaro, S. R. de Echaniz, A. V. Durrant, and J. P. Marangos, J. Opt. B – Quant. Semiclass. Opt. **2**, 252 (2000).

[267] S. E. Harris and L. V. Hau, Phys. Rev. Lett. **82**, 4611 (1999).

[268] M. D. Lukin and A. Imamoglu, Phys. Rev. Lett. **84**, 1419 (2000).

[269] S. E. Harris and Y. Yamamoto, Phys. Rev. Lett. **81**, 3611 (1998).

[270] B. S. Ham and P. R. Hemmer, Phys. Rev. Lett. **84**, 4080 (2000).

[271] M. Yan, E. G. Rickey, and Y. Zhu, Opt. Lett. **26**, 548 (2001); M. Yan, E. G. Rickey, and Y. Zhu, Phys. Rev. A **64**, R041801 (2001).

[272] M. S. Zubairy, A. B. Matsko, and M. O. Scully, Phys. Rev. A **65**, 043804 (2002).

[273] A. B. Matsko, I. Novikova, G. R. Welch, and M. S. Zubairy, Opt. Lett. **28**, 96 (2003).

[274] A. D. Greentree, D. Richards, J. A. Vaccaro, A. V. Durrant, S. R. de Echaniz, D. M. Segal, and J. P. Marangos, Phys. Rev. A **67**, 023818 (2003).

[275] R. W. Boyd, *Nonlinear Optics* (Academic Press, Boston, 1992).

[276] V. S. Smirnov, A. M. Tumaikin, and V. I. Yudin, Sov. Phys. JETP **69**, 913 (1989).

[277] A. V. Taichenachev, A. M. Tumaikin, and V. I. Yudin, JETP **83**, 949 (1996); A. V. Taichenachev, A. M. Tumaikin, and V. I. Yudin, JETP **91**, 67 (2000).

[278] G. Nienhuis, A. V. Taichenachev, A. M. Tumaikin, and V. I. Yudin, Europhys. Lett. **44**, 20 (1998).

[279] V. Milner, and Y. Prior, Phys. Rev. Lett. **80**, 940 (1998).

[280] B. T. H. Varskoe, R. T. Sang, W. R. MacGillivary, M. C. Standage, and P. M. Farrell, J. Mod. Opt. **46**, 787 (1999).

[281] S. Wang, D. G. Ducreay, R. Pina, M. Yan, and Y. Zhu, Phys. Rev. A **61**, 033805 (2000).

[282] M. Fleischhauer, LANL e-print archive quant-ph/9910112 (1999).

[283] J. R. Morris, and B. W. Shore, Phys. Rev. A **27**, 906 (1983).

[284] Z. Diao, M. S. Zubairy, and G. Chen, Zeit. f. Naturforsc. **57a**, 701 (2002).

[285] M. Arditi, and T. R. Carver, Phys. Rev. **124**, 800 (1961).

[286] W. Happer, and B. S. Mathur, Phys. Rev. **163**, 12 (1967);

B. S. Mathur, H. Tang, and W. Happer, Phys. Rev. **171**, 11 (1968).

[287] C. Cohen-Tannoudji and J. Dupont-Roc, Phys. Rev. A **5**, 968 (1972).

[288] P. D. Maker, and R. W. Terhune, Phys. Rev. **137**, A801 (1965).

[289] G. G. Adonts, D. G. Akopyan, and K. V. Arutunyan, J. Phys. B: At. Mol. Phys. **19**, 4113 (1986).

[290] W. V. Davis, A. L. Gaeta, and R. W. Boyd, Opt. Lett. **17**, 1304 (1992).

[291] Y. R. Chiao, J. Bowie, J. Boyce, D. Budker, J. C. Garrison, M. W. Mitchell, V. Yashchuk, T. K. Gustafson, and D. S. Hsiung, *Technical Digest of Conference on Lasers and Electro-Optics, Quantum Electronics and Laser Science*, 259 (1999).

D. Budker, R. Y. Chiao, D. S. Hsiung, S. M. Rochester, and V. V. Yashchuk, *Technical Digest of Conference on Lasers and Electro-Optics, Quantum Electronics and Laser Science*, 252 (2000).

[292] I. Novikova, A. B. Matsko, V. A. Sautenkov, V. L. Velichansky, G. R. Welch, and M. O. Scully, Opt. Lett. **25**, 1651 (2000).

[293] S. M. Rochester, D. S. Hsiung, D. Budker, R. Y. Chiao, D. F. Kimball, and V. V. Yashchuk, Phys. Rev. A **63**, 043814 (2001).

[294] I. Novikova, A. B. Matsko, V. L. Velichansky, M. O. Scully, and G. R. Welch, Phys. Rev. A **63**, 063802 (2001).

[295] D. F. Walls, Nature (London) **306**, 141 (1983), D. F. Walls and G. J. Milburn, *Quantum Optics* (Springer, Berlin, 1995).

[296] See, e.g., the following special issues of journals dealing with squeezing via nonlinear optics: J. Opt. Soc. Am. **4**, 1450-1741; and *Quantum Noise Reduction in Optical Systems*, edited by C. Fabre and E. Giacobino, App. Phys. B **55**, 189ff (1992).

[297] M. Xiao, L.-A. Wu, and H. J. Kimble, Phys. Rev. Lett. **59**, 278 (1987).

[298] P. Grangier, R. E. Slusher, B. Yurke, and A. LaPorta, Phys. Rev. Lett. **59**, 2153 (1987).

[299] H. J. Kimble, in *Fundamental Systems in Quantum Optics*, Les Houches Session LIII, edited by J. Dalibard, J. M. Raimond, and J. Zinn-Justin (Elsevier, Amsterdam, 1992), pp. 549-674.

[300] L.-A. Wu, M. Xiao and H. J. Kimble, J. Opt. Soc. Am. B, **4**, 1465 (1987).

[301] E. S. Polzik, J. Carri and J. H. Kimble, Appl. Phys. B **55**, 279 (1992).

[302] K. Schneider, M. Lang, J. Mlynek, and S. Schiller, Optics Express, **2**, 59 (1998).

[303] P. K. Lam, T. C. Ralph, B. C. Buchler, D. E. McClelland, H. A. Bachor, J. Gao, J. Opt. B – Quant. Semiclass. Opt. **1**, 469 (1999).

[304] A. B. Matsko, I. Novikova,G. R. Welch, D. Budker, D. F. Kimball, and S. M. Rochester, Phys. Rev. A **66** 043815 (2002).

[305] L. Boivin, and H. A. Haus, Opt. Lett. **21**, 146 (1996);

[306] M. Margalit, C. X. Yu, E. P. Ippen, and H. A. Haus, Opt. Express **2**, 72 (1998).

[307] P. Ripka, *Magnetic Sensors and Magnetometers* (Artech House, Boston, 2001).

[308] Y. N. Ning, Z. P. Wang, A. W. Palmer,K. T. V. Grattan, and D. A. Jackson, Rev. Sci. Instrum. **66**, 3097 (1995).

[309] M. N. Deeter, A. H. Rose, G. W. Day, and S. Samuelson, J. Appl. Phys. **70**, 6407 (1991); M. N. Deeter, IEEE Trans. Instrum. Meas. **44**, 464 (1995).

[310] R. B. Wagreich, and C. C. Davis, IEEE Trans. Magn. **33**, 2356 (1997).

[311] A. L. Bloom, Appl. Opt. **1**, 61 (1962).

[312] C. Cohen-Tannoudji, J. DuPont-Roc, S. Haroche, and F. Laloë, Phys. Rev. Lett. **22**, 758 (1969).

[313] D. D. McGregor, Rev. Sci. Instrum. **58**, 1067 (1987).

[314] E. B. Alexandrov, M. V. Balabas, and V. A. Bonch-Bruevich, Pisma Zh. Tekh. Fiz. **12**, 749 (1987).

[315] E. B. Alexandrov, M. V. Balabas, A. K. Vershovskii, A. E. Ivanov, N. N. Yakobson, V. L. Velichanskii, and N. V. Senkov, Opt. Spectr. **78**, 292 (1995).

[316] A. Nagel, L. Graf, A. Naumov, E. Mariotti, V. Biancalana, D. Meschede, and R. Wynands, Europhys. Lett. **44**, 31 (1998).

[317] R. Wynands, and A. Nagel, Appl. Phys. B **68**, 1 (1999); R. Wynands, and A. Nagel, Appl. Phys. B **70**, 315 (2000).

[318] M. Stahler, S. Knappe, C. Affolderbach, W. Kemp, and R. Wynands, Europhys. Lett. **54**, 323 (2001).

[319] F. Bretenaker, B. Lepine, J.-C. Cotteverte, and A. Le Floch, Phys. Rev. Lett. **69**, 909 (1992).

[320] D. Budker, D. F. Kimball, V. V. Yashchuk, and M. Zolotorev, Phys. Rev. A **65**, 033401 (2002).

[321] I. Novikova, and G. R. Welch, J. Mod. Opt. **49**, 349 (2002).

[322] T. Isayama, Y. Takahashi, N. Tanaka, K. Toyoda, K. Ishikawa, and T. Yabuzaki, Phys. Rev. A **59**, 4836 (1999).

[323] S. Yamaguchi, I. Matsuda, and M. Suzuki, IEEE Trans. Instrum. Meas. **28**, 2551 (1992).

[324] J. C. Camparo, and R. P. Frueholz, J. Appl. Phys. **59**, 3313 (1986).

[325] F. Levi, C. Novero, A. Godone, and G. Brida, IEEE Trans. Instrum. Meas. **46**, 126 (1997).

[326] J. Deng, J. Lui, S. An, Y. Tan, and X. Zhu, IEEE Trans. Instrum. Meas. **43**, 549 (1994).

[327] M. Hashimoto, and M. Ohtsu, J. Opt. Soc. Am. B. **6**, 1777 (1989); M. Hashimoto, and M. Ohtsu, IEEE Trans. Instrum. Meas. **39**, 458 (1990).

[328] C. R. Bowers, G. Wäckerle, and M. Mehring, Phys. Rev. A **46**, 7042 (1992).

[329] *WebElements Periodic Table*, http://www.webelements.com/ (1993).

[330] *A Periodic Table of the Elements at Los Alamos National Laboratory's Chemistry Division*, http://pearl1.lanl.gov/periodic/ (2001).

[331] *The Pictorial Periodic Table*, http://chemlab.pc.maricopa.edu/periodic/ (2002).

[332] A. N. Nesmeyanov, *Vapor Pressure Curve of Chemical Elements*, (Elsevier, New York, 1963).

[333] R. W. Ditchburn, and J. C. Gilmoure, Rev. Mod. Phys. **13**, 310 (1941).

APPENDIX A

SOME PROPERTIES OF Rb ATOMS

The chemical element we used in all our experiments is Rubidium (Rb). It belongs to the group of alkali metals (with Li, Na, K, Cs and Fr). The Rb atom has one unbound electron in the electronic configuration [Kr]$5s^1$. Its atomic number is 37, and the atomic weight is 85.4678(3). Twenty four isotopes of Rubidium are known. Naturally occurring Rb is made of two isotopes, ^{85}Rb and ^{87}Rb. The first isotope is stable, and ^{87}Rb is present to the extent of 27.85% in natural rubidium and is a beta emitter with a half-life of $4.9 \cdot 10^{10}$ years [329–331].

Rubidium was discovered spectroscopically in 1861 by R. Bunsen and R. Kirchoff in the mineral lepidolite, from which it is now recovered commercially. The name of the element originated from Latin *rubidus* - deepest red, for its bright spectroscopic lines in near infra-red region.

At room temperature Rb exists in liquid form. The typical atomic cell, which is used in the experiments, is shown in Fig. 69. Glass cylinder contains the drop of liquid Rb and the saturated Rb vapor. The dependence of the pressure of the Rb vapor inside the cell on temperature $T[K]$ is given by empirical formula [332, 333]:

$$\log_{10} P[Torr] = A - \frac{B}{T} + CT + D\log_{10} T, \tag{A.1}$$

where coefficients are $A = -94.04826, B = 1961.258, C = -0.03771687, D = 42.57526$ for solid Rb ($T < 312K$), and $A = 15.88253, B = 4529.635, C = 0.00058663, D = -2.99138$ for liquid Rb.

Rubidium atoms have a hidrogen-like electronic configuration, with the first excited state $5P$. This level is split into two states with total angular momentum

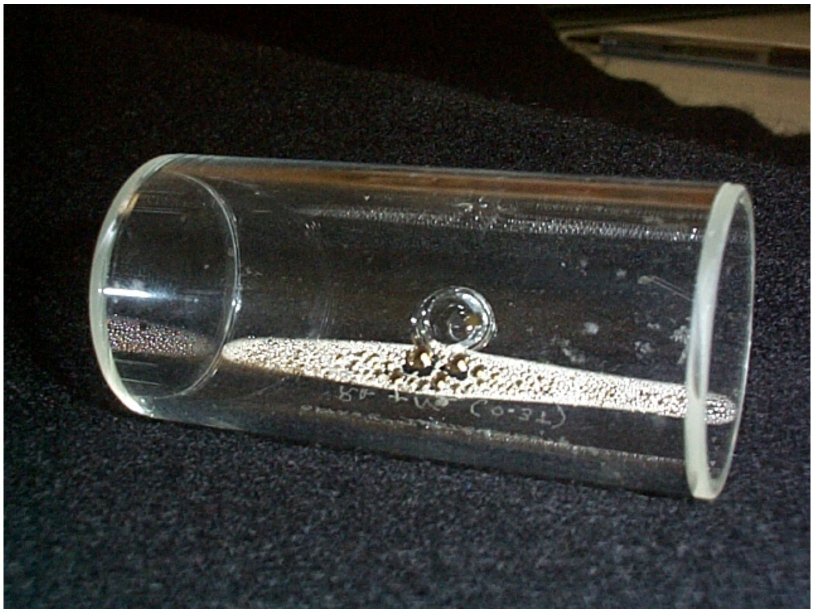

Fig. 69. Glass atomic cell with drops of liquid Rb.

$J = 1/2$ and $J = 3/2$ due to spin-orbit coupling. The optical transition $5S_{1/2} \rightarrow 5P_{1/2}$ (often referred as a D_1 line) has a wavelength of $\lambda = 794.760$nm with the lifetime of the excited state of $\tau = 29.4$ns. The wavelength of the other transition $5S_{1/2} \rightarrow 5P_{1/2}$ (D_2) line is $\lambda = 780.027$nm, with the lifetime of the excited state $\tau = 27.0$ns [161].

Because of the hyper-fine coupling between the electron and nuclear spins, the atomic levels are further split into two ($5P_{1/2}$ and $5P_{1/2}$) or four ($5P_{3/2}$) sublevels. The actual structure of the hyperfine levels depends on the isotope. For ^{87}Rb the nuclear spin is $I = 3/2$, and for ^{85}Rb it is $I = 5/2$. The level scheme and the values of the hyperfine splitting are shown in Fig. 70 for the D_1 and in Fig. 71 for the D_2 lines.

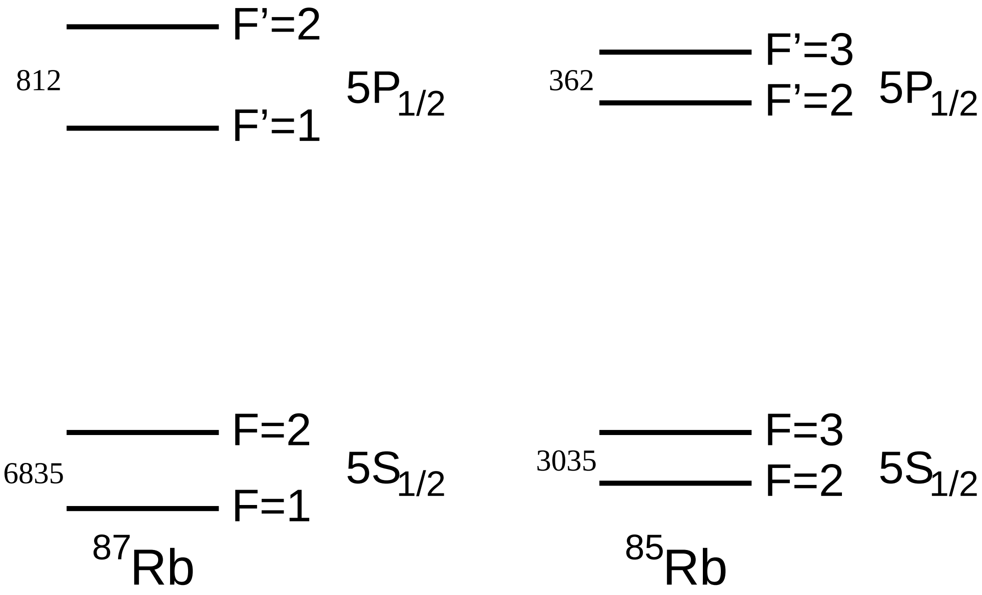
F'=2
812
F'=1
5P1/2
F'=3
362
F'=2
5P1/2
F=2
6835
F=1
5S1/2
87Rb
F=3
3035
F=2
5S1/2
85Rb

Fig. 70. Level scheme for the D_1 line of ^{87}Rb and ^{85}Rb. The splitting between the levels is given in MHz.

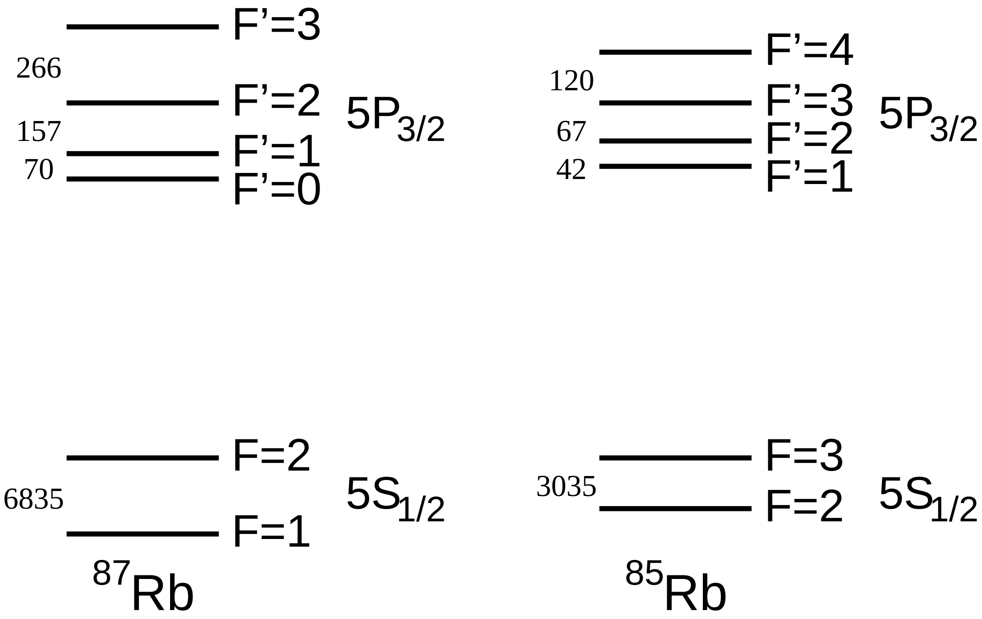
F’=3
266
F’=2
157
F’=1
70
F’=0
5P3/2
F’=4
120
F’=3
67
F’=2
42
F’=1
5P3/2
F=2
6835
F=1
5S1/2
87Rb
F=3
3035
F=2
5S1/2
85Rb

Fig. 71. Same as Fig. 70 for the Rb D_2 line.

The electric dipole moments of the various transitions between the Zeeman sublevels are determined by the following expression:

$$\begin{aligned}\wp_{J,I,F,m_F\to J',I,F',m_{F'}} &= \left|\langle J',I,F',m_{F'}|\vec{d}|J,I,F,m_F\rangle\right| \\ &= \frac{\left|\langle J'|\vec{d}|J\rangle\right|}{\sqrt{2J'+1}}a_{F,m_F\to F',m_{F'}} \end{aligned} \tag{A.2}$$

Here and further the apostrophe, for example "F' ", denotes the values belonging to the excited state.

Coefficients $a_{F,m_F\to F',m_{F'}}$ determine the relative probability of each individual transition within the hyperfine Zeeman substructure of the ground and excited states J and J'. They can be expressed in terms of $3j$ and $6j$ symbols [161]:

$$\begin{aligned}a_{F,m_F\to F',m_{F'}} = & \quad (-1)^{1+I+J'+F'+F-m_{F'}}\sqrt{(2F'+1)(2F+1)(2J'+1)} \\ & \times \begin{pmatrix} F' & 1 & F \\ -m_{F'} & q & m_F \end{pmatrix} \begin{Bmatrix} F' & 1 & F \\ J & I & J' \end{Bmatrix}, \end{aligned} \tag{A.3}$$

where q is the ellipticity coefficient of the laser light ($q=\pm1$ for right/left-circularly polarized light, and $q=0$ for the linearly polarized light.

The numerical values of the coefficients $a_{F,m_F\to F',m_{F'}}$ for the D_1 and D_2 lines of ^{87}Rb are given in Tables III and IV.

Table III. Transition probability coefficients for the ^{87}Rb D_1 line.

	F'		2	2	2	2	2	1	1	1
F	m_F		2	1	0	-1	-2	-1	0	1
2	2	$\frac{1}{2\sqrt{3}}\times$	2	$\sqrt{2}$	0	0	0	$-\sqrt{6}$	0	0
2	1		$-\sqrt{2}$	1	$\sqrt{3}$	0	0	$\sqrt{3}$	$-\sqrt{3}$	0
2	0		0	$-\sqrt{3}$	0	$\sqrt{3}$	0	-1	2	-1
2	-1		0	0	$-\sqrt{3}$	-1	$\sqrt{2}$	0	$-\sqrt{3}$	$\sqrt{3}$
2	-2		0	0	0	$-\sqrt{2}$	-2	0	0	$-\sqrt{6}$
1	1	$\frac{1}{2\sqrt{3}}\times$	$\sqrt{6}$	$\sqrt{3}$	1	0	0	-1	-1	0
1	0		0	$\sqrt{3}$	2	$\sqrt{3}$	0	1	0	-1
1	-1		0	0	1	$\sqrt{3}$	$\sqrt{6}$	0	1	1

Table IV. Transition probability coefficients for the ^{87}Rb D_2 line.

	F'		3	3	3	3	3	3	3
F	m_F		3	2	1	0	-1	-2	-3
2	2		$\sqrt{15}$	$\sqrt{5}$	1	0	0	0	0
2	1		0	$\sqrt{10}$	$2\sqrt{2}$	$\sqrt{3}$	0	0	0
2	0	$\frac{1}{\sqrt{15}}\times$	0	0	$\sqrt{6}$	3	$\sqrt{6}$	0	0
2	-1		0	0	0	$\sqrt{3}$	$2\sqrt{2}$	$\sqrt{10}$	0
2	-2		0	0	0	0	1	$\sqrt{5}$	$\sqrt{15}$

	F'		2	2	2	2	2		1	1	1		0
F	m_F		2	1	0	-1	-2		-1	0	1		0
2	2		-2	$-\sqrt{2}$	0	0	0		$\sqrt{6}$	0	0		0
2	1		$\sqrt{2}$	-1	$-\sqrt{3}$	0	0		$-\sqrt{3}$	$\sqrt{3}$	0		0
2	0	$\frac{1}{2\sqrt{3}}\times$	0	$\sqrt{3}$	0	$-\sqrt{3}$	0	$\frac{1}{2\sqrt{15}}\times$	1	-2	1		0
2	-1		0	0	$\sqrt{3}$	1	$-\sqrt{2}$		0	$\sqrt{3}$	$-\sqrt{3}$		0
2	-2		0	0	0	$\sqrt{2}$	2		0	0	$\sqrt{6}$		0
1	1		$\sqrt{6}$	$\sqrt{3}$	1	0	0		-1	-1	0		1
1	0	$\frac{1}{2\sqrt{3}}\times$	0	$\sqrt{3}$	2	$\sqrt{3}$	0	$\frac{\sqrt{5}}{2\sqrt{3}}\times$	1	0	-1	$\frac{1}{\sqrt{3}}\times$	-1
1	-1		0	0	1	$\sqrt{3}$	$\sqrt{6}$		0	1	1		1

VITA

Name: Irina Borisovna Novikova

Date and Place of Birth: November 16, 1975, Moscow, USSR

Citizenship: Russian

Address: Department of Physics, Texas A&M University,
College Station, TX 77843-4242

E-mails: irina@leona.physics.tamu.edu; i.novikova@osa.org

Education

May 2003	Ph.D. in physics, Texas A&M University, GPR 4.0.
February 1998	Diploma with honors (summa cum laude) in engineering physics/solid state physics, Moscow State Engineering Physics Institute

Experience

1998-2003	Physics Department, Texas A&M University Teaching assistant (undergraduate and graduate courses) Research assistant (Experimental Quantum Optics)
1997-1998	Frequency Standard Laboratory, Lebedev Physics Institute Research assistant (Quantum Electronics)

Honors

Graduate Student Research and Presentation Grant (2002)
Optical Society of America New Focus Student Award (Grand Prize) (2001)
Ethel Ashworth-Tsutsui Memorial award for research (2001)
Finalist in Moscow young scientists competition, Quantum Electronics section (1997)
Phi Kappa Phi

The typist for this dissertation was Irina Novikova.